

**Faculty of Science and Engineering
School of Civil and Mechanical Engineering**

Experimental Study on the Behaviour of Expansive Soils

Farzad Habibbeygi

**This thesis is presented for the Degree of
Doctor of Philosophy
of
Curtin University**

April 2019

DECLARATION

To the best of my knowledge and belief this thesis contains no material previously published by any other person except where due acknowledgment has been made.

This thesis contains no material which has been accepted for the award of any other degree or diploma in any university.

Signature: *Farzad Habibbeygi*

A handwritten signature in blue ink, appearing to read 'Farzad Habibbeygi', written in a cursive style.

Date: 20 April 2019

ABSTRACT

Expansive soils present challenges to geotechnical engineers due to their high swell potential. Understanding the volumetric and mechanical behaviour of such soils is essential to providing more effective means of mitigating their swell potential. In this study, the volumetric behaviour of expansive soils was investigated by carrying out consolidation tests. The effects of initial water content on soil compression curves at both pre-yield and post-yield phases were investigated. The time-tested concept of the intrinsic framework was used to normalise the compression curves. Additionally, the effects of clay mineralogy and initial water content were investigated. Experimental equations are proposed to predict the yield stress, intrinsic constants and intrinsic compression line.

The results indicate that the remoulded yield stress decreases non-linearly with increases in initial water content, and is considerably influenced by the predominant clay type. The remoulded yield stress of a soil consisting predominantly of montmorillonite (smectite) clay is far greater than that of soils containing other clay minerals despite having the same normalised initial void ratio. Furthermore, the remoulded yield stress of an expansive soil consisting predominantly of smectite clay decreases more sharply than that of soils containing other clay minerals. Reconstituted compression indices for clays with considerable amounts of montmorillonite are also greater than those for other clay minerals.

Four models were developed to predict the intrinsic compression indices of reconstituted clays. The effects of clay mineralogy were included in the models to improve their accuracy. A series of sensitivity analyses were performed to investigate the effect of each input parameter on the accuracy of the proposed models. The findings indicate that the void ratio at the liquid limit has the greatest impact on the intrinsic compression indices of clays with a predominant clay of smectite, while the effect of the initial void ratio is the least among the various clay minerals. A modified equation for predicting the virgin compression line of reconstituted clays is proposed that considers the clay mineralogy.

In this study, an equation is proposed to determine the compression index as a function of consistency limits. The intrinsic framework was employed as a normalisation method for the analysis of reconstituted clays. The findings show that there is a unique relationship between the compression indices of reconstituted clays and consistency limits.

The compressibility of expansive soils with various initial water contents was investigated under cyclic loading and reloading. The findings indicate that the unloading/reloading cycle can be approximated by a bi-linear line in a semi-logarithmic plane with three definite slopes (i.e. compression indices). Moreover, the unloading and reloading compression indices can be determined by using the compression and swell indices. The results also show that the reloading component can also be characterised by two initial and final slopes. The disparity in these two above-mentioned slopes can be described by the balance of physico-chemical and mechanical forces. The findings demonstrate that when the consolidation stress is less than the remoulded yield stress, the compression behaviour is mostly governed by physicochemical forces. Actually, the change in the clay micro-structure is small; however, for stresses greater than the remoulded yield stress, the soil structure disintegrates and the clay microstructure is completely affected. Consequently, mechanical forces control the deformation, which results in a sharp decrease in the void ratio.

In this research, twelve series of consolidation tests were carried out on remoulded, reconstituted and undisturbed samples to investigate the impact of high initial water content on the consolidation coefficient. The coefficient of consolidation was found to be affected by the initial water content, stress level and clay mineralogy.

Furthermore, it is demonstrated that the compression behaviour of remoulded samples prepared with initial water contents less than the liquid limit, and reconstituted samples prepared at initial water contents higher than the liquid limit at medium to high-stress levels, are controlled by a physicochemical factor. Therefore, the consolidation coefficient decreases with increases in consolidation pressure for such samples.

Conversely, the compression behaviour of reconstituted samples at low stress levels is governed mostly by a mechanical factor. Moreover, the consolidation coefficient increases with increasing consolidation stress. Furthermore, sample disturbance is another factor affecting the consolidation coefficient. According to the experimental results, sample disturbance can reduce the consolidation coefficient by up to four times the initial value.

In this research, the shear behaviour of expansive clays was investigated. According to the results of direct shear experiments, undrained shear strength is affected by the clay's initial water content. Similar to the compression behaviour analysis, an intrinsic framework was used to normalise the shear strength. The findings illustrate that the normalised undrained shear strength varies according to the initial water content. Furthermore, there is a decreasing trend for the range of pre-consolidation stress studied. Finally, a unique line is proposed for the intrinsic shear strength line of reconstituted clays.

The effect of shear rate on the residual strength of pre-sheared expansive clays was also investigated. The experimental results indicate that there is an instantaneous tendency for the residual strength to increase with increases in shear rate. Subsequently, the fast residual strength continues to rise with further shear displacement, which is referred to as a *positive effect*. Finally, the fast residual strength decreases with increases in shear displacement to a value less than the slow residual strength. This effect is referred to as a *negative effect*. These positive and negative effects, as well as the relationship between the residual strength and the fast shear rates, are discussed in this thesis.

Stabilisation of expansive clays is an effective way to alleviate their swell potential. In this study, the effect of a green stabiliser, magnesium chloride (MgCl_2), on the compression behaviour and geotechnical properties of expansive clays, was investigated. The results indicate that even small amounts of MgCl_2 can improve the consistency limits of clays.

Artificial neural networks (ANNs) were used in this research to predict the compression indices of reconstituted clays. Sensitivity analyses were also carried out to study the impact of each predictor on the accuracy of the results. Five parameters were employed to develop the ANN models: initial water content, specific gravity, liquid and plastic limits and clay mineralogy. One hundred and eighty nine (189) combinations with various numbers of neurons and transfer functions were investigated to discover the optimum ANN for predicting intrinsic constants. Finally, a predictive model was proposed based on the weights and biases found by the ANN models.

ACKNOWLEDGEMENTS

My deep gratitude goes first to my supervisor, Prof. Hamid Nikraz, for his continuous support of my PhD studies and related research, and for his patience, motivation and immense knowledge. His knowledge, guidance and enthusiasm helped me throughout my research and his personal generosity helped make my time at Curtin University enjoyable. I cannot imagine having a better advisor and mentor for my PhD studies.

I would also like to acknowledge the contribution of an Australian Government Research Training Program Scholarship in supporting this research. I acknowledge the use of Curtin University's Microscopy and Microanalysis Facility, whose instrumentation has been partially funded by the university, the State and Commonwealth Governments. I would also like to thank Assoc. Prof. Andrew Whyte, Assoc. Prof. A.H.M. Anwar and Dr Amin Chegenizadeh for their encouragement and support during this period. Special thanks to the Cedar Woods, Douglas Partners, Coffey, and Structerre companies for their kind support in providing samples. Also, my sincere thanks go to the Curtin University technical laboratory staff.

To my immediate family, I would like to thank you for your continuous encouragement, cheer and praise throughout my years of study.

My special and hearty thanks to my friends, Matt Ghanavi and Payam Sadeghi, for their inspiration and encouragement, and a special thanks to Bill Koul for his mentorship and support.

Finally, I would like to give thanks to my loving and supportive wife, Shadi, who provide unending inspiration. I look forward to continuing our lives together with our wonderful son long into the future.

DEDICATION

To:

My love, Shadi

My son, Aren: God's precious gift to me

Table of Contents

1	Introduction	1
1.1	Background	1
1.2	Research Objectives and Significance	2
1.3	Scope of Research	3
1.4	Thesis Outline.....	4
2	Literature Review.....	7
2.1	Background	7
2.2	Intrinsic Framework	8
2.3	Intrinsic Compression Invariables.....	13
2.4	Virgin Compression Line	15
2.5	Remoulded Yield Stress	18
2.6	Coefficient of Consolidation	18
2.7	Intrinsic Strength Line.....	20
2.8	Residual Shear Strength	20
2.9	Swell Pressure	21
2.9.1	Empirical approaches	22
2.9.2	Oedometer approaches	23
2.9.3	Stabilisation.....	24
3	Materials and Experimental Methods	27
3.1	Materials.....	27
3.1.1	Black clay.....	27
3.1.2	Magnesium Chloride.....	33
3.2	Experimental Methods	33
3.2.1	Oedometer tests	33
3.2.2	Direct shear tests	37
3.2.3	Ring shear test.....	39

4	Intrinsic Compression Characteristics Of An Expansive Clay From Western Australia	41
4.1	Introduction	41
4.2	Citation	41
4.3	Manuscript Contents.....	41
4.3.1	Abstract	41
4.3.2	Introduction	42
4.3.3	Material and Test Procedure	43
4.3.4	Results and Discussion.....	47
4.3.5	Conclusions	55
5	Regression Models for Intrinsic Constants of Reconstituted Clays.....	57
5.1	Introduction	57
5.2	Citation	57
5.3	Manuscript Contents.....	57
5.3.1	Abstract	57
5.3.2	Introduction	58
5.3.3	Existing correlations for predicting intrinsic constants.....	59
5.3.4	Estimating the intrinsic constants	60
5.3.5	Experimental data of reconstituted clays	61
5.3.6	Regression models	66
5.3.7	Comparison and discussion.....	79
5.3.8	Virgin compression line estimation	84
5.3.9	Conclusions	86
6	Determination of the compression index of reconstituted clays using intrinsic concept and normalised void ratio	88
6.1	Introduction	88
6.2	Citation	88
6.3	Manuscript Contents.....	88

6.3.1	Abstract	88
6.3.2	Introduction	89
6.3.3	Normalising compression curves of reconstituted clays	91
6.3.4	Determining compression index	95
6.3.5	Conclusions	98
7	The Effect of Unloading and Reloading on the Compression Behaviour of Reconstituted Clays.....	100
7.1	Introduction	100
7.2	Citation	100
7.3	Manuscript Contents.....	100
7.3.1	Abstract	100
7.3.2	Introduction	101
7.3.3	Sample Preparation and Test Procedures	102
7.3.4	Discussion and Results.....	104
7.3.5	Conclusions	107
8	Variation of consolidation coefficient of expansive clays at high initial water content.....	111
8.1	Introduction	111
8.2	Citation	111
8.3	Manuscript Contents.....	111
8.3.1	Abstract	111
8.3.2	Introduction	112
8.3.3	Coefficient of Consolidation (C_v).....	114
8.3.4	Materials, Methods and Tests	114
8.3.5	Discussion and Results.....	117
8.3.6	Conclusions	123
9	Characterisation of the Undrained Shear Strength of Expansive Clays at High Initial Water Content Using Intrinsic Concept	125

9.1	Introduction	125
9.2	Citation	125
9.3	Manuscript Contents.....	125
9.3.1	Abstract	125
9.3.2	Introduction	126
9.3.3	Intrinsic Framework	127
9.3.4	Materials and Test Procedures	128
9.3.5	Discussion and Results.....	129
9.3.6	Conclusions	136
10	Effect of Shear Rate on the Residual Shear Strength of Pre-Sheared Clays....	137
10.1	Introduction.....	137
10.2	Citation.....	137
10.3	Manuscript Contents	137
10.3.1	Abstract	137
10.3.2	Introduction	138
10.3.3	Materials and Test Procedure.....	140
10.3.4	Results and Discussion.....	143
10.3.5	Conclusion	148
11	Compression behaviour of highly expansive clays stabilised with a green stabiliser of magnesium chloride	149
11.1	Introduction.....	149
11.2	Citation.....	149
11.3	Manuscript Contents	149
11.3.1	Abstract	149
11.3.2	Introduction	150
11.3.3	Materials and test program.....	153
11.3.4	Results and discussion	157

11.3.5	Conclusions	160
12	Prediction of intrinsic compressibility parameters of reconstituted clays using artificial neural network	162
12.1	Introduction.....	162
12.2	Manuscript Contents	162
12.2.1	Abstract	162
12.2.2	Introduction	163
12.2.3	Materials and procedure (database)	166
12.2.4	Artificial Neural Networks.....	169
12.2.5	ANN structure used in this study	172
12.2.6	Results and Discussion.....	174
12.2.7	Conclusions	182
13	Conclusions and Recommendations	184
13.1	Summary Discussion	184
13.1.1	Inherent Compressibility and Remoulded Yield Stress	184
13.1.2	Compression, Recompression and Swell Indices	185
13.1.3	Consolidation Coefficient	186
13.1.4	Intrinsic Shear Strength.....	187
13.1.5	Residual Shear Strength	188
13.1.6	Swell Potential	188
13.1.7	Regression models	189
13.1.8	Artificial Neural Network Models	190
13.2	Recommendations.....	190
13.3	Further Research	191
14	REFERENCES.....	192

LIST OF PUBLICATIONS

It is noted that several chapters of this thesis are published papers. However, the content of the following publications is the result of research which was carried out since the official commencement date of the approved research program. All mentioned publications within this chapter are presented in full in this thesis. The pertinent chapter is listed alongside each publication for clarification. Listed publications are presented in the order of the pertinent section appears in this publication.

PEER-REVIEWED MANUSCRIPTS

[Chapter 4 – Page 41] Habibbeygi, F., Nikraz, H., & Chegenizadeh, A. (2017). Intrinsic Compression Characteristics of an Expansive Clay from Western Australia. *International Journal of GEOMATE*, 12(29), 140-147. <https://doi.org/10.21660/2017.29.20455>

[Chapter 5 – Page 57] Habibbeygi, F., Nikraz, H. & Koul B. (2018). Regression Models for Intrinsic Constants of Reconstituted Clays. , *Cogent Geoscience*, 4(1), 1546978. <https://doi.org/10.1080/23312041.2018.1546978>

[Chapter 6 – Page 88] Habibbeygi, F., Nikraz, H., & Verheyde, F. (2017). Determination of the compression index of reconstituted clays using intrinsic concept and normalised void ratio. *International Journal of GEOMATE*, 13(39), 54-60. <https://doi.org/10.21660/2017.39.98271>

[Chapter 7 – Page 100] Habibbeygi, F., & Nikraz, H. (2018). The effect of unloading and reloading on the compression behaviour of reconstituted clays. *International Journal of GEOMATE*, 15(51), 53-59. <https://doi.org/10.21660/2018.51.52643>

[Chapter 8 – Page 111] Habibbeygi, F., & Nikraz, H. (2018). Variation of Consolidation Coefficient of Expansive Clays at High Initial Water Content. *Journal of Engineering Science & Technology*, 13(9), 2644-2654.

[Chapter 9 – Page 125] Habibbeygi, F., & Nikraz, H. (2018). Characterisation of the Undrained Shear Strength of Expansive Clays at High Initial Water Content Using

Intrinsic Concept. *International Journal of GEOMATE*.
<https://doi.org/10.21660/2017.29.20455>

[Chapter 10 – Page 137] Habibbeygi, F., & Nikraz, H. (2018). Effect of shear rate on the residual shear strength of pre-sheared clays. *Cogent Geoscience*, 4(1), 1453989.
<https://doi.org/10.21660/2017.29.20455>

[Chapter 11 – Page 149] Habibbeygi, F., & Nikraz, H. (2018). Compression behaviour of highly expansive clays stabilised with a green stabiliser of magnesium chloride. *International Journal of GEOMATE*, 14(45), 144-150.
<https://doi.org/10.21660/2018.45.10697>

UNPUBLISHED MANUSCRIPTS

[Chapter 12 – Page 162] Habibbeygi, F., & Nikraz, H. (2018). Prediction of intrinsic compressibility parameters of reconstituted clays using artificial neural network. *Unpublished*

All technical contents of above listed papers are sourced from the original content of this thesis. All other contributors of the above publications, have involved in following contributions: method guidance, concept recommendation, introduction/conclusion, critical review, article presentation and technical advice. All other contributors are correctly and consensually attributed as co-authors in relevant papers. Attribution tables are presented in Appendix G.

Copyright permissions and licenses of published papers are also presented in Appendix H.

LIST OF FIGURES

Figure 1-1. Thesis structure	6
Figure 2-1. Typical plot of the compression curve of a normally consolidated clay. 15	
Figure 3-1. Sampling site – Western Australia	27
Figure 3-2. Sampling site – Baldivis, WA	28
Figure 3-3. Sampling procedure: (a) test pit wall and (b) soil spoil	28
Figure 3-4. Sampling extrusion: (a) equipment used and (b) extruded sample	29
Figure 3-5. Four-point Casagrande test of the liquid limit of the study soil	30
Figure 3-6. Specific gravity testing: (a) pycnometer and (b) test setup	30
Figure 3-7. Activity chart for expansive clays	31
Figure 3-8. Particle size distribution test: (a) calibration and (b) hydrometer test	31
Figure 3-9. Particle size distribution curves	32
Figure 3-10. Organic content test – burnout sample	32
Figure 3-11. XRD spectrum of the black clay	33
Figure 3-12. Sample preparation procedure: (a) dried sample and (b) grinding the sample	34
Figure 3-13. One-dimensional consolidation testing	35
Figure 3-14. Direct shear testing: (a) shear box, (b) load cap and bolts and (c) prepared sample	38
Figure 3-15. Direct shear testing setup	38
Figure 3-16. Ring shear test setup	39
Figure 4-1. Plasticity chart	44
Figure 4-2. Particle size distribution curve for the studied soil	45
Figure 4-3. XRD pattern for the studied soil	46
Figure 4-4. Inherent compression curves of Baldivis clay	48
Figure 4-5. Inherent compression curves of Baldivis clay in bi-logarithmic plane ...	49
Figure 4-6. Remoulded yield stress against normalised water content	50
Figure 4-7. Normalised void ratio graphs for Baldivis clay	53
Figure 4-8. Intrinsic compression curves for Baldivis clay	53
Figure 4-9. Comparison of intrinsic parameters against initial water content	54
Figure 4-10. Relationship of intrinsic parameters plot against initial water content:	55
Figure 5-1. Compression curves of the studied clays in e - $\log \sigma v'$ space	64
Figure 5-2. Normalised compression curves of the studied clays in lv - $\log \sigma v'$ space	65
Figure 5-3. Residual graphs of Model 1:	68

Figure 5-4. Plot of residuals against fitted values of Model 1:	69
Figure 5-5. Plot of intrinsic constants e_{100}^* and C_c^* against e_L in Model 1.....	70
Figure 5-6. Residual graphs of Model 2.....	71
Figure 5-7. Plot of residuals against fitted values of Model 2	72
Figure 5-8. Residual graphs of Model 3.....	75
Figure 5-9. Plot of residuals against fitted values of Model 3	76
Figure 5-10. Residual graphs of Model 4.....	78
Figure 5-11. Plot of residuals against fitted values of Model 4	79
Figure 5-12. Comparison of predicted intrinsic constants and measured ones.....	80
Figure 5-13. Comparison of predicted intrinsic constants by different methods for Baldivis clay.....	81
Figure 5-14. The effect of predictors on e_{100}^*	82
Figure 5-15. The effect of predictors on e_{1000}^*	83
Figure 5-16. Intrinsic compression line of Baldivis clay in $Iv - \log \sigma v'$ space	85
Figure 5-17. Comparison of estimated and observed void ratios for Baldivis clay...	86
Figure 6-1. Schematic plot of a compression curve in $e - \log \sigma v'$ space	89
Figure 6-2. Compression curves in semi-logarithmic space	93
Figure 6-3. Normalised compression curves in $Iv - \log \sigma v'$ space.....	95
Figure 6-4. Schematic graph of compression index calculation	96
Figure 6-5. Comparison between estimated and measured compression indices	98
Figure 7-1. Consolidation test set-up	103
Figure 7-2. Compression indices definition on a semi-logarithmic plane	105
Figure 7-3. Oedometer test results with unloading/reloading on the black clay.....	109
Figure 7-4. Oedometer test results with unloading/reloading.....	110
Figure 8-1. Sampling site for the studied clay	115
Figure 8-2. Variation of consolidation parameters with consolidation stress.....	118
Figure 8-3. Variation of C_v with consolidation stress.	120
Figure 8-4. Variation of C_v with consolidation stress for an undisturbed and remoulded sample.	123
Figure 9-1. Comparison of compression curves for the pre-consolidation stage and the one-dimensional consolidometer test	130
Figure 9-2. Semi-logarithmic compression curves ($e - \log \sigma v'$).....	131
Figure 9-3. Semi-logarithmic normalised compression curves ($Iv - \log \sigma v'$).....	132

Figure 9-4. Relationship between undrained shear strength (Su^*) and axial strain	133
Figure 9-5. Undrained shear strength (Su^*) versus normal stress	133
Figure 9-6. Void index versus undrained shear strength (Su^*).....	134
Figure 9-7. Normalised undrained shear strength (Rsu^*) versus normalised initial water content	134
Figure 9-8. Normalised undrained shear strength (Rsu^*) versus normal stress	135
Figure 10-1. Ring shear apparatus used in this study.....	141
Figure 10-2. Sample prepared before the consolidation stage	142
Figure 10-3. Shear rate and test procedure in this study	143
Figure 10-4. Residual shear strength versus time at various shear rates.....	144
Figure 10-5. A comparison of residual shear strength at different normal stresses.	145
Figure 10-6. Residual shear behaviour under $\sigma n' = 200$ kPa at the various shear rates of	147
Figure 11-1. Sampling site, Baldvis Western Australia.....	154
Figure 11-2 Particle size distribution curves of the black clay	155
Figure 11-3. Activity chart for expansive clays	156
Figure 11-4. Variation of the index parameters with the stabiliser content.....	157
Figure 11-5. Variation of the swell pressure against test time for various stabiliser content.....	158
Figure 11-6. Variation of the swell pressure against test time for various stabiliser content in a semi-logarithmic plane	159
Figure 11-7. Variation of the swell strain against time for various stabiliser contents	160
Figure 11-8. A schematic of swell pressure with time.....	160
Figure 12-1. The relationships between intrinsic parameters and input parameters	167
Figure 12-2. Spearman rank correlation coefficients of input parameters.....	169
Figure 12-3. A single layer of neurons	171
Figure 12-4. Schematic of the architecture of a three-layer ANN using abbreviated notation.....	172
Figure 12-5. The ANN structure used in this study	173
Figure 12-6. Performance graph of the number of neurons in the hidden layer	175
Figure 12-7. Performance graph of the number of iterations for 17 neurons	176
Figure 12-8. Performance charts for various ANN structures	177

Figure 12-9. Simulation results for the three steps of data processing, and for all data ($Cc *$).....	178
Figure 12-10. Simulation results for the three steps of data processing, and all data ($e100 *$).....	179
Figure 12-11. Comparison between the target values and outputs ($Cc *$).	180
Figure 12-12. Comparison between target values and outputs ($e100 *$).	181

LIST OF EQUATIONS

(2-1).....	8
(2-2).....	9
(2-3).....	9
(2-4).....	9
(2-5).....	10
(2-6).....	11
(2-7).....	12
(2-8).....	12
(2-9).....	13
(2-10).....	13
(2-11).....	13
(2-12).....	13
(2-13).....	13
(2-14).....	14
(2-15).....	14
(2-16).....	14
(2-17).....	14
(2-18).....	14
(2-19).....	14
(2-20).....	16
(2-21).....	16
(2-22).....	16
(2-23).....	16
(2-24).....	18
(2-25).....	18
(2-26).....	19
(2-27).....	22
(2-28).....	22
(2-29).....	23
(2-30).....	23
(2-31).....	24
(4-1).....	50
(4-2).....	52

(5-1).....	61
(5-2).....	67
(5-3).....	67
(5-4).....	67
(5-5).....	70
(5-6).....	70
(5-7).....	70
(5-8).....	72
(5-9).....	73
(5-10).....	73
(5-11).....	73
(5-12).....	76
(5-13).....	76
(5-14).....	84
(6-1).....	91
(6-2).....	94
(6-3).....	94
(6-4).....	96
(6-5).....	96
(6-6).....	96
(6-7).....	97
(6-8).....	97
(7-1).....	106
(7-2).....	107
(8-1).....	112
(9-1).....	135
(10-1).....	141
(10-2).....	141
(12-1).....	168
(12-2).....	172
(12-3).....	174
(12-4).....	174
(12-5).....	174
(12-6).....	182

This page intentionally left blank

LIST OF TABLES

Table 2-1. ICL experimental relationships.....	13
Table 2-2. Intrinsic compression invariable relationships	15
Table 2-3. Some equations used to estimate the compression index of clays.....	17
Table 3-1. Soil properties of the studied clay	32
Table 3-2. Vertical consolidation stress and cycle of loading/reloading	36
Table 3-3. Consolidometer test procedure	37
Table 3-4. Consolidation stress increments at the preconsolidation stage.....	39
Table 4-1. Physical properties of Baldivis clay	45
Table 5-1. Geotechnical properties of consolidometer tests	63
Table 5-2. Predictor coefficients of Model 3	74
Table 5-3. Predictor coefficients of Model 4	77
Table 6-1. Geotechnical parameters of the studied soils.....	92
Table 7-1. Vertical pressure increments and cycle of loading/reloading in oedometer tests.....	104
Table 7-2. Compression indices for $w_0/w_L=1.0$	106
Table 8-1. Physical properties of black clay.	115
Table 8-2. Consolidometer test procedure.	117
Table 9-1. Consolidation stress increments at the pre-consolidation stage and normal stress for direct shear test	130
Table 12-1. Summary statistics of the data used as input parameters.....	168
Table 12-2. Summary of optimal ANN structures for various transfer functions and numbers of hidden neurons	177
Table 12-3. Mean square errors (<i>MSE</i>) for the optimal ANN structures excluding each input parameter.....	181
Table 12-4. Biases and weights of the optimal ANN model.....	182

LIST OF APPENDICES

Appendix A Test Pitting Photos.....	203
Appendix B One-dimensional Consolidation Results.....	205
Appendix C Direct Shear Test Results	214
Appendix D Torsional Shear Test Results	223
Appendix E Artificial Neural Network Results	226
Appendix F Artificial Neural Network Matlab Codes	256
Appendix G Co-author Attribution Tables	267
Appendix H Copyright Permissions	272

ABBREVIATIONS AND ACRONYMS

Abbreviations	
ASTM	American Society for Testing and Materials
bgs	Below ground surface
DO	Double-Oedometer Swell Test (DO)
ICL	Intrinsic Compression Line
ISuL	Intrinsic Strength Line
PSD	Particle Size Distribution
RS	Restrained Swell Test
SC	Swell-Consolidation Test
VCL	Virgin Compression Line
WA	Western Australia
XRD	X-Ray Diffraction
ZS	Zero Swell Test

NOMENCLATURE

Nomenclatures	
a	Normalisation invariable
b	Normalisation invariable
C_c	Compression index
C_c^*	Intrinsic Compression index
$C_{c,LL}^*$	C_c^* when the initial water content of sample is w_L
$C_{c,2LL}^*$	C_c^* when the initial water content of sample is $2w_L$
C_H	Heave index
C_r	Recompression index
C_s	Swelling index
C_v	Coefficient of consolidation, cm^2/sec
DDL	Defuse Double Layer
e	Void ratio
e_0	Void ratio at an effective stress of σ'_0
e_{100}^*	Void ratio relating to the vertical stresses of 100 kPa
e_{1000}^*	Void ratio relating to the vertical stresses of 1000 kPa
$e_{100,LL}^*$	e_{100}^* when the initial water content of sample is w_L
$e_{100,2LL}^*$	e_{100}^* when the initial water content of sample is $2w_L$
e_L	Void ratio at liquid limit
e/e_L	Normalised void ratio
e_0/e_L	Normalised initial void ratio
G_s	Specific gravity of solid particles
h_i	Thickness of the clay layer
H_0	Total height of the clay layer
I_p	Plasticity index, %
I_s	Shrink index
k	Hydraulic conductivity, cm/hr

m_v	Coefficient of volume change, 1/kPa
n_0	In situ porosity
p	Consolidation stress, kN/m ²
P_0	Initial stress state
P_f	Final stress state
R_C	Invariant for equation of C_c^*
R_E	Invariant for equation of e_{100}^*
R_{su}^*	Normalised shear strength parameter
S_u^*	Undrained shear strength, kN/m ²
u_{w_f}	Final pore-water pressure, kN/m ²
U	Percentage of consolidation
w	Water content, %
w_0	Initial water content, %
w_0^*	Normalised initial water content to liquid limit, %
w_L	Liquid limit, %
w_P	Plastic limit, %
w_{SL}	Shrinkage limit, %
z	Depth, m
Greek Symbols	
σ'_0	Initial effective vertical stress, kPa
σ'_{cv}	Swell pressure from constant volume swell test
σ'_v	Effective vertical stress, kPa
$(\sigma'_{v0})_z$	Effective overburden stress at the middle of soil layer
σ'_{yr}	Effective remoulded yield stress, kPa
γ_w	Unit weight of water, kN/m ³

1 INTRODUCTION

1.1 Background

Expansive soils are one of the major challenges faced by geotechnical engineers all over the world. These soils, also known as *problematic soils*, are substantially affected by changes to their water contents. Expansive soils mainly comprise clay minerals, which have significant swell potential. In fact, the volume of such clays can increase several times when they absorb water. Every year, globally, millions of dollars are spent on financial losses or remedial works related to expansive soils. Generally speaking, the cost of damage to buildings, pavements, irrigation canals, and other infrastructure due to the shrinkage and swelling of expansive soils is greater than the aggregate cost of damage caused by natural disasters such as hurricanes, floods, landslides and earthquakes (Nelson & Miller, 1992; Vanapalli & Lu, 2012). Therefore, comprehending the behaviour of such problematic soils will aid the establishment of effective measures to mitigate the influence of their swelling and shrinkage on infrastructure.

During recent decades, many researchers have endeavoured to introduce an inclusive framework for predicting the compression behaviour of all types of clays independent of their status. One highly-accepted baseline amongst researchers is the ‘intrinsic framework’, which was initially introduced by Burland (1990). Afterwards, this concept was used for investigating the behaviour of many clayey soils all over the world. The intrinsic concept has been employed by many researchers in recent years to explore the compressibility and shear strength of clayey soils (Al Haj & Standing, 2015; Hong, Gao, Cui, Bian, & Zeng, 2013; Hong, Yin, & Cui, 2010; Liu, Zhuang, & Horpibulsuk, 2013; Xu, Gao, Yin, Yang, & Ni, 2014; Zeng, Hong, & Cui, 2015). A unique line, namely, the *intrinsic compression line* (ICL), was proposed by these researchers to normalise the compression curves pertinent to their initial condition (Burland, 1990; Hong, 2006). However, the independence of the ICL to the initial status of a studied soil was recently questioned. It is now understood that the ICL can be affected by the initial state of the sample (Cerato & Lutenecker, 2004; Hong et al., 2010). Nevertheless, this concept is still a useful framework for predicting the behaviour of clays as it incorporates the effects of the initial conditions. In this

research, the major factors affecting the ICL are investigated and some modifications to the ICL are proposed based on the experimental results.

A sustainable resolution to the massive amounts of clayey slurries dredged every year from lakes and rivers has been identified to be used as land reclamation materials. Because of the importance of the settlement of dredged slurries on future coastal developments, the study of the compression behaviour of such clayey soils at high initial water contents is crucial. The intrinsic concept can be used to investigate the behaviour of dredged slurries, as the structure of such soils is completely broken. As the laboratory tests for determining the ICL of such soils are laborious and costly, several indirect methods have been suggested by researchers based on simple geotechnical indices viz. liquid limit, plastic limit and initial void ratio (Xu & Yin, 2015; Zeng et al., 2015). However, these equations have some limitations and may over- or underestimate the intrinsic compression parameters. In this thesis, some relationships are presented that allow more reliable estimates of intrinsic compression parameters for a broad range of initial conditions and mineralogy.

1.2 Research Objectives and Significance

Understanding the mechanical and volumetric behaviour of expansive soils is essential in finding more effective measures to prevent damage to infrastructure built on expansive clays. Therefore, this study was designed to comprehend the behaviour of such soils in both experimental and analytical frameworks. The PhD programme was performed in two major sections: 1) carrying out experimental tests to investigate the volumetric and mechanical behaviour of expansive clays and 2) proposing predictive models to estimate the behaviour of such clays based on simple index parameters.

In the first section—the experimental tests—the effects of several factors on the behaviour of expansive clays were investigated, such as initial water content, clay mineralogy, stress level, cyclic loading/reloading steps and rate of shear displacement. This research also aimed to investigate heave prediction procedures. It uses models to estimate compression indices and the shear strength of expansive clays via regression analyses and artificial neural simulations. The developed models, which include clay mineralogy, initial water content and geotechnical index parameters, are described in the second section of this study.

The swell pressure and heave value of expansive clays are key components used by geotechnical engineers when dealing with expansive soils. Heave can be estimated by

one or a combination of geotechnical indices such as the plasticity index, liquid limit or shrinkage limit. Furthermore, a green stabiliser, magnesium chloride, is introduced to mitigate the swell potential of expansive clays.

Briefly, the following objectives were investigated in this study:

- (1) Study the effect of initial water content and clay mineralogy on the intrinsic compression line.
- (2) Introduce an experimental equation describing the relationship between the void index and the effective vertical stress.
- (3) Propose an inclusive intrinsic line for predicting the compression behaviour of reconstituted clays.
- (4) Develop regression models to predict the intrinsic compression parameters of clayey soils for a wide range of initial water contents and different clay mineralogy.
- (5) Investigate the effect of high initial water content of the prepared specimens on the undrained shear strength of remoulded and reconstituted clays.
- (6) Introduce an inclusive intrinsic line for predicting the shear behaviour of clays.
- (7) Study the changes in the undrained shear strength of reconstituted and remoulded clays prepared at high initial water contents with the change in normal stress.
- (8) Introduce an experimentally-derived equation describing the relationship between the void index and undrained shear strength.
- (9) Investigate the effect of shear rate on the residual shear strength of expansive clays.
- (10) Introduce a green stabiliser for the stabilisation of expansive clays to mitigate their swell potential.
- (11) Investigate the effect of repetitive loading and reloading steps on the compression behaviour of expansive clays.
- (12) Develop artificial neural networks for predicting the compression behaviour of expansive clays with high initial water contents.

1.3 Scope of Research

The scope of work required to achieve the objectives mentioned in Section 1.2 is as follows:

- (1) Carry out geotechnical classification tests on the collected samples to determine the physical properties of the studied clay.
- (2) Carry out consolidation tests with various amounts of initial water content and vertical stress.
- (3) Carry out zero deformation and free swell oedometer tests on untreated samples and samples stabilised with magnesium chloride.
- (4) Carry out shear strength tests (direct shear tests and ring shear tests) to investigate the shear behaviour of the studied clay.
- (5) Perform regression analyses to develop predictive equations for compressibility parameters.
- (6) Perform statistical analyses to investigate the effects of initial water content, consistency limits, specific gravity and clay mineralogy.
- (7) Perform artificial neural network simulations to predict the intrinsic compression parameters based on physical parameters, and to develop the predictive models.

1.4 Thesis Outline

This thesis is presented in 14 chapters, with an outline chart presented in Figure 1-1.

The structure of this thesis is built on nine publications, as follows:

Chapter 1 describes the background, objectives and research significance of this research. The scope of the research and a thesis outline are also presented in this chapter.

Chapter 2 presents a literature review on topics relevant to this research. This chapter includes the knowledge gained throughout this research. The review comprises information about the intrinsic compression behaviour of clays, normalisation methods, methods of estimating compression indices, shear strength of expansive clays and stabilisation methods.

Chapter 3 presents the physical characteristics of the materials used for this research, being expansive clay samples and magnesium chloride. The methodology of the experimental tests, which include one-dimensional consolidation tests, direct shear tests and torsional shear tests, are also described. To avoid possible duplication of the literature review in this chapter, proper citations of publications are made where required in the thesis.

Chapter 1 - Introduction

Chapters 4 to 12 present the results and discussion of the research in the form of eight peer-reviewed published articles and one unpublished chapter. As most of these chapters are based on the publications, each chapter has its own literature review and methodology focusing on a particular aspect of the research. Experimental tests and numerical models are also presented in each chapter alongside their discussions and results.

Chapter 13 summarises the results and conclusions of this research. As the results and discussions are presented in Chapters 4 to 12 in detail, the summary provided in this chapter only presents the key findings and achievements. The final section of this chapter makes recommendations and gives ideas for future research based on the knowledge gained in this thesis.

Chapter 14 lists the references cited in the thesis, using APA 6th.

Test pitting photos, one-dimensional consolidation results, direct shear tests results, torsional shear test results, Artificial Neural Network results, co-author attribution tables and copyright permission are also presented in Appendix A to H respectively.

Chapter 1 - Introduction

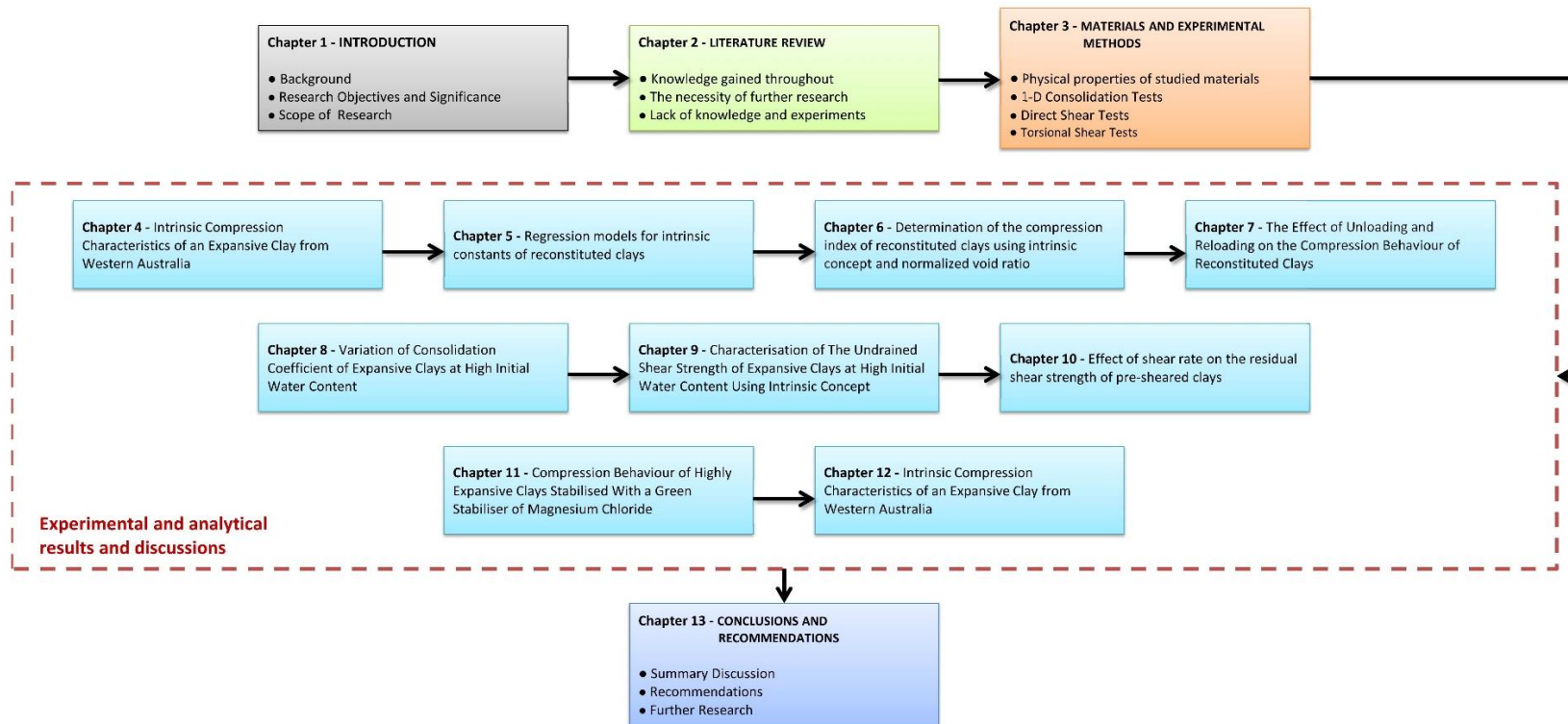


Figure 1-1. Thesis structure

2 LITERATURE REVIEW

2.1 Background

Expansive soils have challenged engineers during past decades; their swelling and shrinkage behaviour causes much damage to dwellings and infrastructure all over the world, such as pavements, irrigational canals, culverts, overland conveyors, residential buildings and airport aprons. Expansive soils are not limited to humid climates and can also be found in arid or semi-arid regions in countries such as the U.S., Canada, Australia, Saudi Arabia and Turkey. These types of soils, which are also called *problematic soils*, are responsible for billions of dollars of damage and/or remediation costs to properties each year. For example, in the United States alone, the annual cost of damage caused by such soils is about \$15 billion (Jones & Jefferson, 2012). Generally, the cost of damage caused by shrinkage and swelling of expansive soils is even greater than that incurred by natural disasters such as floods, earthquakes and tornadoes (Nelson & Miller, 1992; Vanapalli & Lu, 2012).

Expansive soils generally include considerable amounts of montmorillonite (smectite). Clay minerals composed of montmorillonite can expand to several times their initial volume when they absorb water, and shrink to a fraction of their initial volume when lose moisture and dry out. This sensitivity to changes in water content has been the focus of researchers all over the world who wish to understand the behaviour of expansive clays and the effect of water changes on the volumetric and mechanical characteristics of problematic soils (Horpibulsuk, Liu, Zhuang, & Hong, 2016; Puppala, Manosuthikij, & Chittoori, 2014; Puppala, Punthutaecha, & Vanapalli, 2006; Saride, Puppala, & Chikyala, 2013).

Expansive clay is usually referred to as *black clay* in Queensland and *gilgai* in the Pilbara, Western Australia. Recently, expansive clays are becoming a challenge to new suburb developments in southern Perth, the capital city of Western Australia (WA). In fact, some of the newly developed houses have been constructed on expansive clays, especially in southern Perth where remedial work must be carried out prior to construction. One of these newly developed suburbs is Baldivis, where the samples for this research were collected.

One simple traditional solution to mitigating the negative impacts of expansive clays on infrastructure is box-out method. In this method, the problematic soils are replaced

by engineered fill to an appropriate depth. The cost of this method is increasing as sources of good fill materials dwindle. Consequently, other methods comprising chemical stabilisation (traditionally with lime, or with new chemical stabilisers) are becoming economically practical. Therefore, there is a need to comprehend the volumetric and mechanical behaviour of both untreated and treated expansive clays to propose more cost-effective and reliable methods of remediation.

2.2 *Intrinsic Framework*

An effective method for comprehending the volumetric behaviour of clayey soils is to normalise the compression curves of various soils and propose a normalised line for further prediction. This unique line represents all types of clayey soils and can predict the behaviour of the studied clays using some simple indices of geotechnical parameters without needing to carry out cumbersome and expensive laboratory tests. One of the simplest normalising methods was suggested by Nagaraj and Murthy (1983). In their method for standardisation, the void ratio at liquid limit (e_L) of the studied clays was employed as the normalisation index. Simplicity is the main advantage of this method, which makes the prediction of clay parameters easy; however, it has poor accuracy in predicting the volumetric behaviour of clays with high initial water contents (Habibbeygi, Nikraz, & Chegenizadeh, 2017).

Nagaraj and Murthy (1983) presented a single equation to predict the void ratio (e) based on the effective consolidation stress (σ'_v) and the void ratio at liquid limit (e/e_L). The equation predicting the normalised void ratio (e/e_L) is presented in Equation (2-1):

$$e/e_L = a - b(\log \sigma'_v) \quad (2-1)$$

where a and b are constants for the normalisation equation. They initially proposed values of 1.099 and 0.223 for a and b , respectively (Nagaraj & Murthy, 1983), then later, Nagaraj and Murthy (1986) updated these values to 1.122 and 0.2343.

Another method for normalising the compression behaviour of clayey soils was first introduced by Burland (1990). He initiated the concept of *intrinsic baseline* for normalising the compression curves of clayey soils and predicting the behaviour of the studied soil. Afterwards, this concept has been progressively used for predicting the behaviour of clayey soils with various statuses, such as sedimentary clays, reconstituted clays, dredge slurries and marine clays (Al Haj & Standing, 2015; Chen,

Sun, & Lü, 2013; Hong, 2006; Hong et al., 2010; Jung, Choo, Cho, & Chung, 2013; Liu et al., 2013; Polidori, 2014; Shi, Qian, Zeng, & Bian, 2015; Takashi, 2015; Wang & Abriak, 2014; Wang, Zentar, & Abriak, 2016; Xu, Gao, & Xu, 2015; Xu & Yin, 2015; Xu et al., 2014; Yanase et al., 2010; Zeng et al., 2015).

The intrinsic compression line (ICL) was introduced by Burland (1990) in his 40th Rankine lecture. It can predict the compressibility behaviour of either natural or remoulded clays. The *intrinsic* term was invented by Burland (1990) to emphasise that this line is unique for a wide range of liquid limits, and relative constants are independent of the status of the studied clay. Conversely, it was recently demonstrated that the initial condition of a sample such as its initial water content has a great impact on the compressibility of clayey soils (Habibbeygi, Nikraz, & Chegenizadeh, 2017; Hong et al., 2010).

According to the definition first expressed by Burland (1990), a *reconstituted clay* is defined as a sample prepared with a water content equal to or greater than its liquid limit, generally 1.25 times its liquid limit. It is expected that the structure of a clayey sample with a water content exceeding this limit is completely destroyed, and that the compressibility behaviour of a reconstituted clay is solely dependent on the intrinsic characteristics of the sample. An asterisk symbol (*) alongside the indices is used to differentiate the intrinsic compression parameters of reconstituted clays with those of natural clays. These parameters are expressed in Equations (2-2) and (2-3):

$$C_c^* = e_{100}^* - e_{1000}^* \quad (2-2)$$

$$I_v = \frac{e - e_{100}^*}{C_c^*} \quad (2-3)$$

where C_c^* is the intrinsic compressibility of the reconstituted clay, I_v is the void index of the reconstituted clay, and e_{100}^* and e_{1000}^* are the void ratios relating to vertical stresses of 100 kPa and 1000 kPa, respectively.

Equation (2-4) presents the regression equation for the ICL proposed by Burland (1990), which establishes the relationship between the void index and effective consolidation stress:

$$I_v = 2.45 - 1.285(\log \sigma'_v) + 0.015(\log \sigma'_v)^3 \quad (2-4)$$

where σ'_v is the effective vertical consolidation stress.

Hong and Tsuchida (1999) applied the intrinsic framework proposed by Burland (1990) to investigate the compressibility behaviour of a sensitive clay from Ariake. As the in-situ water contents of Ariake clays were between 1.17 and 1.42 w_L , the

remoulded samples used in the study had the characteristics of reconstituted clays according to Burland's definition. The oedometer results for Ariake clays indicated good agreement with the ICL proposed by Burland (1990). However, the measured values for e_{100}^* were higher than the values calculated by Burland's relationship.

Cerato and Lutenecker (2004) prepared reconstituted samples at 1.75 times the liquid limit from four different clays. The results of one-dimensional consolidation tests on reconstituted clay specimens illustrate that there were some disparities between the compression curves of samples subjected to low and high levels of effective consolidation stress. Cerato and Lutenecker (2004) concluded that the ICL may not be unique and can be affected by other factors such as initial water content. Thus, more experimental tests are required to explain this inconsistency and the impact of each factor on the results.

Yanase et al. (2010) employed the intrinsic concept to analyse the influence of cementation on the compressibility behaviour of sedimentary clays from Sri Lanka and Japan. They conducted tests under two different sedimentation environments: freshwater and saline water. The studied clayey samples were collected from depths of 7–32 m and had natural water contents measured to be between 37.4–94.6%. All marine sediments had natural water contents greater than their liquid limits and could be classified as reconstituted clays according to Burland's description. Their findings revealed that Burland's void index can be used to characterise the sedimentation condition well. However, the sedimentation situation, which causes different structural states for a given reconstituted clay, has a considerable impact on the compression behaviour of clays. According to this research, the I_v value of freshwater sediment differed from that of the marine sediments because of changes in their consolidation properties.

Hong et al. (2010) carried out a series of consolidometer tests on reconstituted samples with a wide range of initial water contents. They prepared reconstituted samples with initial water contents ranging from $0.7w_L$ to $2w_L$ to explore the effect of initial water content on compression behaviour. Based on their findings, all the compression curves were inverse S-shaped, which is comparable to the compression lines derived for natural clays. They also proposed a polynomial equation to define the ICL, as presented in Equation (2-5):

$$I_v = 3.0 - 1.87(\log \sigma'_v) + 0.179(\log \sigma'_v)^2 \quad (2-5)$$

Lei, Wang, Chen, Huang, and Han (2015) used Burland's concept to inspect the compressibility behaviour of ultra-soft clays using 1-D consolidation tests. Consolidation tests were carried out on different types of samples: remoulded, reconstituted and undisturbed specimens. All specimens were 60 mm in diameter and 20 mm in height. Preparation of the reconstituted samples was undertaken in accordance with Burland's procedure and the initial water contents of samples were 1.53, 1.84 and 2.2 times their liquid limits. According to the index tests, all samples lay above the A-line of the plasticity chart. They found that for vertical consolidation stresses greater than 40 kPa, the compression behaviour is consistent with the ICL proposed by Burland (1990). However, for consolidation stresses less than 40 kPa, the void index is greater than the predicted values. The maximum tested consolidation stress in their research was approximately 800 kPa. Thus, they calculated e_{1000}^* by extrapolation instead of measuring it directly. Based on these tests, they presented a new relationship for the ICL:

$$I_v = 2.598 - 1.4008(\log \sigma'_v) + 0.0614(\log \sigma'_v)^2 \quad (2-6)$$

Al Haj and Standing (2015) studied the compressibility behaviour of two expansive soils from Sudan using the intrinsic baseline. The initial water content of the reconstituted samples of their study was chosen 1.22 and 1.38 times their liquid limits. Clay mineralogy tests were conducted by X-Ray Diffraction (XRD), which indicated a considerable amount of smectite—approximately 80%—which shows why the clays were categorised as highly expansive. Oedometer tests indicated a good agreement between the measured intrinsic parameters of the Sudanese clays and those calculated by Burland's relationships. However, the measured values were slightly higher than the derived ones. Similar results, where measured values of intrinsic parameters were higher than predicted ones, have also been reported in several studies (Nagaraj & Murthy, 1986; Newland & Allely, 1955).

Zeng et al. (2015) performed 48 consolidation tests on 21 different reconstituted specimens. The initial water contents of the samples varied between 22.3–179.6% and the initial normalised water content (w_0^*) changed between 1.0 and 1.9. The compression curves of the studied reconstituted clays were sigmoid. They used three different methods for preparing specimens for oedometer tests depending on the initial water contents of the samples. First, for samples with initial water contents more than 1.5 times the liquid limit, the slurry was poured into consolidation moulds. A 5 mm

rod was used to remove air bubbles from the slurry. Second, for specimens with initial moisture contents 1.2–1.5 times their liquid limit, specimens were placed into consolidation moulds with a pallet knife. A vibrating 5 mm rod was used to remove air bubbles. Finally, for samples with initial water contents less than 1.2 times the liquid limit, the traditional method for remoulding soils was used. In this method, a consolidation ring is slowly pushed into a sample resting on flat glass. All samples were 61.8 mm in diameter and 20 mm or 40 mm in height.

Xu and Yin (2015) employed Burland's framework to investigate the compressibility of various clay minerals, i.e. kaolin, illite and montmorillonite, at high initial water contents. The initial water content in this study varied from w_L to $2.0w_L$ and the vertical stress varied from a very low stress of 0.5 kPa up to 1600 kPa. The diameter of the oedometer test specimens was 61.8 mm and their height was 20 mm. Each vertical stress increment was applied for one day and then doubled at the next stage. The results emphasise the effect of initial water content on the compressibility of clays with different mineralogy. According to this study, intrinsic parameters increased non-linearly with increases in initial water content. Their findings showed that the influence of initial water content (w_0) on compressibility depends on mineralogy. For example, this effect is the weakest for e_{100}^* on montmorillonite among the clay minerals, and is the strongest for illite. However, the influence of w_0 on the intrinsic compression index remained almost constant for the three different minerals. Additionally, they found that there is an upper limit for the intrinsic parameters with increases in w_0 ; the effect of w_0 decreases at high initial water contents. Moreover, the effect of initial water content on the compression behaviour of clays becomes constantly smaller with increasing initial water content. According to this study, the gap between the compression curves of clay samples prepared at different initial water content were minimal for montmorillonite. They also introduced two new invariants (R_E, R_C) to compare the impact of initial water content on various clay mineralogy, as follows:

$$R_E = (e_{100,LL}^* - e_{100,2LL}^*)/e_L \quad (2-7)$$

$$R_C = (C_{c,LL}^* - C_{c,2LL}^*)/e_L \quad (2-8)$$

where $(e_{100,LL}^*, C_{c,LL}^*)$ and $(e_{100,2LL}^*, C_{c,2LL}^*)$ are intrinsic parameters when the initial water contents of the sample are w_L and $2w_L$, respectively. According to this research, R_E changes with increase in the liquid limit. However, R_C remains almost constant at 0.08–0.09 for a wide range of liquid limits (Lei et al., 2015).

A summary of existing experimental equations for ICL is presented in Table 2-1.

Table 2-1. ICL experimental relationships

Relationship	Equation	Reference
$I_v = 2.598 - 1.4008(\log \sigma'_v) + 0.0614(\log \sigma'_v)^2$	(2-9)	(Lei et al., 2015)
$I_v = 3.0 - 1.87(\log \sigma'_v) + 0.179(\log \sigma'_v)^2$	(2-10)	(Hong et al., 2010)
$I_v = 2.45 - 1.285(\log \sigma'_v) + 0.015(\log \sigma'_v)^3$	(2-11)	(Burland, 1990)

2.3 *Intrinsic Compression Invariables*

Intrinsic invariables can be determined by carrying out one-dimensional consolidation tests. These experimental laboratory tests are expensive, laborious and time-consuming, especially when working with clayey samples with high initial water contents and very low permeability. Such samples require more work to prepare, much more time to test and, consequently, are more expensive.

Therefore, to avoid the necessity of performing expensive laboratory tests, it became the focus of many researchers to develop empirical relationships to predict intrinsic compression invariables using simple geotechnical indices.

Initial water content, Atterberg limits and natural void ratio are some of the physical properties that have been used conventionally as input parameters to forecast the compression behaviour of expansive clays (Cerato & Lutenegeger, 2004; Kootahi & Moradi, 2016; Lee, Hong, Kim, & Lee, 2015; Lei et al., 2015; Takashi, 2015; Xu & Yin, 2015; Zeng, Hong, Cai, & Han, 2011).

Burland (1990) proposed two experimental relationships to determine the intrinsic parameters C_c^* and e_{100}^* indirectly. Equations (2-12) and (2-13) were derived using regression analyses on the data of consolidation tests published by Skempton and Jones (1944).

$$e_{100}^* = 0.109 + 0.679e_L - 0.089e_L^2 + 0.016e_L^3 \quad (2-12)$$

$$C_c^* = 0.256e_L - 0.04 \quad (2-13)$$

Equations (2-12) and (2-13) are suggested for clays lying above the A-line of a plasticity chart.

Yin and Miao (2013) reviewed the data of 42 consolidometer tests on various clays from China. The initial water content of samples ranged from 0.7 to 2 times the liquid

limit of the samples. Equations (2-14) and (2-15) present the results of the regression analyses carried out by Yin and Miao (2013). These equations were verified using 40 independent data from the literature. The initial water content of samples from these datasets varied from 1.0 to 1.75 times their liquid limits.

$$e_{100}^* = 1.13w_L + 0.39 w_0/w_L - 0.084 \quad (2-14)$$

$$C_c^* = 0.91w_L + 0.25 w_0/w_L - 0.461 \quad (2-15)$$

Zeng et al. (2015) proposed some regression relationships for predicting intrinsic compression invariables by analysing the results of 222 consolidometer tests comprising 90 self-carried out tests and more than 132 consolidation tests collected from (Burland, 1990; Cerato & Lutenegeger, 2004; Hong et al., 2010). The specific gravity of soil solids (G_s) of the studied clays ranged between 2.65 and 2.75. The initial water contents (w_0) varied between 22.3% and 163.3%. The liquid limits of the studied clays ranged from 28.1% to 100%.

Equations (2-16) and (2-17) were developed solely based on their experimental data, while a broader range of data comprising their own data and data from the literature were used to derive Equations (2-18) and (2-19).

$$e_{100}^* = 0.357 + 0.171e_0 + 0.223e_L \quad (2-16)$$

$$C_c^* = -0.069 + 0.109e_0 + 0.152e_L \quad (2-17)$$

$$e_{100}^* = 0.223 + 0.261e_0 + 0.282e_L - 0.018e_0^2 - 0.05e_L^2 + 0.015e_L^3 \quad (2-18)$$

$$C_c^* = -0.064 + 0.153e_0 + 0.11e_L - 0.006e_0^2 \quad (2-19)$$

A summary of existing equations for predicting intrinsic compression invariables is tabulated in Table 2-2.

Table 2-2. Intrinsic compression invariable relationships

Relationship	Reference
$e_{100}^* = 0.109 + 0.679e_L - 0.089e_L^2 + 0.016e_L^3$	(Burland, 1990)
$C_c^* = 0.256e_L - 0.04$	
$e_{100}^* = 1.13w_L + 0.39 w_0/w_L - 0.084$	(Yin & Miao, 2013)
$C_c^* = 0.91w_L + 0.25 w_0/w_L - 0.461$	
$e_{100}^* = 0.357 + 0.171e_0 + 0.223e_L$	Hong et al. (2010)
$C_c^* = -0.069 + 0.109e_0 + 0.152e_L$	
$e_{100}^* = 0.223 + 0.261e_0 + 0.282e_L - 0.018e_0^2 - 0.05e_L^2 + 0.015e_L^3$	
$C_c^* = -0.064 + 0.153e_0 + 0.11e_L - 0.006e_0^2$	

2.4 Virgin Compression Line

The rate of compression of a clayey layer can be estimated by the compression index of the in situ clay. The compression index is frequently determined by measuring both the void ratio and the relative effective vertical consolidation stress. Figure 2-1 illustrates the definition of compressibility and the compression line of normally consolidated clay. The linear part of the compression curve is generally referred to as the *virgin compression line* (VCL). The slope of this line, which is the *compression index* (C_c), represents the compressibility of the natural clay.

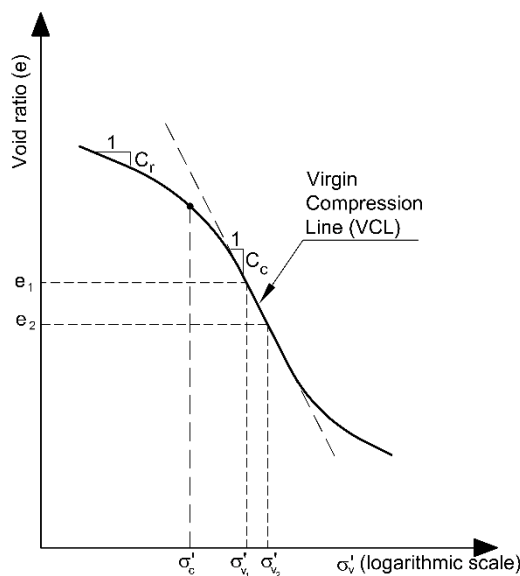


Figure 2-1. Typical plot of the compression curve of a normally consolidated clay

Equation (2-20) can be used to determine the total consolidation (ΔH) of a clayey layer:

$$\Delta H = \frac{\Delta e H_0}{1 + e_0} \quad (2-20)$$

where H_0 is the total height of the clay layer and e_0 is the void ratio at an effective stress of σ'_0 .

Similarly, the change in void ratio (Δe) due to the excessive loading of $\Delta\sigma$ can be estimated by Equation (2-21) for normally consolidated clay, and Equations (2-22) and (2-23) for overconsolidated clays:

$$\Delta e = C_c \log \frac{\sigma'_0 + \Delta\sigma}{\sigma'_0} \quad (2-21)$$

$$\Delta e = C_r \log \frac{\sigma'_0 + \Delta\sigma}{\sigma'_0} \quad \text{when } \sigma'_0 + \Delta\sigma < \sigma'_c, \quad (2-22)$$

$$\Delta e = C_r \log \frac{\sigma'_c}{\sigma'_0} + C_c \log \frac{\sigma'_0 + \Delta\sigma}{\sigma'_c} \quad \text{when } \sigma'_0 < \sigma'_c < \sigma'_0 + \Delta\sigma \quad (2-23)$$

where σ'_0 is the initial effective vertical stress, $\Delta\sigma$ is the increment of stress applied to the clayey layer, σ'_c is the preconsolidation stress of the clayey layer, and C_c and C_r are the compression and recompression indices, respectively.

A summary of some of the experimental relationships used to estimate the compression index using only simple geotechnical parameters is tabulated in Table 2-3.

Table 2-3. Some equations used to estimate the compression index of clays (Habibbeygi, Nikraz, & Verheyde, 2017).

No.	Equations	Reference
1	$C_c = 0.007 (w_L - 7)$	(Skempton & Jones, 1944)
2	$C_c = 0.007 (w_L - 10)$: Remolded clays $C_c = 0.009 (w_L - 10)$: Undisturbed clays	(Terzaghi & Peck, 1967)
3	$C_c = 0.29 (e_0 - 0.27)$	(Hough, 1957)
4	$C_c = 0.43 (e_0 - 0.25)$	(Das, 2013)
5	$C_c = 0.02 + 0.014I_p$	(Arulrajah, Nikraz, & Bo, 2005)
6	$C_c = 0.01 (w_0 - 5)$	(Bo, Choa, Wong, & Arulrajah, 2011)
7	$C_c = 0.5I_p G_s$	(Cozzolino, 1961)
8	$C_c = 0.015 (w_L - 19)$	(Nacci, Wang, & Demars, 1975)
9	$C_c = 0.01 (w_0 - 7.55)$	(Azzouz, Krizek, & Corotis, 1976)
10	$C_c = 0.2237e_L$	(Wroth & Wood, 1978)
11	$C_c = 0.2343e_L$	(Ogawa, 1978)
12	$C_c = 0.274e_L$	(Herrero, 1983)
13	$C_c = 0.156e_0 + 0.0107$	(Nagaraj & Murthy, 1983)
14	$C_c = 0.007(I_s + 18)$	(Nagaraj, Basavapatna, & Murthy, 1985)
15	$C_c = 0.0103w_0$	(Nagaraj, Pandian, Narasimha Raju, & Vishnu Bhushan, 1995)
16	$C_c = 0.015I_p - 0.0198$	(Bowles, 1989)
17	$C_c = \frac{n_0}{371.747 - 4.275n_0}$	(Sridharan & Nagaraj, 2000)

Note: C_c = compression index; w_L = liquid limit; e_0 = initial or in situ void ratio; I_p = plasticity index; w_0 = initial or in situ water content; G_s = specific gravity; e_L = void ratio at liquid limit; I_s = shrink limit; n_0 = in situ porosity.

2.5 Remoulded Yield Stress

The ICLs of both overconsolidated and reconstituted clays are inverse S-shape in such for an effective vertical stress greater than a specific value, the concave of the ICL changes. This definite stress has been named *preconsolidation stress* for natural clays. Similarly, this particular stress for reconstituted clays has been the focus of many researchers. For the sake of distinguishing between preconsolidation stress in sedimentary and reconstituted clays, it has been given different names. Some of the names used by early researchers are *pore-water suction*, *suction pressure*, *apparent consolidation stress*, and *remoulded yield stress* (Alonso, Gens, & Josa, 1990; Hong, 2006; Hong, Lin, Zeng, Cui, & Cai, 2012; Hong et al., 2010). In this thesis, it will be referred to as *effective remoulded yield stress* (σ'_{yr}).

One of the most common techniques for determining the effective preconsolidation stress was proposed by Butterfield (1979). He proposed that the compression curves can be replotted in a bi-logarithmic space with two straight lines. The intersection of these lines (i.e. the pre-yield and post-yield lines) represents the preconsolidation stress. This method has since been successfully employed by other researchers (Hong et al., 2010; Takashi, 2015; Wang et al., 2016).

Hong (2006) used the void ratio at the liquid limit to estimate the remoulded yield stress. He determined an experimental relationship between σ'_{yr} and the normalised initial void ratio (e_0/e_L). Equation (2-24) shows the relationship between initial void ratio and effective remoulded yield stress:

$$e_0/e_L = (2.14/\sigma'_{yr})^{0.22} \quad (2-24)$$

Hong et al. (2010) reported that the initial water content has a great impact on the remoulded yield stress, which decreases with increases in initial water content.

Equation (2-25) represents the relationship between σ'_{yr} and normalised initial void ratio, which was developed for initial water contents ranging between 25–160%:

$$\sigma'_{yr} = 5.66/(e_0/e_L)^2 \quad (2-25)$$

2.6 Coefficient of Consolidation

Consolidation settlement of a clayey layer is time-dependent and can occur over months or even years due to the low permeability of such soils. In fact, the rate of water discharge from a clayey layer depends on the hydraulic conductivity of the soil.

Equation (2-26) represents a relationship that defines the rate of consolidation of a saturated clayey layer (Das, 2013):

$$C_v = \frac{k}{m_v \gamma_w} \quad (2-26)$$

where C_v is the coefficient of consolidation, γ_w is unit weight of water, m_v is the coefficient of volumetric change and k is the hydraulic conductivity of the soil.

Terzaghi and Peck (1967) suggested that C_v remains unchanged with increases in effective consolidation stress. Therefore, the coefficient of volumetric change and the hydraulic conductivity of a clayey soil decrease with increases in effective consolidation stress, which results in a constant value of C_v .

Retnamony, Robinson, and Allam (1998) reviewed published data from consolidation tests. They also carried out a series of consolidation tests on various clays to investigate how the consolidation coefficient varies with soil type. They proposed that C_v varies according to consolidation stress and can be influenced by the clay mineralogy of the studied soil.

Curve fitting is usually employed to evaluate laboratory-derived consolidation curves and determine the consolidation coefficient. Two highly-used graphical methods are the *log-time* and *square-root-time* techniques, which are also recommended in geotechnical standards (ASTM D2435-04).

The log-time method was originally introduced by Casagrande. In this method, two basic points relating to $U = 0\%$ and $U = 100\%$ are established first; U is defined as the percentage of consolidation. The $U = 0$ point can be derived using a parabolic curve for the first half of consolidation curve (from $U = 0-52.6\%$). The end-point of primary consolidation is defined by the intersection of the steepest linear part of the compression curve and backward extension of the secondary compression curve. It is then possible to calculate the settlement corresponding to half of primary consolidation ($U = 50\%$), which is usually used to estimate the coefficient, as the middle part of the compression curve is in close agreement with the theoretical curve.

The square-root-time method was proposed by Taylor (1948); hence, it is also called *Taylor's method*. It assumes that the first half of the root-time/compression curve is almost linear. Backward extension of this linear section gives the consolidation point at $U = 0\%$. A line can be drawn from the origin (i.e. $U = 0\%$). Then, another line is

drawn from origin with 1.15 times the abscissae of the former line. The intersection of the latter line and laboratory results is the point representing $U = 90\%$.

The drawback of the log-time method is that the consolidation process must continue to the secondary consolidation stage in order to estimate the end-point of primary consolidation. On the other hand, the square-root-time method only requires the initial part of the consolidation curve to estimate C_v .

2.7 Intrinsic Strength Line

Investigations of the volumetric behaviour of clays by focusing on the intrinsic baseline were reviewed in the previous sections. In this section, investigation of the mechanical behaviour of clays using the same baseline is discussed.

The concept of using the intrinsic framework to characterise the mechanical behaviour of clays was introduced by Burland, Rampello, Georgiannou, and Calabresi (1996). Afterwards, this framework was continually used by researchers to estimate the shear behaviour of either natural sedimentary clays or remoulded clays (Cerato & Lutenecker, 2004; Habibbeygi, Nikraz, & Verheyde, 2017; Hong et al., 2013; Zeng et al., 2015).

Chandler (2000) proposed the intrinsic strength line (IS_uL) to predict the mechanical behaviour of reconstituted clays. He also defined a normalised shear strength parameter for reconstituted clays (R_{su}^*), defined as the ratio of its undrained shear strength to the effective vertical stress. The plasticity of the soils in his study varied between 12 and 60, and the void index ranged between -1 and 0 . Chandler (2000) concluded that R_{su}^* is independent of the initial state of the soil and assessed it to be 0.34 .

2.8 Residual Shear Strength

The minimum shear strength of clay is generally expressed as its residual shear strength when the sample is sheared at large shear deformations; the stress remains almost unchanged with increases in shear deformation (ASTM D647). Furthermore, the shear strength along a pre-developed shear area is known as the *residual shear strength* of clay. A pre-existing zone can be established by a change in groundwater, blasting, seismic and tectonic forces, or an old landslide.

Gratchev and Sassa (2015) carried out experimental tests to investigate the major factors influencing the residual shear strength of cohesive soils. They found that clay

structure, mineralogy, soil particle size grading, rate of shear deformation and excess pore water pressure are some of the major factors affecting residual shear strength.

Tika, Vaughan, and Lemos (1996) carried out some shear tests on clayey soils to explore the impact of the rate of shearing. Their results illustrated that the shear strength of their studied clays increased with increasing shear rate. They also explained that there was dissimilarity between the effects of shear rate on shear strength. In fact, shear strength can increase or decrease due to the mode of failure relating to the residual shear strength. Based on their findings, three modes of failure were proposed: *sliding*, *transitional* and *turbulent*.

Tika and Hutchinson (1999) undertook a series of ring shear tests on in situ clays from Italy. Their results indicate that residual shear strength decreases with increases in the shear rate and drops to approximately 60% of the residual shear strength when carried out at a slow rate.

Li, Wen, Aydin, and Ju (2013) undertook a series of large ring shear tests comprising 27 specimens collected from various existing landslides. Shear rates of 0.1, 1 and 10 mm/s were selected to investigate the effect of shear rate. Particle size grading, liquid and plastic limits, and the plasticity index and fine fraction were some of the major parameters found to affect residual shear strength.

Gratchev and Sassa (2015) carried out experimental tests on the shear strength of clayey samples. Residual shear strength was affected by shear rate in all of the studied samples. Moreover, the shear strength increased marginally with decreases in shear rate, which was also affected by the confining pressure.

Scaringi and Di Maio (2016) carried out experimental tests on blends of sand, kaolinite and bentonite. Direct shear tests were performed for shear rates ranging from 0.0001 to 100 mm/min. Their findings illustrate that the residual strength of clayey soils increases with increases in the shear displacement rate. Moreover, clay fractions higher than 50% and/or shear rates greater than 1 mm/min resulted in increases of residual shear strength. Conversely, shear rates less than 1 mm/min had no major impact on residual shear strength.

2.9 Swell Pressure

Investigation of the swell potential of expansive soils in engineering practice is generally carried out by simple swell and shrink tests. For example, conducting a swell test and a simplified core shrinkage test on undisturbed samples is common in

Australian residential projects, especially for light residences where the swelling problem is more crucial. In these types of tests with reactive soils, the swelling potential of the soil is prescribed by a shrink-swell index without the need for suction measurement (Standards Australia 2003). Various techniques have been proposed by several researchers to measure the swelling potential of reactive soils. Despite a diversity of proposed methods, they can be grouped into two major categories based on the techniques used to measure the swell and shrink displacement and loading procedure: *empirical approaches* and *consolidation approaches* using an oedometer (*oedometer approaches*). According to this classification, several relationships and predictive procedures for these categories are introduced herein, and the pros and cons of each method are discussed.

2.9.1 Empirical approaches

Empirical methods use basic geotechnical parameters that can be defined easily by basic soil classification tests (i.e. particle size distribution, Atterberg limits) to predict the swelling potential of reactive soils. Seed, Woodward, and Lundgren (1962) presented one of the earliest relationships for predicting the swell potential of expansive soils. In their relationship, swell potential was related to the plasticity index, which can be computed simply by basic classification tests.

$$\text{Swell Potential } \% = 0.00216 I_p^{2.44} \quad (2-27)$$

where the plasticity index $I_p = w_L - w_p$, w_L is the liquid limit and w_p is the plastic limit of the studied soil. Another attempt to correlate the swelling potential of expansive soil with geotechnical parameters of the soil was done by Ranganatham and Satyanarayana (1965):

$$\text{Swell Potential} = 0.000413 I_s^{2.67} \quad (2-28)$$

where shrinkage index $I_s = w_L - w_{SL}$, w_{SL} is the shrinkage limit of the studied soil. These relationships are simple and straightforward to use and little information is required to investigate the swell potential of expansive soils. Thus, they are very useful for the preliminary study of swelling and shrinkage movements. However, these approaches are based on regional and limited databases and can only give rough estimates of swell potential.

2.9.2 Oedometer approaches

Among the aforementioned methods, oedometer methods are very popular among researchers for evaluating the swelling potential of expansive soils and have been properly established during recent decades. In these techniques, the results from one-dimensional oedometer tests are used to determine the swell pressure and compression index (the two key parameters in heave value computation). Several methods have been suggested based on the loading procedure and stress paths in this category, such as the zero swell test (ZS), swell-consolidation test (SC), restrained swell test (RS) and double-oedometer swell test (DO) (Basma, Al-Homoud, & Husein, 1995; Nelson, Reichler, & Cumbers, 2006). A brief description of two common oedometer tests is presented in this section.

One common test from this group is the zero-swell (ZS) test. In the ZS test, distilled water is added to the sample, which is under a 7 kPa seating pressure. The applied pressure is increased gradually to maintain zero expansion in the specimen during the saturation process. The test is continued until no further swelling is observed in the specimen. The maximum pressure applied to the sample to prevent it from swelling is termed *swell pressure*. In contrast to the ZS test, a free swell condition is allowed in the swell-consolidation (SC) test. The specimen is soaked and permitted to swell freely under a seating pressure of 7 kPa. The pressure required to return the expanded sample to its initial height is *swell pressure*. Then, a conventional consolidation test is performed by applying loads successively. During the test, the increment of applied load begins from 25 kPa and finally reaches 1600 kPa. (Basma et al., 1995). After swell displacement is completed, the test is followed by a standard consolidation test. The main difference between these two methods is that while the strain changes (i.e. the heave value increases) during SC testing, strain is kept constant during ZS testing. Fredlund (1983) proposed an equation to derive the heave value for an expansive layer.

$$\Delta h_i = h_i \frac{C_s}{1 + e_0} \log \frac{P_f}{P_0} \quad (2-29)$$

$$P_f = \sigma_0 \pm \Delta \sigma_v - u_{wf} \quad (2-30)$$

where h_i is the thickness of the clay layer, C_s is the swelling index (which can be computed by an oedometer test), P_0 is the initial stress state (which is equal to the corrected swelling pressure), P_f is the final stress state, σ_0 is the initial overburden

pressure, $\Delta\sigma_v$ is the change in vertical stress due to excavation of fill placement, u_{wf} is the final pore-water pressure and e_0 is the initial void ratio.

The swell pressure should be corrected for the compressibility of the oedometer equipment and sample disturbance (Fredlund, 1983; Fredlund & Rahardjo, 1993). Compressibility can be measured using a steel plug instead of a soil specimen and subtracting the displacement measurement from the soil test results. Furthermore, for measuring disturbance correction, Fredlund and Rahardjo (1993) used an empirical method originally proposed by Casagrande (1936).

Similarly, many researchers have used oedometer results in predicting the swelling displacement of expansive soils (Nelson & Chao, 2014; Nelson & Miller, 1992; Nelson et al., 2006). Nelson et al. (2006) suggested using a heave index C_H to calculate the heave value. The heave index is defined as the ratio of the swell measured in oedometer testing to inundation stress (i.e. the vertical stress applied to the specimen during a saturation procedure). According to their methodology, the heave index and swell movement can be derived from Equation (2-31).

$$\Delta h_i = h_i C_H \log \frac{\sigma'_{cv}}{(\sigma'_{v0})_z} \quad (2-31)$$

where σ'_{cv} is the swelling pressure (determined from a constant volume swell test), $(\sigma'_{v0})_z$ is the effective overburden stress at the middle of the soil layer (at any depth of z) and h_i is the thickness of the clay layer.

Oedometer test results show that the swell potential decreases with the increase of applied vertical stress. On the other hand, the swell potential of dry samples is much higher than that of wet samples and swell potential increases with increases in soil dry density (Basma et al., 1995; Basma, Al-Homoud, Husein Malkawi, & Al-Bashabsheh, 1996; Powell, Siemens, Take, & Remenda, 2013). This indicates that the initial moisture content and dry density of expansive soil have great effects on its swell potential.

2.9.3 Stabilisation

Stabilisation and treatment of expansive clays are appropriate methods for reducing or eliminating the effects of such problematic soils on infrastructure. Based on the stabiliser (agent) used for treatment and the acceptance of the method amongst researchers and engineers, stabilisers can be classified into two categories: *traditional* and *non-traditional stabilisers*.

Portland cement, hydrated and/or quick lime, fly ash, gypsum, zeolite and manufacturing waste are categorised as traditional stabilisers. These agents have been widely used in various projects to mitigate the swell and shrinkage potential of expansive clay. Moreover, there are extensive case studies and research on the effectiveness of such materials in the literature (Al-Mukhtar, Lasledj, & Alcover, 2014; Alrubaye, Hasan, & Fattah, 2016; Bourokba Mrabent, Hachichi, Souli, Taibi, & Fleureau, 2015; Hossanlourad, Rokni, Hassanlo, & Badrlou, 2017; Jha & Sivapullaiah, 2015; Kang, Ge, Kang, & Mathews, 2015; Phanikumar, Sreedharan, & Aniruddh, 2014; Wang, Abriak, & Zentar, 2014).

Lime, which can be used in the form of dolomitic quick lime [CaO.MgO], quick lime (CaO), hydrated lime [Ca(OH)₂] or hydrated dolomitic lime [Ca(OH)₂.Mg(OH)₂] is one of the most popular agents for the treatment of expansive clays. Hydrated lime [Ca(OH)₂] is very effective in stabilising expansive clays because it comprises large amounts of free calcium (Ca²⁺ ions).

Portland cement, which is similar to lime, produces calcium oxide in the hydration procedure, which is essential to the stabilisation process. Ca²⁺ ions exchange monovalent ions, which decreases the swell potential by decreasing inter-layer electrochemical forces. In treated clay, this cation replacement improves engineering properties such as shear strength, workability and density, and also reduces the swell and shrink potential (Khemissa & Mahamedi, 2014; Ouhadi, Yong, Amiri, & Ouhadi, 2014).

Alternatively, there are other chemical stabilisers known as *non-traditional agents*. The usage of these chemical agents is gradually increasing due to the environmental issues raised by traditional agents (Latifi, Rashid, Siddiqua, & Horpibulsuk, 2015; Ouhadi et al., 2014; Turkoz, Savas, Acaz, & Tosun, 2014; Yunus, Wanatowski, & Stace, 2013). Chemical agents consist of one or a combination of resins, ions, polymers, acids and silicates (Latifi et al., 2015; Yunus et al., 2013).

Magnesium chloride hexahydrate (with the industrial name Bischofite) has the chemical formula of (MgCl₂.6H₂O) and has lately been considered for use as a chemical stabiliser for expansive clays. Magnesium chloride hexahydrate is generally used as a dust controller and ice melter in the road and pavement industry (Thenoux & Vera, 2002). There is very little research on the effectiveness of clays stabilised with MgCl₂; however, what does exist illustrates that MgCl₂ is potentially a new and

Chapter 2 - Literature Review

effective environmentally-friendly stabiliser for expansive clays (Latifi et al., 2015; Turkoz et al., 2014; Yunus et al., 2013).

3 MATERIALS AND EXPERIMENTAL METHODS

3.1 Materials

3.1.1 Black clay

Experimental tests were carried out on expansive clay from Western Australia (WA). Clay samples were collected from Baldivis, a newly-developed suburb 46 km south of Perth, WA (Figure 3-1).

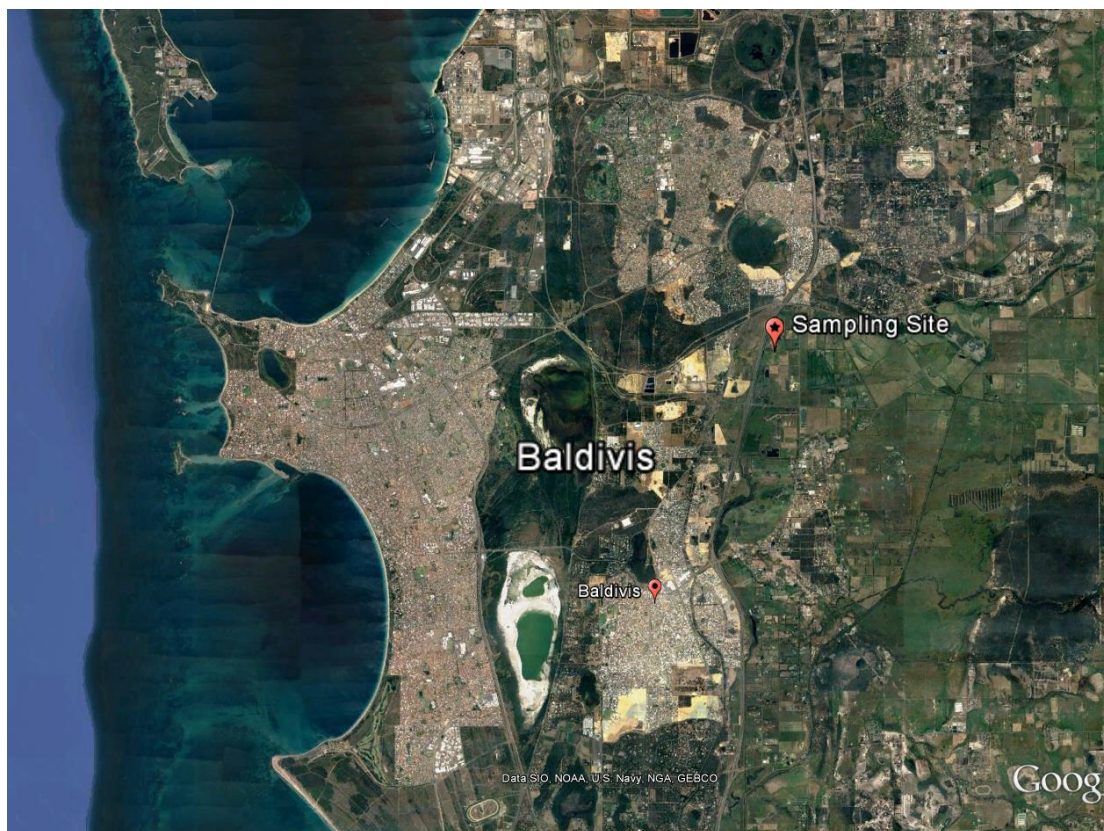


Figure 3-1. Sampling site – Western Australia (Google Maps)

According to the Geological Map (AusGIN Geoscience Portal 2017-1:250,000 scale), the geological unit of the area is alluvium (Qa), comprising clay, sand and loam (Geoscience Australia and Australian Stratigraphy Commission, 2017).

3.1.1.1 Sampling procedure

First, the vegetation and topsoil were removed from the ground surface; then, samples were collected from depths between 0.3 m and 0.5 m bgs (below ground surface). Two types of samples were collected for this research: disturbed and intact

(undisturbed). Bulk sampling (digging by hand) was used to obtain disturbed samples. Additionally, two undisturbed samples were collected from a test pit dug by an excavator. The procedure of sample preparation for each type of sample is discussed in *Section 3.2 - Experimental Methods*. Figure 3-2 illustrates the sampling site and the vegetation at the time of sampling. As seen, the area was level and covered by abundant grass with frequent small trees. Figure 3-3 shows the test pit and the spoil which bulk samples were collected from. More photos describing the test pitting procedure are presented in Appendix A.



Figure 3-2. Sampling site – Baldvis, WA

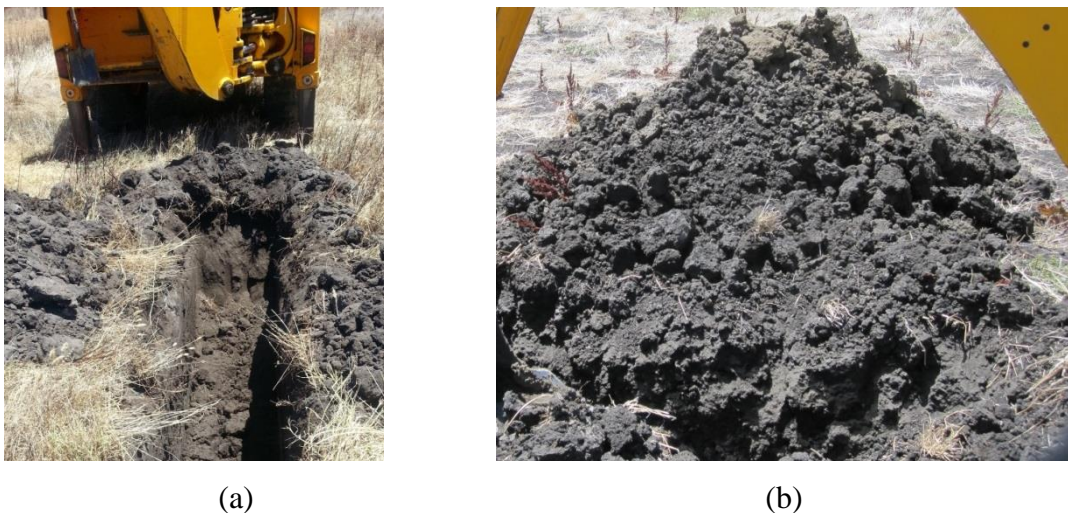


Figure 3-3. Sampling procedure: (a) test pit wall and (b) soil spoil

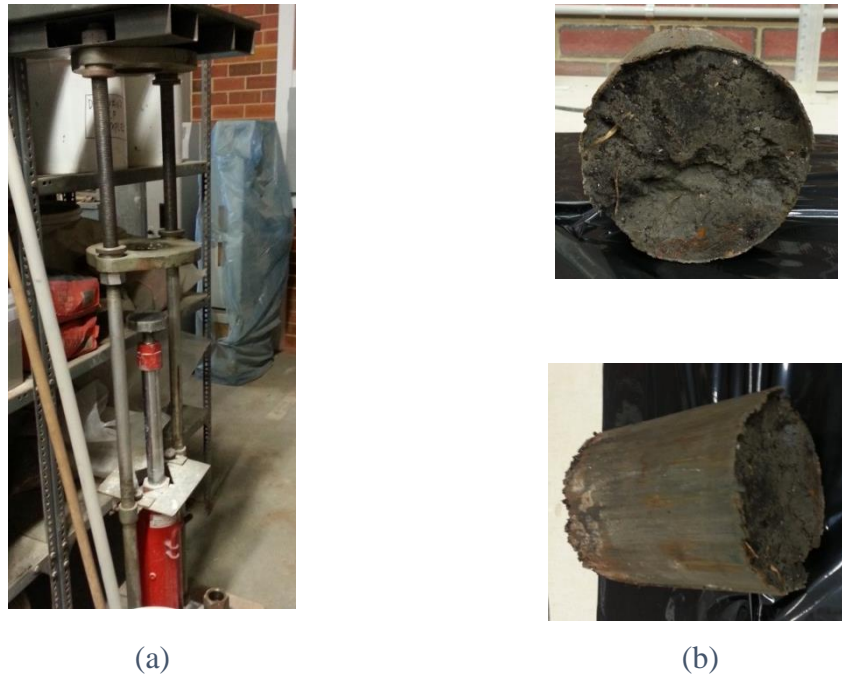


Figure 3-4. Sampling extrusion: (a) equipment used and (b) extruded sample

Undisturbed (intact) samples were taken from the test pit by pushing a 250 mm long steel tube into the ground to a depth of 0.5 m bgs. Then, undisturbed samples were carefully removed from the sampling tubes with a hydraulic jack. The equipment and the extruded sample are presented in Figure 3-4. Extruded samples were wrapped in multiple layers of cling foil to retain the in situ water and stored in a temperature-controlled room until required. As the studied soil had a natural black colour and was an expansive clay, it is referred to as *black clay (or Baldivis clay)* in this research.

3.1.1.2 Geotechnical index tests

Basic geotechnical index tests were carried out in accordance with ASTM standards to determine the physical characteristics of the studied clay. The liquid limit was measured by the four-point Casagrande procedure and plastic limit tests were performed using the thread rolling technique in accordance with ASTM D4318. The measured liquid limit and plastic limit (3 series) of the studied clay were 82% and 35%, respectively (Figure 3-5).

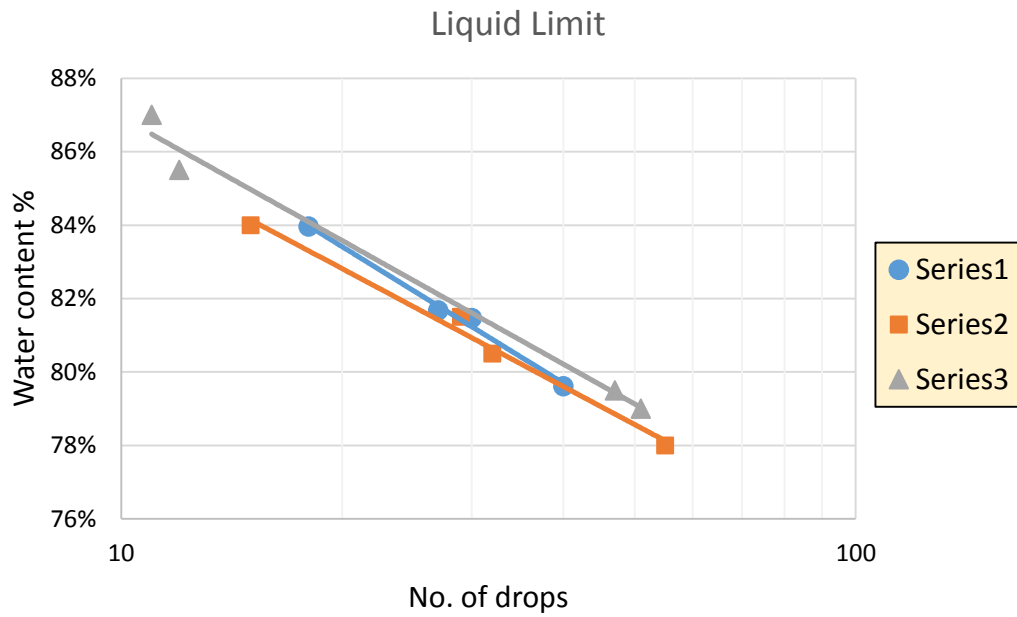


Figure 3-5. Four-point Casagrande test of the liquid limit of the study soil

Figure 3-6 shows the specific gravity test carried out using pycnometers in accordance with ASTM D854. The specific gravity of the solid particles was measured as 2.58. The consistency limit data for the black clay was also plotted on a plasticity chart (Figure 3-7). As shown, the clay lies marginally above the A-line of the plasticity chart. The plasticity index proposed by Chen (1988) classifies the swell potential of the black clay as *high to very high*.



(a)



(b)

Figure 3-6. Specific gravity testing: (a) pycnometer and (b) test setup

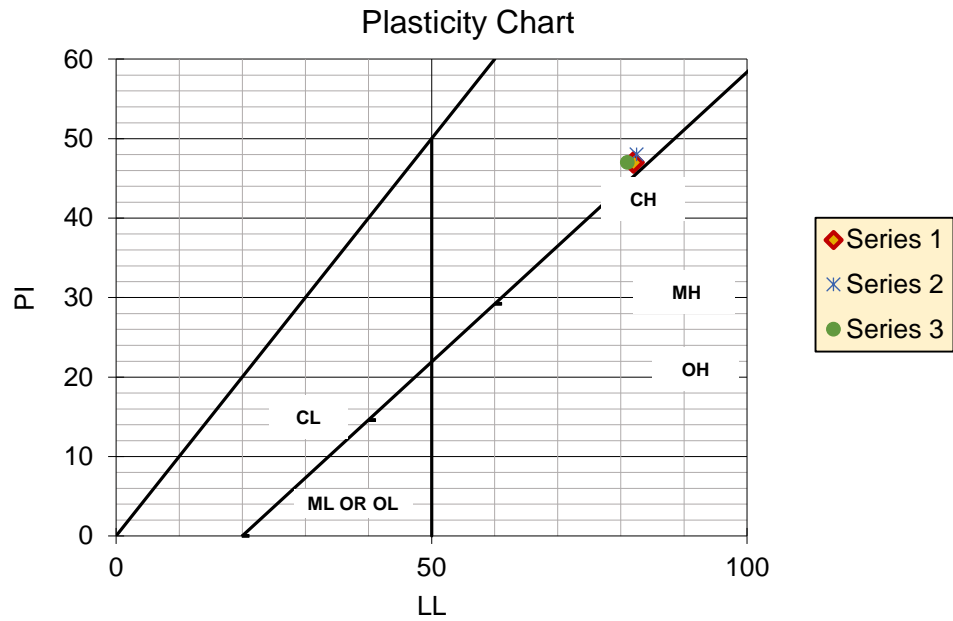


Figure 3-7. Activity chart for expansive clays

The particle size distribution (PSD) of the studied clay was determined by wet sieving and hydrometer tests. The test setup used for the soil analysis - hydrometer test is shown in Figure 3-8. Figure 3-9 presents three PSDs of the studied clay. Based on the results, the black clay comprised 20% sand, 12% silt and 68% clay. The soil properties and geotechnical indices of the studied clay are also summarised in Table 3-1.

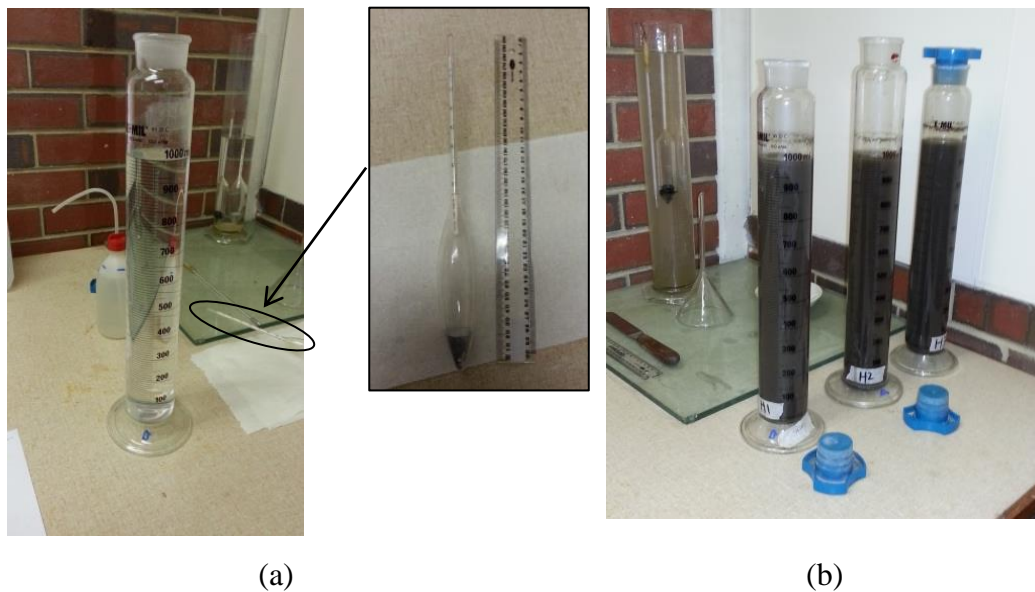


Figure 3-8. Particle size distribution test: (a) calibration and (b) hydrometer test

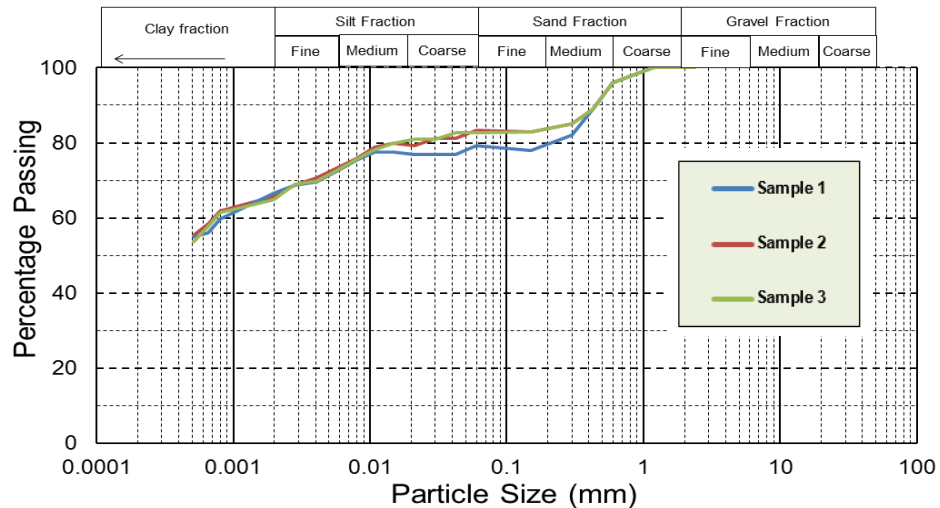


Figure 3-9. Particle size distribution curves (Habibbeygi & Nikraz, 2018a)

Table 3-1. Soil properties of the studied clay

Sand	Silt	Clay	Liquid limit	Plastic limit	Plasticity index	Specific gravity
%	%	%	w_L	w_P	I_P	G_s
20	12	68	82	35	47	2.58

The organic content of the black clay was assessed by the ignition technique. The clay was burnt out in a furnace at a temperature of 400 ± 5 °C for one day. The measured weight loss due to the burning-off of organic content ranged between 5.3% and 6.6%. Figure 3-10 shows the sample after the test.



Figure 3-10. Organic content test – burnout sample

The clay mineralogy of the black clay was investigated using X-ray diffraction (XRD) tests. Air-dried specimens were run on a D8 Advance powder diffractometer (Bruker AXS, Germany) with a copper tube (K-alpha radiation, wavelength 1.54 Å) at 40 kV

and 40 mA using a LynxEye detector (Habibbeygi, Nikraz, & Chegenizadeh, 2017).

Figure 3-11 illustrates the results.

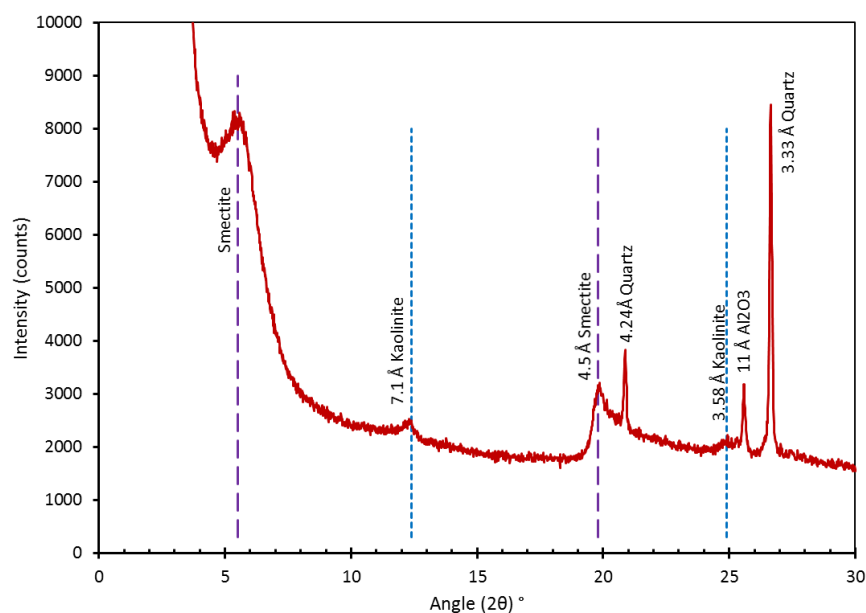


Figure 3-11. XRD spectrum of the black clay

As shown in Figure 3-11, the studied clay comprised montmorillonite (smectite), kaolinite (basal order reflection of 7.15 Å), aluminium oxide (basal order reflection of 11 Å) and quartz (basal order reflection of 3.33 and 4.24 Å).

3.1.2 Magnesium Chloride

Magnesium chloride hexahydrate was used in this research as a stabiliser for expansive clays. The industrial name of this salt is *bischofite*, which is white in colour and has the chemical formula $MgCl_2 \cdot 6H_2O$. This product was provided in the form of flakes with a purity of 98–100%.

3.2 Experimental Methods

3.2.1 Oedometer tests

Samples were prepared by three methods, namely: *reconstituted*, *remoulded* and *undisturbed*.

First, collected bulk samples were dried in ovens at temperatures of 105–110 °C. The samples were then ground to a powder by using a rubber pestle and mortar until they passed a 2-mm sieve. Figure 3-12 shows a dried sample and the sample preparation procedure.

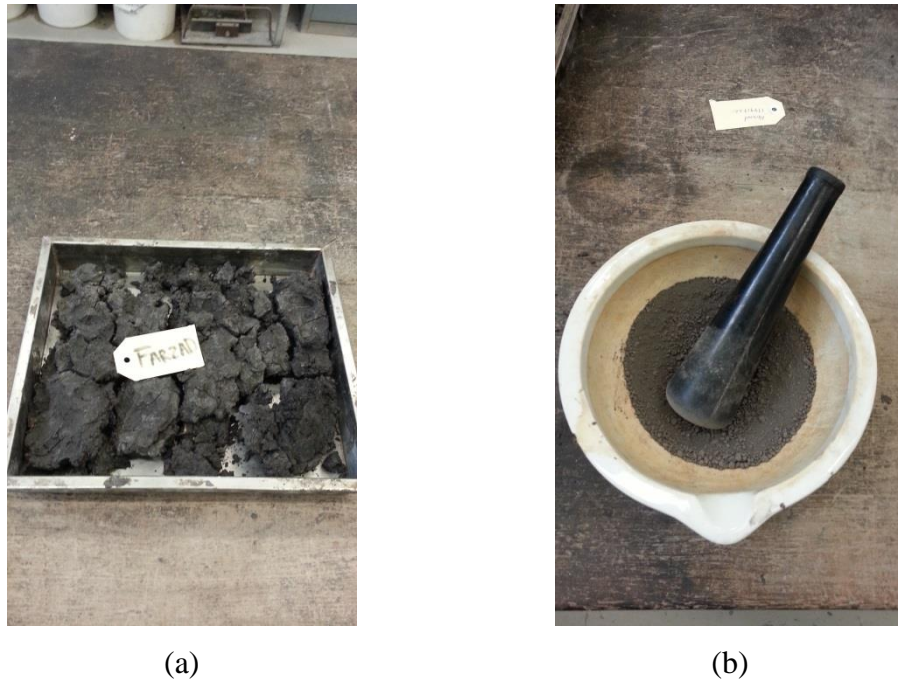


Figure 3-12. Sample preparation procedure: (a) dried sample and (b) grinding the sample

Reconstituted specimens were then prepared by mixing the powder with predefined amounts of distilled water in accordance with Burland's procedure (Burland, 1990). The second type of sample was the remoulded sample. These samples were prepared by mixing predefined amounts of distilled water gradually to the clay to achieve the desired water content following the procedure proposed by (Head, 1986). The mixed soil was placed on flat glass and a consolidation ring was gently pushed into it. The specimen was then trimmed and the remaining trimmings were used for measuring its water content (Figure 3-13).

Finally, the undisturbed specimens were trimmed from the 250 mm disks cut from the undisturbed samples. The in situ water content of the sample was measured prior to carrying out any tests. All remoulded and reconstituted specimens were wrapped in multiple cling foils and kept in three successive airtight plastic bags for one day to homogenise. The temperature of the room where samples were kept was controlled at 25 ± 2 °C.

One-dimensional consolidation tests were carried out on specimens 64 mm in diameter and 25.4 mm in height. The wall of the consolidation ring was covered by a thin layer of silicone grease to decrease friction and alleviate the effect of the steel ring on the compression behaviour.

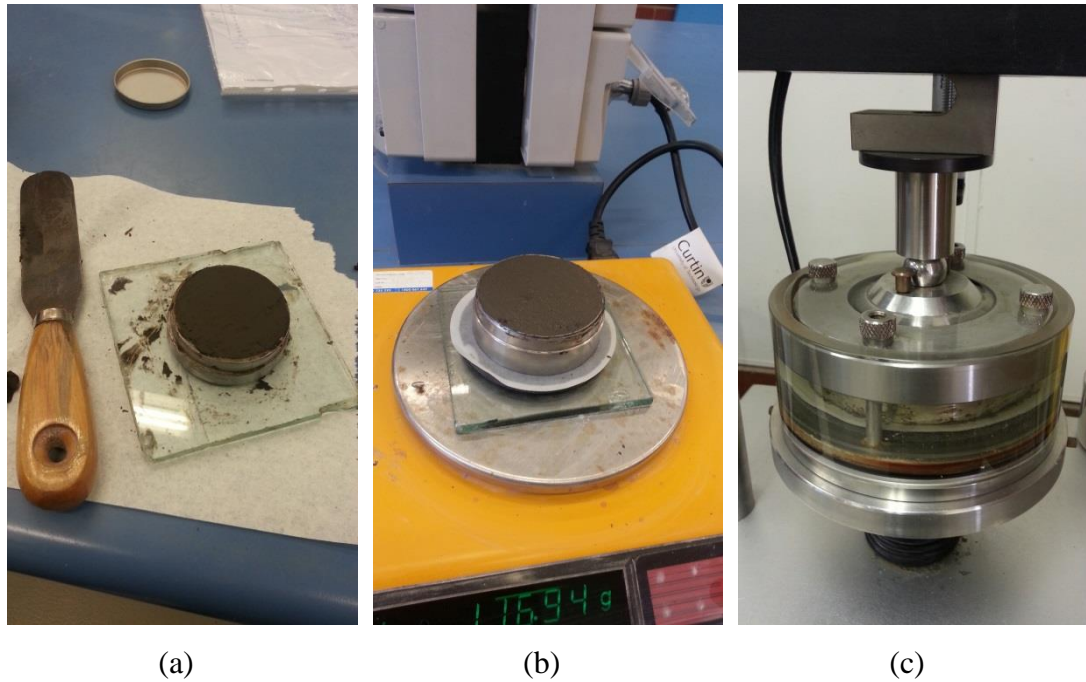


Figure 3-13. One-dimensional consolidation testing (a) sample preparation (b) before test measurement (c) consolidation cell set-up

Twenty-three one-dimensional consolidation tests were conducted on reconstituted/remoulded and undisturbed samples in an auto consolidation apparatus. All tests were carried out under fully-saturated conditions. The consolidation tests began at low stress of 1 kPa to explore the impact of low stress on compression behaviour. The initial water content of the reconstituted samples ranged between 0.67 and 1.25 times the liquid limit. The stress increments considered in these tests were 1, 3, 6, 12.5, 25, 50, 100, 200, 400, 800 and 1600 kPa, which were then unloaded to 800, 400 and 100 kPa. The maximum and minimum time for primary consolidation of each stage were 24 hours and 8 hours respectively. Deformation was recorded over time to investigate the primary consolidation of the samples at each initial water content. Table 3-2 and Table 3-3 present the details of stress increment, initial water content and cycle of loading/reloading for the tests. More information about the sample preparation for each test is presented in Chapters 4 to 11.

Table 3-2. Vertical consolidation stress and cycle of loading/reloading (Habibbeygi & Nikraz, 2018c)

Sample ID	Normalised initial water content ratio	Loading/reloading cycle	Vertical consolidation stress increments (kPa)
1	0.8	No 1	1, 3, 6, 12.5, 3
		No 2	6, 12.5, 25, 50, 100, 25, 6
		No 3	12.5, 25, 50, 100, 200, 400, 100, 25
		No 4	50, 100, 200, 400, 800, 200, 50
		No 5	100, 200, 400, 800, 1600
2	0.9	No 1	1, 3, 6, 12.5, 3
		No 2	6, 12.5, 25, 50, 100, 25, 6
		No 3	12.5, 25, 50, 100, 200, 400, 100, 25
		No 4	50, 100, 200, 400, 800, 200, 50
		No 5	100, 200, 400, 800, 1600
3	1.0	No 1	1, 3, 6, 12.5, 3
		No 2	6, 12.5, 25, 50, 100, 25, 6
		No 3	12.5, 25, 50, 100, 200, 400, 100, 25
		No 4	50, 100, 200, 400, 800, 200, 50
		No 5	100, 200, 400, 800, 1600
4	1.1	No 1	1, 3, 6, 12.5, 3
		No 2	6, 12.5, 25, 50, 100, 25, 6
		No 3	12.5, 25, 50, 100, 200, 400, 100, 25
		No 4	50, 100, 200, 400, 800, 200, 50
		No 5	100, 200, 400, 800, 1600
5	1.2	No 1	1, 3, 6, 12.5, 3
		No 2	6, 12.5, 25, 50, 100, 25, 6
		No 3	12.5, 25, 50, 100, 200, 400, 800, 1600, 400, 100

Table 3-3. Consolidometer test procedure (Habibbeygi & Nikraz, 2018d)

Sample No.	Sample Type	Initial	
		Water Content %	Vertical Consolidation Stress, (kPa)
1	Rem.	41%	25-50-100-200-400-800-1,600
2	Rem.	55%	12.5-25-50-100-200-400-800-1,600
3	Rem.	58%	12.5-25-50-100-200-400-800-1,600
4	Rem.	66%	12.5-25-50-100-200-400-800-1,600
5	Recons.	74%	6-12.5-25-50-100-200-400-800-1,600
6	Recons.	82%	6-12.5-25-50-100-200-400-800-1,600
7	Recons.	90%	6-12.5-25-50-100-200-400-800-1,600
8	Recons.	99%	3-6-12.5-25-50-100-200-400-800-1,600
9	Recons.	104	3-6-12.5-25-50-100-200-400-800-1,600
10	Recons.	109%	3-6-12.5-25-50-100-200-400-800-1600
11	Undist.	40%	100-200-400-800-1600
12	Undist.	43%	200-400-800-1600

where Rem.: Remoulded sample; Recons.: Reconstituted sample and Undist.: Undisturbed sample.

3.2.2 Direct shear tests

Twenty-four direct shear tests were carried out on the black clay in accordance with ASTM D3080 (American Society for Testing and Materials, 2011) in this research. Normal stresses of 50, 100, 200 and 400 kPa were adopted for these tests. Additionally, initial water content ratios were varied from 0.6 to 1.1 times the liquid limit to investigate the effect of high initial water contents on shear behaviour (i.e. $w_0/w_L = 0.6, 0.7, 0.8, 0.9, 1.0$ and 1.1).

Friction between the specimen and shear box was alleviated by applying small amounts of silicone grease to the walls of the shear box. The inner dimensions of the shear box were 63.5 mm x 63.5 mm x 31 mm (Figure 3-14). To provide draining conditions in both directions, two porous stones were placed at the top and bottom of the specimen. Figure 3-15 illustrates the setup used for the direct shear tests.

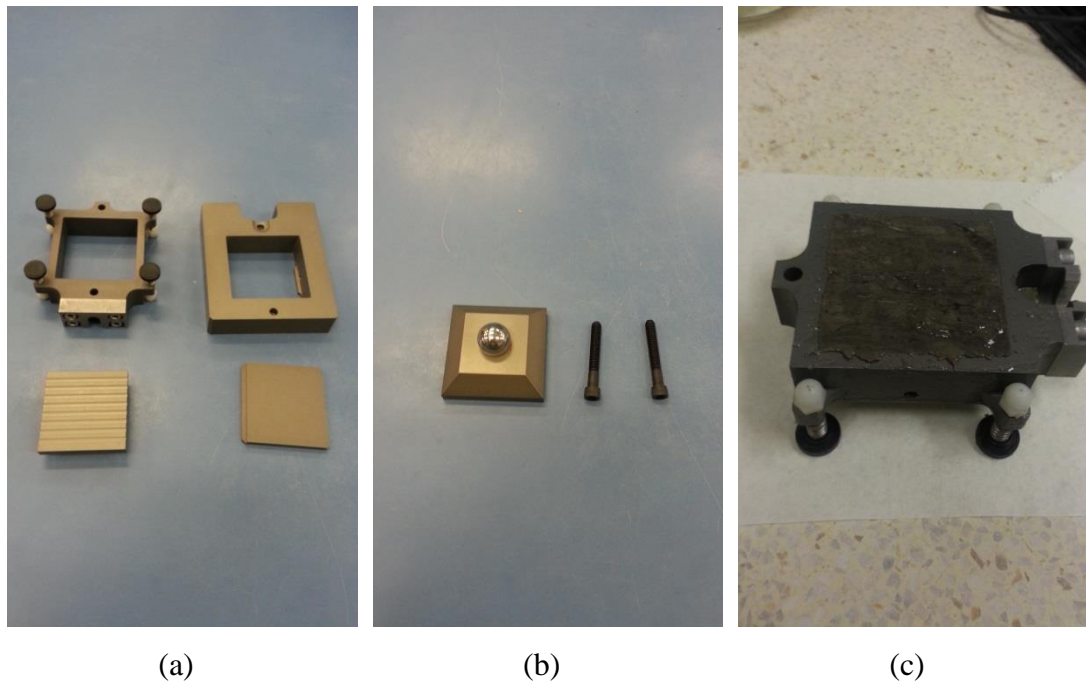


Figure 3-14. Direct shear testing: (a) shear box, (b) load cap and bolts and (c) prepared sample

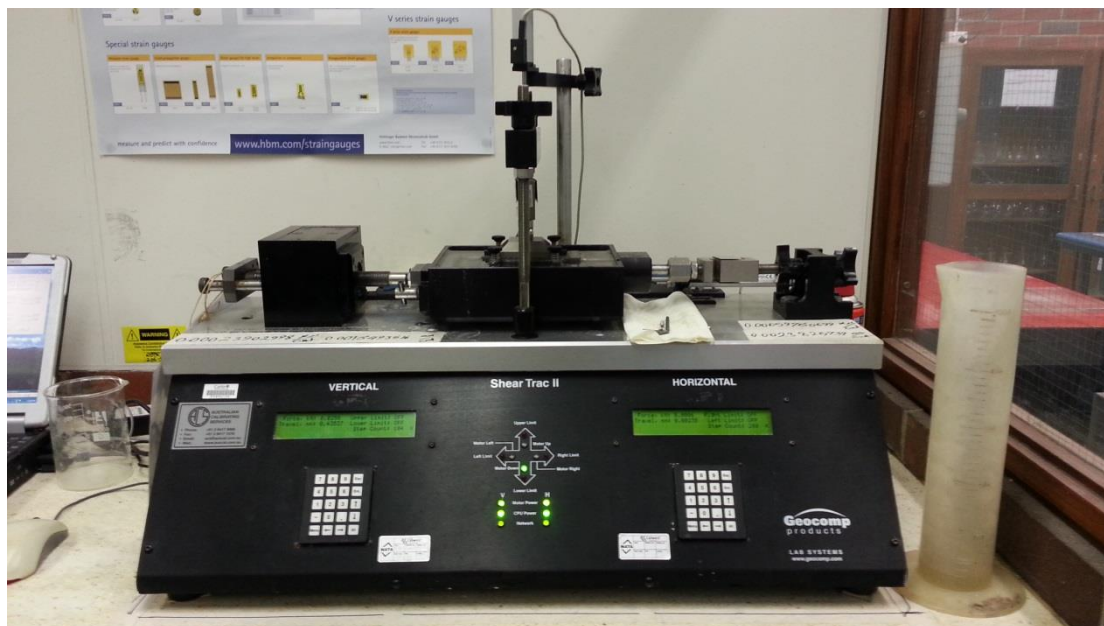


Figure 3-15. Direct shear testing setup

Before the shear stage, consolidation stress was progressively exerted on the samples for the consolidation step. Table 3-4 presents the preconsolidation stress prior to applying shear. More information on the test procedure and sample preparation is discussed in Chapter 9.

Table 3-4. Consolidation stress increments at the preconsolidation stage (Habibbeygi & Nikraz, 2018a)

Sample No.	Initial water content ratio (w_0/w_L)	Normal stress (kPa)	Vertical consolidation stress increments (kPa)
1 – 4	0.6	50, 100, 200 and 400	3, 6, 12.5, 25, 50, 100, 200, 400
5 – 8	0.7	50, 100, 200 and 400	3, 6, 12.5, 25, 50, 100, 200, 400
9 – 12	0.8	50, 100, 200 and 400	6, 12.5, 25, 50, 100, 200, 400
13 – 16	0.9	50, 100, 200 and 400	1, 3, 6, 12.5, 25, 50, 100, 200, 400
17 – 20	1.0	50, 100, 200 and 400	1, 3, 6, 12.5, 25, 50, 100, 200, 400
21 – 24	1.1	50, 100, 200 and 400	1, 3, 6, 12.5, 25, 50, 100, 200, 400

3.2.3 Ring shear test

Figure 3-16 presents the setup used for the ring shear tests. A predefined torsional shear force could be applied on an annular sample to explore the shear strength of the studied soil. A pre-sheared surface was created by rotating the sample after the initial shear failure. Sample preparation was similar to that discussed in *Section 3.2.1 - Oedometer test*.



Figure 3-16. Ring shear test setup

Prior to applying shear rotation, the samples were consolidated to the normal stresses of 50, 100 and 200 kPa. Then, the sample was sheared for one day to create a

predefined shear surface. The rate at the pre-shear step was controlled at 0.1 mm/min. A slow shear rate was adopted to mitigate the effect of soil extrusion, as well as to dissipate any pore water pressure generated in the sample. Shear rates of 200, 100, 50, 10 and 1 mm/min were adopted in this research. For more details of the shear testing procedure, refer to Chapter 10.

4 INTRINSIC COMPRESSION CHARACTERISTICS OF AN EXPANSIVE CLAY FROM WESTERN AUSTRALIA

4.1 Introduction

This chapter presents the first published document of a series of publications pertaining to this research. This peer-reviewed manuscript introduces the results of one-dimensional consolidation tests alongside the interpretation of the results. More importantly, the intrinsic framework is reviewed in this manuscript based on the experimental results. Additionally, the effectiveness of this framework to estimate the compression behaviour of expansive clays is investigated.

The list of references, keywords, and acknowledgements were excluded from this manuscript. The acknowledgements, abbreviations and references are combined on pages vi, xxiv and 192 of the current manuscript, respectively.

Minor changes were made for the inclusion of the published manuscript into the current document. The differences comprise removing repetitions, referencing, style and numbering of table captions and figure captions, wherever it was necessary to keep the uniformity and consistency of the current document. Repetitions comprise equations and literature reviews which have already been addressed in Chapter 2. Thus, some equations may refer to Chapter 2. Furthermore, the numbering of equations, figures and tables follow the current manuscript numbering and may differ from those of the published manuscript.

4.2 Citation

Habibbeygi, F., Nikraz, H., & Chegenizadeh, A. (2017). Intrinsic Compression Characteristics of an Expansive Clay from Western Australia. *International Journal of GEOMATE*, 12(29), 140-147. <https://doi.org/10.21660/2017.29.20455>

4.3 Manuscript Contents

4.3.1 Abstract

Intrinsic compression behaviour of an expansive clay from Western Australia is investigated using the intrinsic framework in this study. Oedometer results conform with the intrinsic concept at post-yield phase. However, there is a great impact of initial

water content on the compression curves at pre-yield stage. It specifies that there is an initial structure similar to a natural clay structure which resists applied forces at this phase and it is related to the amount of initial water content at the preparation stage. Nonetheless, this interparticle bonding is demolished when vertical stress becomes greater than remoulded yield stress. The findings also show that the remoulded yield stress of a reconstituted clay decreases non-linearly with the increase of initial water content, and is remarkably affected by its clay mineralogy. The remoulded yield stress of a soil with the predominant clay of smectite is far greater than those of other clay minerals despite having the same normalised initial void ratio value (e_0/e_L). Moreover, remoulded yield stress of an expansive soil with main clay mineral of smectite decreases more abruptly than for other clay minerals reported in the literature. Reconstituted compression indices (C_c^* , e_{100}^*) for clays with a considerable amount of smectite are also greater than respective values for other clay minerals.

4.3.2 Introduction

Expansive soils are a major problem in new residential developments in some arid and semi-arid areas all over the world. These types of soils, which mostly contain a considerable amount of smectite (montmorillonite), are very sensitive to the change of their water content. They expand with an increase in their moisture content while contract as they dry. Every year, millions of dollars are expended on both financial losses and stabilisation of these problematic soils. Overall, expansive soils damage dwellings, roadways, irrigational waterways, and other assets so significantly that the cost of the damage is greater than the cumulative cost of loss caused by natural disasters such as typhoons, cyclones, floods, earthquakes, and so forth (Nelson & Miller, 1992).

As the population of Western Australia has been increasing continuously during past decades, the need for new affordable housing grows rapidly. The answer to this amplified demand has been found in developing new residential communities near Perth city. Several new suburbs and cities have been constructed both to the south and the north of the capital city in the recent years. Some of these new suburbs are being constructed on expansive soil layers, where expansion of these problematic soils is a real challenge to the geotechnical engineers of those projects. As stabilisation methods consist of laying sand cover layers, and chemical treatments are costly and

cumbersome, new research on understanding the compressibility of these expansive soils is worthwhile to develop more efficient methods of stabilisation. In this study, several samples were collected from Baldivis, a newly-developed suburb in the south of Perth, to investigate the compression behaviour of this highly expansive soil by using the intrinsic concept.

In this study, the compression behaviour of an expansive clay from Western Australia was investigated by performing 1-D consolidation tests on reconstituted samples. All tests began from a very low consolidation stress level of 1 kPa to consider the influence of low levels of stress, increasing to high stress levels to also test this influence. Two different methods of normalising inherent compression curves were used to determine the most suitable method for characterisation the compressibility of expansive clays. As a part of this study, clay mineralogy was investigated by X-ray diffraction tests to analyse the impact of clay mineralogy on the intrinsic parameters. An empirical relationship then was proposed for determining the remoulded yield stress of expansive soils with the dominant clay mineral of smectite.

Most research on inherent compressibility of clays, to the authors' knowledge, has focused on geotechnical invariants so far. This chapter presents the influence of clay mineralogy as well as initial water content on the compressibility of expansive soils based on intrinsic framework. There is also a lack of information about the relationships for predicting the remoulded yield stress of clays with predominant mineral of smectite. Furthermore, existing experimental relationships underestimate the value of remoulded yield stress of such expansive soils. Overall, the following questions will be discussed in this chapter:

Is it possible to use existing relationships for predicting intrinsic parameters (C_c^* , e_{100}^*) of an expansive soil with chief clay mineral of smectite?

How susceptible is the expansive soils' structure to the initial water content?

How much does clay mineralogy affect the value of remoulded yield stress?

What is the best method of normalising inherent compression curves of expansive soils?

4.3.3 Material and Test Procedure

Soil samples used in this research were collected from an under development residential site at Baldivis, a suburb 46 km south of Perth, the capital city of Western

Chapter 4 - Intrinsic Compression Characteristics Of An Expansive Clay From Western Australia

Australia. All disturbed samples were hand dug from a depth of 0.3 m to 0.5 m below ground surface after grass was removed. Basic soil index tests were performed in accordance to ASTM standards (American Society for Testing and Materials, 2011) to identify the physical properties of the studied soil. The liquid limit test was performed using a Casagrande device and the plastic limit was measured with thread rolling in accordance to ASTM D4318; a specific gravity test was carried out using a pycnometer (ASTM D854). The result of consistency limits for Baldivis clay is plotted on the plasticity chart in Figure 4-1; the data lies slightly above the A-line in the plasticity chart. The high value of plasticity index indicates that the studied soil is highly expansive.

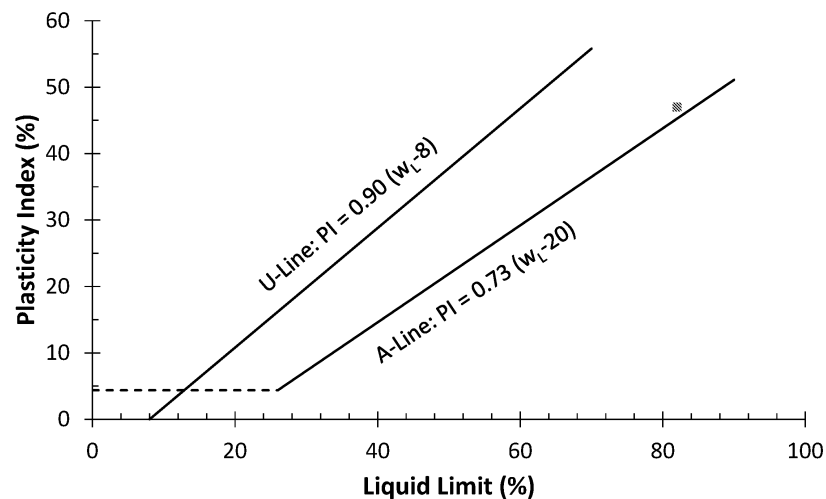


Figure 4-1. Plasticity chart

Particle size distribution of the studied soil performed is shown in Figure 4-2. It can be seen that Baldivis soil consists 20% sand, 12% silt and a considerable amount of clay (68%). Physical properties of the studied clay are also tabulated in Table 4-1. The organic content of Baldivis clay was measured by ignition method; the studied soil was burnt out at a furnace to $400 \pm 5^\circ\text{C}$ for 24 hrs. The measured loss was approximately 5.3% to 6.6% for soil at the studied depth.

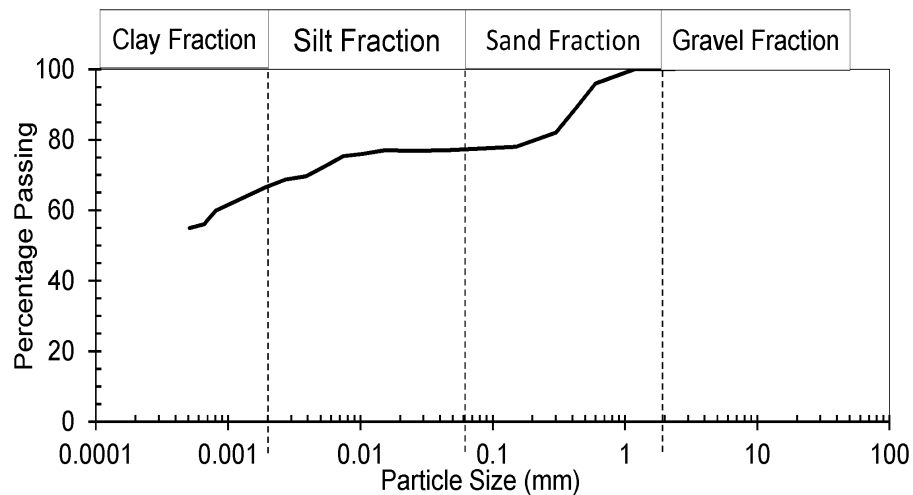


Figure 4-2. Particle size distribution curve for the studied soil

Table 4-1. Physical properties of Baldvis clay

Liquid Limit (w_L)	Plastic Limit (w_P)	Plasticity Index (PI)	Specific Gravity (G_s)	Sand (%)	Silt (%)	Clay (%)
82	35	47	2.6	20	12	68

X-ray diffraction tests were conducted to analyse the mineralogical component of Baldvis clay. Air-dried samples were run on powder diffractometer D8 Advance (Bruker AXS, Germany) with a copper tube (K-alpha radiation, wavelength 1.54Å) at 40kV and 40mA and with a LynxEye detector. The results, presented in Figure 4-3, show a considerable amount of smectite (montmorillonite) in the studied soil. However, smectite is the main clay mineral; kaolinite was also detected with a basal order reflection of 7.15 Å and 3.58 Å.

Reconstituted samples were prepared according to the sample preparation proposed originally by Burland (1990) and followed by Hong et al. (2010). First, samples obtained from the site were oven-dried at 105-110°C. The samples were then ground to a powder by using a pestle and mortar to pass a 2 mm sieve. The determined amount of distilled water was added to the measured oven-dried soil to achieve the prescribed initial water content (w_0); initial water content of sample preparation ranged from 0.67 to 1.33 times liquid limit (w_L) in this study. Prepared samples were kept in an air-tight container at a controlled room temperature ($25 \pm 2^\circ\text{C}$) for 24 hours to equilibrate before

performing consolidation tests. The initial water content of each specimen was measured before the consolidation test to determine the precise value of initial water content.

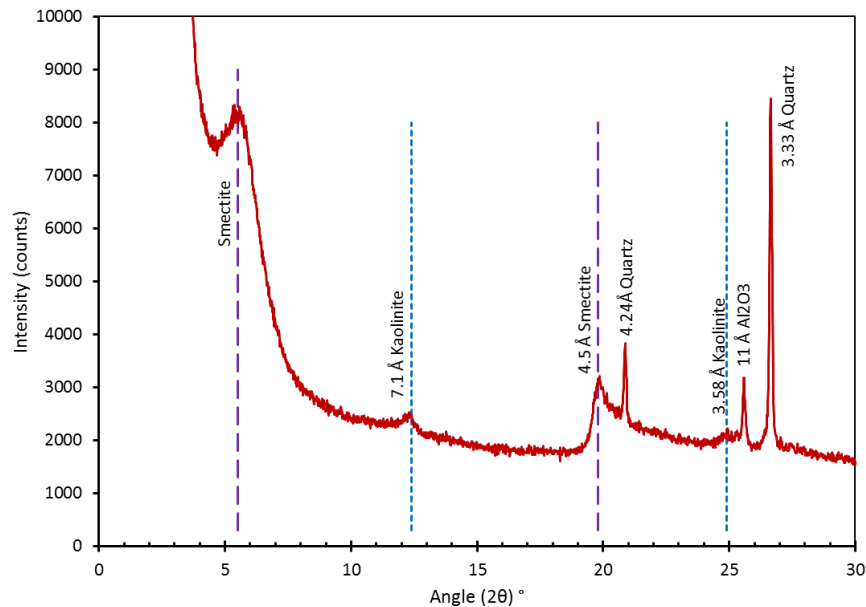


Figure 4-3. XRD pattern for the studied soil

One-dimensional consolidation tests were conducted on specimens of 64 mm in diameter and 25.4 mm in height (i.e., area of the specimen was 3217 mm²). Sample preparation techniques were chosen based on the relative value of initial water content of each specimen to the liquid limit. For specimens with an initial water content more than the liquid limit, the prepared soil was carefully spooned into the consolidation rim to avoid trapping any air bubbles in the specimen. However, the traditional method of sample preparation of a remoulded sample was chosen for those with an initial water content of less than the liquid limit (Head, 1986). The mixed soil was placed on a flat glass, and a consolidation ring was gently pushed into the soil. The specimen was then trimmed, and remaining trimmings were used for measuring its water content.

Eight series of 1-D consolidation tests were conducted on reconstituted samples in an auto consolidation apparatus in fully saturated conditions. The initial vertical consolidation stress was kept as low as possible to investigate the effect of low stresses on the compression behaviour. The stress increments used in this study were 1, 3, 6, 12.5, 25, 50, 100, 200, 400, 800, 1600 kPa in the loading phase. The deformation curves versus time were employed to define the end of primary consolidation of each

stage by using the log-time method introduced by Casagrande (Head, 1986). The maximum and minimum time for primary consolidation of each stage were 24 hours and 8 hours respectively. Two porous stones were used at top and bottom of the specimen. Thus, drainage was allowed at both surfaces of the specimen during the test. Room temperature during all tests was kept constant at $25 \pm 2^\circ\text{C}$.

4.3.4 Results and Discussion

4.3.4.1 Inherent Compressibility and Remoulded Yield Stress

To investigate a complete intrinsic compression line (ICL) of Baldvis clay, one-dimensional tests began at a very low stress of 1 kPa and ended at 1600 kPa in the loading phase.

Compression curves of Baldvis clay for various initial water content, $0.67w_L$ to $1.33w_L$, are presented in Figure 4-4 in a semi-logarithmic space of $e - \log \sigma'_v$. It is clear from this figure that all compression curves are an inverse S-shape and slightly concave upwards, similar to those of natural clays. The same shape of ICL was reported by other researchers with different degrees of plasticity for reconstituted clays as well (Hong et al., 2010; Zeng et al., 2015). Moreover, Figure 4-4 depicts that the compression behaviour of Baldvis clay is highly sensitive to its initial water content. It is evident from this figure that samples with higher initial water content have relatively greater values of void ratio at the same vertical consolidation stress. However the gap between curves decreases gradually when vertical stress increases. It indicates that even reconstituted clays have a definite structure which withstands the external force. However this bonding is destroyed with increasing the vertical stress.

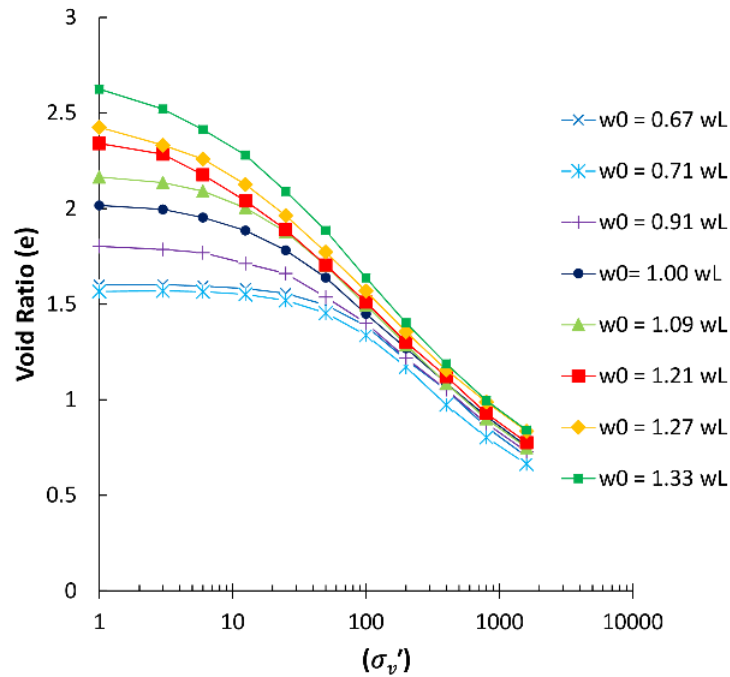


Figure 4-4. Inherent compression curves of Baldivis clay

The term *structure* in this study is used as the combination of inter-particle bonding of clay particles and fabric (clay particle arrangement) following Mitchell and Soga (1976). After applying a certain amount of external force (i.e. vertical consolidation stress) to specimen, soils cannot keep their original structures and the gap between compression curves will reduce.

ICLs of either natural or reconstituted clays are an inverse S-shape, and for consolidation stresses greater than a particular stress, become marginally concave upwards. This particular stress, which is very comparable to pre-consolidation stress for natural clays, has been named differently by earlier researchers: pore-water suction, suction pressure, apparent consolidation stress, and remoulded yield stress (Hong et al., 2012; Hong et al., 2010). In the interest of not being confused with unsaturated definitions, as well as natural clay pre-consolidation stress, it seems *remoulded yield stress* (σ'_{yr}) employed by Hong et al. (2012) is the appropriate term to describe this definite stress. As the ICL of a reconstituted clay is similar to the compression curve of a natural clay, the remoulded yield stress can be defined by methods such as those presented for preconsolidation stress of sedimentary clays. Butterfield (1979) firstly used bilogarithmic space to present 1-D consolidation results of natural clays. He proposed the inverse S-shape of $e - \log \sigma'_v$ compression curves can be simply presented by two straight lines in the bi-logarithmic plane. In fact, this method is highly

useful when the compression curves of those clays with ambiguous yield stress are being investigated. In this method, the intersection point of pre-yield and post-yield states can be defined as the yield stress. This technique has been successfully used by several researchers (Hong et al., 2010; Wang et al., 2016).

Intrinsic compression curves of Baldvis clay are replotted in Figure 4-5 in the bi-logarithmic plane of $\ln(1+e)$ vs. $\log(\sigma'_v)$. All compression curves can be well characterised by two individual lines which intersect at the remoulded yield stress. For different values of initial water content, the reconstituted clay has low compressibility for stresses less than σ'_{yr} , while its compressibility increases abruptly when the vertical consolidation stress is greater than σ'_{yr} . The slope of compression line in $\ln(1+e)$ - $\log(\sigma'_v)$ plane increased from about 0.01-0.04 for pre-yield state to 0.13 for post-yield state. There is a sharp escalation of compressibility at σ'_{yr} , 3.2 to 13 times its initial value, because the bond of clay inter-particles is destroyed and the original structure is lost. Oedometer test results presented in Figure 4-5 depicts a clear value of remoulded yield stress for the studied range of water contents for the studied soil. The remoulded yield stress of Baldvis clay varies between 19 kPa to 70 kPa.

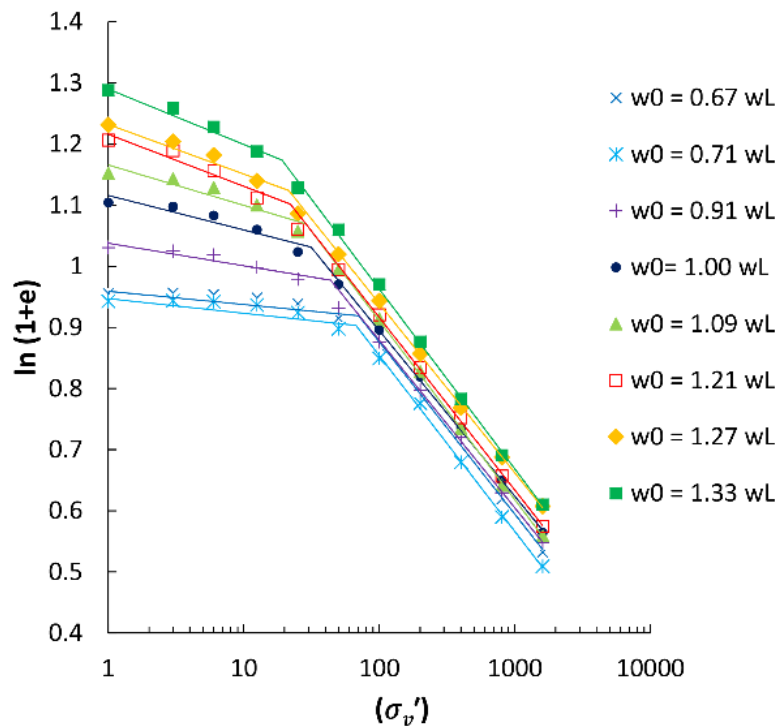


Figure 4-5. Inherent compression curves of Baldvis clay in bi-logarithmic plane

It is well established that the remoulded yield stress (σ'_{yr}) of clays reduces with the growth in initial moisture content (Hong, 2006; Hong et al., 2010). Remoulded yield stress for various values of initial water content have been normalised against the normalised initial water content (w_0/w_L) as seen in Figure 4-6 (for equations, refer to Chapter 2). It can be seen in this figure that the remoulded yield stress decreases non-linearly with an increase of normalised initial water content (w_0/w_L). The relationship between σ'_{yr} and normalised initial water content can be presented by the following power equation:

$$\sigma'_{yr} = 33.5/(w_0/w_L)^{1.96} \quad (4-1)$$

where σ'_{yr} is in kPa. Hong (2006) extrapolated compression curves to calculate the remoulded yield stress (σ'_{yr}) in a bi-logarithmic plane. He also used e_L to normalise the relationship between σ'_{yr} and initial void ratio (e_0). He suggested that there is a unique relationship between σ'_{yr} and normalised initial void ratio e_0/e_L using an extrapolation method to find e_0 ; e_L is the void ratio at liquid limit (Equation (2-24)). Hong et al. (2010) correlated the ICL for a wider range of initial water contents (25% to 160%) using a normalising invariant of I_v . Hong et al. (2010) also developed an equation to determine the remoulded yield stress by knowing the normalised initial void ratio (Equation (2-25)).

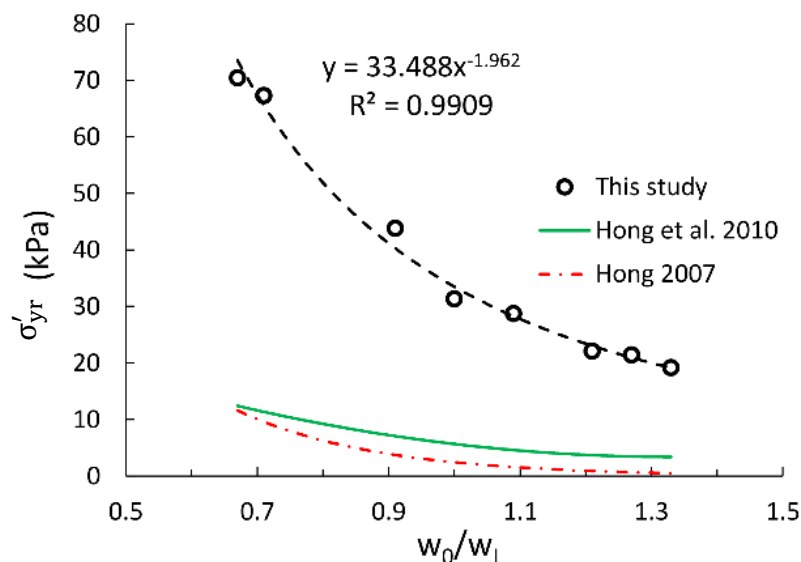


Figure 4-6. Remoulded yield stress against normalised water content

A comparison of the remoulded yield stress derived from the aforementioned relationships and the results of this study are also given in Figure 4-6. As all samples

were saturated and the specific gravity was the same, the value of (w_0/w_L) is equal to (e_0/e_L) for each clay and the graph can be drawn against normalised initial water content. Figure 4-6 shows that the remoulded yield stress for Baldvis clay is far greater than the values calculated by Equation (2-24) and (2-25). Although the tendency of decreasing σ'_{yr} with w_0/w_L is almost the same for all test results, the disparity between the results of this study and the other data is enormous. Fortunately, this gap can be explained by studying clay mineral composition of studied soils. Recent studies show that the predominant clay mineral of past research were mostly illite and the amount of smectite mineral was noticeably low (Hong et al., 2013). However, the main clay mineral of Baldvis clay which has been studied herein was known to be smectite. This indicates that for the studied clays, the principal clay minerals has a crucial impact on the value of σ'_{yr} . According to Figure 4-6, the remoulded yield stress of Baldvis clay plummets rapidly with the increase of initial water content, and almost levelled off for w_0/w_L greater than 1.21. This sharp plunge in the value of remoulded yield stress indicates that expansive clay with the main clay mineral of smectite is more susceptible to initial water content rather than other minerals. Furthermore, the structure of expansive clay becomes weak so rapidly with an increase of initial water content that σ'_{yr} drops more suddenly than for other clay minerals reported in the literature. Thus, the variation of the remoulded yield stress of clays with different predominant clay varies considerably when the initial water content changes. In fact, most of the relationships for estimating the remoulded yield stress of reconstituted clays presented in the literature have been derived from a limited range of clay mineralogy. However, while these relationships can effectively predict σ'_{yr} of clays with a principal clay of either kaolinite or illite, they underestimate the value of the remoulded yield stress for clays with a considerable amount of smectite.

4.3.4.2 Normalising Inherent Compression Curves

In this study, two of the most popular frameworks for normalising inherent compression curves have been used. First, void ratio at liquid limit (e_L) was used as a normalising parameter following Nagaraj and Murthy (1983). Second, void index – introduced originally by Burland (1990) – was employed for standardisation. Then the effectiveness of each method was investigated in characterising the compressibility behaviour of reconstituted Baldvis clay.

Nagaraj and Murthy (1983) introduced a unique relationship between the effective consolidation stress (σ'_v) and the normalised void ratio (e/e_L) as follows:

$$e/e_L = a - b(\log \sigma'_v) \quad (4-2)$$

where a and b are constants. They suggested the values of a and b to be 1.099 and 0.223 (Nagaraj & Murthy, 1983). Then they revised a and b invariants to 1.122 and 0.2343 respectively (Nagaraj & Murthy, 1986).

The inherent compression curves of Baldivis clay normalised by e_L is presented in Figure 4-7. For comparison, the normalised compression lines proposed by Nagaraj and Murthy (1983, 1986) are also plotted in this figure. As it can be seen in Figure 4-7, the results are highly dependent on the value of initial water content. However, the results approach the values estimated by above relationships when vertical stress increases. This consistency at high levels of stress is due to loss of the original structure of clay. Thus, the normalised void ratio approached the value determined by Equation (4-2).

Intrinsic compression curves for Baldivis clay which have been normalised using Burland's concept are presented in Figure 4-8 at different initial water contents, from 0.67 to 1.33 times liquid limit. It can be seen that the results conform well with both Burland (1990) and Hong et al. (2010) at post-yield state, i.e. when the vertical stress is greater than the remoulded yield stress. However, the void index is less than the calculated value of aforementioned relationships at pre-yield phase. On the other hand, compression curves cannot be normalised at pre-yield states by using the intrinsic framework. Moreover, the value of the void index is completely affected by the initial water content for the studied soil. It shows that there is a certain structure at the pre-yield state, i.e. the vertical stress is less than the remoulded yield stress, which bears the deformation, and this structure depends on the value of initial water content.

Chapter 4 - Intrinsic Compression Characteristics Of An Expansive Clay From Western Australia

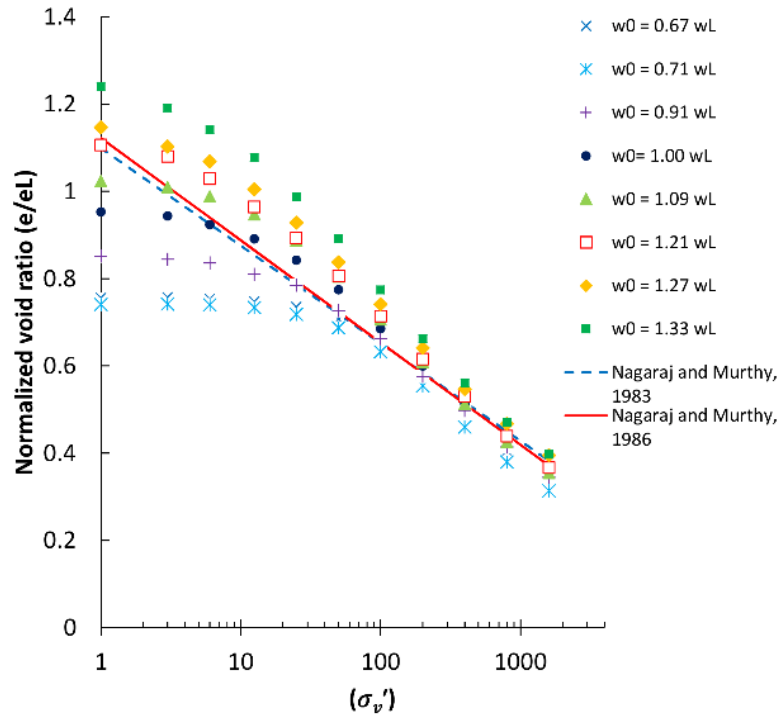


Figure 4-7. Normalised void ratio graphs for Baldvis clay

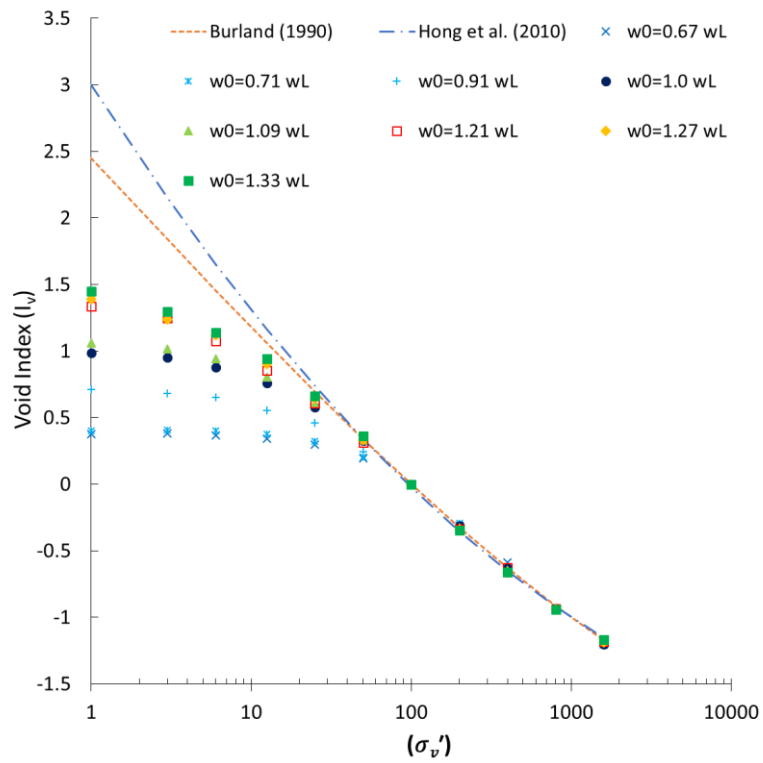


Figure 4-8. Intrinsic compression curves for Baldvis clay

Figure 4-9 shows the measured values of intrinsic parameters of e_{100}^* and C_c^* for various initial states (i.e. $w_0/w_L = 0.67$ to 1.33) and those calculated from Equations (2-12) and (2-13). As it can be seen in this graph, e_{100}^* increases gradually with an increase of water content. Moreover, for all ranges of initial water content, e_{100}^* is higher than the values calculated by the empirical relationship. On the other hand, the rate of variation of C_c^* against normalised water content is less than the rate of e_{100}^* . However, C_c^* has an almost positive correlation with the normalised water content to a lesser degree. C_c^* is approximately uniform for the range of the normalised water content of 1.0 to 1.33, which is in good agreement with Burland (1990). Overall, the empirical relationships proposed by Burland (1990) underestimated intrinsic parameters for the studied range of initial water content for the studied soil.

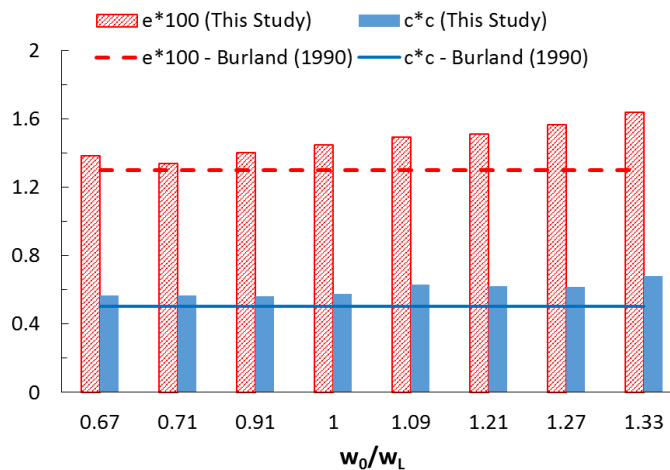


Figure 4-9. Comparison of intrinsic parameters against initial water content

Figure 4-10 shows the measured values of intrinsic parameters for Baldvis clay as well as derived value for this soil using some more recent empirical relationships. The graph depicts that the measured values of both intrinsic parameters are higher than the derived ones through relationships proposed by Zeng et al. (2015) and Yin and Miao (2013). However, the increasing trend is almost the same for all these relationships and measured values. These results show how important the impact of clay minerals is on the values of intrinsic parameters, such as with Baldvis clay, with the chief clay of smectite, having unique values for intrinsic parameters regarding average values derived from empirical relationships. Therefore, the intrinsic framework can be used to properly characterise the inherent compression curves for various clays including expansive clays, yet the empirical relationships should be used cautiously as they

underestimate the intrinsic parameters for clays with a considerable amount of smectite.

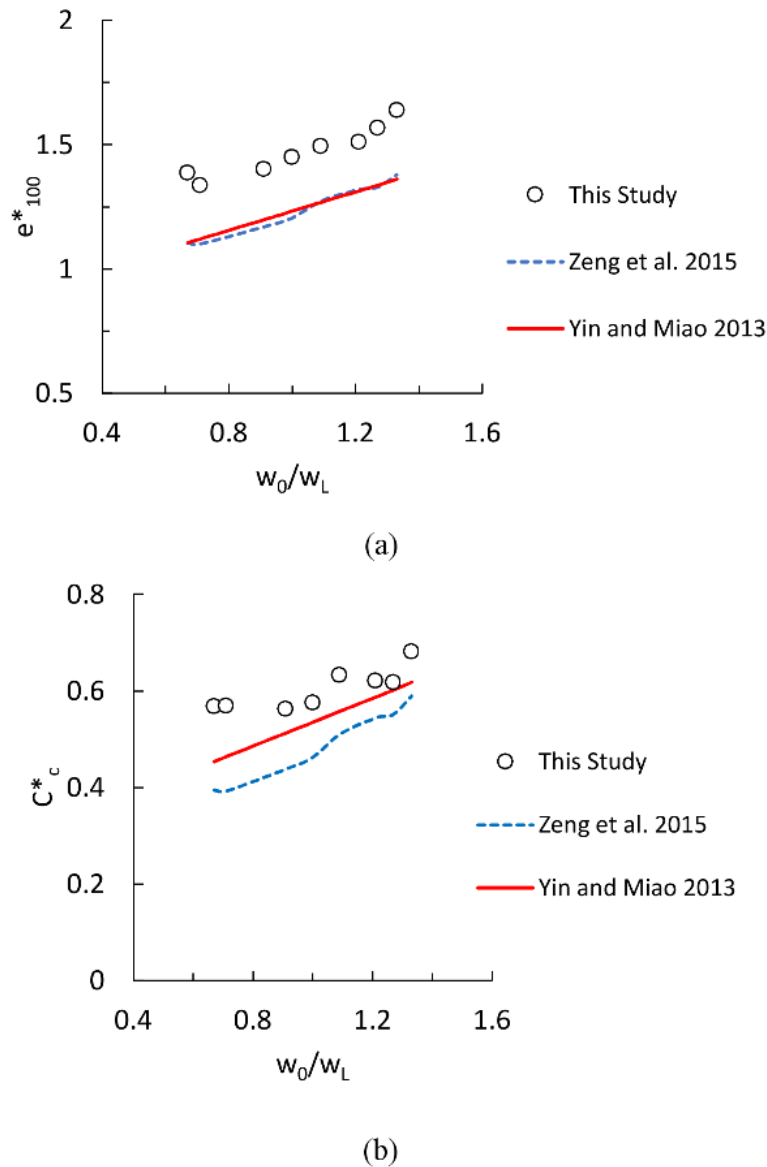


Figure 4-10. Relationship of intrinsic parameters plot against initial water content: (a) e_{100}^* graph (b) C_c^* graph

4.3.5 Conclusions

Intrinsic compression behaviour of Baldivis clay from Western Australia was investigated in this chapter using two different methods of normalisation (i.e. normalised void ratio and void index). The following results were observed for the studied soil based on XRD and 1-D consolidation tests:

- All compression curves of reconstituted Baldivis clay were an inverse S-shape similar to those of natural clays. The intrinsic concept can explain well the compression behaviour of reconstituted Baldivis clay beyond the remoulded yield stress. However, the behaviour is completely affected by the initial water content at stresses lower than the remoulded yield stress.
- Inherent compression curves of an expansive clay can be well defined by two straight lines in a bi-logarithmic plane with a definite remoulded yield stress. However, the gap between normalised void ratios for different initial states decreases when the vertical stress increases and the original structure is destroyed. The remoulded yield stress has a negative non-linear correlation with normalised initial water content.
- Intrinsic compression curves of the studied soil cannot be effectively standardised using normalised void ratio. However, the disparity decreases when the vertical stress increases. Nevertheless, the inherent compression curves can be normalised satisfactory for the post-yield phase by using the intrinsic concept and void index.
- Most experimental relationships for estimating the remoulded yield stress of reconstituted clays in literature are based on consolidation tests on clays with the principal clay of illite. These relationships underestimate the value of remoulded yield stress if predominant clay is smectite. A new relationship has been presented in this study for predicting the remoulded yield stress, especially for expansive soils in which the predominant clay is smectite.
- However, while the intrinsic frame of reference can be used to satisfactorily explain the compressibility of reconstituted clays, the experimental relationships developed for estimating the void index can underestimate the intrinsic compression parameters of expansive clays.

5 REGRESSION MODELS FOR INTRINSIC CONSTANTS OF RECONSTITUTED CLAYS

5.1 Introduction

This published manuscript employs regression analyses to predict the compression behaviour of expansive clays. Four predictive models are presented based on the experimental laboratory results. Furthermore, the clay mineralogy is also included in the models.

The list of references, keywords, and acknowledgements were excluded from this manuscript. The acknowledgements, abbreviations and references are combined on pages vi, xxiv and 192 of the current manuscript, respectively.

Minor changes were made for the inclusion of the published manuscript into the current document. The differences comprise removing repetitions, referencing, style and numbering of table captions and figure captions, wherever it was necessary to keep the uniformity and consistency of the current document. Repetitions comprise equations and literature reviews which have already been addressed in Chapter 2. Thus, some equations may refer to Chapter 2. Furthermore, the numbering of equations, figures and tables follow the current manuscript numbering and may differ from those of the published manuscript.

5.2 Citation

A summary of this chapter was published:

Habibbeygi, F., Nikraz, H. & Koul B. (2018). Regression Models for Intrinsic Constants of Reconstituted Clays. , Cogent Geoscience, 4(1), 1546978.

<https://doi.org/10.1080/23312041.2018.1546978>

5.3 Manuscript Contents

5.3.1 Abstract

In this study, four models were developed to predict intrinsic constants based on some simple physical parameters as well as clay mineralogy of a reconstituted clay sample.

The effect of each predictor on the response was evaluated for each individual clay mineralogy. According to the results, it appears that the void ratio at liquid limit has the greatest effect on clays with a considerable amount of smectite, while the effect of the initial void ratio of such clays is the least amongst other clay minerals. A simplified method is also presented to determine the virgin compression line of reconstituted clays using the initial void ratio, the void ratio at the liquid limit, and its clay mineralogy.

5.3.2 *Introduction*

Dredged slurry sedimentation is currently used frequently in land reclamations as a sustainable solution to manage the huge quantities of slurries dredged from lakes and rivers every year. The deposited slurries can be found all over the world where reclamation is considered to be an essential step in developing new urban areas. Over the past seven decades, researchers and geotechnical engineers across the world have been interested in better comprehending the compression behaviour of dredged slurries at high initial water content due to the potential effect of their settlement on future coastal development projects.

During the dredging process, the structure of a clayey material is broken down such that the sedimented dredged clay can be considered as a reconstituted soil. A reconstituted soil is defined as a type of remoulded sample which is prepared at a water content equal to or greater than its liquid limit following Burland's procedure (Burland, 1990). During the past seven decades, many researchers have performed a considerably large number of consolidation tests on remoulded/reconstituted samples to investigate the compressibility of clays (Butterfield, 1979; Habibbeygi, Nikraz, & Verheyde, 2017; Hong & Tsuchida, 1999; Hong, 2006; Mesri & Olson, 1971; Mitchell & Soga, 1976; Nagaraj & Miura, 2001; Nagaraj & Murthy, 1983; Sridharan & Gurtug, 2005; Sridharan & Nagaraj, 2000). However, a relatively accurate prediction of the compressibility behaviour of dredged slurries can be derived by performing modified oedometer (consolidation) tests on these types of materials; unfortunately, consolidation tests on reconstituted clays are always time-consuming, costly and cumbersome. The determination of compression index is considered to be a relatively expensive and time-consuming test in most geotechnical projects, especially when undertaken on clays with high initial water content. Considering all these difficulties

and limitations in assessing the compressibility of reconstituted clays at high initial water content, geotechnical engineers estimating the volumetric behaviour of reconstituted clays often tend to use empirical correlations instead of performing one-dimensional consolidation tests. Accordingly, having some reliable empirical equations to predict the compression behaviour of such soils is beneficial. In this case, compressibility can be estimated by understanding some simple physical characteristics of the soil sample under study (i.e. initial water content, liquid and plastic limits, natural void ratio), which can be determined conveniently in the laboratory.

To the authors' knowledge, some research has previously been conducted to consider the effect of initial water content and soil properties on the compression behaviour of reconstituted clays (Cerato & Lutenecker, 2004; Kootahi & Moradi, 2016; Lee et al., 2015; Lei et al., 2015; Takashi, 2015; Xu & Yin, 2015; Zeng et al., 2011), but only a few studies have taken into account the influence of clay mineralogy (Habibbeygi, Nikraz, & Chegenizadeh, 2017; Xu & Yin, 2015). In this chapter, the intrinsic concept was used as a basic frame of reference for interpreting and evaluating the compressibility of reconstituted clays. Furthermore, the effect of clay mineralogy on compression behaviour has been assessed using a broad range of geotechnical data from the literature. Eventually, four series of practical relationships were developed to estimate the intrinsic constants and compressibility of a reconstituted clay based on some simple physical parameters, as well as the clay's mineralogy.

5.3.3 Existing correlations for predicting intrinsic constants

Burland (1990) proposed a unique framework for normalising the compression behaviour of reconstituted clays by introducing the intrinsic concept in his 40th Rankine lecture. The intrinsic concept has since been consistently used worldwide to explain the behaviour of clays (Al Haj & Standing, 2015; Habibbeygi, Nikraz, & Chegenizadeh, 2017; Hong et al., 2012; Hong et al., 2010; Horpibulsuk et al., 2016). Intrinsic compression behaviour can be interpreted by two constants of compressibility - compression index (C_c^*) and e_{100}^* - and a void ratio invariant, named the void index (I_v). Existing equations have been already addressed in Chapter 2. Thus, the equations and literature review have been removed from this chapter to avoid repetition.

Habibbeygi, Nikraz, and Chegenizadeh (2017) performed eight series of consolidation tests on reconstituted samples to investigate the impact of mineralogy on the compressibility of expansive clays. The initial water content of their study ranged from $0.67w_L$ to $1.33w_L$, and vertical consolidation stress varied from as low as 1 kPa to as high as 1,600 kPa to consider a broad range of consolidation stress. Their studies depicted that the initial water content had a considerable impact on the intrinsic constants for the studied soil. In fact, e_{100}^* and C_c^* increased with increases in the initial water content. Furthermore, the intrinsic constants of the studied clay with smectite as the predominant clay mineral were higher than the estimated values from existing empirical equations.

In summary, it appears that there is considerable influence of clay mineralogy on the intrinsic constants of a reconstituted clay. While some experimental equations have been proposed to estimate the intrinsic constants of reconstituted clays (e_{100}^* and C_c^*) by past researchers (Burland, 1990; Yin & Miao, 2013; Zeng et al., 2015), none of these equations has taken into account the effect of clay mineralogy on the intrinsic constants. Given past research, the main objective of this chapter has been to investigate the effect of clay mineralogy on the value of intrinsic constants, and to suggest some equations for estimating these constants and compressibility based on simple, measureable, physical geotechnical parameters considering the influence of clay mineralogy.

5.3.4 *Estimating the intrinsic constants*

To develop some empirical equations that are able to predict values of the intrinsic constants under different circumstances, a large series of 1-D consolidation test data was collected in this study to include not only diverse initial states and physical properties, but also the variety of clay mineralogy in the predicting relationships. The collected data was then used to derive some regression models based on the availability of the input data. Finally, the proposed model, including the clay mineralogy, was compared to the existing models, and the influence of each parameter in the model on the response was evaluated for various clay minerals.

5.3.5 Experimental data of reconstituted clays

A broad range of experimental data of ninety-four (94) consolidation tests on various reconstituted/remoulded clays, with different mineralogy and initial water contents, was used in this study. A summary of the geotechnical properties, initial state, and references to these tests is tabulated in Table 5-1. Density of soil particles ranged from 2.57 g/cm^3 to 2.80 g/cm^3 and the initial water content varied from 22.4% to 528.7%. The liquid and plastic limits of the studied soils were in the range of 39.8% to 258.9% and 15% to 42.8%, respectively. As can be seen from Table 5-1, the data includes three different clay minerals - kaolinite, illite and smectite.

Figure 5-1 illustrates the compression curves of all these clays in the form of e vs $\log \sigma'_v$ relationship. The initial consolidation stress in the tests was as low as 0.5 kPa and reached high stress levels of 1,600 kPa to 4,000 kPa. As expected, most curves are inverse S-shaped, with a distinct remoulded yield stress. Remoulded yield stress of a reconstituted clay, which is similar to pre-consolidation stress of a natural clay, is a particular stress beyond which the inherent structure of a reconstituted clay breaks down, and the compressibility (the slope of virgin compression line) increases abruptly.

The compression curves of the studied soils are replotted in a normalised plane, using the void index in Figure 5-2 (I_v vs $\log \sigma'_v$). However, there is a considerable disparity between normalised compression curves of reconstituted clays at low stress level; Burland's equation can express these well when the vertical consolidation stress is higher than the vertical consolidation stress at the remoulded yield stress. A new polynomial equation (Equation (5-1)) has also been fitted to the data with the method of least squares (correlation coefficient of 0.93), to refine the existing ICL equations:

$$I_v = 1.906 - 0.392(\log \sigma'_v) - 0.457(\log \sigma'_v)^2 + 0.088(\log \sigma'_v)^3 \quad (5-1)$$

The refined equation, as well as the Burland's equation, has been plotted in Figure 5-2 for comparison. It is noted that Burland's empirical equation has been developed for the reconstituted soils, with e_L lower than 4.44, while the proposed equation used data with e_L up to 7.04. However, Burland's equation and the refined equation are close to each other for the medium level of effective vertical stress (50 to 100 kPa), and even overlap for some stresses in this range. The modified equation becomes slightly more

concave upwards than Burland's equation for consolidation stresses higher than 100 kPa.

Table 5-1. Geotechnical properties of consolidometer tests

Soil Description	w ₀	G _s	w _L	w _P	Chief clay mineral	Clay %	Stress range	No. of tests	Reference
Kleinbell Ton	≥ w _L	2.77	127	36			10-2000 kPa	1	Burland (1990)
London Clay	≥ w _L	2.71	67.5	26.5			10-2000 kPa	1	
Wiener Tegel	≥ w _L	2.76	46.7	22			10-2000 kPa	1	
Baldivis clay	55-109	2.6	82	35	Smectite	68	1-1600 kPa	8	Habibbeygi et al. (2017)
Atchafalaya	101-177	2.8	101	35	montmorillonite	66.6	Up to 2MPa	8	Cerato and Lutenegger (2004)
Boston blue clay	45-79	2.8	45	23	Illite	48.4			
Kaolinite	42-74	2.68	42	26	Kaolinite	36.2			
Kaolin	45-113	2.69	55.3	25.2	Kaolinite	62	0.5-1600kPa	9	Xu and Yin (2015)
Illite	45-104	2.7	52.7	29.6	Illite	40	0.5-1600kPa	10	
Montmorillonite	190-529	2.72	258.9	42.8	Smectite	84	0.5-1600 kPa	8	
Lianyungang clay	50-146	2.71	74	33		23	0.5-1600kPa	14	Hong et al. (2010)
Baimahu clay	64-180	2.65	91	38		20	0.5-1600kPa	14	
Kemen clay	43-122	2.67	61	30		19	0.5-1600kPa	14	
Lin-Gang Clay 1 (undisturbed)	46-124	2.8	56.4	26.5	Illite	55.4	2-827 kPa	4	Lei et al. (2015)
Central Fishing Port Clay (undisturbed)	22.4	2.8	39.8	15	Illite	46		1	
Qing-Fang Clay 1 (undisturbed)	43.4	2.8	40.8	22.1	Illite	38.1		1	
Qing-Fang Clay 2 (remoulded)	43.3							1	

Note: Some geotechnical parameters were not available to the authors which left 'blank' in the table.

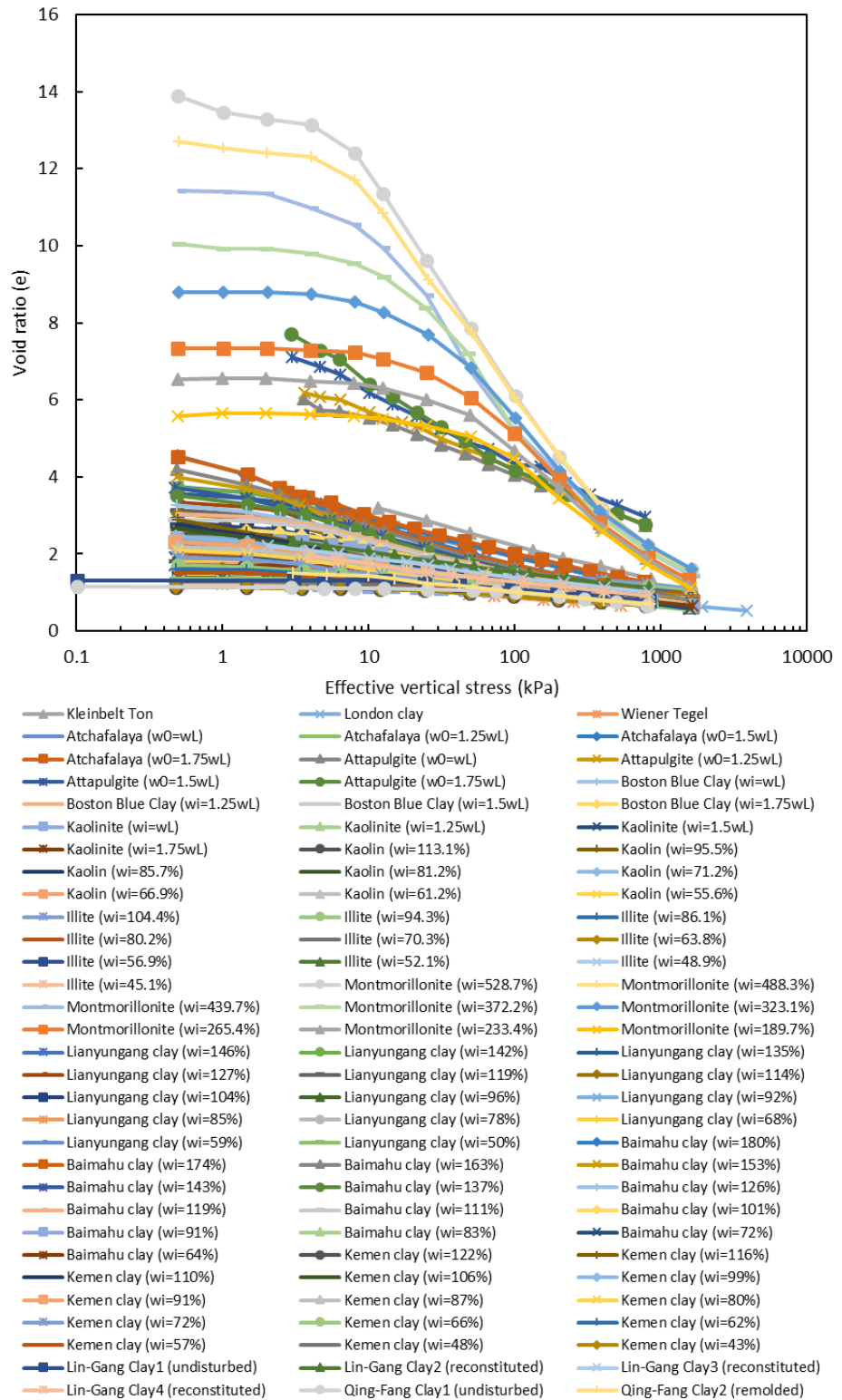


Figure 5-1. Compression curves of the studied clays in e - $\log \sigma'_v$ space (references for experimental data are listed in Table 5-1)

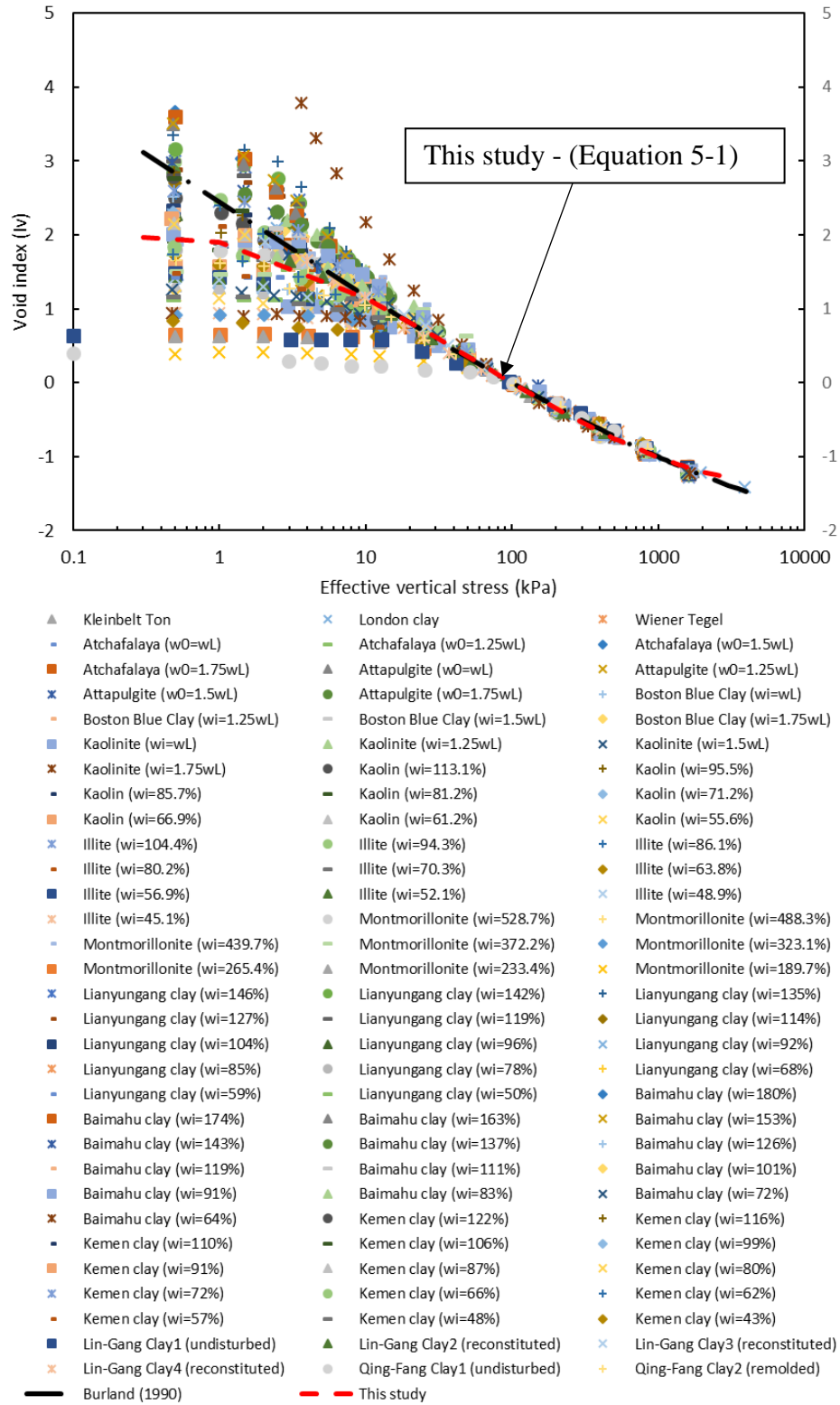


Figure 5-2. Normalised compression curves of the studied clays in I_v - $\log \sigma'_v$ space (references for experimental data are listed in Table 5-1)

5.3.6 Regression models

Following the introduction of the intrinsic concept by Burland (1990), the void index has been used herein to normalise the compression curves and to interpret the compressibility of reconstituted clays. Based on Burland's work, the compressibility of a reconstituted clay can also be estimated by knowing the values of e_{100}^* and e_{1000}^* . These two void ratios can also be used to determine the intrinsic compression index (I_v) and to predict the compression behaviour of a reconstituted clay.

Two simple geotechnical parameters, i.e. the void ratio at initial condition (e_0) and the void ratio at liquid limit (e_L), along with the type of clay mineralogy (CLM), were adopted as predictors to obtain the empirical equations for estimating the intrinsic constants in this study. The following four regression models were developed based on the degree of availability of geotechnical parameters of the investigated soil:

- Model 1: If only the void ratio at the liquid limit (e_L) is available.
- Model 2: If both the void ratio at the liquid limit (e_L) and the initial void ratio (e_0) are known.
- Model 3: If, in addition to the void ratios of (e_0 and e_L), clay mineralogy (CLM) is also available.
- Model 4: A simplified form of Model 3, which is easier to use without losing much accuracy from Model 3.

5.3.6.1 Model 1

Three different regression models were developed to estimate e_{100}^* and e_{1000}^* depending on the information obtainable for the studied reconstituted clay. The first model, which is the simplest one, uses only one parameter, e_L , to estimate the intrinsic parameters. The void ratio at the liquid limit can be calculated by assuming saturated condition for the clayey soil, using the relationship $e_L = G_s \cdot w_L$, where G_s is the specific gravity, and w_L is the liquid limit of the studied clay. The equations (Equations (5-2) to (5-4)) for this model can be summarised as follows:

$$e_{100}^* = 1.167 - 0.334e_L - 0.242e_L^2 - 0.016e_L^3 \quad (5-2)$$

$$e_{1000}^* = 2.093 - 1.712e_L - 0.637e_L^2 - 0.057e_L^3 \quad (5-3)$$

$$C_c^* = -0.926 - 2.046e_L - 0.879e_L^2 - 0.073e_L^3 \quad (5-4)$$

Residual analyses of these two intrinsic parameters are presented in Figure 5-3 to give a comparison of the overall accuracy of the model in predicting intrinsic constants in such a broad range of e_L . The residual of a response can be computed by the subtraction of the measured values and the fitted values. As can be seen from the histogram plots (Figure 5-3a and b), the data have been distributed almost normally for both parameters. Furthermore, their probability graphs lie on a straight line (Figure 5-3c and d), which indicates that there is a reasonably accurate fit for the normally distributed data. The values of R-squared for the regression analyses of e_{100}^* , and e_{1000}^* are as high as 0.978 and 0.931, respectively.

Figure 5-4 shows the plot of residuals of the intrinsic parameters against the fitted values. A large number of fitted values for e_{100}^* are in the range of 1.0 to 2.0, while only some have values greater than 4.0. Similarly, most of e_{1000}^* values range between 0.75 and 0.9, and only a few are above 1.8. The relationship of e_L and the intrinsic constants predicted from this model are illustrated in Figure 5-5. The values of intrinsic constants increase continuously when e_L increases in this model, which is in good agreement with the observed data and the results of past research (Burland, 1990; Hong et al., 2010).

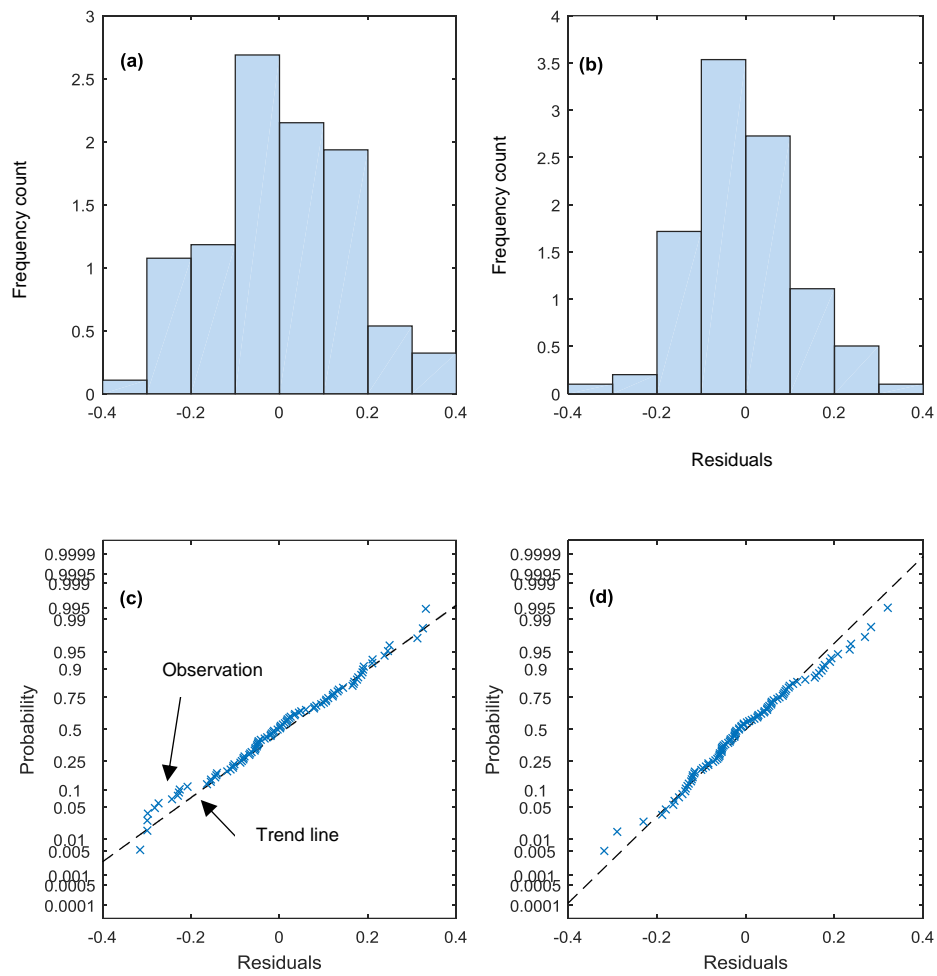


Figure 5-3. Residual graphs of Model 1: (a) histogram plot e_{100}^* (b) histogram plot e_{1000}^* (c) probability graph e_{100}^* (d) probability graph e_{1000}^*

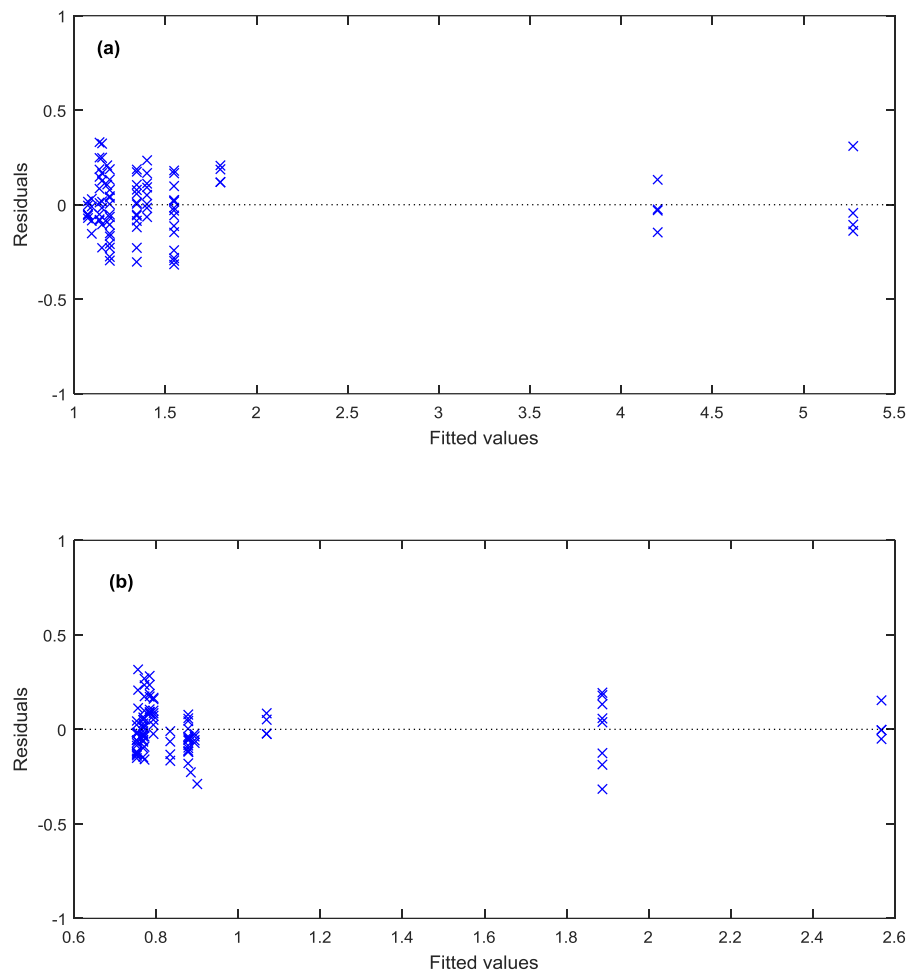


Figure 5-4. Plot of residuals against fitted values of Model 1: (a) e_{100}^* (b) e_{1000}^*

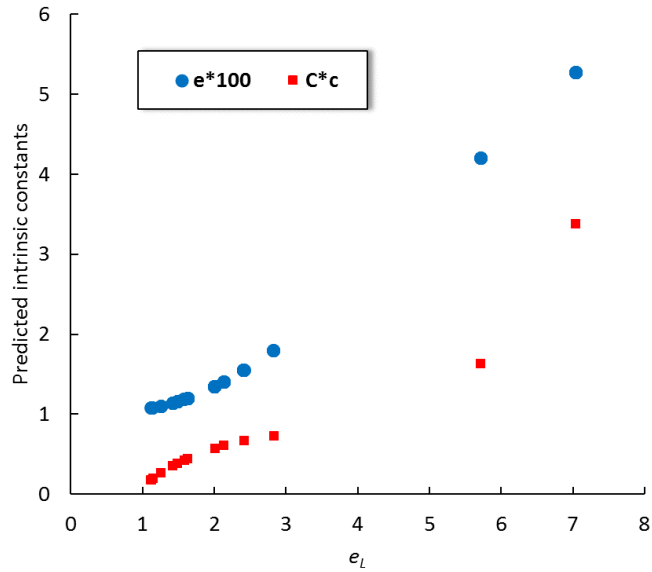


Figure 5-5. Plot of intrinsic constants e^*_{100} and C^*_c against e_L in Model 1

5.3.6.2 Model 2

In Model 2, the effect of initial state has been applied to the model by adding the initial void ratio into the predicting relationships. Equations (5-5) to (5-7) estimate the intrinsic parameters of a reconstituted clay when both initial state (e_0) and e_L are accessible:

$$e^*_{100} = 0.813 + 0.182e_0 - 0.112e_L - 0.001e_0^2 + 0.075e_L^2 \quad (5-5)$$

$$e^*_{1000} = 0.777 + 0.101e_0 - 0.166e_L - 0.003e_0^2 + 0.033e_L^2 \quad (5-6)$$

$$C^*_c = 0.036 + 0.081e_0 + 0.054e_L + 0.002e_0^2 + 0.042e_L^2 \quad (5-7)$$

Similar to Model 1, Figure 5-6 shows the results of residual analyses for this model. The data are slightly skewed to the right in Model 2 for both intrinsic parameters (Figure 5-6a and b). The probability graphs (Figure 5-6c and d) are almost linear, which indicates normally distributed data were accurate enough. The values of R-squared for the regression analyses of e^*_{100} , and e^*_{1000} are considerably high, 0.987 and 0.877, respectively. The values of residuals of the intrinsic parameters are plotted in Figure 5-7. As can be seen from this figure, the residuals are distributed well around the line of zero residual (horizontal line). Moreover, residuals for this model are less than related values for Model 1. Hence, the accuracy of prediction has been increased

by having a better understanding of the initial state (i.e. the initial water content) of the investigated soil.

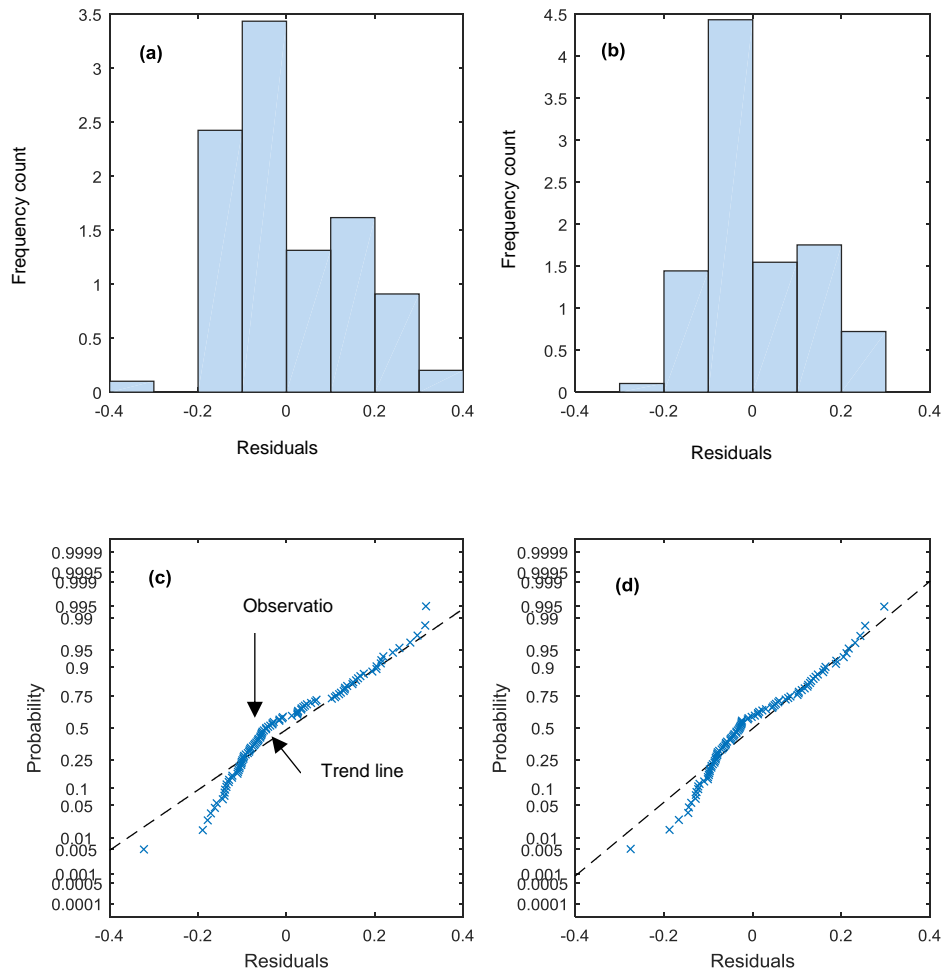


Figure 5-6. Residual graphs of Model 2 : (a) histogram plot e_{100}^* (b) histogram plot e_{1000}^* (c) probability graph e_{100}^* (d) probability graph e_{1000}^*

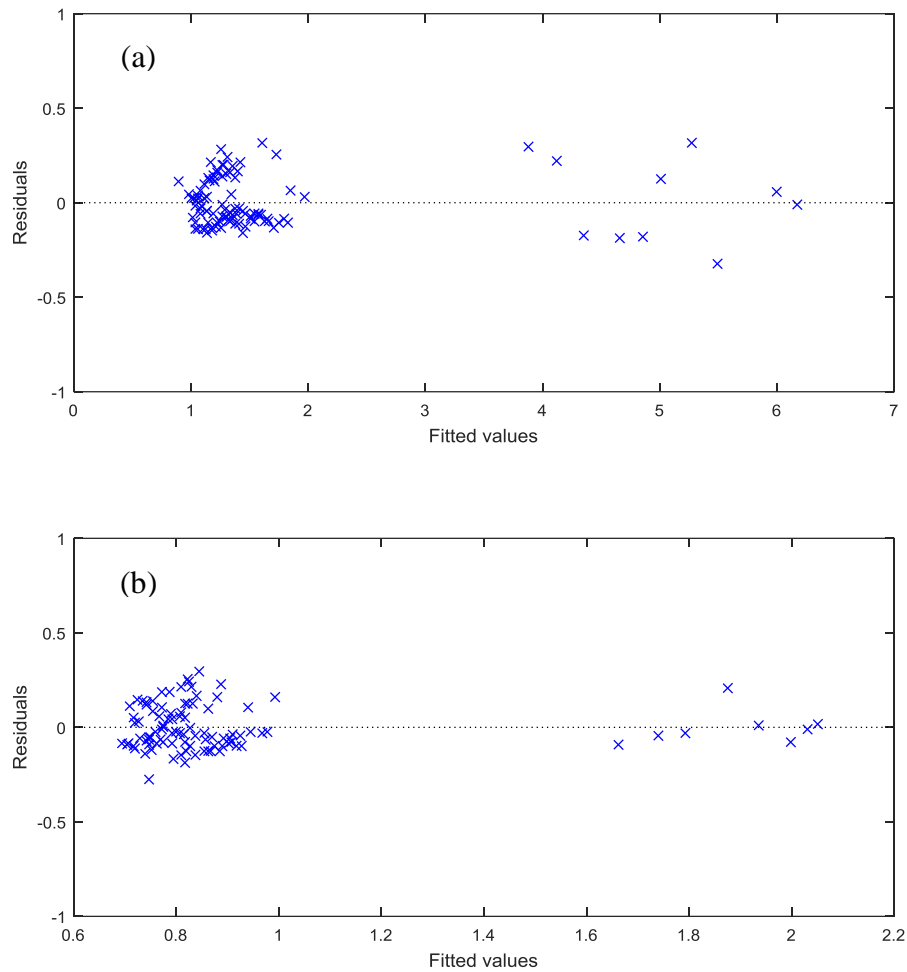


Figure 5-7. Plot of residuals against fitted values of Model 2: (a) e_{100}^* (b) e_{1000}^*

5.3.6.3 Model 3

In the third model, which is the most sophisticated model to predict intrinsic constants, in addition to initial state parameters, e_0 and e_L , the clay mineralogy is also included. Clay mineralogy of the investigated soil was assumed to be represented by its most predominant clay mineral. Clay was implied into the regression analysis by a dummy parameter named CLM. Intrinsic equations and the values of dummy parameters of CLM_1 to CLM_3 , depending on the type of principal clay mineral, are presented as follows in Equations (5-8) to (5-10):

$$e_{100}^* = CLM_1 + 0.2e_0 - 0.208e_L - 0.002e_0^2 + 0.081e_L^2 \quad (5-8)$$

$$e_{1000}^* = \text{CLM}_2 + 0.111e_0 - 0.209e_L - 0.003e_0^2 + 0.035e_L^2 \quad (5-9)$$

$$C_c^* = \text{CLM}_3 + 0.081e_0 + 0.054e_L + 0.002e_0^2 + 0.042e_L^2 \quad (5-10)$$

$$\text{CLM}_1 = \begin{cases} 0.956 & \text{for chief clay mineral of kaolinite} \\ 0.887 & \text{for chief clay mineral of illite} \\ 1.094 & \text{for chief clay mineral of smectite} \end{cases}$$

$$\text{CLM}_2 = \begin{cases} 0.862 & \text{for chief clay mineral of kaolinite} \\ 0.796 & \text{for chief clay mineral of illite} \\ 0.924 & \text{for chief clay mineral of smectite} \end{cases}$$

$$\text{CLM}_3 = \begin{cases} 0.094 & \text{for chief clay mineral of kaolinite} \\ 0.091 & \text{for chief clay mineral of illite} \\ 0.170 & \text{for chief clay mineral of smectite} \end{cases}$$

It is much easier to use the Wilkinson notation to express the regression equations (Wilkinson & Rogers, 1973), as it is a very powerful notation in presenting a complex regression model. The notation is used to present a model in terms of response and predictors in the form of a simple equation with a table of predictor coefficients. In this notation, '1' stands for constants and each predictor is separated with a symbol of '+'. If there is a powered predictor in the equation, it means that all lower order terms of the predictor are included in the equation, unless otherwise noted. By using this notation, Equations (5-8) to (5-10) can be summarised to a single equation, Equation (5-11). The coefficients of predictors (e_0 , e_L , e_0^2 , e_L^2 , and CLM) for this relationship are tabulated in Table 5-2. CLM is the categorical invariant of clay mineralogy and can be expressed in this model by two dummy variables, CLM_K and CLM_M .

$$e_{100}^*, e_{1000}^*, C_c^* \sim 1 + \text{CLM} + e_0 + e_L + e_0^2 + e_L^2 \quad (5-11)$$

Similar to the two previous models, the data have also been distributed normally in this model for both intrinsic parameters (Figure 5-8a and b), and the probability graphs (Figure 5-8c and d) are also practically linear. The R-squared values for the regression analyses of e_{100}^* , and e_{1000}^* are 0.99 and 0.896, respectively. As can be seen in Figure 5-9, the residuals are well distributed normally around the zero residual line.

Table 5-2. Predictor coefficients of Model 3

Coefficients	e_{100}^*	e_{1000}^*	C_c^*
Constants	0.887	0.796	0.091
e_0	0.200	0.111	0.081
e_L	-0.208	-0.209	0.054
CLM_K	0.069	0.066	0.003
CLM_M	0.207	0.128	0.079
e_0^2	-0.002	-0.003	0.002
e_L^2	0.081	0.035	0.042

where CLM_K , and CLM_M are 1.0 when the principal clay of the studied soil is Kaolinite and Smectite respectively, otherwise they are zero.

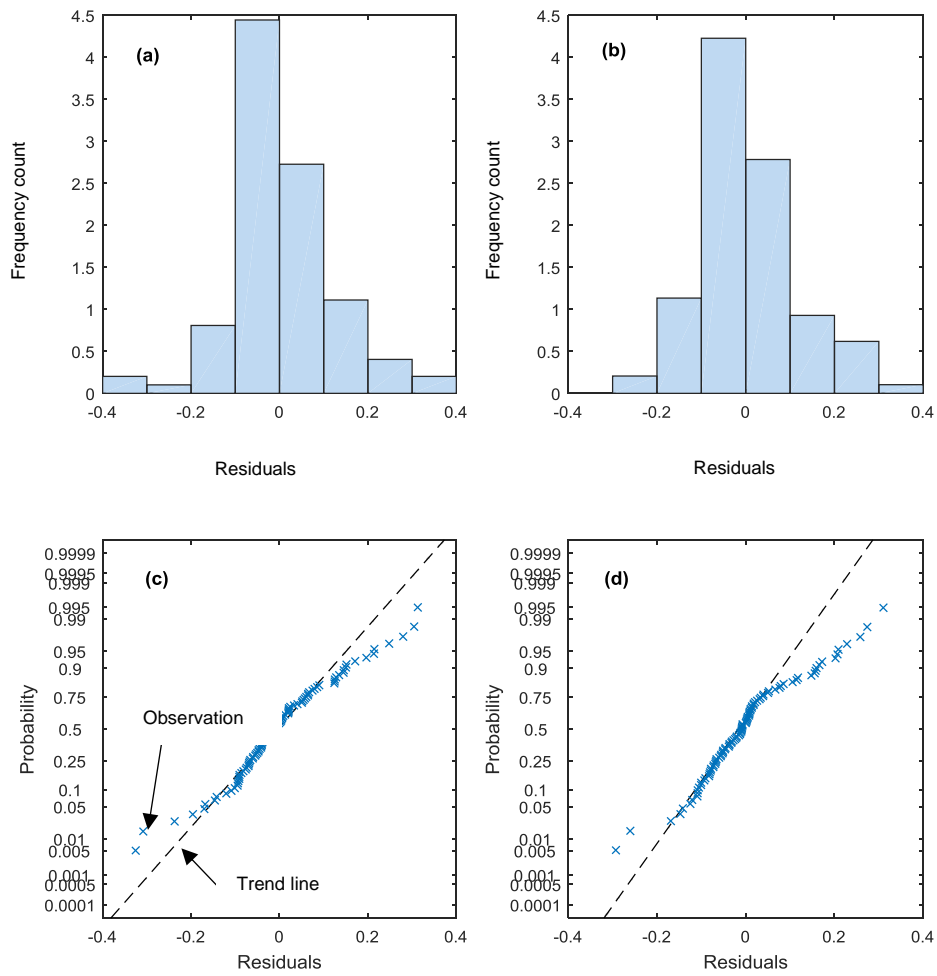


Figure 5-8. Residual graphs of Model 3 : (a) histogram plot e_{100}^* (b) histogram plot e_{1000}^* (c) probability graph e_{100}^* (d) probability graph e_{1000}^*

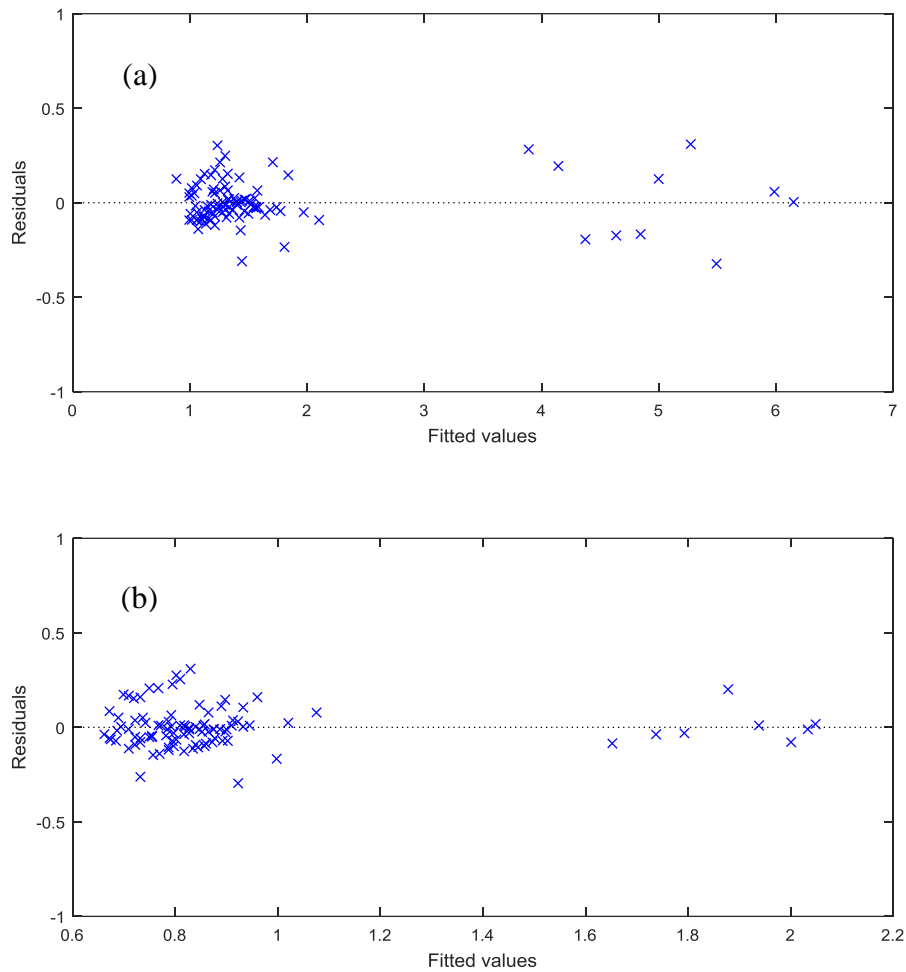


Figure 5-9. Plot of residuals against fitted values of Model 3 : (a) e_{100}^* (b) e_{1000}^*

5.3.6.4 Model 4

Model 4 is a simplified version of Model 3. The model still considers the clay mineralogy, initial state, and properties of the studied soil, yet it retains its simplicity. Despite the fact the model is simple, it still has good accuracy in predicting the intrinsic parameters of e_{100}^* and e_{1000}^* . The correlation coefficients of R-squared are 0.99 and 0.85 for e_{100}^* and e_{1000}^* , respectively.

$$e_{100}^* \sim 1 + e_0 + e_0 : \text{CLM} + e_L : \text{CLM} + e_L^2 + e_0^2 \quad (5-12)$$

$$e_{1000}^* \sim 1 + e_L + e_L : \text{CLM} \quad (5-13)$$

Wilkinson notation has been used to express Equations(5-12) and (5-13). A symbol of ‘:’ means only the product of two predictors without the lower order terms of the predictor. The coefficient of each predictor and dummy variables are presented in Table 5-3.

Similar to the two previous models, the data have also been distributed normally in this model (Figure 5-10a and b), and the probability graphs (Figure 5-10c and d) are practically linear. The R-squared values for the regression analyses of e_{100}^* , and e_{1000}^* are 0.99 and 0.84, respectively. The normally distributed residuals around the zero residual line in Figure 5-11 indicate the good ability of the model to estimate the intrinsic constants.

Table 5-3. Predictor coefficients of Model 4

Coefficients	e_{100}^*	Coefficients	e_{1000}^*
Constants	0.696	Constants	0.502
e_0	0.157	e_L	0.147
e_0 : CLM _K	0.139	e_L : CLM _K	0.092
e_0 : CLM _{MM}	-0.096	e_L : CLM _{MM}	0.059
e_L : CLM _K	-0.110		
e_L : CLM _{MM}	0.215		
e_0^2	0.005		
e_L^2	0.040		

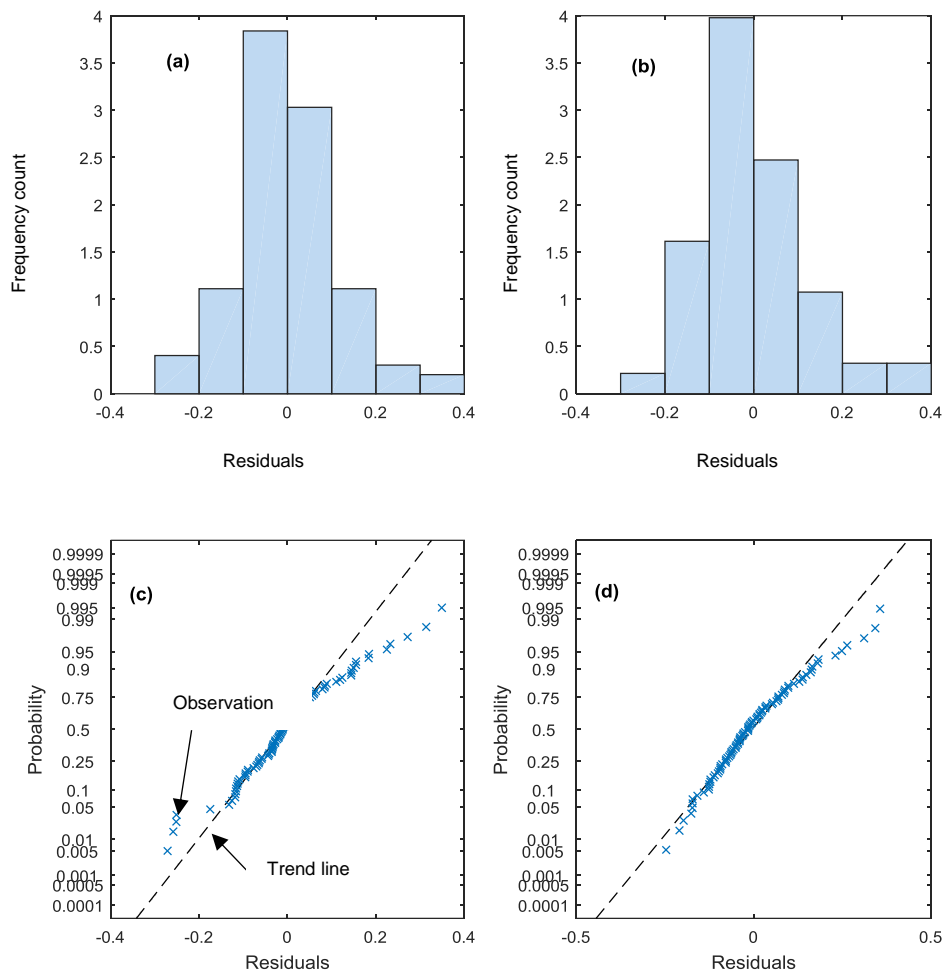


Figure 5-10. Residual graphs of Model 4 : (a) histogram plot e_{100}^* (b) histogram plot e_{1000}^* (c) probability graph e_{100}^* (d) probability graph e_{1000}^*

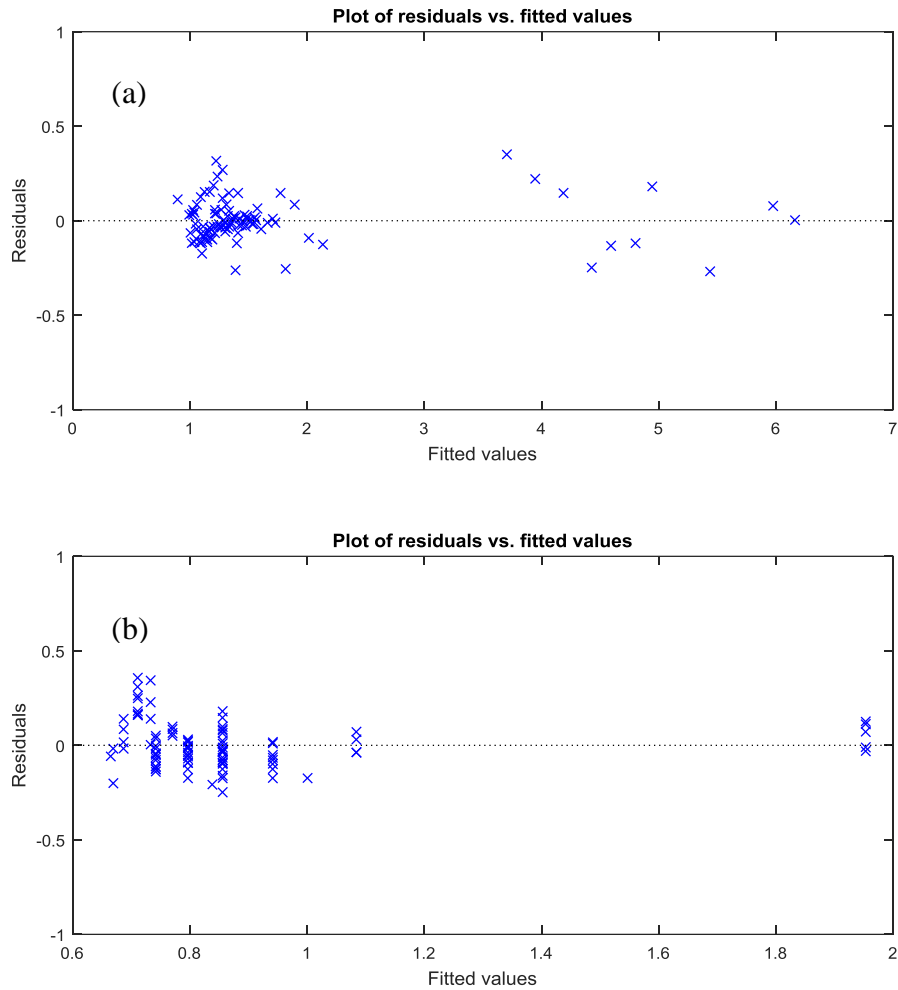
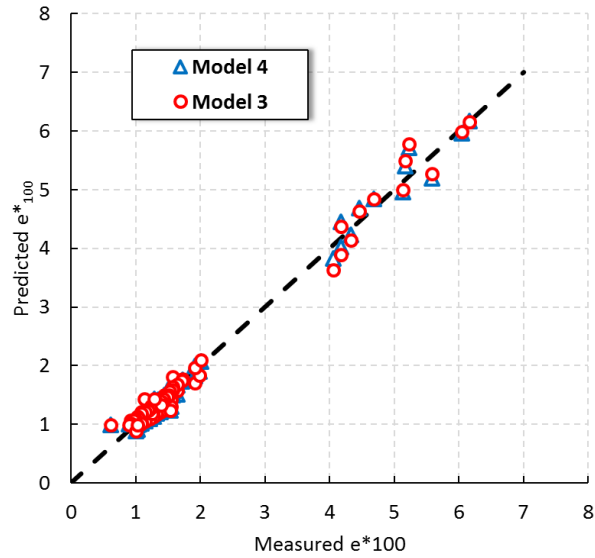


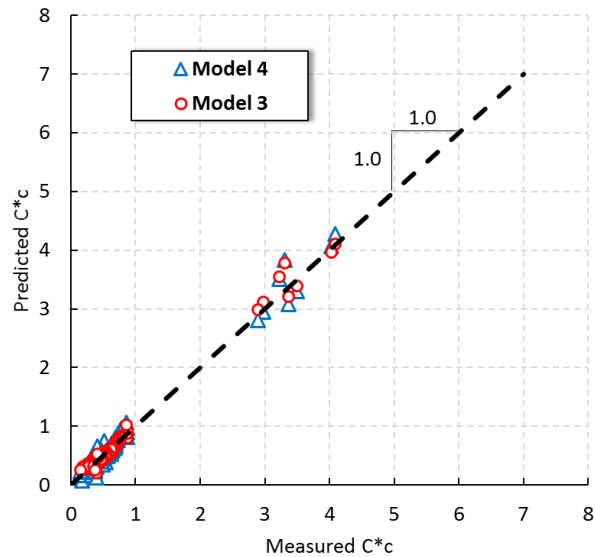
Figure 5-11. Plot of residuals against fitted values of Model 4 : (a) e_{100}^* (b) e_{1000}^*

5.3.7 Comparison and discussion

A comparison of the ability of the proposed models to predict intrinsic constants has been presented in this section. Figure 5-12 demonstrates the values of predicted e_{100}^* and C_c^* against the related measured values obtained from the experimental data. It can be seen that the estimated values of e_{100}^* and C_c^* are in good agreement with the observed values. Moreover, Model 4 can estimate the parameters accurately even though it has relatively lesser order of terms of predictors than Model 3.



(a)



(b)

Figure 5-12. Comparison of predicted intrinsic constants and measured ones : (a) e_{100}^* (b) C_c^*

The dataset reported by Habibbeygi, Nikraz, and Chegenizadeh (2017) was used to compare the different empirical equations existing in the literature. The e_{100}^* and C_c^* values of Baldivis clay, estimated for different conditions of initial water content, are plotted in Figure 5-13. The geotechnical and physical parameters for the studied clay are presented in Table 5-1. According to Burland’s equation, intrinsic constants are independent of the initial state (for example, e_0 or w_0). Zeng et al. (2015) modified Burland’s equation to consider the effect of the initial state. The values estimated by equations suggested by Zeng et al. (2015) increase with an increase in the value of w_0 , in a trend similar to the observed values. However, both these equations underestimate

the intrinsic constants of the investigated clays with a considerable amount of smectite in its mineralogy. On the other hand, as depicted in Figure 5-13, the estimated values of intrinsic constants using the proposed model of this study are higher than the predicted values from other methods, and are close to the observed values. Thus, the predicted intrinsic constants from the proposed model are in good agreement with the measured constants for the investigated clay.

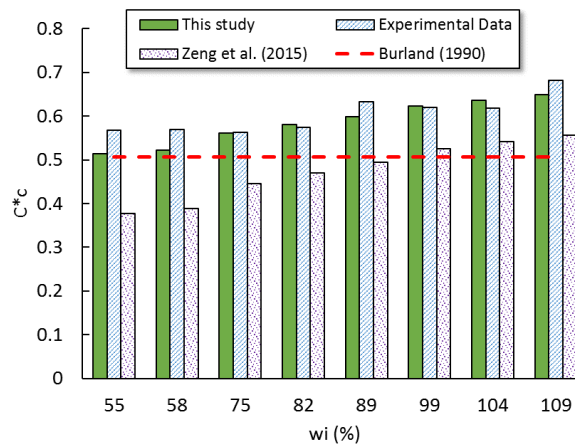
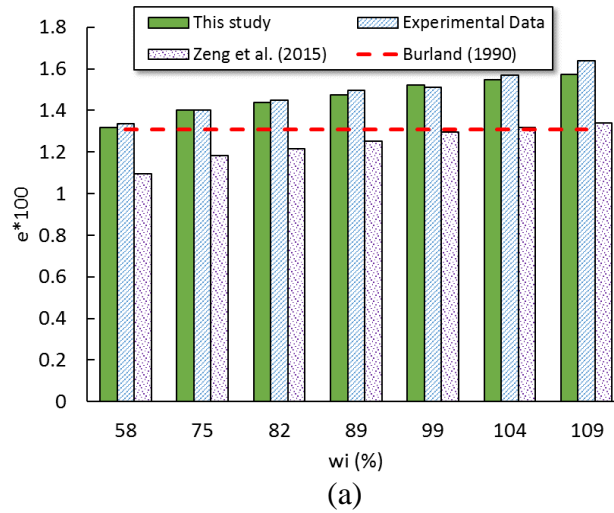


Figure 5-13. Comparison of predicted intrinsic constants by different methods for Baldvis clay : (a) e^*_{100} (b) C^*_c

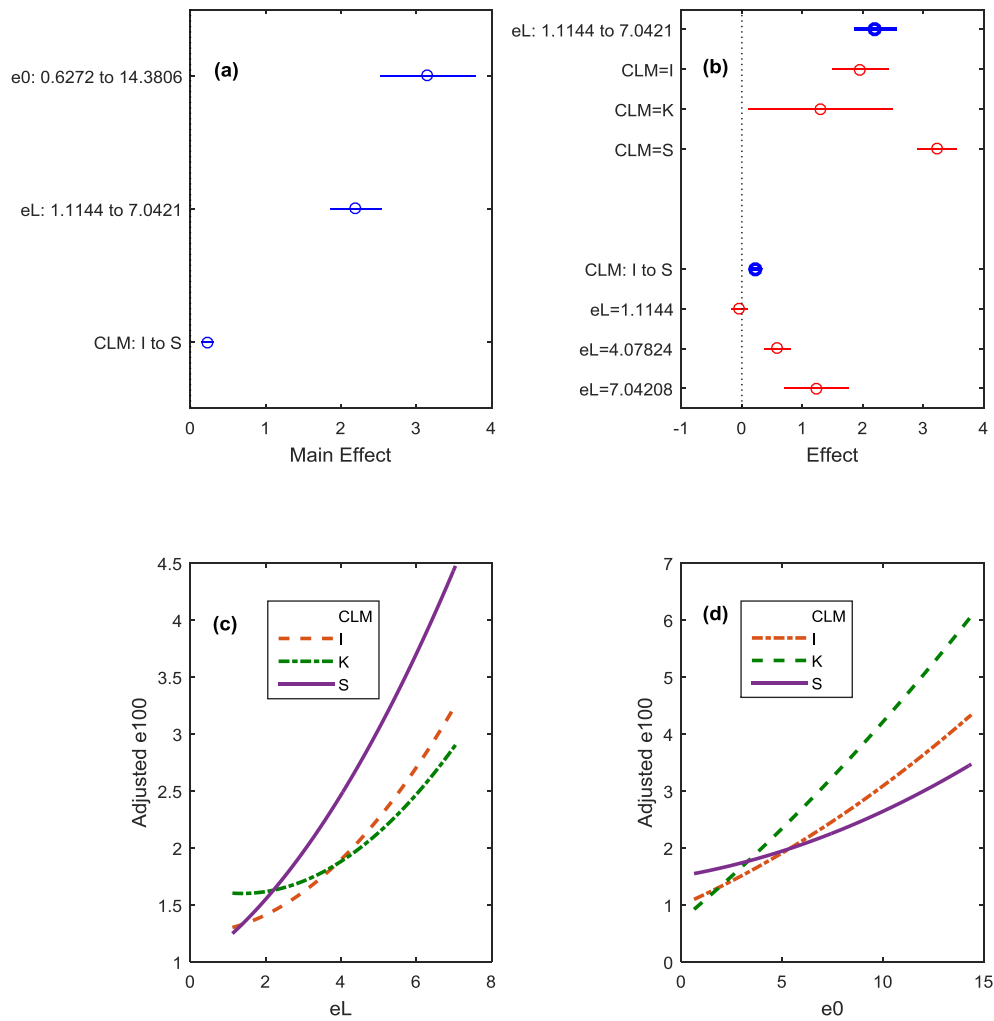


Figure 5-14. The effect of predictors on e_{100}^* (I: illite, K: kaolonite, S: smectite): (a) predictor effect (b) predictor effect with CLM (c) e_L effect (d) e_0 effect

The effect of each predictor on the response of the proposed model has been examined for Model 4. Figure 5-14 presents the influence of a change in each predictor on e_{100}^* . As can be seen from Figure 5-14a, the change in e_0 has the greatest effect on e_{100}^* among other predictors. It shows that changing e_0 from 0.63 to about 14 increases e_{100}^* by about 3. Moreover, it also shows that changing e_L from 1.11 to 7 raises e_{100}^* by about 2. Figure 5-14b shows the interaction plot for observing the effect of changing one predictor while keeping others fixed. For example, the increase in e_L (from 1.11 to 7.0) is much more effective on the growth of e_{100}^* when the principal mineral of clay is smectite, with an increase of 3, whereas the increase of e_{100}^* is two (2) when the principal clay mineral is illite. Interaction graphs for e_0 and e_L are plotted in

Figure 5-14c and d for comparison. The increase in both e_0 and e_L lead to an increase in e_{100}^* , but with different rates for different clay minerals. For example, the rate of increase of e_{100}^* with e_0 for smectite is the lowest. On the other hand, the rate of increase of e_{100}^* with the increase of e_L is the highest in smectite. In Model 4, e_{1000}^* is only a function of e_L and its mineralogy. The effect of the variation of these predictors are plotted in Figure 5-15. While the increase in e_L leads to an increase in e_{1000}^* , the variation is the least for illite, with a growth of about 0.8.

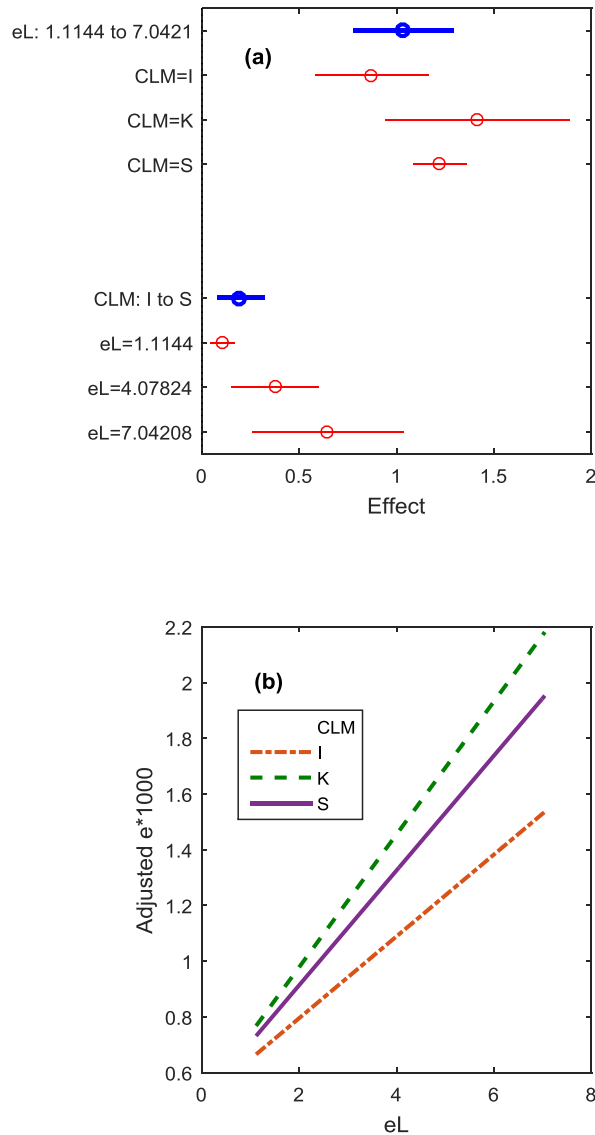


Figure 5-15. The effect of predictors on e_{1000}^* (I: illite, K: kaolinite, S: smectite):
 (a) predictor effect (b) e_L effect

5.3.8 Virgin compression line estimation

An advantage of using the void index for normalisation is that it allows estimation of compression curves without performing consolidation tests. In other words, the virgin compression line (VCL) of a reconstituted clay can be determined by substituting the modified equation of ICL (Equation (5-1)) into the void index definition equation (Equation (2-3)) as follows:

$$e = C_c^*(1.906 - 0.392x - 0.457x^2 + 0.088x^3) + e_{100}^* \quad \text{For } \sigma'_v \geq \sigma'_{yr} \quad (5-14)$$

where $x = \log \sigma'_v$; σ'_v is in kPa, and σ'_{yr} is the remoulded yield stress of a reconstituted clay. This equation can be used for a broad range of e_L (1.1 to 7.0) and the initial state of e_0 (0.63 to 14.38).

Depending on the availability of information about the studied soil, intrinsic constants of e_{100}^* and e_{1000}^* can be calculated from any of the four models – Models 1 to 4. In cases where the three main physical parameters of clay mineralogy, the initial void ratio and the void ratio at liquid limit are available, Equations (5-8) and (5-10) can be used. Otherwise, if clay mineralogy is not known with any degree of accuracy, either groups of equations, Equations (5-2) to (5-4) or Equations (5-5) to (5-7), can be used for two different conditions of accessibility to the initial state. Moreover, the void ratio at liquid limit can always be computed by knowing the specific gravity of the investigated soil and the liquid limit. Therefore, the VCL of a reconstituted clay can be computed indirectly, without performing time-consuming laboratory 1-D consolidation tests, by knowing simple physical geotechnical parameters.

To sum up, the steps are as follows:

- First determine the initial state, including clay mineralogy and the liquid limit of the studied soil;
- Secondly, the intrinsic parameters should be estimated by using one of the four proposed models – Models 1 to 4 – based on the degree of understanding of the initial state; and
- Finally, the VCL can be determined by Equation (5-14).

The ICL calculated by this method has been plotted for Baldivis clay in Figure 5-16 for consolidation stress greater than 100 kPa (i.e. stress range higher than the remoulded yield stress of Baldivis clay).

Figure 5-16 identifies that the refined equation of the void index can satisfactorily predict the void index of the studied reconstituted clay for stresses higher than the remoulded yield stress. Predicted values of the void ratio of Baldivis clay using this method are illustrated in Figure 5-17 for models 3 and 4. As can be seen, there is good agreement between the measured values and predicted values for both models. The estimated void ratios are in the range of $\pm 10\%$ of the observed value for the studied soil.

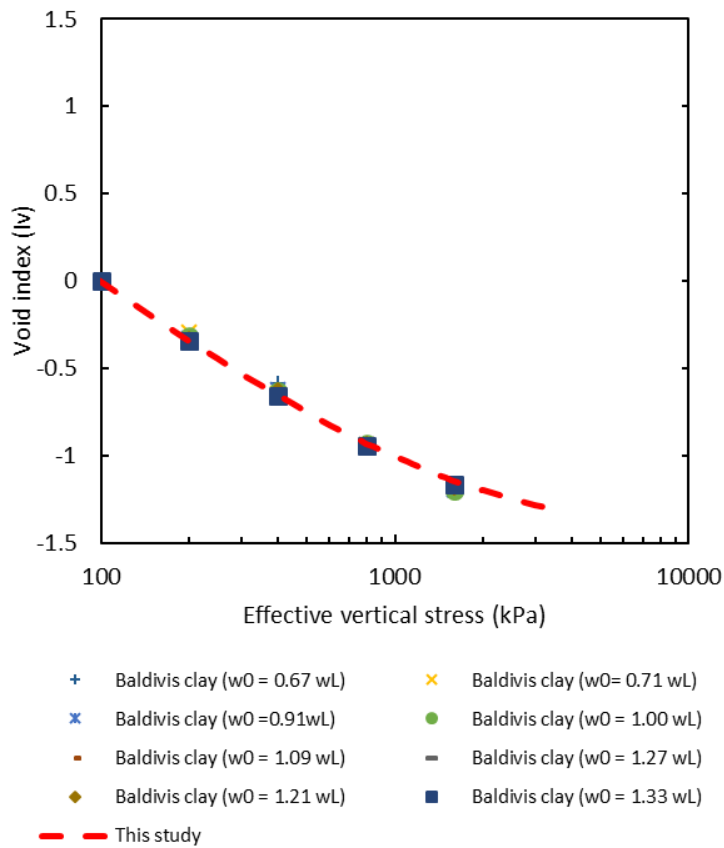
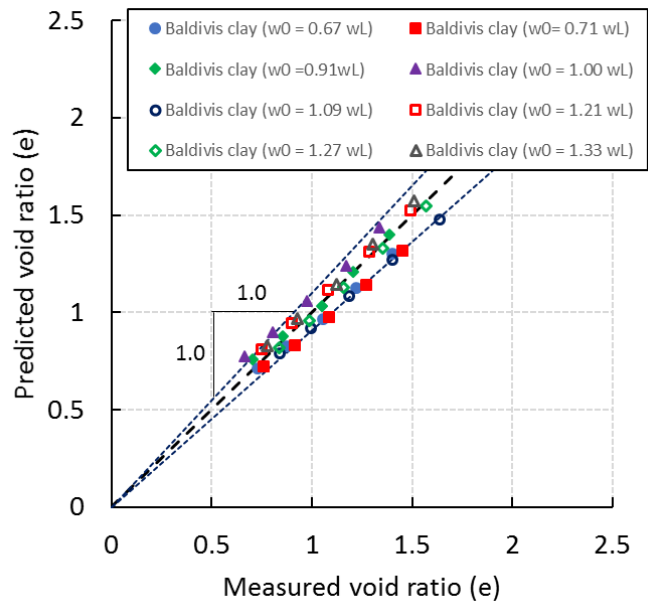
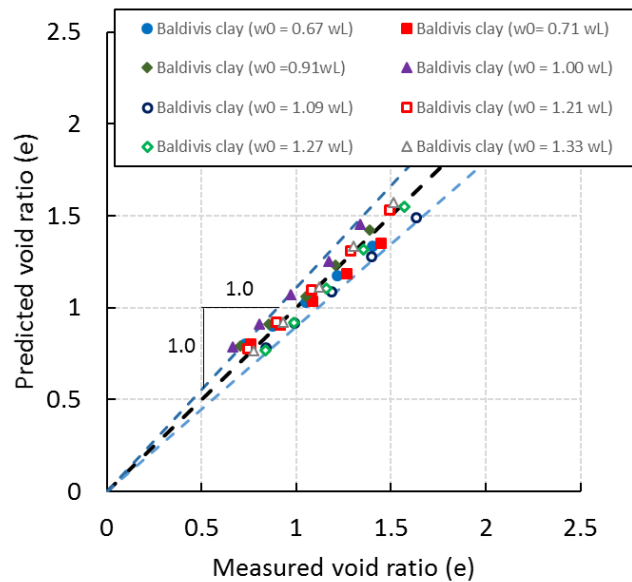


Figure 5-16. Intrinsic compression line of Baldivis clay in I_v - $\log \sigma'_v$ space (reference for experimental data is listed in Table 5-1)



(a)



(b)

Figure 5-17. Comparison of estimated and observed void ratios for Balddivis clay
(a) Model 3 (b) Model 4

5.3.9 Conclusions

Based on the intrinsic concept, the compression behaviour of a reconstituted clay can be estimated if the intrinsic constants are known. Four regression models are proposed for estimating the intrinsic constants based on the degree of available data for the studied clay. The proposed models use the maximum advantage of the available data so that when enough information is obtainable, accuracy increases significantly. The results show that the clay mineralogy of a reconstituted clay has a considerable impact

on the values of intrinsic constants. The effect of each predictor on the response of the suggested model is also investigated in this chapter. The results show that, however, e_{100}^* increases with an increase in e_L for all types of clay minerals, but the increase is greatest in clays with smectite in their mineralogy. On the other hand, it seems that e_0 has a lesser effect on e_{100}^* for a clay with smectite as its principal mineral as compared to other clay minerals. The refined equation of the void index is also used to predict the compression behaviour of a reconstituted clay from Baldivis, Western Australia. The results show that the predicted void ratios are in good agreement with measured values from consolidation tests for a wide range of initial water content.

6 DETERMINATION OF THE COMPRESSION INDEX OF RECONSTITUTED CLAYS USING INTRINSIC CONCEPT AND NORMALISED VOID RATIO

6.1 Introduction

This peer-reviewed manuscript reviews the existing experimental relationship for predicting the compression index of reconstituted clays. Then, a new relationship based on the experimental results and the intrinsic concept is proposed.

The list of references, keywords, and acknowledgements were excluded from this manuscript. The acknowledgements, abbreviations and references are combined on pages vi, xxiv and 192 of the current manuscript, respectively.

Minor changes were made for the inclusion of the published manuscript into the current document. The differences comprise removing repetitions, referencing, style and numbering of table captions and figure captions, wherever it was necessary to keep the uniformity and consistency of the current document. Repetitions comprise equations and literature reviews which have already been addressed in Chapter 2. Thus, some equations may refer to Chapter 2. Furthermore, the numbering of equations, figures and tables follow the current manuscript numbering and may differ from those of the published manuscript.

6.2 Citation

Habibbeygi, F., Nikraz, H., & Verheyde, F. (2017). Determination of the compression index of reconstituted clays using intrinsic concept and normalised void ratio. *International Journal of GEOMATE*, 13(39), 54-60. <https://doi.org/10.21660/2017.39.98271>

6.3 Manuscript Contents

6.3.1 Abstract

Measurement of the compression indices of clayey soils, particularly reconstituted clays with a high initial water content, is generally time-consuming and costly. A mitigation of these constraints could include a correlation between the compression indices and the consistency limits of the clay soil that can be measured reliably. In

this chapter, the time-tested concepts of intrinsic framework and normalisation methods were used to derive a correlation between the compression indices of reconstituted clays and the soil void ratios at consistency limits. The proposed method is based on the assumption that a unique relationship exists between consolidation pressures and consistency limits. Furthermore, the equation was simplified to estimate the compression index as a function of consistency limits. Then, the equation was validated via comparison with a wide range of results reported in the literature regarding various types of clay. Results of this comparison suggest that there is an exclusive relationship between compression index and consistency limits for reconstituted clays.

6.3.2 Introduction

The compression characteristic of soils, is a critical parameter in geotechnical engineering for the prediction of the settlement of structures, in particular if the foundation material is a clayey soil (Hough, 1957; Skempton & Jones, 1944; Terzaghi & Peck, 1967). The rate of consolidation of a clayey layer can be identified by its compressibility, which is often expressed in terms of void ratio and effective vertical stress (Das, 2013). The slope of the linear portion of a compression curve (Figure 6-1), which is usually referred to as ‘Virgin Compression Line’ (VCL), is often used to represent the compressibility behaviour of a soil (Das, 2013).

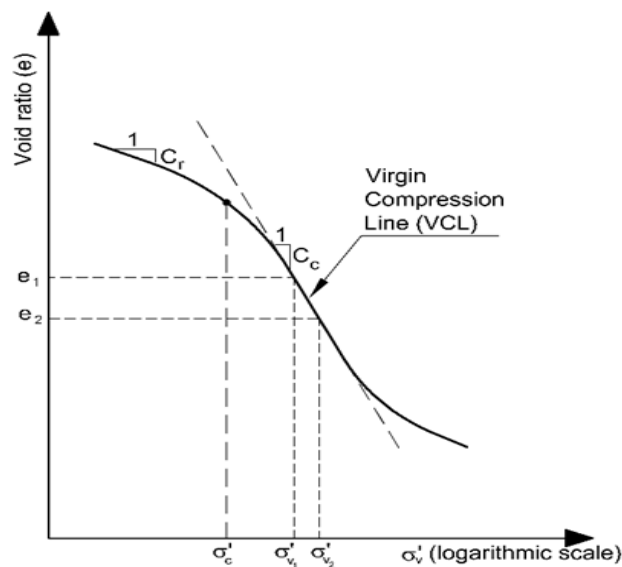


Figure 6-1. Schematic plot of a compression curve in e - $\log \sigma'_v$ space (Redrawn from (Das, 2013))

Existing equations have been already addressed in Chapter 2. Thus, the equations and literature review have been removed from this chapter to avoid repetition. Compressibility can be conventionally determined by laboratory or field tests (Das, 2013; Skempton & Jones, 1944). However, such tests are cumbersome and expensive. They are particularly difficult for reconstituted samples such as marine clays that have been prepared at a water content greater than their liquid limit (Arulrajah et al., 2005; Bo et al., 2011). Therefore, it may be useful to estimate the compression index by simply measuring soil classification parameters such as liquid limit, plastic limit, natural water content, in situ void ratio, or porosity (Cozzolino, 1961). These parameters can also be measured reasonably accurately in most traditional geotechnical laboratories without the requirement for sophisticated testing. In the past six to seven decades, many researchers have proposed empirical relationships for a broad range of soil types and sample conditions to predict soil compressibility using the previously-mentioned geotechnical parameters (Azzouz et al., 1976; Bowles, 1989; Cozzolino, 1961; Herrero, 1983; Hough, 1957; Nacci et al., 1975; Nagaraj & Miura, 2001; Nagaraj & Murthy, 1983; Nagaraj et al., 1995; Nagaraj et al., 1985; Nath & Dedalal, 2004; Ogawa, 1978; Park & Koumoto, 2004; Skempton & Jones, 1944; Sridharan & Nagaraj, 2000; Terzaghi & Peck, 1967; Wroth & Wood, 1978). To name a few, a summary of some of these relationships is provided in Table 2-3.

Most empirical relations are supposed to estimate a soil compression index under a wide range of conditions. However, representing a unique equation to reliably estimate the compression index (C_c) for all types of soil classifications and soil states is almost impractical due to the complexity of soil structures, mineralogy, and inevitable sample disturbance. Thus, any suggested equation must be used carefully and be suited to the relevant soil conditions. In fact, the assessment of the compression index (C_c) for a clayey soil (which is determined by laboratory oedometer tests) is highly influenced by the soil state. Another parameter that affects the compression behaviour of clays is the sampling procedure. Sampling disturbance has an especially great impact on sensitive clays with compression curves that are no longer linear. It is now well established that compression curves for reconstituted clays are non-linear (Habibbeygi, Nikraz, & Chegenizadeh, 2017; Hong et al., 2010). However, there are several different relationships used to link compression index to consistency limits, and only a few have been developed especially for high level of moisture content. To the authors' knowledge, there is also a lack of experimental data for predicting the

compression index of a soil with high initial water content. In the present research, a new equation for estimating the compression index of reconstituted clays is proposed, using the intrinsic and normalisation concepts. First, a regression normalisation line is proposed based on the results of one-dimensional consolidation tests on four studies that were performed on reconstituted clays. Then an empirical equation is derived by using the equation of normalisation line as well as the theoretical criterion for shear strength at consistency limits proposed by Wroth and Wood (1978). Finally, the derived equation is validated using a broader range of data available from the literature regarding clayey soils with different mineralogy, soil conditions and soil classifications to evaluate the applicability of the equation to other clays.

6.3.3 Normalising compression curves of reconstituted clays

The concept of using void ratio at the liquid limit to normalise compression results was originally proposed by Nagaraj and Murthy (1983, 1986). In this study, nineteen series of compression data from seven different reconstituted clays were used to plot normalised compression curves (graph of normalised void ratio versus effective vertical stress) within the stress range of 50 to 2000 kPa. Geotechnical parameters, such as consistency limits and specific gravity values from the consolidation database, are tabulated in Table 6-1. Liquid and plastic limits (w_L , w_P) of the studied soils ranged from 42% to 200% and 23% to 108%, respectively; plasticity index (I_P) varied broadly, from 16% to 94%; specific gravity (G_s) ranged from 2.60 to 2.83. Compression curves of the investigated soils are presented in Figure 6-2 (a) in the form of void ratio versus effective vertical stress in a semi-logarithmic plane. Consolidation data is also normalised in Figure 6-2 (b) using normalised void ratio (e/e_L). As illustrated in Figure 6-2 (b), for consolidation stresses greater than 50 kPa, compression curves are confined within a narrow band of e/e_L against vertical consolidation stress (σ'_v) in a semi-log plane. Moreover, the equation of the narrow band can be fitted with a straight line with an acceptable correlation coefficient ($R^2 = 0.96$) as follows:

$$e/e_L = 1.3402 - 0.3162 \log \sigma'_v \quad (6-1)$$

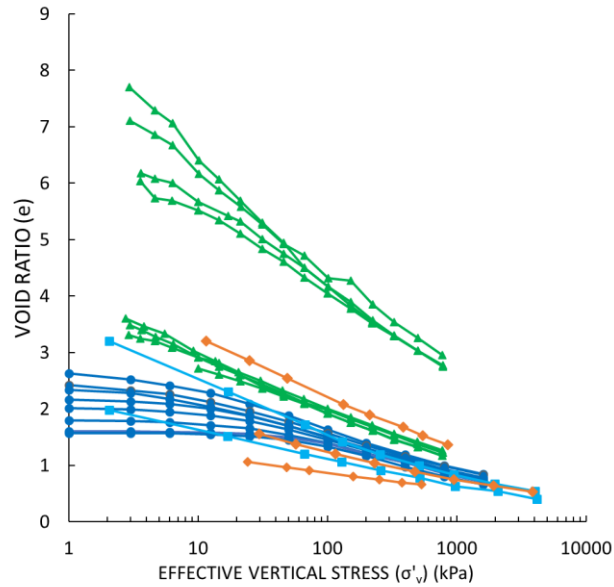
where e is the void ratio, e_L is the void ratio at the liquid limit, and σ'_v is the effective vertical stress in kPa.

Chapter 6 - Determination of the compression index of reconstituted clays using intrinsic concept and normalised void ratio

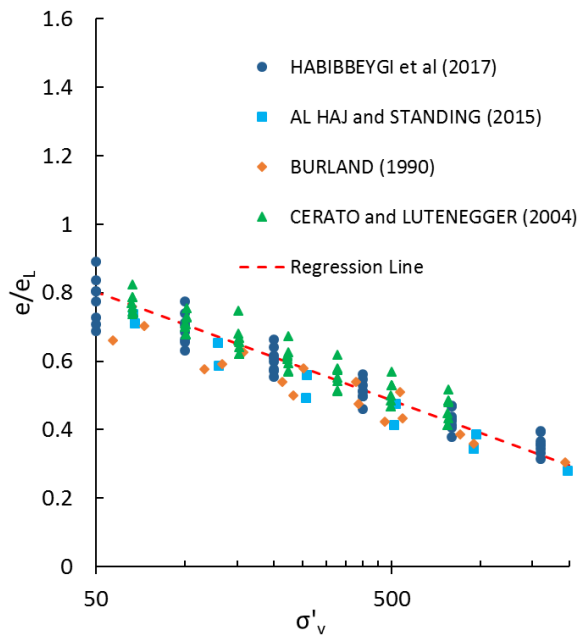
Table 6-1. Geotechnical parameters of the studied soils

Soil Description	w_L (%)	w_P (%)	I_P (%)	G_s	Reference
Kleinbelt Ton	127	36	91	2.77	(Burland, 1990)
London clay	67	27	40	2.71	(Burland, 1990)
Wiener Tegel	47	22	25	2.76	(Burland, 1990)
Black soil	60	30	30	2.72	(Al Haj & Standing, 2015)
Red soil	87	33	54	2.78	(Al Haj & Standing, 2015)
Kaolinite	42	26	16	2.68	(Cerato & Lutenegro, 2004)
Boston Blue clay	45	23	22	2.80	(Cerato & Lutenegro, 2004)
Atchafalaya	101	35	66	2.80	(Cerato & Lutenegro, 2004)
Attapulgate	202	108	94	2.83	(Cerato & Lutenegro, 2004)
Baldivis clay	82	35	47	2.60	(Habibbeygi, Nikraz, & Chegenizadeh, 2017)

Chapter 6 - Determination of the compression index of reconstituted clays using intrinsic concept and normalised void ratio



(a)



(b)

Figure 6-2. Compression curves in semi-logarithmic space, data extracted from references (Al Haj & Standing, 2015; Burland, 1990; Cerato & Lutenegger, 2004; Habibbeygi, Nikraz, & Chegenizadeh, 2017; Horpibulsuk et al., 2016)

(a) $e - \log \sigma'_v$ space

(b) Normalised compression curves in $e/e_L - \log \sigma'_v$ space

The compression curves of the reconstituted clays presented in Figure 6-2 are replotted in Figure 6-3 using the intrinsic framework. The ‘intrinsic concept’ was first termed by Burland (1990) for correlating the inherent compression curves of reconstituted clays and was widely used afterwards by other researchers to present the compression behaviour of clays. Burland (1990) introduced an ‘Intrinsic Compression Line’ (ICL),

which is derived by plotting the void index (I_v) against vertical stress in a semi-log plane to study the compression behaviour of reconstituted clays. The void index (I_v) used in the intrinsic concept is defined as follows:

$$I_v = \frac{e - e_{100}^*}{e_{100}^* - e_{1000}^*} \quad (6-2)$$

where the values of e_{100}^* and e_{1000}^* are the void ratios of the vertical stresses at 100 kPa and 1000 kPa, respectively. Burland (1990) also proposed a polynomial equation to express the unique intrinsic compression line (ICL) in terms of effective vertical consolidation stress at a range of liquid limits varying widely between 25 and 128%: where σ'_v is the effective vertical stress expressed in KPa (Equation (2-4)).

The ICL can normalise the virgin compression curves of a clayey soil reasonably well for medium to high levels of vertical consolidation stress (Habibbeygi, Nikraz, & Chegenizadeh, 2017). Although there is an impact of initial water content on the compression behaviour of reconstituted clays at low stress levels (Habibbeygi, Nikraz, & Chegenizadeh, 2017; Hong et al., 2010), both methods of normalisation, i.e. void index and normalised void ratio at the liquid limit, plot the compressibility of reconstituted clays in a narrow band as vertical consolidation stress increases (greater than 50 kPa). The relation of the void index (Figure 6-3) can be expressed by linear regression, with a correlation coefficient of 0.98, of the form:

$$I_v = 2.142 - 1.055(\log \sigma'_v) \quad (6-3)$$

As seen in Figure 6-3, in the range of studied stresses, a good agreement exists between the ICL proposed by Burland (1990), Equation (2-4), and the regression line proposed in this study (Equation (6-3)). Although there is a slight disparity at stress levels higher than 2000 kPa, the proposed equation almost coincides with Burland's results for stresses between 50—2000 kPa. Similarly, Horpibulsuk et al. (2016) proposed that virgin compression curves using an intrinsic framework are nearly unique for stresses higher than 100 kPa. However, this boundary stress can be reduced to 50 kPa for clayey soils with high initial water content to reflect a wider range of stress. In fact, the aforementioned linear regression equations can be used to express the compressibility of reconstituted clays above the A-line of the plasticity chart, which is the soil type considered in this study.

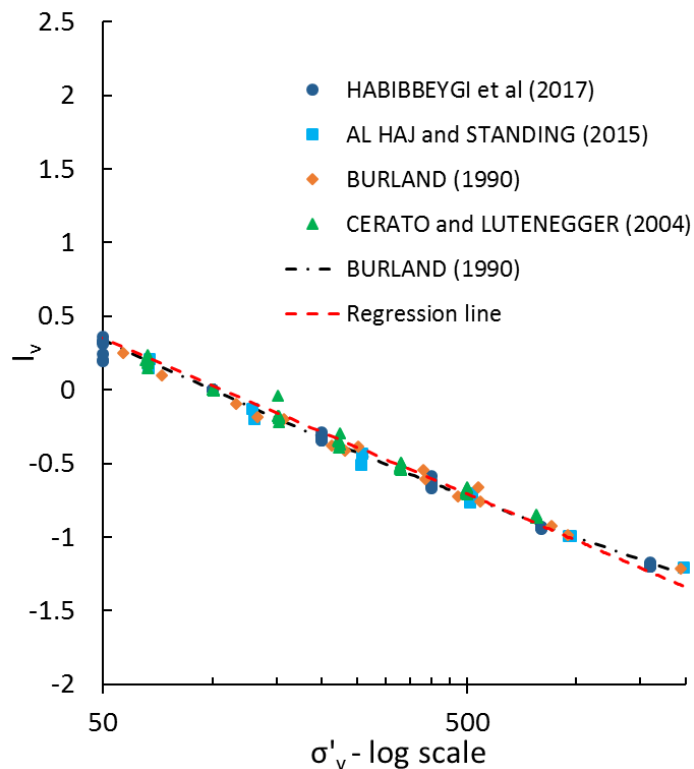


Figure 6-3. Normalised compression curves in I_v - $\log \sigma'_v$ space

6.3.4 Determining compression index

Skempton and Bishop (1954) showed that a relationship exists between the shear strength of clayey soils and their liquid limit. Moreover, it is now well-established that the shear strength of all clayey soils at water contents near the liquid limit is consistently 1.7 kPa (Sharma & Bora, 2004; Sharma & Bora, 2003; Wood & Wroth, 1976; Wroth & Wood, 1978). Wroth and Wood (1978) also reported that the major principal effective vertical stress in a normally consolidated soil is almost constant for all types of fine grained soils and is equal to 6.3 kPa at the liquid limit. Furthermore, according to Wroth and Wood (1978), the shear strength of a clayey soil at its plastic limit is approximately 100—150 times the correlated shear strength at its liquid limit. Therefore, it can be presumed that the stress at the plastic limit of a clayey soil would be 100—150 fold greater than the related vertical stress at its liquid limit (6.3 kPa), i.e. approximately 800 kPa. This assumption will be verified later in this research by testing the reliability of the estimated compression index values by comparing them with measured values. The compression index (C_c), by definition, is the slope of the compression curves in a semi-log plane (Figure 6-4):

$$C_c = -\frac{\Delta e}{\Delta \log \sigma'_v} = \frac{e_1 - e_2}{\log \sigma'_{v_2} - \log \sigma'_{v_1}} \quad (6-4)$$

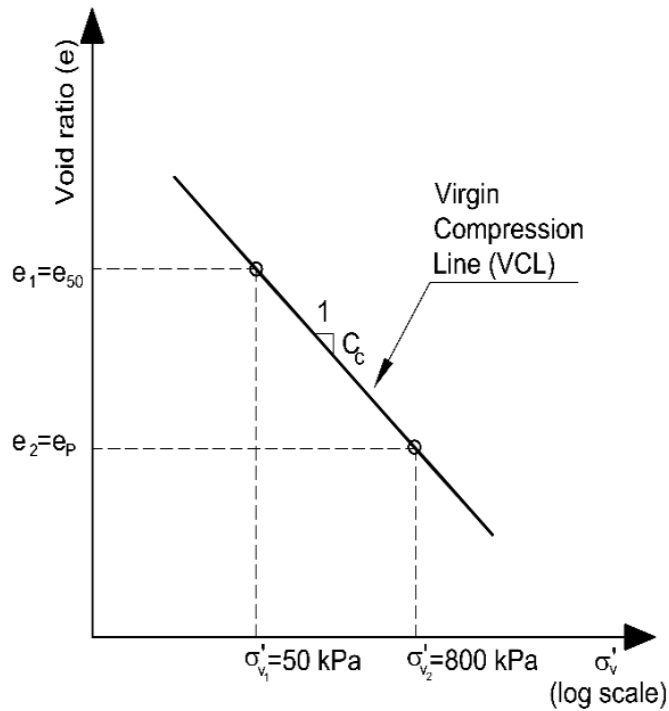


Figure 6-4. Schematic graph of compression index calculation

As shown by both methods of normalisation, the relationship between void ratio invariants (void index (I_v) and normalised void ratio (e/e_L)) and vertical stress is linear beyond 50 kPa for the primary consolidation stage. Thus the void ratio at a vertical stress of 50 kPa (e_{50}), has been chosen as the first point for calculating the slope of the virgin compression line. The second point chosen for slope calculation, based on Wroth and Wood (1978), is the void ratio at the plastic limit (e_p) and its corresponding vertical stress of 800 kPa. By substituting the void ratios at a vertical stress of 50 kPa and at the soil plastic limit (e_{50} , and e_p), and their related vertical stresses (50 kPa and 800 kPa) into Equation (6-4), the compression index can be expressed in the form:

$$C_c = \frac{e_{50} - e_p}{\log 800 - \log 50} = 0.830 (e_{50} - e_p) \quad (6-5)$$

By using the regression equation (Equation (6-1)), e_{50} can be written using the void ratio at the liquid limit e_L , and the compression index can be written in the form:

$$e_{50} = 0.803e_L \quad (6-6)$$

Chapter 6 - Determination of the compression index of reconstituted clays using intrinsic concept and normalised void ratio

$$C_c = 0.666e_L - 0.830e_P \quad (6-7)$$

Equation (6-7) suggests that the compressibility of a reconstituted clay is exclusively a function of the soil void ratio at its consistency limits. By replacing the void ratio with water content using the equation $w \cdot G_s = S_r \cdot e$ (where w is the water content, G_s is the specific gravity, and S_r is the degree of saturation), Equation (6-7) can be rewritten for consistency limits in a saturated condition ($S_r = 100\%$) by taking into account the average specific gravity for clays (2.6) in the form:

$$C_c = 0.0173w_L - 0.0216w_P \quad (6-8)$$

Ninety-two consolidation tests conducted under various mineralogy and soil conditions, and reported in the literature, were used as an independent database to estimate compression indices using Equations (6-7) and (6-8). Results were then compared with values measured from consolidation tests, to validate the efficiency of the proposed relationships. The results of this comparison are presented in Figure 6-5, which shows a reasonable agreement between the predicted values and the measurements reported in the literature (Adams, 2011; Biscontin, Cola, Pestana, & Simonini, 2007; Coutinho & Bello, 2011; Coutinho, Oliveira, & Oliveira, 1998; Devin & Sandford, 1990; Garga, Khan, & Vanapalli, 2006; Hong et al., 2010; Hou, Wang, & Jeng, 2011; Hunt, Pestana, Bray, & Riemer, 2002; Lee, Kayen, & McArthur, 1990; Mohd Amin et al., 1997; Rashwan & Koumoto, 2007; Samang, Miura, & Sakai, 2005; Sharma & Bora, 2015; Simons, Menzies, & Matthews, 2002; Sridharan & Nagaraj, 2000; Tan, 2004; Walton, Sangrey, & Miller, 1983; Whittle, 1974; Yan & Ma, 2010). As discussed before, a unique relation exists between consolidation stress and plastic limit (Wood & Wroth, 1976; Wroth & Wood, 1978). The result of this study also suggests that the assumption of the mean vertical consolidation stress at the plastic limit being 125 times that at the liquid limit is acceptable for the studied soils. Hence, it can be concluded that void ratios at 50 kPa and at the plastic limit can be employed for determining the compression index of reconstituted clays with acceptable accuracy.

Chapter 6 - Determination of the compression index of reconstituted clays using intrinsic concept and normalised void ratio

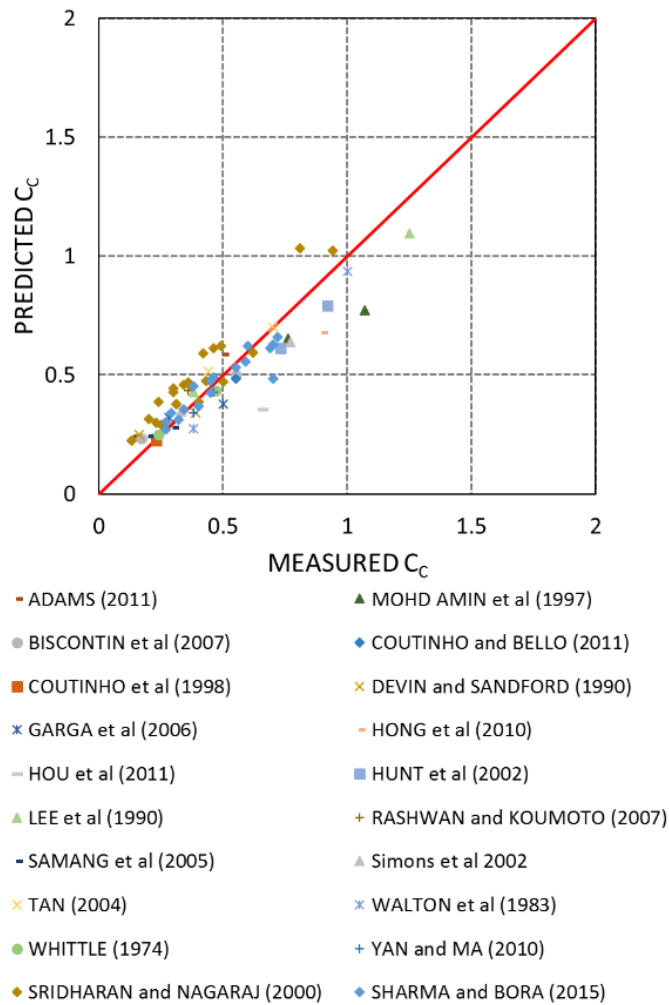


Figure 6-5. Comparison between estimated and measured compression indices

6.3.5 Conclusions

Compression curves of normally consolidated reconstituted clays were normalised in the present research using two methods of normalisation, i.e. void ratio and void ratio at liquid limit (e_L). Both methods show that the consolidation curves (e - $\log \sigma'_v$) are linear at stresses between 50—2000 kPa. It has also been shown that consolidation stress at the plastic limit can be assumed to be about 125 times greater (i.e. 800 kPa) than the correlated consolidation stress at the liquid limit based on the theoretical criteria proposed by Wroth and Wood (1978). This unique point on the compression curve together with the point associated to a void ratio at 50 kPa (e_{50}) were used to estimate the compression index of reconstituted soils. In fact, the compression index was found to be a unique function of the consistency limits (i.e. liquid limit w_L and

Chapter 6 - Determination of the compression index of reconstituted clays using intrinsic concept and normalised void ratio

plastic limit w_p) for saturated reconstituted clays over the A-line in the plasticity chart. Based on these findings, an equation was proposed that uses consistency limits to estimate the compression index of reconstituted clays. The accuracy of the estimates was verified by comparison with a broad range of measured data from the literature. Findings indicate that the equation proposed in this study is suitable to predict the compression index of reconstituted clays above the A-line in the plasticity chart, with reasonable accuracy.

7 THE EFFECT OF UNLOADING AND RELOADING ON THE COMPRESSION BEHAVIOUR OF RECONSTITUTED CLAYS

7.1 Introduction

This peer-reviewed manuscript investigates the compression behaviour of reconstituted clays under the cycles of loading, reloading and unloading. The importance of various factors such as initial water content is investigated in this manuscript. Additionally, some new experimental relationships for predicting the unloading and reloading compression indices are presented.

The list of references, keywords, acknowledgements were excluded from this manuscript. The acknowledgements, abbreviation and references are combined on pages vi, xxiv and 192 of the current manuscript respectively.

Minor changes were made for the inclusion of the published manuscript into the current document. The differences comprise referencing, style and numbering of table captions and figure captions, wherever it was necessary to keep the uniformity and consistency of the current document. Furthermore, the numbering of equations, figures, and tables follows the current manuscript numbering and may differ from those of the published manuscript.

7.2 Citation

Habibbeygi, F., & Nikraz, H. (2018). The effect of unloading and reloading on the compression behaviour of reconstituted clays. *International Journal of GEOMATE*, 15(51), 53-59. <https://doi.org/10.21660/2018.51.52643>

7.3 Manuscript Contents

7.3.1 Abstract

Oedometer tests were carried out on reconstituted clays to investigate the compressibility of soft clays with high initial water content under repetitive cycles of unloading/reloading. It is necessary to estimate the compression indices under repetitive loadings to predict the settlement of clayey layers. The results indicate that the unloading/reloading loop can be represented by a bi-linear line in a semi-

logarithmic plane with three definite slopes (compression indices). Furthermore, the compression indices of unloading and reloading can be estimated using the compression and swell indices with reasonable accuracy. The reloading part can also be defined by two initial and final slopes. The difference in these two aforementioned slopes can be explained by the balance of physico-chemical and mechanical forces. When the consolidation stress is less than the remoulded yield stress, the compression behaviour is mainly controlled by the physicochemical effect. In fact, the change in the clay micro-structure is small; however, for stresses greater than remoulded yield stress, the soil structure demolishes and the clay microstructure is completely affected. Consequently, it results in a sharp decrease in the void ratio.

7.3.2 Introduction

Soft clayey soils may experience cycles of unloading/reloading over decades for several reasons, such as preloading, stage construction, natural phenomena (e.g. shifting rivers, heavy rainfalls, drought) and groundwater fluctuation (e.g. dewatering and pumping for industrial or agriculture uses). The ongoing consolidation of these soft clayey deposits can lead to catastrophic problems in many metropolitan areas all over the world (Bucx, Van Ruiten, Erkens, & De Lange, 2015; Hung, Hwang, Liou, Lin, & Yang, 2012; Peduto, Huber, Speranza, Van Ruijven, & Cascini, 2016). In some situations, even though external conditions influenced by humans are controlled, the groundwater still changes due to natural phenomena such as gradual changes in river alignment, heavy rainfall, drought, and so on; as a consequence, fluctuations in groundwater are often inevitable. The groundwater fluctuations induce cycles of unloading/reloading which results in irreversible deformation in clayey soils. Understanding the volumetric behaviour of soft clayey soils in loading and unloading/reloading conditions can help engineers to predict the settlement (permanent and temporary deformation) of clayey deposits more accurately and to design an appropriate method to mitigate the damage to infrastructures.

Numerical modelling is a useful method to forecast the settlement of the clayey soils. An elastoplastic model is a simple model used to predict the behaviour of the clayey deposit during consolidation; however, the estimated settlement values with such simple models are not very accurate and can be over- or under-estimated, especially when complex conditions such as unloading and reloading occur. Recently, some more elaborate models have been developed to predict the ground deformation in such cases

Chapter 7 - The Effect of Unloading and Reloading on the Compression Behaviour of Reconstituted Clays

(Butterfield, 2011; Le, Fatahi, & Khabbaz, 2012, 2015; Li, Zhang, Hicher, & Wei, 2016; Ni, Indraratna, Geng, Carter, & Chen, 2014).

Experimental laboratory tests can be used to monitor the volumetric behaviour of soft clays in cycles of loading, unloading and reloading. Based on the results of oedometer tests, the plastic deformation induced during the repetitive loads can be investigated. In this study, one-dimensional consolidation tests on reconstituted clayey samples with high initial water content were conducted under repetitive unloading and reloading conditions to investigate the compression behaviour of the studied clay. Additionally, the consolidation tests were undertaken for various initial water contents to study the influence of this parameter on the results.

7.3.3 Sample Preparation and Test Procedures

7.3.3.1 Test Procedure and Materials

Five series of one-dimensional consolidation tests were conducted on reconstituted specimens to study the compression behaviour of soft clays with high initial water content under several cycles of loading and unloading. Five different initial water content ratios (i.e. $w_0/w_L = 0.8, 0.9, 1.0, 1.1$ and 1.2) were adopted to investigate the effect of initial water content on the results.

All samples were bulk collected from an under-developed suburb (Baldivis), south of the capital of Western Australia, Perth. X-ray diffractometer test results show that the dominant clay mineral of the studied soil is smectite (Habibbeygi, Nikraz, & Chegenizadeh, 2017). Index tests undertaken on the samples, in accordance with ASTM D4318, show high values of Atterberg limits (liquid limit and plastic limit - $w_L = 82\%$ and $w_P = 35\%$ respectively) (American Society for Testing and Materials, 2011). High values of liquid limit (i.e. 82%) and plasticity index (47%) result in high potential of expansion and shrinkage with water content fluctuation. The specific gravity of the studied soil was measured using a hydro-pycnometer and assessed to be 2.60 (ASTM D854). More than 65% of the studied soil comprised clay; 20% sand; and the remainder was silt (ASTM D1140). As the colour of collected samples were dark grey to black, the studied clay is herein referred to as 'black clay'. The normalised shear strength of the black clay is measured to be between 0.25 and 0.5 (Habibbeygi, Nikraz, & Chegenizadeh, 2017).

7.3.3.2 Sample preparation

Sample preparation in this study followed the sample preparation procedure proposed by Head (1986) for reconstituted samples. Firstly, all collected samples were dried at 105°C in the oven for at least 48 hours. Since samples were completely wet during collection, the constant weight method was used to make sure that samples were fully dried before sample preparation. Secondly, some homogenous powder was prepared by grinding the oven-dried materials, then passing them through a 2.36 mm sieve. Later, a predefined volume of water was added to the clayey powder and mixed thoroughly for at least 15 minutes to prepare a homogenous slurry.

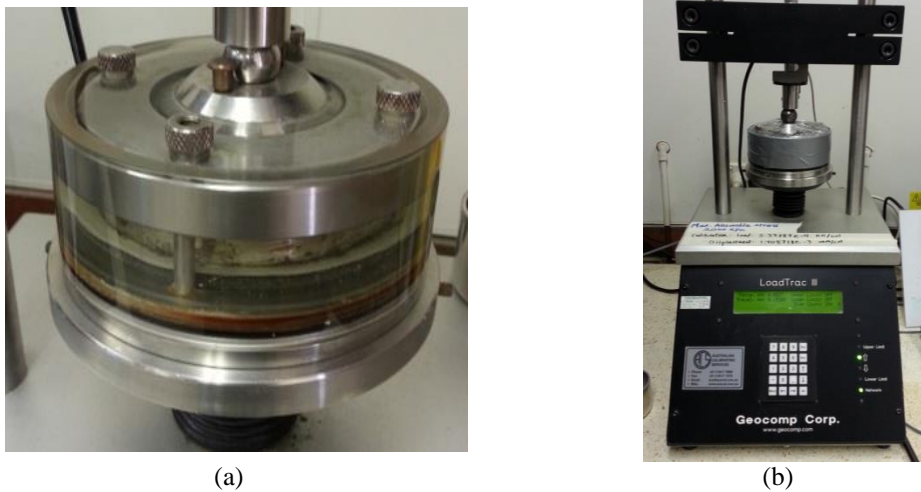


Figure 7-1. Consolidation test set-up

(a) Consolidation cell (b) Auto-consolidation apparatus

The slurry was kept in several air-tight bags for more than 24 hours before consolidation tests. One-dimensional consolidation tests were performed on specimens prepared from the slurry in accordance with the incremental loading procedure (ASTM D2435). The wall of consolidation steel ring was covered by a thin layer of silicone grease to reduce friction and mitigate the effect of the ring on the results. One-dimensional consolidation tests were carried out by an automotive oedometer on specimens with a size of 63.5 mm diameter and 31 mm height. Specimens were drained in both upward and downward directions during the consolidation process by placing two porous stones with filter papers at the top and bottom of the specimen. Figure 7-1 shows the set-up of the test and auto-consolidation apparatus used in this study. Table 7-1 presents the vertical consolidation stress and the related cycle of loading/reloading for each sample.

Chapter 7 - The Effect of Unloading and Reloading on the Compression Behaviour
of Reconstituted Clays

Table 7-1. Vertical pressure increments and cycle of loading/reloading in oedometer tests

Sample ID	Initial Water Content Ratio (w_0/w_L)	Loading/reloading Cycle	Vertical Consolidation Pressure Increments (kPa)
1	0.8	Cycle 1	1, 3, 6, 12.5, 3
		Cycle 2	6, 12.5, 25, 50, 100, 25, 6
		Cycle 3	12.5, 25, 50, 100, 200, 400, 100, 25
		Cycle 4	50, 100, 200, 400, 800, 200, 50
		Cycle 5	100, 200, 400, 800, 1600
2	0.9	Cycle 1	1, 3, 6, 12.5, 3
		Cycle 2	6, 12.5, 25, 50, 100, 25, 6
		Cycle 3	12.5, 25, 50, 100, 200, 400, 100, 25
		Cycle 4	50, 100, 200, 400, 800, 200, 50
		Cycle 5	100, 200, 400, 800, 1600
3	1.0	Cycle 1	1, 3, 6, 12.5, 3
		Cycle 2	6, 12.5, 25, 50, 100, 25, 6
		Cycle 3	12.5, 25, 50, 100, 200, 400, 100, 25
		Cycle 4	50, 100, 200, 400, 800, 200, 50
		Cycle 5	100, 200, 400, 800, 1600
4	1.1	Cycle 1	1, 3, 6, 12.5, 3
		Cycle 2	6, 12.5, 25, 50, 100, 25, 6
		Cycle 3	12.5, 25, 50, 100, 200, 400, 100, 25
		Cycle 4	50, 100, 200, 400, 800, 200, 50
		Cycle 5	100, 200, 400, 800, 1600
5	1.2	Cycle 1	1, 3, 6, 12.5, 3
		Cycle 2	6, 12.5, 25, 50, 100, 25, 6
		Cycle 3	12.5, 25, 50, 100, 200, 400, 800, 1600, 400, 100

7.3.4 Discussion and Results

Figure 7-2 presents the definition of compression indices for a cycle of unloading/reloading. As shown, the slope of a Virgin Compression Line (VCL) is

Chapter 7 - The Effect of Unloading and Reloading on the Compression Behaviour of Reconstituted Clays

denoted as C_c ; the slope of the unloading (swelling) line is C_s ; the initial and final slopes of the reloading line are C_r and C_{rc} , respectively.

Figure 7-3 shows the results of consolidation tests on the black clay (i.e. $e - \log \sigma'_v$ curves in a semi-logarithmic scale) under repetitive cycles of unloading and reloading (3 to 5 cycles).

The results of simple consolidation tests on the samples, including single loading and unloading, at the last stage of loading, are also replotted on the figure for comparison. As shown, the reloading curve of the consolidation curves is converging to the VCL and coincides with the VCL for stresses greater than the maximum applied consolidation stress before unloading. Figure 7-3 also shows that the VCL is almost linear for a wide range of consolidation stresses (i.e. 50 – 800 kPa). Moreover, the unloading part of loading/reloading curves is linear for all initial water contents, which is in agreement with the results of other researchers for soils under a cycle of loading and reloading (Butterfield, 2011); however, the unloading part for the single loading/reloading graphs is clearly non-linear for a stress of 1600 kPa. The slope of the unloading line for a constant value of initial water content is almost the same for different cycles of unloading independent of the number of cycles.

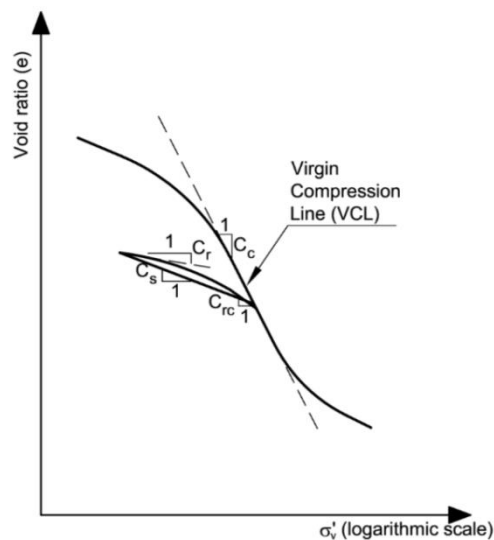


Figure 7-2. Compression indices definition on a semi-logarithmic plane

The results of consolidation tests can be used directly to measure the compression indices; for instance, the compression indices measured using compression curves for $w_0/w_L = 1.0$ are shown in Table 7-2.

Chapter 7 - The Effect of Unloading and Reloading on the Compression Behaviour of Reconstituted Clays

Table 7-2. Compression indices for $w_0/w_L=1.0$

Cycle	C_c	C_s	C_r	C_{rc}
1	-	0.0452	0.0450	0.0445
2	0.5756	0.1004	0.0230	0.1957
3	0.5746	0.1205	0.0281	0.1954
4	0.5750	0.1264	0.0290	0.1955
Single	0.5748	0.0950	0.0282	0.1897

As can be seen, the compression reloading indices for the reloading/loading cycles are nearly constant; however, the compression indices for the first cycle is far less than for the other cycles. The reason can be found in the change of the structure of clays with the increase of consolidation stress. It states that there is a definite structure for the studied clay even at the initial stage. Furthermore, the deformation in the initial stage is reversible and the soil behaves almost linearly elastic. Subsequently, when the deformation increases gradually with the increase in consolidation stress, the structure weakens. Then, it increases sharply when the clayey sample de-structures. The results also show that the unloading/reloading compression curve is a hysteresis loop. In fact, the unloading (swell) part is almost linear, but the reloading part is clearly non-linear. It is understood that irreversible deformation is controlled by the orientation of clay particles. Moreover, the balance of mechanical and physicochemical forces governs the volumetric behaviour of clayey soils (Mesri & Olson, 1971). The compressibility of clayey soils is controlled by physicochemical forces when the clay particles are parallel. On the other hand, compressibility is more affected by mechanical forces when the contact of clay particles are more skewed relative to each other (Mesri & Olson, 1971). As shown in the compression curves, the swell occurs during unloading and is mostly controlled by physico-chemical forces. The higher void ratios under unloading show the higher repulsion caused by the parallel orientation of the clay particles. This reasoning also explains how a small change in the void ratio (i.e. volume decrease) in the reloading stage is a result of balancing external loads with the repulsive force. Afterwards, when the external force exceeds the repulsive force, it results in higher deformation and a steeper slope of the compression curve.

Based on Table 7-2, it can be concluded that compression indices can be estimated using the compression and unloading indices as follow:

$$C_r = 0.23C_s \quad (7-1)$$

$$C_{rc} = 0.34C_c \quad (7-2)$$

Similarly, Equations (7-1) and (7-2) can estimate the reloading compression indices for the other initial water content ratios (i.e. $w_0/w_L=0.8, 0.9, 1.1$ and 1.2). As shown in Figure 7-3, the VCL of the studied clay in both single loading/reloading and multiple cycles of loading/reloading are not completely linear, especially when the consolidation stress increases and reaches the higher stress levels (i.e. greater than 800 kPa). This result can be explained by the de-structuring effect as the reconstituted samples lose their micro-structure during the sample preparation procedure. This result is in good agreement with other experimental tests on various reconstituted clays which support the idea that the VCL is non-linear (Habibbeygi, Nikraz, & Chegenizadeh, 2017; Habibbeygi, Nikraz, & Verheyde, 2017; Zeng et al., 2015).

The results also show that plastic deformation (irreversible void ratio) occurs when the consolidation stress is greater than a specific stress level. This specific stress level was named as the preconsolidation stress for natural clays; however, for the purpose of clarifying between natural and reconstituted clays, this definite stress level is referred to as remoulded yield stress (σ'_{yr}) (Habibbeygi, Nikraz, & Chegenizadeh, 2017; Hong et al., 2012). There are several methods to estimate the remoulded yield stress for reconstituted clays. One of the most used methods is to replot the compression index on a bi-logarithmic plane and present the compression line with two straight lines in this space; the intersection of these two lines (i.e. pre-yield and post-yield stages) defines the remoulded yield stress (Butterfield, 1979).

The bi-linear compression curves for various initial water content were plotted in Figure 7-4 ($\ln(1+e)$ vs $\log \sigma'_v$). As shown, the bi-linear technique can be employed to predict the value of remoulded yield stress of reconstituted clays with reasonable accuracy. Findings depict how the compression index increases slightly with an increase in initial water content ratio (w_0/w_L); however, the variation is not significant. The compression index for initial water content ratios greater than 1.0 is almost constant, which is in agreement with Burland (1990).

7.3.5 Conclusions

Oedometer tests were carried out with repetitive unloading/reloading cycles on reconstituted samples of black clay from Western Australia. The effect of loading/unloading/reloading on compression curves has been explained in this study

Chapter 7 - The Effect of Unloading and Reloading on the Compression Behaviour of Reconstituted Clays

by using the mechanical and physicochemical effects. The oedometer tests were undertaken on reconstituted samples with different initial water contents to investigate the influence of water content in the preparation stage (i.e. $w_0/w_L = 0.8, 0.9, 1.0, 1.1$ and 1.2). The following conclusions are drawn to interpret the findings:

- Deformation is reversible for stresses smaller than the initial remoulded yield stress of the reconstituted samples, at very low-stress levels. Moreover, the reloading compression indices are almost constant for the very first reloading stage, while being far smaller than the reloading indices of the other cycles.
- The swell (unloading) index for the first cycle is 45% and 38% of the one for cycles 2 and 3 respectively. The final reloading index for the first cycle is approximately 22% of the one for the cycles 2 to 4.
- Rebound compression indices of the reloading stage can be estimated with good accuracy using the compression and swell indices.
- The bi-logarithmic technique can be used to derive the remoulded yield stress of reconstituted clays both for single loading and multiple unloading/reloading conditions.

Chapter 7 - The Effect of Unloading and Reloading on the Compression Behaviour of Reconstituted Clays

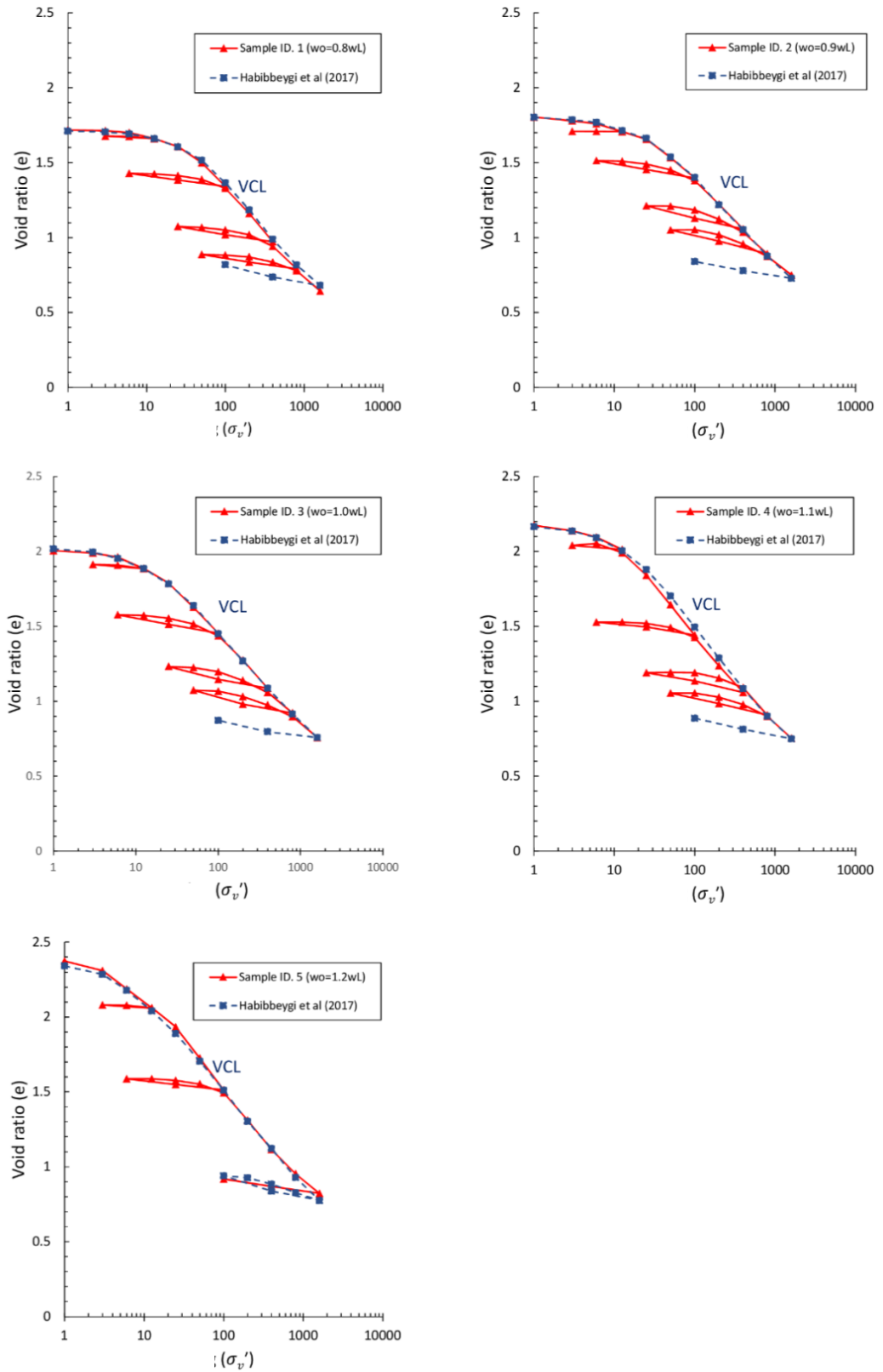


Figure 7-3. Oedometer test results with unloading/reloading on the black clay

Chapter 7 - The Effect of Unloading and Reloading on the Compression Behaviour of Reconstituted Clays

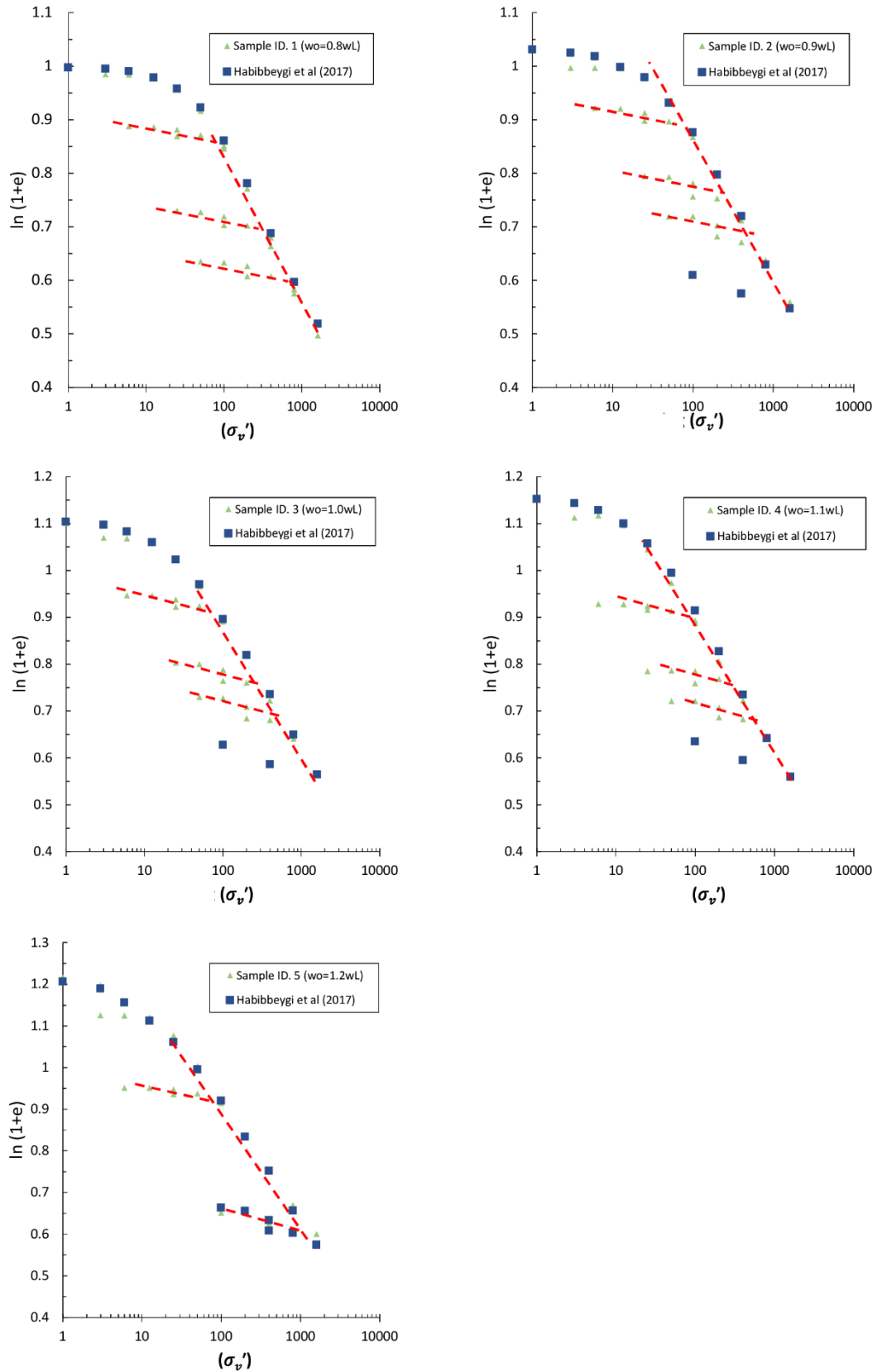


Figure 7-4. Oedometer test results with unloading/reloading

8 VARIATION OF CONSOLIDATION COEFFICIENT OF EXPANSIVE CLAYS AT HIGH INITIAL WATER CONTENT

8.1 Introduction

This peer-reviewed manuscript explores another aspect of the compression behaviour of expansive clays by studying the rate of consolidation. One-dimensional consolidation tests were carried out on various types of samples viz. remoulded, reconstituted and undisturbed samples to study the importance of disturbance. Additionally, the effect of initial condition on the results are studied in this manuscript. The list of references, keywords, acknowledgements were excluded from this manuscript. The acknowledgements, abbreviation and references are combined on pages vi, xxiv and 192 of the current manuscript respectively.

Minor changes were made for the inclusion of the published manuscript into the current document. The differences comprise referencing, style and numbering of table captions and figure captions, wherever it was necessary to keep the uniformity and consistency of the current document. Furthermore, the numbering of equations, figures, and tables follows the current manuscript numbering and may differ from those of the published manuscript.

8.2 Citation

Habibbeygi, F., & Nikraz, H. (2018). Variation of Consolidation Coefficient of Expansive Clays at High Initial Water Content. *Journal of Engineering Science & Technology*, 13(9), 2644-2654.

8.3 Manuscript Contents

8.3.1 Abstract

The coefficient of consolidation is a fundamental parameter for estimating the rate of settlement of structures found on saturated clayey layers. In this study, twelve series of one-dimensional consolidometer tests were performed on both undisturbed and remoulded/reconstituted samples of an expansive clay from Western Australia. The aim of this study is to investigate the variation in coefficient of consolidation at high initial water contents. The consolidometer tests start at very low consolidation stress

(3 kPa) and increase to the relatively high-stress level of 1600 kPa to consider the effect of stress level on the results. The results show that the initial water content, stress level, and clay mineralogy have a great impact on the coefficient of consolidation. Moreover, the physicochemical factor governs the compression behaviour of remoulded samples prepared at initial water contents less than the liquid limit, and reconstituted samples at initial water contents higher than the liquid limit at medium to high-stress levels. Therefore, the coefficient of consolidation decreases with increasing consolidation stress for such samples. On the other hand, the mechanical factor mainly controls the compression behaviour of reconstituted samples at low-stress levels, and there is an increasing trend of the coefficient of consolidation with consolidation stress. In addition, the results also show that sample disturbance has a great influence on the coefficient of consolidation by decreasing the value by approximately four times.

8.3.2 Introduction

The settlement in a granular soil occurs shortly after an excess load is applied, whereas that in a saturated clayey soil occurs over a longer period. In fact, this the settlement, which is referred to as ‘consolidation settlement’, can be completed over months, years, or even decades for clayey soils as a result of the low permeability of such soils. In the other words, the rate of water expulsion from a clayey soil controls the rate of settlement, and this rate is affected mainly by the hydraulic conductivity of the soil. Therefore, the coefficient of consolidation (C_v), which expresses the rate of consolidation in saturated clays, can be defined in terms of hydraulic conductivity (k), unit weight of water (γ_w), and coefficient of volume change (m_v), as follows (Das & Sobhan, 2013):

$$C_v = \frac{k}{m_v \gamma_w} \quad (8-1)$$

Terzaghi and Peck (1967) expected C_v to remain constant with increasing the consolidation stress in an oedometer test. In their opinion, both k and m_v decrease with increasing effective consolidation stress (σ'_v) at a virtually identical rate that maintains C_v at an almost constant value (Terzaghi & Peck, 1967). Retnamony et al. (1998) criticised this idea by reviewing various published data of C_v - σ'_v variations in the literature and conducting laboratory tests on different clay minerals. Based on their

findings, the variation in C_v and σ'_v for clayey soils is not constant; it is dependent on the vertical consolidation stress and clay mineralogy (Retnamony et al., 1998).

However, the effect of index properties and clay mineralogy on the compressibility properties of clayey soils have been investigated by several researchers (Habibbeygi, Nikraz, & Chegenizadeh, 2017; Habibbeygi, Nikraz, & Verheyde, 2017; Horpibulsuk, Yangsukkaseam, Chinkulkijniwat, & Du, 2011; Lei et al., 2015; Xu & Yin, 2015) but the effect of the initial conditions (such as initial water content) and level of sample disturbance on the coefficient of consolidation have received less attention. Moreover, there is a lack of experimental data regarding an investigation of the effect of high initial water content on the mechanism of compressibility and the coefficient of consolidation of expansive clays. As a result, the following questions are investigated in this study:

- What is the effect of initial water content on the coefficient of consolidation of expansive clays?
- What is the trend of the coefficient of consolidation with vertical consolidation stress when the initial water content is high?
- What is the main factor controlling the compressibility and rate of consolidation for expansive clays?
- How does the value of consolidation stress affect the coefficient of consolidation of expansive clays?
- What is the effect of sample disturbance on the value of consolidation coefficient of expansive clays?

Based on these questions, the impact of initial water content on the coefficient of consolidation is investigated for highly expansive clays. To consider the effect of stress level, the consolidation pressure initiates at a low stress of 3 kPa (low- stress level) that increases to 1600 kPa (high-stress level) in the consolidometer tests. The stress level is adapted to cover the range of stresses normally being applied to the clay during construction. Moreover, consolidometer tests were performed on both undisturbed and remoulded samples (prepared with the same water content as that in-situ) to study the effect of sample disturbance on the coefficient of consolidation.

8.3.3 *Coefficient of Consolidation (C_v)*

Compression curves of clayey soils can be divided into three phases for analytical purposes: initial compression, primary consolidation, and secondary compression (Das & Sobhan, 2013). The initial compression phase occurs almost instantly with the application of the first load increment in the consolidometer test. The primary consolidation phase, which is the most important part of the compression curve, is time-related and completed when the excess pore water pressure dissipates (Terzaghi & Peck, 1967).

Terzaghi and Peck's one-dimensional theory of consolidation is thus far the most broadly employed framework to estimate the rate of consolidation. The only parameter required to compute the degree of consolidation of a clay layer is the coefficient of consolidation (C_v). By knowing the amount of C_v , it is possible to assess the percentage of consolidation and the amount of stress transferred to the skeleton at any stage of the consolidation process. However, the consolidation process is really a three-dimensional phenomenon, but for the most practical applications, the result of the one-dimensional analysis is sufficiently accurate, especially for such a laterally confined clayey soil deposit bounded between two porous layers as the drainage patterns are so similar to one-dimensional theory (Das & Sobhan, 2013).

The coefficient of consolidation is a fundamental parameter for estimating the rate of settlement of structures built on saturated clayey layers. However, several methods, including empirical and computational relationships, have been proposed over the past six to seven decades to determine C_v . Two standard methods, namely log-time and square-root-time, remain the most practical and reliable methods to estimate the rate of consolidation (Casagrande & Fadum, 1940; Taylor, 1948). In this study, the log-time technique has been used to compute the coefficient of consolidation of the studied clay in light of the high acceptance between geotechnical engineers and the recommendations in the standard (ASTM D2435-04) (American Society for Testing and Materials, 2011).

8.3.4 *Materials, Methods and Tests*

Twelve series of consolidometer tests (on both undisturbed and remoulded/reconstituted samples) were performed on expansive clay with various initial water contents to investigate the variation of coefficient of consolidation. The

Chapter 8 - Variation of consolidation coefficient of expansive clays at high initial water content

studied clay, referred to in this study as ‘black clay’, was collected from Baldivis, 46km south of Perth, the capital city of Western Australia (Figure 8-1). The geotechnical parameters, sample preparation and test procedure are explained in this section.



Figure 8-1. Sampling site for the studied clay (Google Maps)

8.3.4.1 Geotechnical properties

Table 8-1 illustrates the initial water content as well as soil properties of the studied soil (Habibbeygi, Nikraz, & Chegenizadeh, 2017). All soil classification tests were carried out according to ASTM standards (American Society for Testing and Materials, 2011). Based on the results of the X-ray Diffraction (XRD) tests conducted at Curtin University’s Microscopy and Microanalysis Facility, the predominant clay mineral of the black clay is smectite (Habibbeygi, Nikraz, & Chegenizadeh, 2017). The physical properties of the black clay are tabulated in Table 8-1.

Table 8-1. Physical properties of black clay.

Geotechnical property	Value
Liquid limit % (w_L)	82
Plastic limit % (w_p)	35
Plasticity index % (I_p)	47
Specific gravity (G_s)	2.6
Sand (%)	20
Silt (%)	12
Clay (%)	68
Unified soil classification system	CH
Swell pressure (kPa)	83 (Habibbeygi & Nikraz, 2018b)

8.3.4.2 Sample preparation and test procedure

Three different soil sample preparation methods were chosen in this study: undisturbed, remoulded and reconstituted samples. Two undisturbed samples were collected from the Baldivis site from a 0.5-m deep of a test pit. Undisturbed samples were collected by pushing a large 250-mm tube into the soil.

Samples were extruded in the laboratory, wrapped in multiple cling foils, and sealed to keep the initial moisture before the one-dimensional consolidometer tests. The in-situ moisture content of the undisturbed samples measured soon after collection from the site was approximately 40%. Disks were cut from the undisturbed sample and trimmed carefully for placement in the oedometer ring.

To decrease the disturbance effect of the tube walls at the outer part of the sample during pushing of the sample into the soil, only one sample was trimmed from each soil disk.

To investigate the influence of disturbance on the consolidation characteristics of the studied soil, remoulded samples were prepared by adding the desired amount of water to the soil to correct the water content of the specimen. Unit weight of in-situ samples was measured to be 16.7 kN/m^3 . Moreover, remoulded samples were compacted using a metal tamper to achieve the same unit weight.

Reconstituted samples were prepared by mixing oven-dried ground clay with a predefined amount of water, following Burland's procedure of preparing reconstituted samples (Burland, 1990). When the initial water content of the sample was more than the liquid limit (i.e., reconstituted samples), the prepared soil was carefully spooned into the consolidation rim to avoid trapping any air bubbles in the sample. As the samples were too soft, just a vibrating metal rod was used to exhaust air bubbles.

All remoulded and reconstituted samples were sealed in three successive airtight plastic bags for 24 hr to mature. The inner face of the consolidation ring was covered by a thin layer of silicon grease prior to sample preparation to reduce the friction between the soil and the ring. Consolidometer tests were conducted on various samples (total of 12 samples) with different degrees of disturbance (i.e., remoulded/reconstituted and undisturbed samples) and several different initial water contents in an automatic one-dimensional consolidation apparatus. The soil samples were 25.4 mm high and 64 mm in diameter. Table 8-2 illustrates the sample number, initial water content, sample condition, and vertical stress increments of the consolidometer tests.

Table 8-2. Consolidometer test procedure.

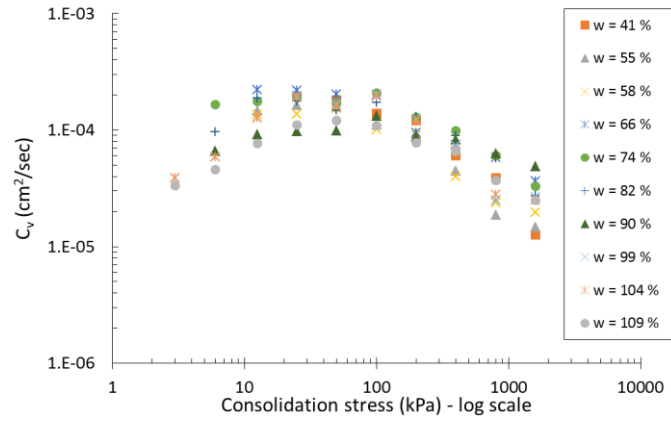
Sample no.	Sample type	w(%)	Vertical consolidation stress (kPa)
BC-R1	Remoulded	41	25, 50, 100, 200, 400, 800, 1600
BC-R2	Remoulded	55	12.5, 25, 50, 100, 200, 400, 800, 1600
BC-R3	Remoulded	58	12.5, 25, 50, 100, 200, 400, 800, 1600
BC-R4	Remoulded	66	12.5, 25, 50, 100, 200, 400, 800, 1600
BC-R5	Reconstituted	74	6, 12.5, 25, 50, 100, 200, 400, 800, 1600
BC-R6	Reconstituted	82	6, 12.5, 25, 50, 100, 200, 400, 800, 1600
BC-R7	Reconstituted	90	6, 12.5, 25, 50, 100, 200, 400, 800, 1600
BC-R8	Reconstituted	99	3, 6, 12.5, 25, 50, 100, 200, 400, 800, 1600
BC-R9	Reconstituted	104	3, 6, 12.5, 25, 50, 100, 200, 400, 800, 1600
BC-R10	Reconstituted	109	3, 6, 12.5, 25, 50, 100, 200, 400, 800, 1600
BC-U1	Undisturbed	40	100, 200, 400, 800, 1600
BC-U2	Undisturbed	43	200, 400, 800, 1600

8.3.5 Discussion and Results

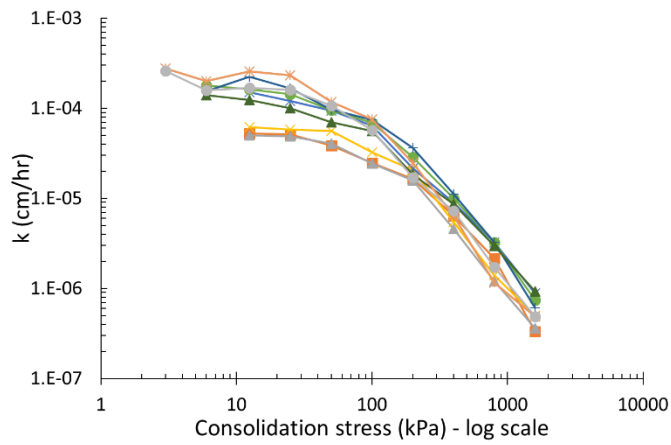
8.3.5.1 Vertical stress effect

Figure 8-2 shows the variation in consolidation parameters (i.e., C_v , k and m_v) with vertical consolidation stress for the remoulded and reconstituted samples. As shown in Figure 8-2(b) and (c), k and m_v decrease with increasing vertical consolidation stress, which is in agreement with past researches (Retnamony et al., 1998; Terzaghi & Peck, 1967). However, there is a decreasing trend in both consolidation parameters (i.e., k and m_v), although they decrease at different rates. This difference in rates results in C_v varying with the change in consolidation stress. For instance, m_v decreases from 3.1×10^{-3} 1/kPa at $\sigma'_v=6$ kPa to 6.4×10^{-5} 1/kPa at $\sigma'_v=1600$ kPa ($w=74\%$) while k decreases from 1.84×10^{-5} cm/hr to 7.43×10^{-7} cm/hr for the same range of consolidation stress. This shows the ratio of the rate of decrease of k is almost half of m_v 's rate for the same consolidation stress range.

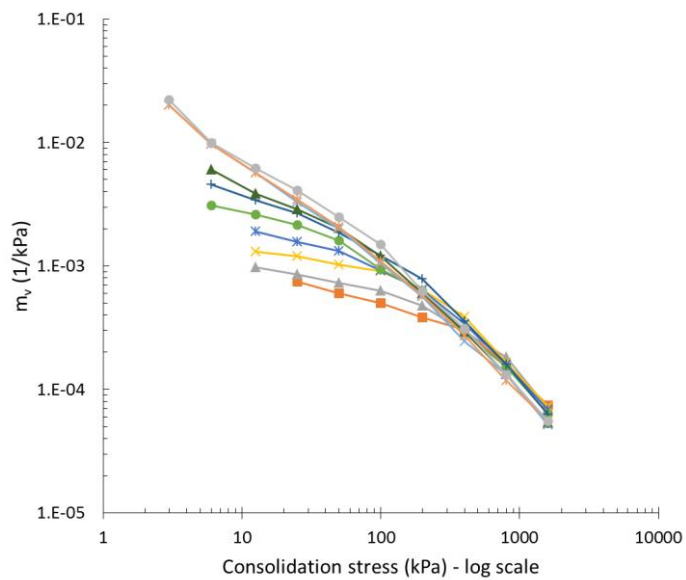
Chapter 8 - Variation of consolidation coefficient of expansive clays at high initial water content



(a) C_v variation with consolidation stress



(b) k variation with consolidation stress



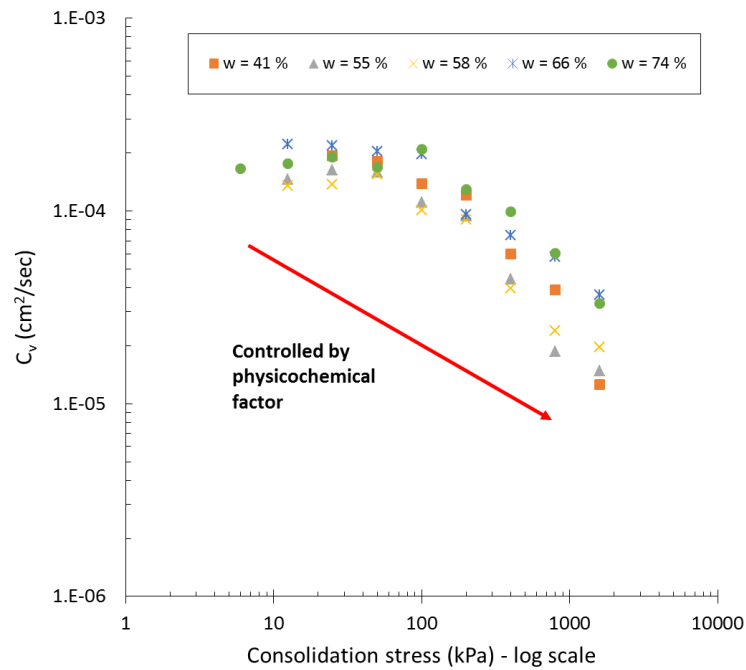
(c) m_v variation with consolidation stress

Figure 8-2. Variation of consolidation parameters - with consolidation stress.

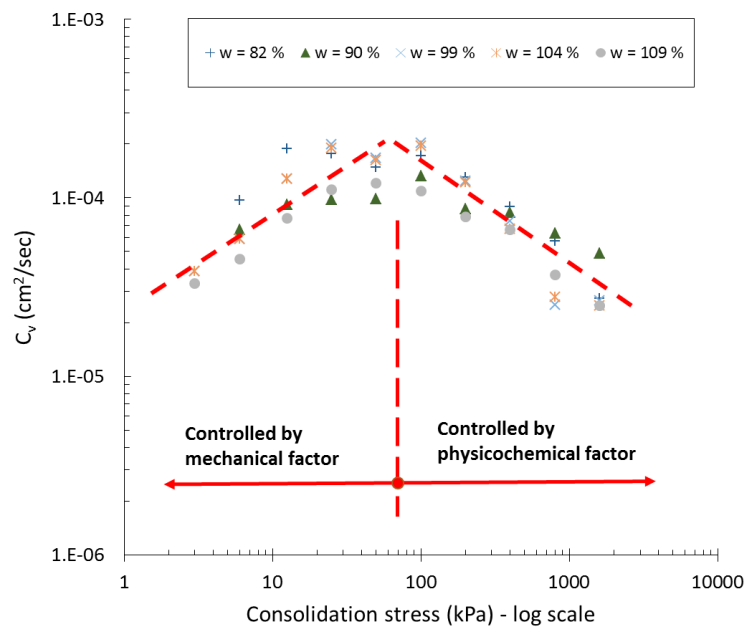
In addition, the results show that the variation of C_v is dependent on the level of stress and the initial water content. The $C_v - \sigma'_v$ graphs are plotted in Figure 8-3 for two ranges of initial water content: Initial water content less than the liquid limit (i.e., $w=41\%$, 58% , 66% , and 74%) and initial water content equal to or greater than the liquid limit (i.e., $w=82\%$, 90% , 99% , 104% , and 109%). For initial water contents less than the liquid limit, C_v decreases continuously with increasing consolidation stress (Figure 8-3a).

For instance, C_v decreases from 1.65×10^{-8} m²/s at $\sigma'_v=6$ kPa to 3.31×10^{-9} m²/s at $\sigma'_v=1600$ kPa ($w=74\%$). The trend differs for reconstituted samples prepared at initial water contents greater than the liquid limit (Figure 8-3b). For the studied clay, the C_v of the reconstituted samples with high initial water contents (i.e., samples BC-R6 to BC-R10) increases for consolidation stresses less than 100 kPa, whereas it decreases for consolidation stresses greater than 100 kPa (Figure 8-3b). For instance, C_v increases continuously from 3.89×10^{-9} m²/s at $\sigma'_v=3$ kPa to 1.96×10^{-8} m²/s at $\sigma'_v=100$ kPa, then it decreases to 2.48×10^{-9} m²/s at $\sigma'_v=1600$ kPa ($w=104\%$). These different trends for the variation of coefficient of consolidation in reconstituted clays can be explained by the mechanism governing the compression behaviour of clayey soils.

Chapter 8 - Variation of consolidation coefficient of expansive clays at high initial water content



(a) $w < w_L$



(b) $w \geq w_L$

Figure 8-3. Variation of C_v with consolidation stress.

Retnamony et al. (1998) proposed that the coefficient of consolidation depends on clay mineralogy. According to their research, C_v of clays with montmorillonite (smectite) as the main mineral decreases with increasing consolidation stress; whereas those with main minerals of illite and kaolinite minerals exhibit an increasing trend. The present

study confirms this finding for the remoulded samples prepared at initial water contents less than the liquid limit. Similarly, C_v decreases with increasing consolidation stress for the reconstituted samples for medium to high-stress levels. On the contrary, C_v increases with the increasing consolidation stress for low-stress levels of reconstituted samples prepared at initial water contents greater than the liquid limit. Furthermore, it seems that the C_v trend depends not only on the clay mineralogy but also on the stress level of such clayey soils.

The trend with consolidation stress can be explained by the mechanism controlling the compression behaviour. Two main factors govern the compression behaviour of clays, namely mechanical and physicochemical factors (Mesri & Olson, 1970). The mechanical factor is employed for short-range inter-particle forces governed only by the physical characteristics of soil particles, such as strength, flexibility, and surface friction (Retnamony et al., 1998). In this case, the physical properties of the minerals and the lubricating influence of water are the two factors controlling the compression behaviour. On the other hand, physicochemical effects specify almost long-range inter-particle forces particularly in diffuse double layers (Retnamony et al., 1998).

The results of this study show that the variation of C_v with consolidation stress depends on different factors such as clay mineralogy, initial water content, and stress level. For reconstituted samples at high initial water contents, the variation of consolidation coefficient is controlled mainly by the mechanical factor rather than the physicochemical factor, even for clays predominantly composed of smectite (montmorillonite). It seems that the high initial water content in montmorillonite clays suppresses the diffuse double layer formation; thus, the compression behaviour of such clays is influenced mainly by mechanical factors.

Nevertheless, for initial water contents less than the liquid limit, there is a decreasing trend of C_v with consolidation stress and the governing mechanism of compression behaviour is physicochemical. Similarly, when the consolidation stress is high at high initial water contents, the mechanism controlling the compression behaviour is mainly physicochemical and there is a decreasing C_v trend.

8.3.5.2 Initial water content effect

Figure 8-2c presents the $m_v - \sigma'_v$ curves of the remoulded and reconstituted samples. The results show that the m_v values of the remoulded samples are generally lower than

those of the reconstituted samples at the same consolidation stress. Moreover, the m_v value mostly decreases with increasing consolidation stress.

The test results further illustrate that there is a general increasing trend of C_v for the reconstituted samples with decreasing initial water content (Figure 8-2a). For example, the C_v value for $w=90\%$ ($4.88 \times 10^{-9} \text{ m}^2/\text{s}$) is almost 1.5 and 3.9 times that for $w=74\%$ and 41% ($3.31 \times 10^{-9} \text{ m}^2/\text{s}$ and $1.26 \times 10^{-9} \text{ m}^2/\text{s}$), respectively at the same consolidation stress of 1600 kPa.

8.3.5.3 Sample disturbance effect

Figure 8-4 presents the variation of C_v for two levels of sample disturbance (i.e., undisturbed sample and remoulded sample). The results show that the values of C_v for the two undisturbed samples are greater than that of the remoulded sample. For instance, the C_v value of BC-U1 is $5.15 \times 10^{-9} \text{ m}^2/\text{s}$ at a consolidation stress of 1600 kPa, while at the same stress and for the remoulded sample (BC-R1) the C_v is $1.26 \times 10^{-9} \text{ m}^2/\text{s}$. So it is almost four times more than that of the remoulded soil.

Figure 8-4 further illustrates that the C_v values of both undisturbed samples decrease with increasing consolidation stress. It is expected that the physicochemical mechanism controls the compression behaviour of the undisturbed samples as the in-situ water contents of the undisturbed samples are lower than the liquid limit of the black clay. Only two undisturbed samples were studied in this research. More laboratory tests are recommended to be carried out to compare the results.

Chapter 8 - Variation of consolidation coefficient of expansive clays at high initial water content

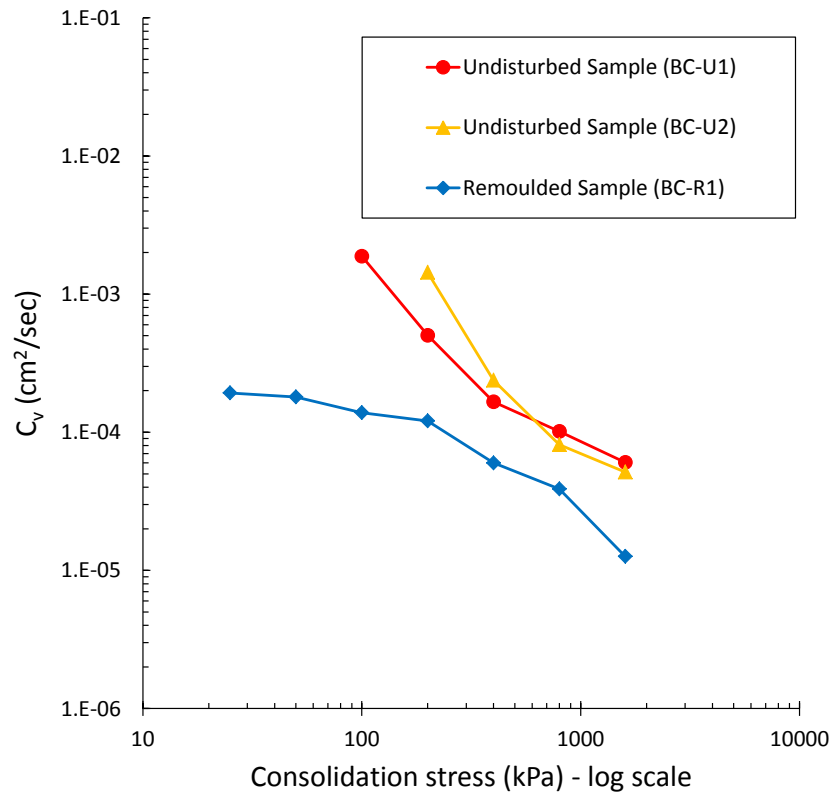


Figure 8-4. Variation of C_v with consolidation stress for an undisturbed and remoulded sample.

8.3.6 Conclusions

Twelve series of consolidometer tests were performed on both undisturbed and remoulded/reconstituted samples with various initial water contents to investigate the effect of the initial water content and sample disturbance on the coefficient of consolidation. Based on the results of the consolidometer tests, the following is concluded:

- The C_v of expansive clays varies with increasing consolidation stress and is dependent on clay mineralogy, stress level, and initial water content.
- The variation of C_v with consolidation stress depends on the initial water content of the studied clay with the predominant clay of smectite. For an initial water content less than its liquid limit, the compression behaviour is governed mainly by the physicochemical mechanism. Moreover, the same trend for C_v is expected at medium to high-stress levels, even for those samples with initial water contents greater than their liquid limit. On the other hand, C_v increases with increasing consolidation stress when the stress level is low and initial

Chapter 8 - Variation of consolidation coefficient of expansive clays at high initial water content

water content is high. It is recommended that further experimental tests be carried out on the reconstituted samples, especially at low-stress levels, to investigate the governing mechanism of the compression behaviour.

- There is a general decreasing trend of C_v with increasing initial water content for the remoulded and reconstituted samples (at mid to high stress level and initial water content less than the liquid limit).
- Sample disturbance reduces the C_v of expansive clays; C_v of undisturbed samples were almost four times that of the remoulded ones at the same water content.

9 CHARACTERISATION OF THE UNDRAINED SHEAR STRENGTH OF EXPANSIVE CLAYS AT HIGH INITIAL WATER CONTENT USING INTRINSIC CONCEPT

9.1 Introduction

This peer-reviewed manuscript explains the mechanical behaviour of expansive clays. The intrinsic framework is used to predict the shear strength of the reconstituted samples. A new relationship for the normalised line of intrinsic shear line is introduced based on the results of direct shear tests.

The list of references, keywords, and acknowledgements were excluded from this manuscript. The acknowledgements, abbreviations and references are combined on pages vi, xxiv and 192 of the current manuscript, respectively.

Minor changes were made for the inclusion of the published manuscript into the current document. The differences comprise removing repetitions, referencing, style and numbering of table captions and figure captions, wherever it was necessary to keep the uniformity and consistency of the current document. Repetitions comprise equations and literature reviews which have already been addressed in Chapter 2. Thus, some equations may refer to Chapter 2. Furthermore, the numbering of equations, figures and tables follow the current manuscript numbering and may differ from those of the published manuscript.

9.2 Citation

Habibbeygi, F., & Nikraz, H. (2018). Characterisation of the Undrained Shear Strength of Expansive Clays at High Initial Water Content Using Intrinsic Concept. *International Journal of GEOMATE*. <https://doi.org/10.21660/2017.29.20455>

9.3 Manuscript Contents

9.3.1 Abstract

Twenty-four direct shear tests were conducted on remoulded/reconstituted specimens to study the effect of initial water content on the undrained shear strength of expansive clays. The laboratory tests illustrate that the shear behaviour of the studied clayey soil

is dependent on both the confining pressure and the initial water content at which the specimen was prepared. In fact, the undrained shear strength decreases with increasing initial water content. Similarly to the compression behaviour, the intrinsic concept can also be used to predict the undrained shear strength of the studied soil. Additionally, the relationship between the void index, which is a normalised invariant of void ratio, and the undrained shear strength can be defined uniquely by a straight line. The experimental results also show that the normalised undrained shear strength, which is defined as the ratio of the peak undrained shear strength to the normal stress, varies with the initial water content from 0.25 to 0.50. Moreover, a decreasing trend is found for the range of pre-consolidation stress between 50 and 400 kPa.

9.3.2 Introduction

The mechanical and volumetric characteristics of clays can be predicted by assessing the behaviour of remoulded and reconstituted samples. In fact, these samples can be used as a framework to evaluate the behaviour of natural clays. Burland (1990) proposed an intrinsic concept as a basic reference for studying the compression behaviour of reconstituted clays. According to Burland (1990), the void ratio of a reconstituted clay can be uniquely normalised by using the void index invariant. Additionally, the intrinsic parameters are understood to be related only to the properties of soil materials, and are not affected by the initial state of natural soils (Burland, 1990). Furthermore, Burland et al. (1996) extended the intrinsic framework to predict the shear behaviour of reconstituted clays. Since then, this notable concept has been widely used by researchers to predict the compressibility and shear behaviour of remoulded/reconstituted and natural clays all over the world (Cerato & Lutenegeger, 2004; Chandler, 2000; Habibbeygi, Nikraz, & Chegenizadeh, 2017; Habibbeygi, Nikraz, & Verheyde, 2017; Hong et al., 2013; Hong et al., 2010; Zeng et al., 2015).

To the best of the authors' knowledge, there is a lack of experimental data regarding the effect of initial water content on the shear behaviour of reconstituted/remoulded clays. Similarly to the intrinsic compression line (ICL), a reference line may be used to correlate the void index and undrained shear strength of reconstituted clays. Although the intrinsic characteristics are supposed to be independent of the initial state of the studied soil, it is anticipated that the shear behaviour of a reconstituted clay may be affected by additional factors such as effective consolidation pressure and initial

moisture content. Consequently, the following questions were investigated in this study:

- What is the impact of high initial moisture content of the preparation stage on the undrained shear strength of remoulded/reconstituted clays?
- Is the proposed intrinsic framework for studying the compressibility of reconstituted clays applicable to predict the undrained shear strength of clayey soils?
- What is the trend of the undrained shear strength of reconstituted/remoulded clays with normal stress when the initial water content of the preparation phase is high?
- What is the relationship between the void index and the undrained shear strength for reconstituted/ remoulded clays?

Based on these questions, the influence of the initial water content of the preparation stage is investigated in this study for highly expansive clays. To consider the effect of the initial water content on the results, six series of initial water content were considered in the experimental tests. Additionally, the compression behaviour of the studied clay was investigated to confirm the compatibility of the compression curves of a remoulded/reconstituted specimen in the pre-consolidation stage with that of an identical sample consolidated in a standard one-dimensional consolidation apparatus.

9.3.3 *Intrinsic Framework*

Burland (1990) proposed a baseline reference by introducing the ICL to predict the compressibility of reconstituted clays. A review of intrinsic framework and the related relationships are presented in Chapter 2.

Habibbeygi, Nikraz, and Chegenizadeh (2017) performed eight series of one-dimensional consolidometer tests on expansive clays from Western Australia at different initial water content levels. Based on their results, the intrinsic compression behaviour of expansive clays can be explained well by the ICL. However, the initial water content has a significant influence on the void index for stresses below the remoulded yield stress. Furthermore, the intrinsic compression parameters are also dependent on the clay mineralogy, which must be considered in the ICL relationship. Habibbeygi, Nikraz, and Verheyde (2017) reviewed nineteen one-dimensional consolidation test results of seven clays from all over the world, of which the liquid

and plastic limits varied from 42% to 200% and 23% to 108%, respectively; the soil particle density varied from 2.60 to 2.83. Their findings showed that the void ratio can be normalised well by the void index. Consequently, a linear relationship can be used with reasonable accuracy to estimate the relationship between the void index and the effective consolidation pressure within the range of 50 to 2000 kPa (Equation (6-3)). Chandler (2000) employed the intrinsic concept to explain the shear behaviour of reconstituted clays by introducing an intrinsic strength line (ISuL). Chandler (2000) reviewed the shear strengths of various clayey soils with plasticity and void indices ranging from 12 to 60, and -1 to approximately zero, respectively. It was concluded that the normalised shear strength of the reconstituted clays (R_{su}^*), which is defined as the ratio of undrained shear strength to the effective confining stress, is independent of the plasticity index of the studied soil, and is equal to 0.34.

9.3.4 Materials and Test Procedures

9.3.4.1 Geotechnical Properties

Twenty-four series of direct shear tests on reconstituted /remoulded samples were performed to study the undrained shear strength of clays at high initial water content. Six different initial water content ratio values (i.e. $w_0/w_L = 0.6, 0.7, 0.8, 0.9, 1.0,$ and 1.1) were adopted to investigate the effect of initial water content on the undrained shear strength.

Disturbed samples were collected in bulk from an underdeveloped suburb, named Baldivis, south of the capital city of Western Australia. The studied clay is referred as 'Black clay' herein owing to the dark grey to black colour of the clayey soil. The main clay mineral of the studied soil is assessed as smectite based on the results of X-ray diffractometry tests. The high level of smectite in clay minerals explains the high potential of swelling and expansion of the studied soil with the change in water content. The Atterberg limits (w_L and w_p) were measured in accordance with ASTM D4318 (American Society for Testing and Materials, 2011) and assessed to be 82% and 35%, respectively. A hydro pycnometer was used to measure the soil particle density (G_s) of the studied clay in accordance with ASTM D854 ($G_s = 2.6$). According to the wet-sieve test results, the clayey soil comprised 20% sand, 12% silt, and 68% clay. Finally, direct shear tests were performed for various normal stresses of 50, 100, 200, and 400 kPa (ASTM D3080) (American Society for Testing and Materials, 2011).

9.3.4.2 Sample Preparation and Test Procedure

Disturbed samples were initially oven dried at 105 ± 5 °C for at least two days prior to preparation to achieve a constant weight. Then, the samples were ground manually by a rubber pestle and mortar to prepare a homogenous powder. A predefined amount of water was then added to the powder to prepare a specimen following Burland's procedure of reconstituted sample preparation (Burland, 1990). Finally, all specimens were kept in multiple airtight bags for at least one day to be homogenised prior to testing. To mitigate the effect of friction between the specimen and the shear box, the inner faces of the box was covered by a small amount of silicone grease. The specimen size was measured to be 63.5 x 63.5 x 31 mm. Two porous stones were used at the top and bottom of the specimen, respectively, to allow free draining in both directions.

Prior to applying the shear displacement, the consolidation pressures were applied gradually to the specimens to be consolidated to the predefined normal stresses, in accordance with Table 9-1. For this purpose, the specimens were prepared at the predefined initial water content and carefully poured into the mould by controlling the total mass. The total mass of every specimen was calculated based on the completely saturated condition and the related water content. Then, the theoretical total mass of the specimens was compared with the measured total mass. An error of less than 3% was accepted in the overall mass measurement. Consolidation pressure increments were applied to each specimen in accordance with Table 9-1. The specimens were maintained at the consolidation pressure of each stage until the completion of the primary settlement of that stage of loading. After the pre-consolidation stage, direct shear tests were performed on four series of specimens at normal stress (24 specimens in total) in accordance with ASTM D3080 to investigate the effect of the initial water content and normal stress on the shear behaviour.

9.3.5 Discussion and Results

9.3.5.1 Pre-Consolidation Stage

In this study, the specimens were initially pre-consolidated to a predefined pressure in accordance with Table 9-1. Each consolidation stress increment remained on the specimen to complete the primary consolidation of the stage. Then, compression curves were plotted for four different normal stresses (i.e. 50, 100, 200, and 400 kPa), as shown in Figure 9-1. The compression curves of the specimens for each stage were

then compared to the corresponding compression curve of an identical specimen, which was consolidated in a one-dimensional oedometer. Figure 9-1 shows the compression curves for the pre-consolidation stage and the one-dimensional consolidation for different initial water contents. As shown in this figure, the $e - \log \sigma'_v$ curves of the pre-consolidation stage are well-matched with the compression curves derived from the consolidometer test.

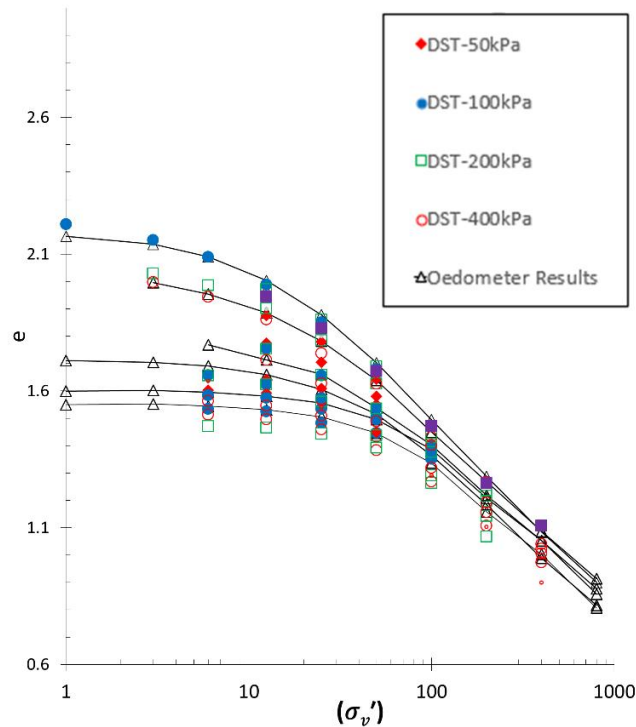


Figure 9-1. Comparison of compression curves for the pre-consolidation stage and the one-dimensional consolidometer test

Table 9-1. Consolidation stress increments at the pre-consolidation stage and normal stress for direct shear test

Sample	Initial Water Content Ratio (w_0/w_L)	Normal stress (kPa)	Vertical Consolidation Pressure Increments (kPa)
1 – 4	0.6	50, 100, 200 and 400	3, 6, 12.5, 25, 50, 100, 200, 400
5 – 8	0.7	50, 100, 200 and 400	3, 6, 12.5, 25, 50, 100, 200, 400
9 – 12	0.8	50, 100, 200 and 400	6, 12.5, 25, 50, 100, 200, 400
13 – 16	0.9	50, 100, 200 and 400	1, 3, 6, 12.5, 25, 50, 100, 200, 400
17 – 20	1.0	50, 100, 200 and 400	1, 3, 6, 12.5, 25, 50, 100, 200, 400
21 – 24	1.1	50, 100, 200 and 400	1, 3, 6, 12.5, 25, 50, 100, 200, 400

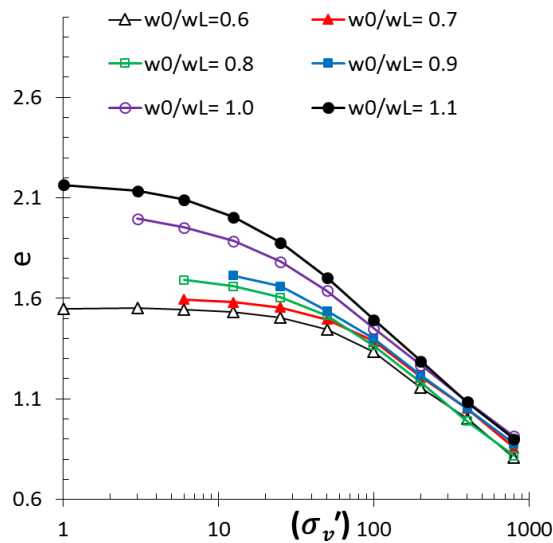


Figure 9-2. Semi-logarithmic compression curves ($e - \log \sigma'_v$)

In addition to verifying the compression curves of the pre-consolidation stages, the effectiveness of the intrinsic framework in normalising the void ratios of reconstituted/remoulded clays was investigated in this study. Figure 9-2 illustrates the intrinsic compression curves ($e - \log \sigma'_v$) of the Black clay prepared at various initial water contents in a semi-logarithmic space of $e - \log \sigma'_v$. As expected, the compression curves are inverse S-shape curves with a slight upward concave. Similar S-shape compression curves were reported in the literature for clays with different predominant clay minerals and degrees of plasticity (Habibbeygi, Nikraz, & Chegenizadeh, 2017; Habibbeygi, Nikraz, & Verheyde, 2017; Hong et al., 2010; Zeng et al., 2015).

The compressibility results of the pre-consolidation stages normalised using the intrinsic framework are replotted in Figure 9-3. As shown, the relationship between the void index and the compression pressure can be correlated by a linear line in a semi-log plane. The ICL equation (Equation (2-3)) is also plotted in the figure for comparison. As shown, the ICL can predict reasonably well the compressibility of the studied soil. However, there is a disparity between the calculated values of I_v from the experimental tests and the estimated values from the linear line of the ICL for lower consolidation pressures. This indicates that the initial water content at which the specimen was prepared has a great impact on the void index of reconstituted/remoulded clays at low stress levels.

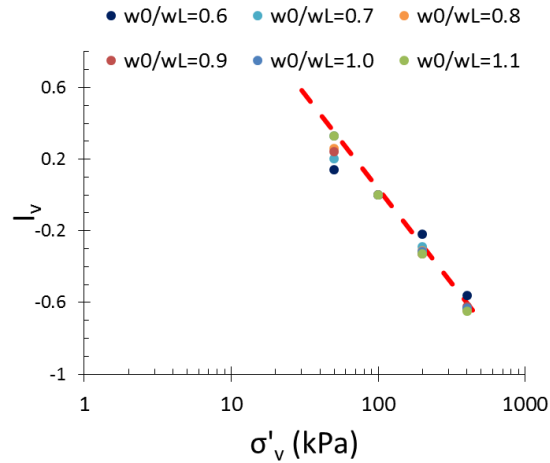


Figure 9-3. Semi-logarithmic normalised compression curves ($I_v - \log \sigma'_v$)

9.3.5.2 Undrained Shear Strength

After the pre-consolidation stage, direct shear tests were undertaken to assess the undrained shear behaviour of the pre-consolidated specimens. Figure 9-4 presents the relationship between the undrained shear strength and axial strain for four different normal stresses of 50, 100, 200, and 400 kPa. As seen in Figure 9-4a, the maximum undrained shear strength and undrained residual shear strength are nearly equal for different initial water contents. However, the gap between the peak shear strength and residual shear strength increases with increasing normal stress (Refer to Figure 9-4a to d). For instance, the peak undrained shear strength (S_u^*) is greater than 1.5 times the residual shear strength at a normal stress of 400 kPa.

According to the direct shear test results, w_0 has a great effect on the shear behaviour of the studied soil. In fact, S_u^* decreases with increasing w_0 at the same normal stress. Furthermore, this gap increases significantly when the normal stress increases. The gap between the shear strength of the specimen prepared at different initial water contents is significant, especially for high normal stress values (i.e. 200 and 400 kPa; refer Figure 9-4c and d). The results are presented in Figures 9-4 to 9-8.

Chapter 9 - Characterisation of the Undrained Shear Strength of Expansive Clays at High Initial Water Content Using Intrinsic Concept

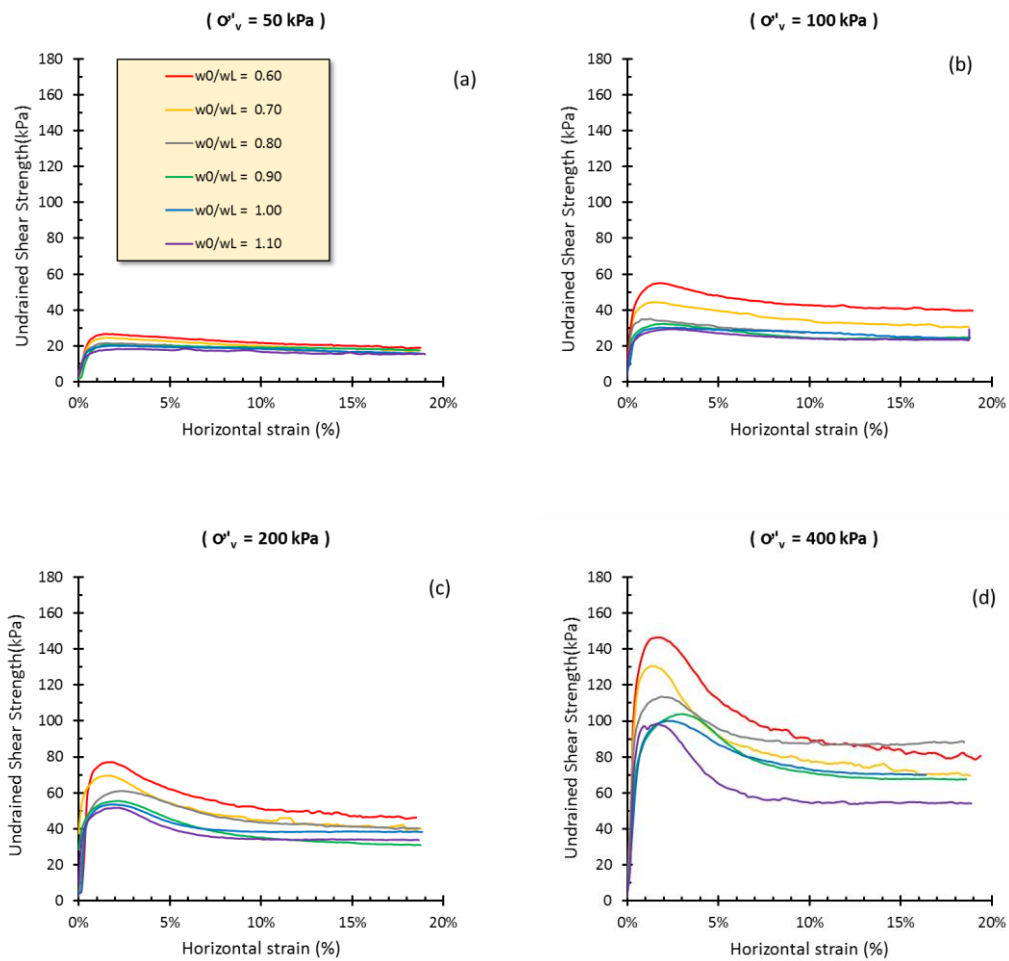


Figure 9-4. Relationship between undrained shear strength (S_u^*) and axial strain

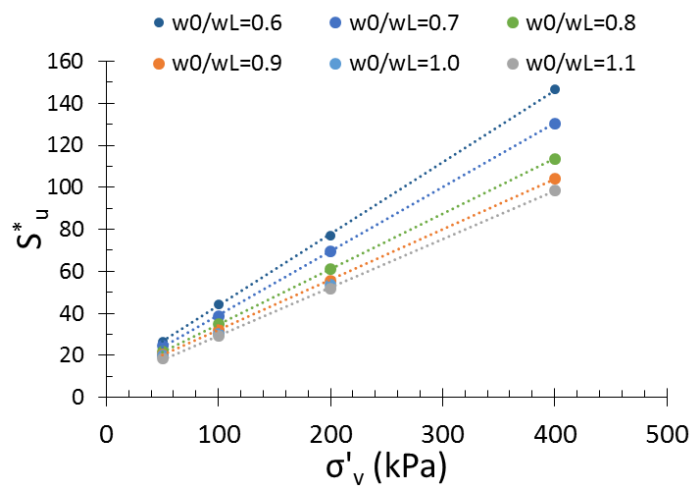


Figure 9-5. Undrained shear strength (S_u^*) versus normal stress

Figure 9-5 illustrates the relationship between the peak undrained shear strength (S_u^*) and the normal stress applied to the specimen prior to applying the shear displacement.

S_u^* is defined as the maximum undrained shear strength that can be applied to the clayey soil before it decreases and the axial strain increases rapidly. As shown, S_u^* has a linear relationship with the normal stress for different initial water contents (Figure 9-5). As expected, the undrained shear strength of a specimen prepared at a higher initial water content is less than that of a specimen prepared at a lower initial water content. S_u^* increases with increasing normal stress, and the difference between S_u^* at different initial water contents increases with increasing normal stress. The values of S_u^* at 50 kPa normal stress are similar for various initial water contents. However, S_u^* is greater at low initial water contents than the related values at high values of w_0 .

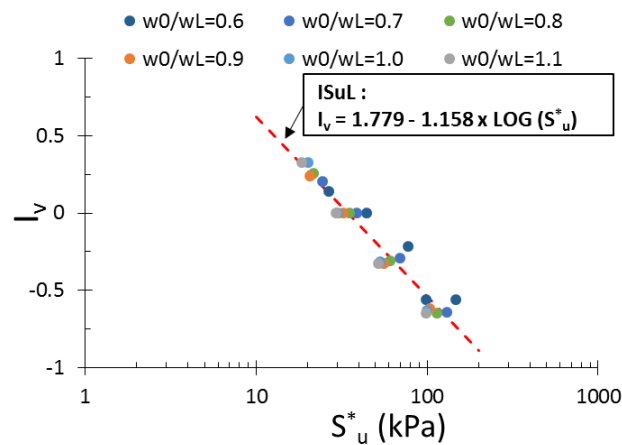


Figure 9-6. Void index versus undrained shear strength (S_u^*)

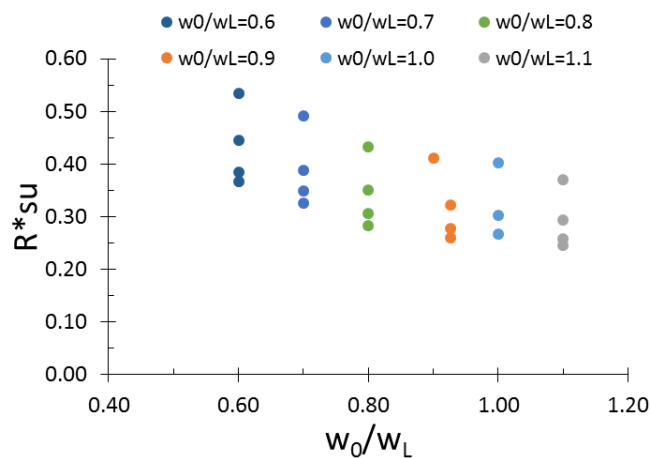


Figure 9-7. Normalised undrained shear strength (R^*_{su}) versus normalised initial water content

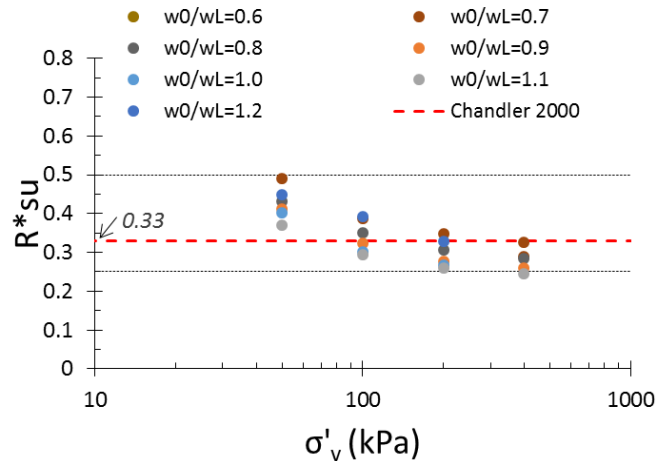


Figure 9-8. Normalised undrained shear strength (R_{su}^*) versus normal stress

To investigate the advantage of using the intrinsic frame of reference, the void index is plotted against S_u^* in Figure 9-6. Similarly to the ICL for compressibility of reconstituted samples, a line can be drawn on the results to correlate the undrained shear strength of such samples. This line is called the intrinsic strength line (IS_{uL}) in accordance with Burland et al. (1996), and can be defined by a straight line with an acceptable correlation coefficient ($R^2=0.94$) as follows:

$$I_v = 1.779 - 1.158(\log S_u^*) \quad (9-1)$$

To study the effect of w_0 and the normal stress on the related undrained shear strength, R_{su}^* is defined as the ratio of undrained shear strength to the effective normal stress in accordance with Chandler (2000).

Figure 9-7 displays the relationship between R_{su}^* and w_0/w_L for the studied clayey soil. As shown, R_{su}^* has a decreasing trend with increasing of w_0/w_L . This can be explained by the fact that specimens with greater w_0 values have higher void ratios in comparison to identical specimens at lower initial water contents.

Figure 9-8 indicates the relationship between R_{su}^* and the normal stress in a semi-log plane. As shown, R_{su}^* has a decreasing trend with increasing normal stress, and varies between 0.25 and 0.50 for the range of normal stresses of 50 to 400 kPa. However, the graph almost becomes level at higher normal stresses and reaches approximately 0.25 to 0.30 for the normal stress of 400 kPa. Accordingly, R_{su}^* is not constant for the studied clayey soil; this is in opposition to the constant value of 0.33 proposed by Chandler (2000). For comparison, the constant line of $R_{su}^*=0.33$ is also plotted in this figure. As shown, R_{su}^* is greater than 0.33 for lower normal stresses, and decreases to below 0.33 for normal stresses as high as 400 kPa.

9.3.6 Conclusions

Twenty-four series of direct shear tests were undertaken on remoulded/reconstituted specimens with different initial water contents to study the impact of the moisture content of the preparation stage and the normal stress on the undrained shear strength of clayey soils. The following conclusions are drawn based on employing the intrinsic framework to interpret the results:

- Shear behaviour of a reconstituted clay depends on the initial water content of the pre-consolidation stage. In fact, the shear strength of the reconstituted sample decreases with increasing initial water content. The difference between the undrained shear strength of samples pre-consolidated at different initial water contents increases with increasing initial water content.
- There is a significant difference between the peak undrained shear strength and the residual shear strength when the normal stress increases.
- Similar to the ICL for compression behaviour, the relationship between the undrained shear strength and the normal stress of reconstituted/remoulded clays can be expressed with a reasonable accuracy by a straight line (ISuL).
- The normalised undrained shear strength (R_{su}^*) depends on the normal stress, and has a decreasing tendency with increasing initial water content.
- The normalised undrained shear strength (R_{su}^*) varies between 0.25 and 0.5 with the normal stress. Moreover, R_{su}^* decreases with increasing normal stress and is almost constant at approximately 0.30 for normal stresses higher than 200 kPa.

10 EFFECT OF SHEAR RATE ON THE RESIDUAL SHEAR STRENGTH OF PRE-SHEARED CLAYS

10.1 Introduction

This peer-reviewed manuscript describes the shear behaviour of presheared clays. The residual shear strength of expansive clays is explored in this manuscript. The effect of shear rate is also studied in this manuscript.

The list of references, keywords, acknowledgements were excluded from this manuscript. The acknowledgements, abbreviation and references are combined on pages vi, xxiv and 192 of the current manuscript respectively.

Minor changes were made for the inclusion of the published manuscript into the current document. The differences comprise referencing, style and numbering of table captions and figure captions, wherever it was necessary to keep the uniformity and consistency of the current document. Furthermore, the numbering of equations, figures, and tables follows the current manuscript numbering and may differ from those of the published manuscript.

10.2 Citation

Habibbeygi, F., & Nikraz, H. (2018). Effect of shear rate on the residual shear strength of pre-sheared clays. *Cogent Geoscience*, 4(1), 1453989. <https://doi.org/10.21660/2017.29.20455>

10.3 Manuscript Contents

10.3.1 Abstract

This chapter presents the result of an experimental study on the shear behaviour of a pre-sheared clayey soil. The effect of shear rate on the residual strength of pre-sheared clays was investigated in a ring shear apparatus. A pre-sheared surface was initially developed at a slow rate of 0.1 mm/min. Fast shear rates were then applied to the pre-sheared specimens to investigate the impact of the shear rates on the results. The laboratory results show that there is an immediate tendency for the residual strength to increase with increasing shear rate. Following this, the fast residual strength continues to increase with further displacement, reaching the peak value of fast residual strength

(i.e. positive rate effect). Finally, the fast residual strength drops with increasing displacement to a value less than slow residual strength (i.e. negative rate effect). Overall, the relationship between the residual strength and the fast shear rates indicates a positive and negative rate effect based on the shear rates and the shear displacement.

10.3.2 Introduction

A residual shear strength of clayey soil under a prescribed normal stress is defined as the minimum shear strength of the soil under relatively large shear displacement (ASTM D647) (American Society for Testing and Materials, 2015). The displacement required to develop the residual strength is greater than the displacements corresponding to the peak shear strength (maximum shear strength) and the critical state shear strength (fully softened) in over consolidated soils. Accordingly, the residual shear strength is not related to the first slide of slopes but related to the existence of slip surface such as old landslides (Skempton, 1985). The orientation of clay particles parallel to the shear direction results in post peak drop of undrained shear strength and the shear strength reaches to the critical state value at the end of the first step (smaller shear displacement). When the particle reorientation completes at larger displacement, the shear strength reaches the residual value and remains constant with the increase of displacement (Skempton, 1985).

Moreover, the residual shear strength of the clayey soil is the shear strength along a pre-developed shear zone. In fact, this pre-existing movement can be developed by various factors, such as an old landslide, tectonic forces, a change in groundwater, earthquake forces, blasting, and dynamic/seismic loadings.

The residual shear strength of cohesive soils has been the centre of focus for many researchers all over the world for the past few decades to predict the behaviour of landslides (Gratchev & Sassa, 2015; Li et al., 2013; Tika & Hutchinson, 1999; Tika et al., 1996; Vulliet & Hutter, 1988). It is anticipated that the soil skeleton, clay type, particle size distribution, displacement rate, and pore water have considerable effect on the residual shear strength of cohesive soils (Gratchev & Sassa, 2015; Mesri & Olson, 1970).

Tika et al. (1996) performed a series of experimental tests on natural clays to investigate the effect of fast shearing on their shear behaviour. Their findings indicate that the shear strength of the soils studied increases when the shear rates are high. However, the shear strength of the fast rate test drops to a residual of shear strength,

which may be greater, equal or even less than the residual shear strength at a slow rate. Tika et al. (1996) also proposed three modes of failure (i.e. sliding, transitional, and turbulent failure) to explain the dissimilar tendency observed for the shear rate effect. Tika and Hutchinson (1999) carried out several ring shear tests on two natural samples collected from a slip surface failure in Italy. Their laboratory results show that there is a negative correlation between the residual strength and the shear displacement rate for the samples studied. In fact, the residual shear strength at a fast rate of displacement was assessed and found to be up to 60% less than that performed at a slow rate.

Li et al. (2013) carried out twenty-seven large ring shear tests on the specimens collected from the slip surfaces of three existing landslides. Three different shear rates were employed in their investigation to study the effect of fast rate on the results (i.e. 0.1, 1 and 10 mm/s). According to Li et al. (2013), the Atterberg limits and the particle size distribution, as well as the gravel and the fine fraction are additional factors that affect the residual shear strength. It was also found that the residual shear strength for the natural soils studied has a negative correlation with the plasticity index and the surface smoothness. This means that the residual strength decreases with an increase in either of these parameters. On the other hand, the particle symmetry defined by the elongation of the soil particles has a positive effect on the residual strength of the soil studied.

Gratchev and Sassa (2015) studied the shear strength of three different clays at different rates of shear displacement. It was concluded that the displacement rate had a considerable impact on all three clays studied. Based on their findings, the shear strength increases slightly when the shear rate decreases. It was also discovered that the increase of the shear strength depends on the confining pressure. Additionally, the increase of the shear strength is significant for confining pressures greater than 100 kPa.

Scaringi and Di Maio (2016) performed a series of controlled, direct shear tests on several mixtures of bentonite, kaolin and sand. In their study, the shear rate varied between 0.0001 and 100 mm/min. It was concluded that there is a positive correlation between the shear displacement rate and the residual strength of clayey soils when the clay fraction is higher than 50% and the displacement rate is greater than 1 mm/min. However, the displacement rate has no effect on the results for rates ranging from 0.0001 to 1 mm/min. Ring shear tests with various rates were also performed on a mixture of the soils and sodium chloride solution to study the effect of salt

concentration on the results. The results revealed that the salt concentration has a positive rate effect. In other words, the rate impact increases with an increasing salt concentration. It was also established that this increase can be explained well by the decrease in the void ratio and the increase of the solid particle contacts due to the solution concentration.

Most studies on the shear-rate effect show that the excess pore-water pressure developed at the shearing stage affects the undrained shear strength of clayey soils. Casacrande and Wilson (1951) proposed that the pore-water pressure generated in the sample at the low shear rate is higher than at higher shear rate. Accordingly, a change in the generated pore-water pressure during the shearing stage results in the dependency of undrained shear strength (Casacrande & Wilson, 1951; Richardson & Whitman, 1963).

Studies carried out on the residual shear strength of cohesive soils show some inconsistency or even opposite results (Gratchev & Sassa, 2015; Scaringi & Di Maio, 2016). It indicates that there is still a lack of experimental data on this topic. Correspondingly, more laboratory tests are required to ascertain the shear behaviour of clayey soils at large shear displacements. In this study, the residual shear strength of an expansive clay was measured after pre-shearing at various shear rates and normal stresses to investigate the effect of these factors on the shear behaviour of the soil studied.

10.3.3 Materials and Test Procedure

A clayey soil collected from the south of Perth, Western Australia was used in this study. This clay referred herein as ‘black clay’, is a highly expansive clay containing 68% clay, 20% sand, and 12% silt. The clay had a high value liquid limit (w_L) of 82%, and a plasticity index (I_p) of 47%. (Habibbeygi, Nikraz, & Chegenizadeh, 2017; Habibbeygi, Nikraz, & Verheyde, 2017). Analyses of the mineralogy of the samples indicate that the predominant clay mineral is smectite. The results of one-dimensional consolidation tests illustrate a high potential of expansion and compressibility for the black clay (Habibbeygi, Nikraz, & Chegenizadeh, 2017). The in-situ water content of the black clay was measured shortly after sample collection, and then assessed and found to be approximately 40% (Habibbeygi, Nikraz, & Verheyde, 2017).

The ring shear device used in this study is shown in Figure 10-1. This device can provide predefined torsional shear on an annular specimen under a fully saturated

Chapter 10 - Effect of Shear Rate on the Residual Shear Strength of Pre-Sheared Clays

condition to measure the residual shear strength of the specimen. The specimen is placed vertically between two porous stones. A counter balance (10:1 ratio lever) loading system is employed to apply the required pressure. A variable speed motor controlled by computer applies the rotation to the lower platen. A pair of load cells automatically measure the torque transmitted to the specimen. Both load cells and linear transducer are connected to a data acquisition system to record and process data. The shear strength of the specimen and the vertical load can be calculated for the predefined normal stress and shear rate using Equations (10-1) and (10-2):

$$P = 4\pi(R_2^2 - R_1^2) \cdot \sigma'_n \quad (10-1)$$

$$\tau = \frac{0.75 L (F_1 + F_2)}{4\pi(R_2^3 - R_1^3)} \quad (10-2)$$

where τ is the shear stress (MPa), F_1, F_2 are the shear forces being measured by load cells (N), R_1, R_2 are the inner radius and outer radius of the specimens respectively (mm), L is the length of the torque arm (mm), P is the vertical load being applied to the specimens (N), and σ'_n is the normal stress being applied vertically to the specimens (MPa).



Figure 10-1. Ring shear apparatus used in this study

First, the specimens were prepared following Head's procedure for preparing a remoulded sample (Head, 1986). Remoulded specimens were prepared by crushing an

Chapter 10 - Effect of Shear Rate on the Residual Shear Strength of Pre-Sheared Clays

air-dried sample using a rubber pestle and mortar. A predefined amount of water was then added to the oven-dried soil to achieve a water content equal to the in-situ water content. All samples were kneaded on a glass plate in order to be mixed uniformly and were stored in a three-layer air-tight bag for one day to mature prior to torsional shear tests. Finally, the specimens were placed into an annular mould using a spatula. The specimen filling was carried out in small horizontal layers to avoid any voids in the cell. The top of the specimen was flattened with the specimen container. They were then kept for 24 hr in the container fully filled with water to be saturated before applying the normal stress increments (Figure 10-2). The container was kept full during the consolidation stage.

Secondly, the specimens were consolidated under the stress increments to achieve the final desired normal stresses of 50, 100, and 200 kPa. Prior to proceeding to the pre-shear step, the normal stress increment at each stage of consolidation and the completion of each increment was verified following the test method, ASTM D2435. The vertical load required to be applied to the annular specimen was calculated using Equation (10-1).



Figure 10-2. Sample prepared before the consolidation stage

Following this, the specimens were pre-sheared to develop a shear surface. The specimens were sheared slowly at the rate of 0.1 mm/min for one day. A slow rate of shear displacement was selected to prevent any sample extrusion or to generate any pore water pressure during this step. To investigate the effect of shear rate on the shear behaviour of the pre-sheared specimens, various shear rates were applied to the specimens (i.e. 200, 100, 50, 10, 1 mm/min). The test procedure used in this study is schematically presented in Figure 10-3. According to this figure, the pre-sheared

specimens were sheared subsequently at five faster shear rates. The shear rates begin with a high value of 200 mm/min and eventually decrease to a relatively slow rate of 1 mm/min. The shear strength of the specimens at each step was then calculated for the predefined normal stress and shear rate of that step using Equation (10-2).

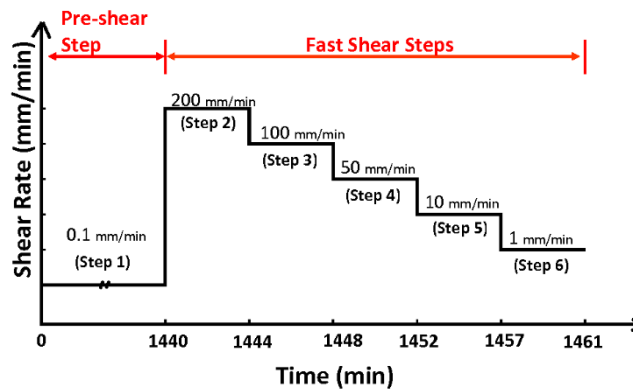


Figure 10-3. Shear rate and test procedure in this study

10.3.4 Results and Discussion

The ring shear tests under controlled shear displacement were performed on the black clay specimens consolidated at various normal stresses (i.e. 50, 100, 200 kPa). The specimens were sheared initially at a slow rate of 0.1 mm/min to develop a predefined shear surface. The shear rate was retained at a slow rate to prevent any sample extrusion, and to develop pore water pressure (step 1). In accordance with ASTM D6467, at least one revolution of the ring was employed to create a pre-sheared surface. At this stage, the shear strength neither increased nor decreased when the shear displacement increased. Therefore, it can be concluded that an existing sheared surface was present before conducting fast shearing stages. The experimental tests show that the residual shear strength of the clayey soil studied is 14.9, 45.3, and 51.1 kPa for the applied normal stresses of 50, 100, and 200 kPa, respectively. Figure 10-4 illustrates the results of the shear behaviour for the fast shear steps for different normal stresses (i.e. steps 2 to 6). As illustrated, the fast residual strength increases the slow residual strength at all fast shear rates after a relatively small shear displacement. For example, the increase in percentage relative to the slow residual strength is approximately between 5% and 10% for various shear rates at the normal stress of 200 kPa. This increase in comparison with the slow residual strength occurs at the maximum shear rate (i.e. 200 mm/min) and step 4 (i.e. 50 mm/min). The increase to the slow residual strength decreases with a decreasing shear rate, from 50 mm/min to the minimum shear

Chapter 10 - Effect of Shear Rate on the Residual Shear Strength of Pre-Sheared Clays

rate of 1 mm/min. However, the fast residual strengths are greater than the slow residual strengths under all normal stresses and at the shear rates.

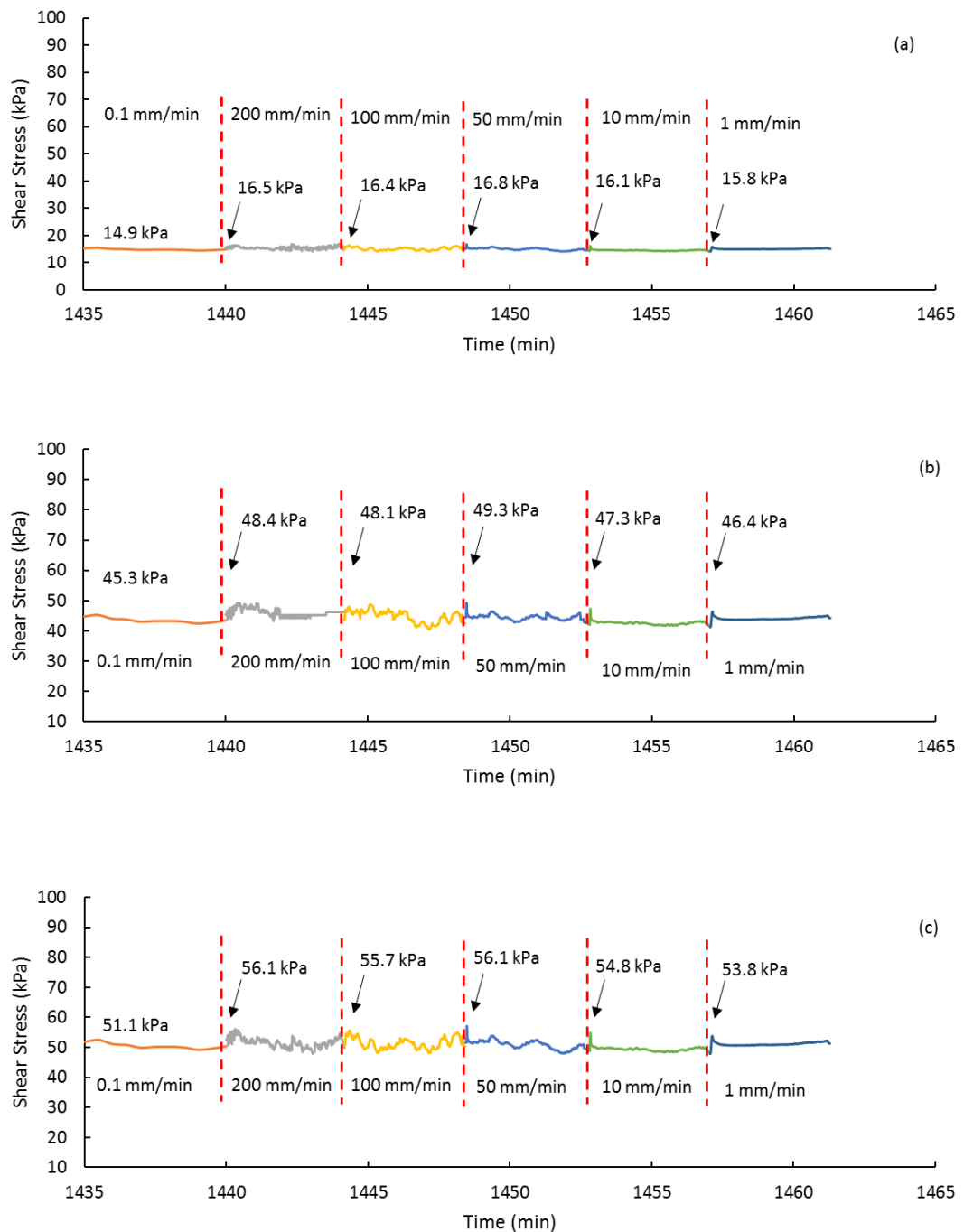


Figure 10-4. Residual shear strength versus time at various shear rates

(a) $\sigma'_n=50$ kPa, (b) $\sigma'_n=100$ kPa, and (c) $\sigma'_n=200$ kPa

The fast residual strengths of the clay studied versus time were replotted in Figure 10-5 to illustrate the effect of the applied normal stress on the results. As expected, the

Chapter 10 - Effect of Shear Rate on the Residual Shear Strength of Pre-Sheared Clays

residual strength increases with increasing applied normal stress. In fact, under the normal stress of 200 kPa, the slow residual strength of the soil studied is equal to 51.1 kPa, which is 342% and 112% of those under the normal stresses of 50 kPa and 100 kPa, respectively. Similarly, the same trend is nearly identical for the peak residual strength at faster rates. The fast residual strength under 100 kPa is nearly 10% higher than that under 50 kPa. Furthermore, the fast residual strength increases to three times the relative strength when the normal stress increases to 200 kPa.

Figure 10-6 presents the relationship between the fast residual strengths and time for various shear rates under the normal stress of 200 kPa. As illustrated, the fast residual strength increases immediately to a value greater than the slow residual stress (i.e. 54.1 kPa in comparison with 51.1 kPa) when the shear rate increases. The fast residual strength at the rate of 200 mm/min then continues to increase with time and reaches the peak fast residual strength (56.1 kPa). Tatsuoka, Di Benedetto, Enomoto, Kawabe, and Kongkitkul (2008) called this positive impact of fast shear rates on the residual strength of the clayey soils, ‘Isotach behaviour’. This positive effect is likely followed by a negative effect with a further displacement. In fact, the fast residual strength decreases from 51.1 to 47.9 kPa (i.e. 6% drop). Such an increase and decrease in the residual strength was also observed by other researchers for clayey soils (Tika et al., 1996). Likewise, such similar behaviour is also observed in this study for other rates of shear displacement. However, for the last two steps (steps 5 and 6), there is a sharp increase in the fast residual strength when the rate changes, which is followed by a drop in the fast residual strength. The positive and negative effect of shear rate is virtually the same for other normal stresses. However, only the results of the normal stress of 200 kPa are presented herein for the sake of brevity and simplicity.

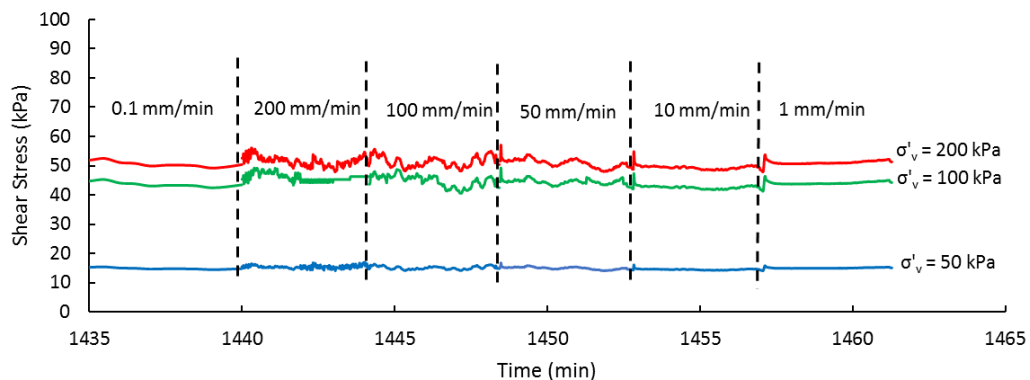


Figure 10-5. A comparison of residual shear strength at different normal stresses

Chapter 10 - Effect of Shear Rate on the Residual Shear Strength of Pre-Sheared Clays

Overall, when a pre-sheared surface developed at residual shear strength by slow shearing was subjected to more rapid shear displacement rate, the Isotach behaviour was observed. The observed behaviour includes an increase in shear strength (positive effect) at a negligibly small displacement followed by a drop reaches the minimum value (negative effect). The studies on the mechanism of the negative effect suggest that the main reason for the observed loss of strength is the penetration of water along the shear surface. Fast shearing results in an increase in the void ratio and thus the water content. The water is then free to penetrate along the shear surface and reduces the shear strength (Tika et al., 1996). On the other hand, the increase in the shear strength at small displacement may be related to volume and structural changes within the shear surface during the fast shearing stage. Fast shearing can cause disordering the structure of the shear surface and result in an increase in the strength (Figure 10-6).

Chapter 10 - Effect of Shear Rate on the Residual Shear Strength of Pre-Sheared Clays

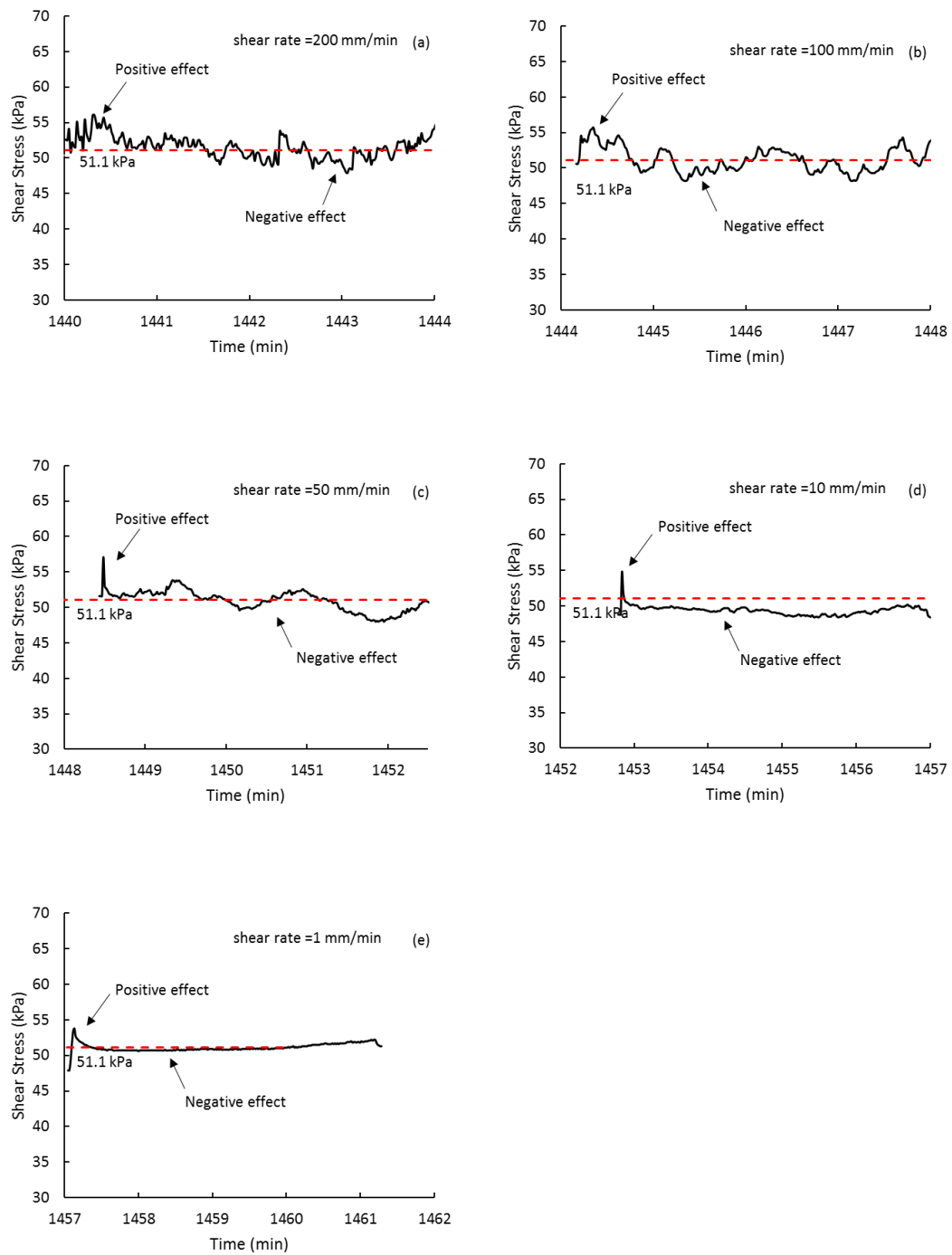


Figure 10-6. Residual shear behaviour under $\sigma'_n=200$ kPa at the various shear rates of (a) 200 mm/min, (b) 100 mm/min, (c) 50 mm/min, (d) 10 mm/min, and (e) 1 mm/min

10.3.5 Conclusion

The shear behaviour of a pre-sheared clay was investigated in this study to examine the effect of shear rate on residual shear strength. Based on the results of the ring shear tests, the following has been concluded:

- There is an immediate increase of residual strength in comparison with the slow residual strength when the shear rates increase. In fact, there is a positive rate effect on the residual strength at a small displacement.
- The fast residual strength of pre-sheared clays increases with an increasing applied normal stress.
- The peak residual strengths of the pre-sheared clay in the fast shear steps are dependent on the rates of shear displacement. The fast residual strengths increase the slow residual strength when the rates increase. Moreover, the maximum peak residual strength of the fast steps occurs at the displacement rates of 50 and 200 mm/min.
- There is a drop in the fast residual strength on top of the increase in the displacement for all various shear rates and the applied normal stresses.
- There is a positive and negative effect of displacement rate on the residual strength for the rates greater than 50 kPa, which requires more research on the shear behaviour of pre-sheared clayey soils at fast shearing conditions.

11 COMPRESSION BEHAVIOUR OF HIGHLY EXPANSIVE CLAYS STABILISED WITH A GREEN STABILISER OF MAGNESIUM CHLORIDE

11.1 Introduction

This peer-reviewed manuscript investigates the swell potential of the studied expansive clays. This manuscript also introduces a green stabiliser for treatment of expansive clays. The results show that magnesium chloride is effective in reducing the swell pressure of the studied clays as well as improving the geotechnical parameters.

The list of references, keywords, acknowledgements were excluded from this manuscript. The acknowledgements, abbreviation and references are combined on pages vi, xxiv and 192 of the current manuscript respectively.

Minor changes were made for the inclusion of the published manuscript into the current document. The differences comprise referencing, style and numbering of table captions and figure captions, wherever it was necessary to keep the uniformity and consistency of the current document. Furthermore, the numbering of equations, figures, and tables follows the current manuscript numbering and may differ from those of the published manuscript.

11.2 Citation

Habibbeygi, F., & Nikraz, H. (2018). Compression behaviour of highly expansive clays stabilised with a green stabiliser of magnesium chloride. *International Journal of GEOMATE*, 14(45), 144-150. <https://doi.org/10.21660/2018.45.10697>

11.3 Manuscript Contents

11.3.1 Abstract

The presence of expansive clays underlying infrastructures has been responsible for damages to the structures in many cases all over the world when the moisture content of these problematic soils changes. One of the effective methods to alleviate the swell potential of expansive clays is to stabilise them with an additive such as lime, cement, resins, chemicals and so on. In this study, the use of magnesium chloride ($MgCl_2$) as a

green stabiliser to improve the geotechnical properties of the treated clays has been investigated by conducting several laboratory tests. Currently, $MgCl_2$ is mainly used as an anti-icing materials in pavement industry; however, it has been recently received more attention as a stabiliser for clayey soils. Firstly, the effect of $MgCl_2$ on the consistency limits of the treated clayey soils was studied in this study. Next, the swell pressure and free swell strain of the treated samples were measured and the results compared with the one of the untreated samples. Overall, the results state that even a small dose of $MgCl_2$ can be used as a stabiliser for expansive clays to improve the geotechnical properties considerably and to mitigate their swell potential effectively.

11.3.2 Introduction

Expansive clayey soils with high potential of swelling are mostly found in arid and semi-arid regions all over the world. These soils are highly susceptible to the variation of their water content and cause huge problems to pavements, embankments, drinking water networks, irrigation open canals, railways, mining structures (e.g. overland conveyors), and light residential buildings for excessive settlement and expansion. Globally, billions of dollars have been spent on either financial losses or treatment work of these problematic soils every year (Basma et al., 1995; Habibbeygi, Nikraz, & Chegenizadeh, 2017; Shi, Jiang, Liu, & Fang, 2002). Generally speaking, the cost of damage to the structures due to shrinkage and swelling of expansive clays is even greater than the cumulative cost of damage caused by all natural disasters such as hurricanes, volcanic eruptions, earthquakes, floods, and tornadoes (Nelson & Miller, 1992; Vanapalli & Lu, 2012).

The damage to structures can be eliminated or significantly mitigated by stabilisation of expansive clays prior to construction of the structures on problematic soils. The stabiliser agents can be used to improve the engineering properties and to reduce the swelling and shrinkage potential of expansive clays. Based on the usage frequency of the stabilisers and the popularity of them amongst engineers, they may be categorised into two major groups: Traditional and non-traditional stabilisers.

Traditional stabilisers comprising cement, hydrated lime, zeolite, industrial waste, fly ash and gypsum are frequently used in industrial projects and extensive case studies as well as laboratory tests have been performed on the ability of these additives to improve the compressibility of soft clayey soils and alleviate the swelling pressures (Al-Mukhtar et al., 2014; Alrubaye et al., 2016; Bourokba Mrabent et al., 2015;

Hossanlourad et al., 2017; Jha & Sivapullaiah, 2015; Kang et al., 2015; Phanikumar et al., 2014; Wang et al., 2014).

Lime as the most popular type of stabilisers is used generally as one of the forms of hydrated dolomitic lime $[\text{Ca}(\text{OH})_2 \cdot \text{Mg}(\text{OH})_2]$, dolomitic quick lime $[\text{CaO} \cdot \text{MgO}]$, hydrated lime ($\text{Ca}(\text{OH})_2$) and quick lime (CaO). Among aforementioned types of lime, hydrated lime is preferably used in the construction industry because there is no need of extra water for hydration process. Moreover, it can produce a considerable amount of free calcium which is essential for the stabilisation of expansive clays.

Another traditional stabiliser is cement which is mostly used as Portland cement. Similar to lime, calcium oxide is produced in hydration process of cement which is the basis of the stabilisation of the clayey soils. Adding cement and lime as the stabiliser agents to the expansive clays with an adequate amount of water produces Ca^{2+} ions. Free calcium ions replace monovalent ions which reduce the interlayer electrochemical forces and increase the particle packing. This cation exchange improves the soil properties of the treated clay such as increasing the soil density, workability and shear strength and reducing the soil plasticity, dispersive properties and expansion potential (Khemissa & Mahamedi, 2014; Ouhadi et al., 2014).

It is well established that pozzolanic reaction of clayey soil and cement/lime improves the engineering properties of the treated clays and alleviate the sensitivity of the expansive clays. Nevertheless, the usage of these traditional stabilisers (i.e. lime and Portland cement) is decreasing recently due to the increase of awareness of environmental issues and waste disposal difficulties as well as an increase in cost and treatment procedure.

On the other hand, there are a number of non-traditional chemical stabilisers which are increasingly being investigated for their effectiveness in treating expansive clays for the past two decades (Latifi et al., 2015; Ouhadi et al., 2014; Turkoz et al., 2014; Yunus et al., 2013). Chemical stabilisers as an alternative to the traditional calcium-based stabilisers are comprised of combinations of liquid polymers, resins, ions, silicates, acids, and lignin derivatives (Latifi et al., 2015; Yunus et al., 2013). These chemical stabilisers are normally concentrated liquids diluted with water or powder dissolved in water and then sprayed on the problematic clayey soils (e.g. expansive clays) prior to compaction. Polymers are also very effective to mitigate the swelling potential by developing bonds between clay minerals and polymers. Non-traditional stabilisers not only reduce the cost of transportation but also are easy to be employed as only small

amounts of chemicals are required and the process of applying them to the problematic soils is practical. Chemical stabilisers are also highly effective for high sulphate soils in comparison to calcium-based stabilisers (i.e. cement and calcium) as some traditional stabilisers have no major effect on soils with a high amount of sulphate and even distress excessive heave called sulphate-induced heave (Mitchell & Soga, 1976; Puppala et al., 2014).

Bischofite with the chemical name of “Magnesium Chloride Hexahydrate” ($\text{MgCl}_2 \cdot 6\text{H}_2\text{O}$) is one of the non-traditional stabilisers which has recently been the centre of focus of researchers. Bischofite is normally used for dust control and also for decreasing coarse particle scattering and preventing ice formation in road and pavement industry (Thenoux & Vera, 2002). In comparison to calcium-based stabilisers such as cement which produces a large amount of green-house gas, Magnesium chloride is a sea salt which has been recognised as a green stabiliser worldwide as it has no harm to plants and animals as well as no corrosion to asphalt or concrete pavements and vehicles (Goodrich, Koski, & Jacobi, 2009). In Europe, the ordinary salt (NaCl) is replaced by MgCl_2 almost completely as the regular salt is ineffective at very low temperature and cause a lot of damages to trees and asphalt every year. On the other hand, magnesium chloride has more prolong effectiveness as an ice melter with little damage to pavements and vegetation. It caused magnesium chloride as a popular environmentally friendly ice melter in countries experiencing cold winters.

As the use of magnesium chloride is becoming more common especially in pavement industry, its potential to mitigate the swelling potential of expansive soils is getting more attention amongst researchers. There is quite limited research on the performance of treated clays with MgCl_2 in the literature (Latifi et al., 2015; Turkoz et al., 2014; Yunus et al., 2013). Nevertheless, more research is still required to investigate the effect of MgCl_2 on the swelling pressure of expansive clays with different mineralogies.

To the best of authors' knowledge, there is also a lack of study on the free swell of the treated clays with MgCl_2 . This investigation is important to understand the behaviour of the stabilised clay when subjected to excavation loadings in future. In this research, the effect of magnesium chloride on the mitigation of the expansion potential of a highly plastic clayey soil from Australia is investigated.

Accordingly, the following questions are addressed in this study:

Chapter 11 - Compression behaviour of highly expansive clays stabilised with a green stabiliser of magnesium chloride

- What is the effect of magnesium chloride on the plasticity of the high plastic clayey soils?
- What is the effectiveness of various percentage of magnesium chloride in mitigating the swell pressure of expansive clays?
- What is the effect of magnesium chloride on the free swell of the treated clayey soils in comparison with the untreated soil?

11.3.3 Materials and test program

11.3.3.1 Materials

The expansive clayey samples used in this research were collected from the southern part of Perth, Western Australia (Figure 11-1). Due to the colour of the studied soil, it is referred herein as the 'black clay'. To characterise the soil sample, soil classification tests including soil classification (ASTM D2487), organic content, moisture content (ASTM D2216), Atterberg limits (i.e. liquid limit, plastic limit and plasticity index (ASTM D4318) were performed (American Society for Testing and Materials, 2011). According to the Unified Soil Classification System, the black clay can be classified as a high plasticity clay (CH). The liquid limit (w_L) and plasticity limit (w_P) of the black clay are measured to be 82% and 35% respectively. The in-situ water content of the samples were measured immediately after collection and was 40% (Habibbeygi, Nikraz, & Verheyde, 2017). The laboratory tests also state that the shear strength of the black clay is highly dependent on the initial water content (Habibbeygi & Nikraz, 2018a). The particle size distribution (PSD) curves of the studied soil are illustrated in Figure 11-2; the PSD tests were performed on three samples (sample no.1-3). Based on the particle density test performed on the studied sample using a hydro-pycnometer, the specific gravity is measured to be 2.6 (ASTM D854). As shown, 84% of the soil consisted of fine materials of which a hefty percentage (68%) is clay. Based on X-ray diffraction (XRD) test results, smectite is the dominant clay mineral of the black clay (Habibbeygi, Nikraz, & Chegenizadeh, 2017).

There are several methods to indicate the swell potential of an expansive soil based on only the physical properties. One of the simplest methods proposed by Building Research Establishment (BRE) is to use plasticity index (Anon, 1979). According to this method, the potential for volume change of a soil with a plasticity index greater than 35% is classified as very high, between 22% and 48% as high, between 12% and

Chapter 11 - Compression behaviour of highly expansive clays stabilised with a green stabiliser of magnesium chloride

32% as medium, and less than 18% as low. For the studied soil, the plasticity index of 47% makes the potential for volume change of the black clay be categorised as ‘very high’. Another method for assessing the swell potential is to employ the soil activity chart proposed by Van Der Merwe (Van Der Merwe, 1956). In this method, the expansiveness of a soil is analysed by both the plasticity index and the clay content of the soil. As can be seen in Figure 11-3, the black clay is placed into the high expansion category based on the soil classification and the results of consistency tests.



Figure 11-1. Sampling site, Baldyvis Western Australia (Google Maps, 2018)

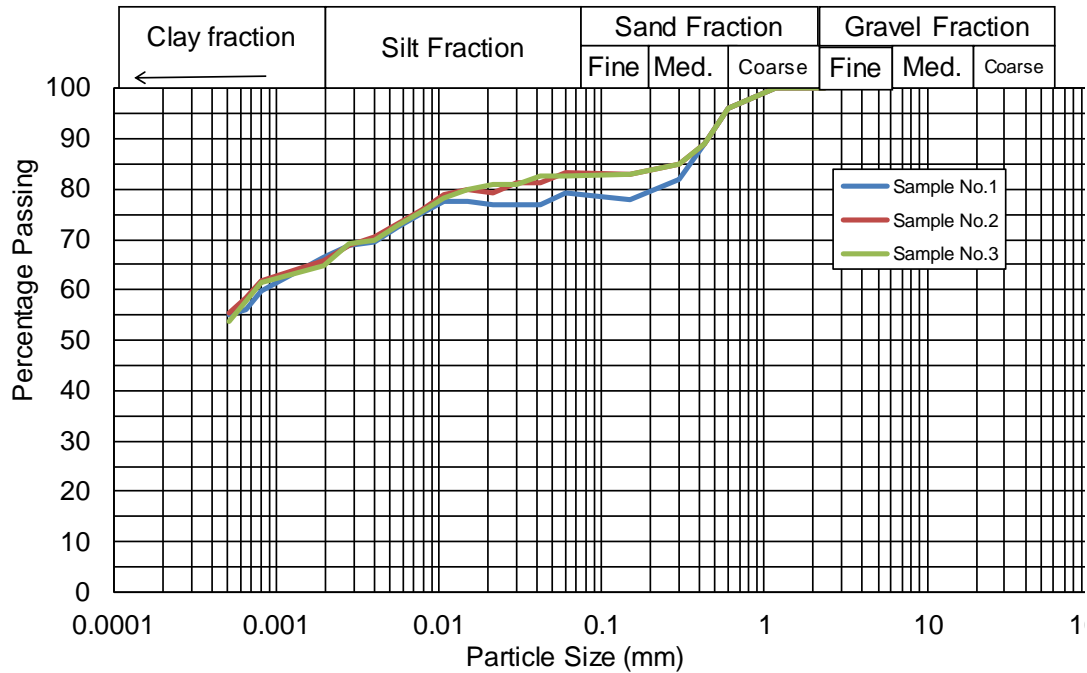


Figure 11-2 Particle size distribution curves of the black clay

Bischofite (Magnesium chloride, $MgCl_2$) has been used effectively as a de-icing material in winter for road maintenance in many countries all over the world such as the U.S., Canada, Russia, Netherlands, Belgium, France, Scandinavia, the U.K. and Germany. $MgCl_2$ can be found in the forms of flake, powder and liquid.

The salt used in this study was in the form of flake with white colour and a chemical formula of ($MgCl_2 \cdot 6H_2O$), Magnesium Chloride Hexahydrate, and a purity of 98 – 100%.

11.3.3.2 Sample Preparation

Samples were prepared in accordance with the sample preparation procedure proposed for remoulded samples (Head, 1986). Initially, the collected samples were oven-dried at $105^\circ C \pm 5$ until the constant weight achieved. The dried samples were then ground and sieved using a 2 mm nominal opening size to obtain a uniform soil powder before using them in the laboratory tests. Different percentages of $MgCl_2$ (2, 4, 6, 8, 10, and 12%) were added to distilled water to make $MgCl_2$ solution. The quantity of water was measured for all samples to simulate the in-situ water content. Then samples were kneaded manually until a homogeneous mixture formed. A measured weight of the wet clay relating to the in-situ soil unit weight (1.67 g/cm^3) was then placed into the oedometer ring and compacted to reach the in-situ density. The specimen was fully

covered with multiple cling foils and cured for 24 hours in a temperature-controlled room ($22^{\circ}\text{C} \pm 2$) to reach a uniform moisture distribution prior to conducting the laboratory tests.

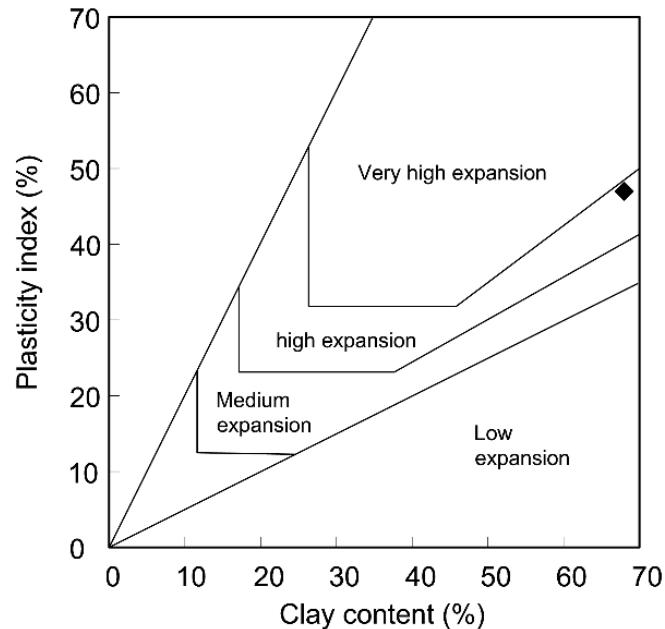


Figure 11-3. Activity chart for expansive clays (redrawn from Nelson & Miller, 1992)

11.3.3.3 Test Procedure

An automotive one-dimensional consolidation apparatus was used for measuring the swelling pressure and free expansion of the treated and the untreated clays. The swell tests were carried out on 64 mm x 25.4 mm (diameter x height) specimens with two porous stones and filter papers on top and bottom of the specimens. To reduce the friction between the specimen and the consolidation ring, a thin layer of silicone grease was used. Zero-deformation method and free swell tests were used to investigate the effect of stabilisation agent on the compressibility and the swell pressure of the studied expansive clays (Basma et al., 1995).

A small amount of seating pressure, 3 kPa, was applied on the specimen in zero-deformation test prior to filling the cell with water. As swelling starts, consolidation pressure is increased continuously to prevent the specimen from any expansion. The maximum pressure applied to the specimen to avoid any swelling (zero deformation), is called the swell pressure. This procedure was undertaken for all various percentage

of $MgCl_2$ for the treated samples and the untreated one (zero per cent of magnesium chloride).

In free swell tests, a specimen was allowed to swell completely under no seating pressure. The vertical displacement was measured by LVDT.

11.3.4 Results and discussion

11.3.4.1 Atterberg Limits

Index tests including liquid limit and plastic limit were conducted on the untreated clayey sample (zero per cent of $MgCl_2$) and the treated samples with various percentage of magnesium chloride (2 to 12%) based on ASTM D4318. The results of consistency limits are presented in Figure 11-4. As seen, the index parameters are decreasing with the increase of the stabiliser dose. Moreover, the index parameters virtually flatten when the stabiliser dose is greater than 8%. The results state that the use of $MgCl_2$ as the stabiliser is significantly effective for reducing both the liquid limit and the plastic limit; however, the liquid limit decreases in a great extent in comparison with the plastic limit. The reason for the decrease of index parameters can be explained by a reduction in the thickness of Defuse Double Layer (DDL) because of the influence of $MgCl_2$ on the cation exchange.

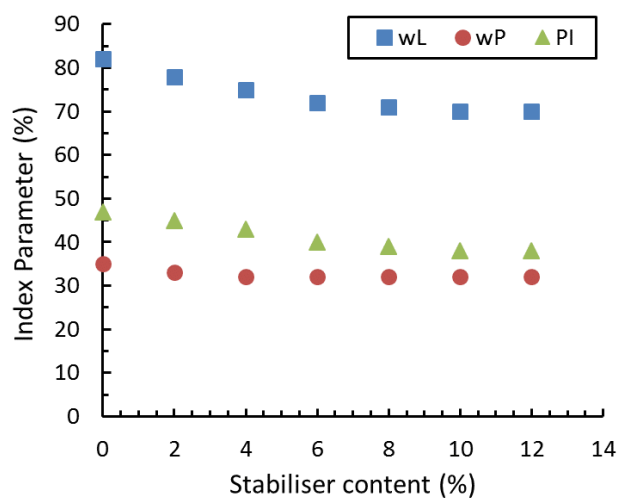


Figure 11-4. Variation of the index parameters with the stabiliser content

11.3.4.2 Swell Pressure

Based on the activity chart, the studied clay is classified as a soil with very high potential for expansion. Likewise, according to another classification, the clayey soil with the plasticity index greater than 35% can also be considered as a soil with very high potential for expansion (Chen, 1988). The results for measuring the swell pressure with the zero-deformation technique are plotted in Figure 11-5. The results are replotted on a semi-logarithmic plane in Figure 11-6. As seen, the curves can be divided into three distinct stages of initial swelling, primary swelling and secondary swelling. The swell pressure increases gradually in the initial phase; the swell pressure then rises considerably with elapsed test time after this stage. Moreover, the swell pressure reaches nearly the final value at the primary swell stage. As seen in Figure 11-6, the primary phase which is responsible for the main portion of the value of swell pressure, begins after approximately 40 – 60 minutes of the start of inundation. Moreover, after about 16 – 24 hours, 90 per cent of the swell pressure occurs in all of the stabiliser contents. Results depict that the swell pressure of the untreated sample is 83 kPa; however, the swell pressure of the treated samples reduces considerably with the use of the stabiliser even with a low dose of $MgCl_2$ (i.e. 2%). In fact, the swell pressure plunges to 16 kPa, one-fifth of the initial value, with 8% of $MgCl_2$. The swell pressure remains almost constant with the increase of stabiliser content from 8% to 12% from 16 kPa to 14.2 kPa.

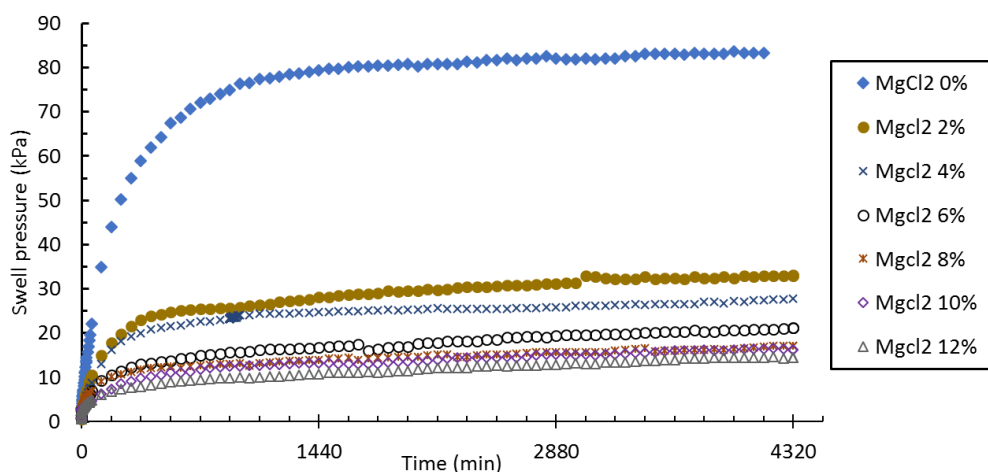


Figure 11-5. Variation of the swell pressure against test time for various stabiliser content

11.3.4.3 Free Swell

The swell displacements against test time of the treated and the untreated samples were measured directly to determine the free swell strain. A soil specimen of 25.4 mm height and 64 mm diameter was placed between two porous stones and filter papers were used in the free swell tests. Then, the sample soaked to swell freely; no seating stress was applied during the free swell tests. Vertical displacement was measured with test time and the swell strain was calculated correspondingly. Figure 11-7 shows the swell strain vs elapsed test time in a semi-logarithmic scale. Similarly to the results of zero-deformation swell, all free swell curves can be divided in to three distinctive stages. A schematic of the free swell curve is presented in Figure 11-8 to define these stages. At the initial swelling stage, the vertical displacement increases gradually with time for the first 40 – 60 min. Then, it increases sharply and reaches approximately 90% of the total swell strain in the second stage which referred to as the primary swelling stage. Finally, the vertical displacement levels with time when the elapsed time is greater than 4 days. Recording the vertical displacement continued until no further displacement observed. As the main clay mineral of the studied soil is smectite (Habibbeygi, Nikraz, & Chegenizadeh, 2017), it is expected that the swelling displacement continues in the secondary stage; the secondary swell strain is approximately 5 – 10% of the total swell for the studied clay. Overall, the secondary swell strain decreases when the $MgCl_2$ content increases.

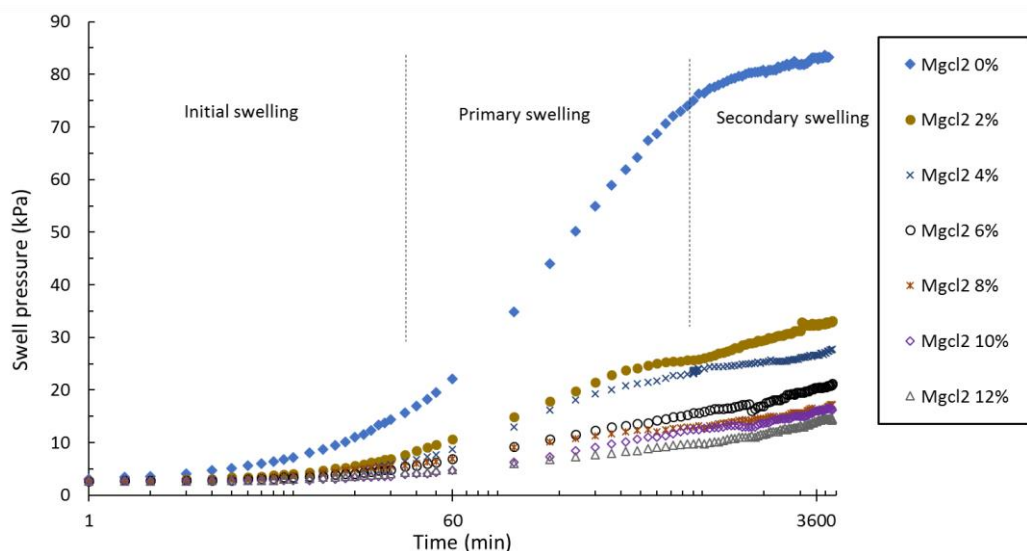


Figure 11-6. Variation of the swell pressure against test time for various stabiliser content in a semi-logarithmic plane

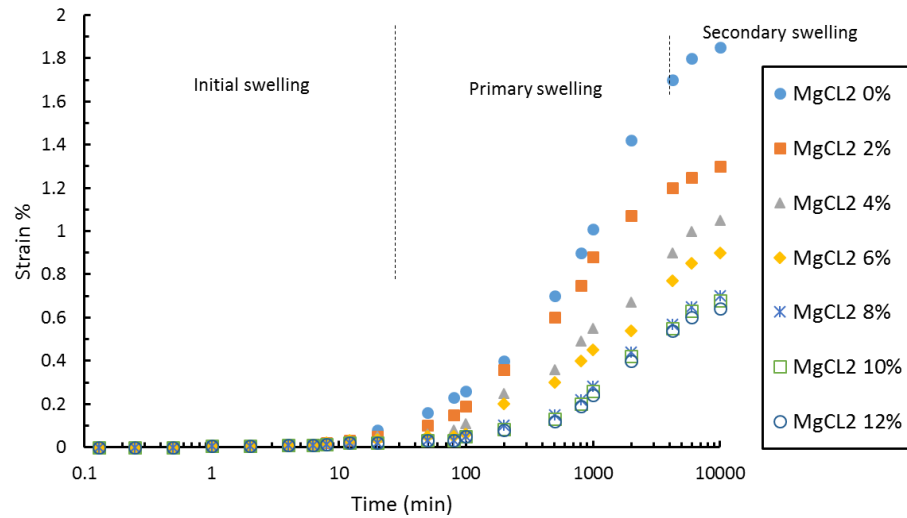


Figure 11-7. Variation of the swell strain against time for various stabiliser contents

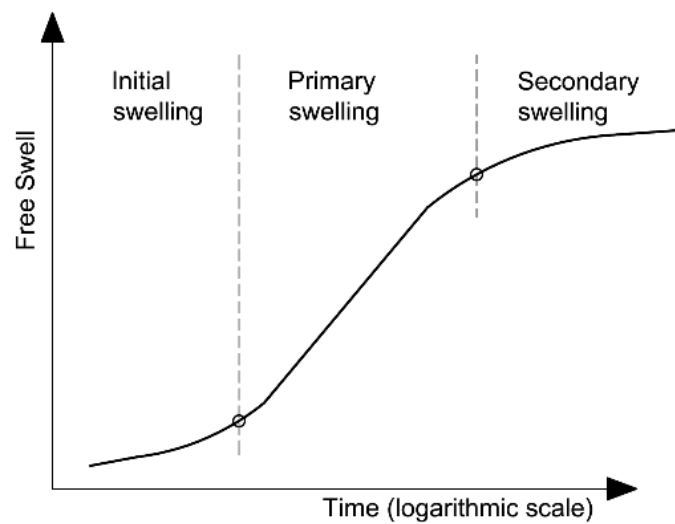


Figure 11-8. A schematic of swell pressure with time
(Sridharan & Gurtug, 2004)

11.3.5 Conclusions

In this study, the following conclusions were drawn:

- Adding $MgCl_2$ as a stabiliser to the clayey soil decreases the consistency limits (i.e. liquid limit and plastic limit). However, the tendency is decreasing for both of consistency limits, the decreasing effect is greater for the liquid limit rather than the plastic limit.

Chapter 11 - Compression behaviour of highly expansive clays stabilised with a green stabiliser of magnesium chloride

- The swell strain of the treated samples with MgCl_2 is decreasing considerably to one-fifth of the initial value of the untreated sample. The swell strain remains nearly constant for the MgCl_2 content higher than 8%.
- Zero-deformation test results show that the swell pressure of the treated expansive clays decreases from 83 kPa to 16 kPa with the use of 8% of MgCl_2 as the stabiliser. The tendency is decreasing with the increase of additive content; however, the use of higher values of MgCl_2 (> 8%) slightly alleviates the swell potential of the treated samples in comparison with the sample treated with 8% of MgCl_2 .
- The zero-deformation test and the free swell test results show that the swell curves can be divided into three separate stages of initial, primary and secondary swelling. However, the swell displacement mainly occurs in the primary stage, a 5-10 % of the total displacement happens in the secondary stage because of the existence of smectite in the clay mineralogy.

12 PREDICTION OF INTRINSIC COMPRESSIBILITY PARAMETERS OF RECONSTITUTED CLAYS USING ARTIFICIAL NEURAL NETWORK

12.1 Introduction

This chapter employs artificial neural networks to predict the compression behaviour of expansive clays. The simulated intrinsic compression parameters are compared with ones measured in laboratory tests. The findings show that ANN models are an effective method for predicting the behaviour of expansive clays.

The acknowledgements, abbreviations and references relevant to this chapter are provided on pages vi, xxiv and 192 of the current manuscript, respectively.

12.2 Manuscript Contents

12.2.1 Abstract

The precise determination of the compressibility parameters of reconstituted clays is essential for accurately evaluating long-term compression behaviour and estimating the settlement of clayey soils. As conventional experimental procedures are time-consuming and relatively expensive, various attempts have been made to correlate intrinsic compressibility parameters with soil index parameters such as the liquid limit, plastic limit, specific gravity, initial water content and so forth. However, regression models mostly either under- or overestimate the intrinsic compression parameters due to their limited numbers of input parameters. Moreover, the reliability of these formulas is generally limited to their own test series and they cannot accurately predict the compression parameters of other test series. This chapter presents an artificial neural network model that predicts intrinsic compression parameters based on the index parameters and mineralogy of reconstituted clays. A series of sensitivity analyses were carried out to investigate the effect of each input parameter on the compression parameters. In these analyses, the number of neurons in the hidden layer was varied from 5 to 25 and various transfer functions adopted to determine the best performance. Nine combinations of transfer functions with 21 different models, a total of 189 ANN models, were experimented with to optimise the ANN model. A

Chapter 12 - Prediction of intrinsic compressibility parameters of reconstituted clays using artificial neural network

relationship for the neural model is also developed based on the weights and biases of the optimised neural network model. The results show that the ANN models are able to predict the intrinsic compression parameters accurately.

12.2.2 Introduction

The use of dredged slurry clays in land reclamation has become increasingly popular in recent years for the following reasons. First, the high amount of slurry sediment dredged annually from rivers and lakes can be used environmentally-friendly in developing new land as part of sustainable development. Second, the prices of granular materials such as sand and gravel for use in new developments are soaring. There are dwindling sources of borrow materials, which pushes engineers to use available materials instead. Third, the dumping of mining waste materials, which include silty and clayey sands with high amounts of initial water, is becoming increasingly challenging for mining industries as suitable dumping areas are limited by restrictive environmental regulations and proper dumping procedures are costly. Consequently, the reuse of mining waste as fill material may be envisaged as a sustainable solution to both dumping issues (environmentally and practically) and the depletion of granular materials.

The very first step in employing dredged sediments in land reclamation is to comprehend the compression behaviour of such clayey soils, which have high initial water contents. In fact, compression parameters are key to settlement estimation and most other engineering practices where highly compressible layers, such as slurry clays, are used. The structures of dredged sediments and mining waste is completely broken down during the dredging or mining process, such that they can be classified as reconstituted soils. By definition, a reconstituted clayey sample is a completely remoulded sample that is prepared at a water content equal to or higher than its liquid limit (Burland, 1990).

Burland (1990) proposed a new concept of normalisation for understanding the compression behaviour of reconstituted clays by introducing a new normalised parameter coined the *void index*. This concept has been used extensively by other researchers as a reference framework for new compressibility models, experimental correlations and interpreting the compression or mechanical behaviour of reconstituted clays (Al Haj & Standing, 2015; Habibbeygi & Nikraz, 2018a, 2018d; Hong et al., 2010; Liu et al., 2013).

Many researchers have conducted consolidometer tests on reconstituted clays to investigate the compression behaviour of these soils under different initial water contents, mineralogies and levels of consolidation stress. The results of some recent consolidation tests on reconstituted clays illustrate: (i) the intrinsic concept and normalised parameter of the void index can be used effectively to predict the compression behaviour of reconstituted clays (Habibbeygi, Nikraz, & Verheyde, 2017; Hong et al., 2012). (ii) The initial water content has a great impact on the compression behaviour of reconstituted clays (Cerato & Lutenegeger, 2004; Habibbeygi, Nikraz, & Chegenizadeh, 2017; Hong et al., 2013). (iii) Clay mineralogy has a great influence on the compression behaviour and compression parameters of reconstituted clays (Habibbeygi, Nikraz, & Chegenizadeh, 2017). (iv) Reconstituted compression parameters can be estimated indirectly by experimental relationships using some simple geotechnical parameters rather than conducting consolidometer tests (Burland, 1990; Liu et al., 2013). Although the compression behaviour of reconstituted clays may be studied relatively accurately by one-dimensional consolidation tests, these are time-consuming and relatively costly, which makes the derivation of compression parameters relatively expensive for many practical engineering projects. Correspondingly, many researchers have endeavoured to develop reliable empirical equations for estimating compression parameters from simple physical parameters. In the past decade, some research has been conducted on correlating the compression parameters of reconstituted clays with the physical properties of soils via laboratory tests. Initial water content, liquid and plastic limits, and void ratio are the main parameters adopted in regression formulas to predict compression parameters (Habibbeygi, Nikraz, & Chegenizadeh, 2017; Habibbeygi, Nikraz, & Verheyde, 2017; Kootahi & Moradi, 2016; Lee et al., 2015; Lei et al., 2015; Takashi, 2015; Xu & Yin, 2015; Zeng et al., 2011). One common limitation of all these empirical relationships is over-simplification, which reduces the accuracy of compression parameter estimates. For instance, most experimental equations consider only one or two physical parameters, such as the liquid limit and/or void ratio, which reduces the accuracy of the estimates. On the other hand, experimental equations with more than two parameters based on multiple regression are too complex to use, which negates the main point of their development. Therefore, there is a need for a simple approach to predicting the complex behaviour of reconstituted clay compressibility. It must be able

Chapter 12 - Prediction of intrinsic compressibility parameters of reconstituted clays using artificial neural network

to estimate the compression parameters from physical parameters with reasonable accuracy.

An artificial neural network (ANN) is a computational procedure for solving complex problems that simulates the structure of the human nervous system (Hagan, Demuth, Beale, & De Jesús, 1996). One advantage of ANNs is their mechanism of learning, which makes them capable of solving complex multi-invariant problems accurately and rapidly. The ability of the ANN to solve non-linear complex problems with multiple invariants makes it a powerful tool for solving almost all logical and mathematical problems. In the past decade, ANNs have been used to solve many problems in various fields of science and engineering, such as marketing, mining, aerospace, banking, medical, real estate, insurance, finance, electronics, robotics, transportation and so forth.

In this chapter, an ANN model was employed to predict the compressibility parameters of reconstituted clays. It uses geotechnical index parameters as well as clay mineralogy as input invariants. The objective of this study was to achieve much more accurate results in comparison with the regression-based relationships proposed by other studies. To the authors' knowledge, most previous studies of reconstituted soil compressibility prediction only consider the effect of index parameters and initial water content on the compressibility parameters of reconstituted clays (Cerato & Lutenecker, 2004; Kootahi & Moradi, 2016; Lee et al., 2015; Lei et al., 2015; Takashi, 2015; Xu & Yin, 2015; Zeng et al., 2011). Only a few studies have taken into account the influence of clay mineralogy (Habibbeygi, Nikraz, & Chegenizadeh, 2017; Xu & Yin, 2015). In this chapter, the effect of clay mineralogy on the compressibility parameters of reconstituted clays is assessed using a broad range of geotechnical data from the literature and from laboratory experiments. In addition, most previous studies employ only one of the intrinsic parameters (compression index or void ratio) as the output. In this study, both intrinsic parameters (e_{100}^* and C_c^*) were predicted by the ANN considering the following input parameters: initial water content (w_0), specific gravity (G_s), liquid limit (w_L) and plastic limit (w_P). A multiple-output ANN model was used in this study to decrease processing time and workload while maintaining accuracy.

A total of 103 laboratory consolidometer and geotechnical index tests on reconstituted clays were investigated and used in this study. Various ANN models were developed and trained based on the laboratory results to achieve the best performance. The best

Chapter 12 - Prediction of intrinsic compressibility parameters of reconstituted clays using artificial neural network

models were then engaged to predict the compressibility of reconstituted clays. Finally, a sensitivity analysis was performed and the impact of each parameter on the results is investigated and discussed.

12.2.3 Materials and procedure (database)

The results of 103 consolidometer tests and laboratory index tests were collected from experimental tests conducted for this thesis and from the literature (Al Haj & Standing, 2015; Burland, 1990; Cerato & Lutenegeger, 2004; Habibbeygi & Nikraz, 2018b; Habibbeygi, Nikraz, & Chegenizadeh, 2017; Hong et al., 2013; Hong et al., 2012; Hong et al., 2010; Lei et al., 2015; Liu et al., 2013; Polidori, 2014; Shi & Herle, 2015; Sridharan & Nagaraj, 2000; Sun, Lu, Guo, Yan, & Jia, 2016; Xu & Yin, 2015). This broad dataset was used to train the developed ANN under different conditions and verify its performance accurately. Based on past research, the compressibility of reconstituted clays is understood to be affected by the soil's intrinsic characteristics, such as the liquid limit, plastic limit and specific gravity. It is also well-known that the compressibility of reconstituted clays is highly dependent on the initial water content (Habibbeygi, Nikraz, & Chegenizadeh, 2017). Consequently, the initial water content was also selected as one of the input invariants in the ANN models. In addition to the four numerical variable (i.e. w_0 , G_s , w_L and w_P) describing the geotechnical index parameters of the reconstituted samples, clay mineralogy (*CLM*) was also considered in the model as a categorical variable to allow for the effect of mineralogy on the intrinsic compressibility parameters. Finally, a total of five input parameters were chosen for use in the ANN models.

The relationships between the input invariants and the outputs (i.e. intrinsic compressibility parameters of e_{100}^* and C_c^*) are presented in Figure 12-1. As shown, the intrinsic parameters clearly have nonlinear relationships with the input parameters. Moreover, the compression parameters are highly affected by two of these parameters (i.e. initial water content (w_0) and liquid limit (w_L)). The influence of specific gravity on the intrinsic compression parameters is partial. Similarly, the effect of plastic limit on the intrinsic compression parameters is mostly limited by the variation of this parameter ranging between 20–50%. A summary of the input parameter statistics is provided in Table 12-1. As summarised in this table, the liquid limit and plastic limit of the studied soils vary dramatically between 39.8–258.9% and 15–108%,

Chapter 12 - Prediction of intrinsic compressibility parameters of reconstituted clays using artificial neural network

respectively. Furthermore, the initial water content of the samples ranges from 22.4% to a hefty value of 528.7%.

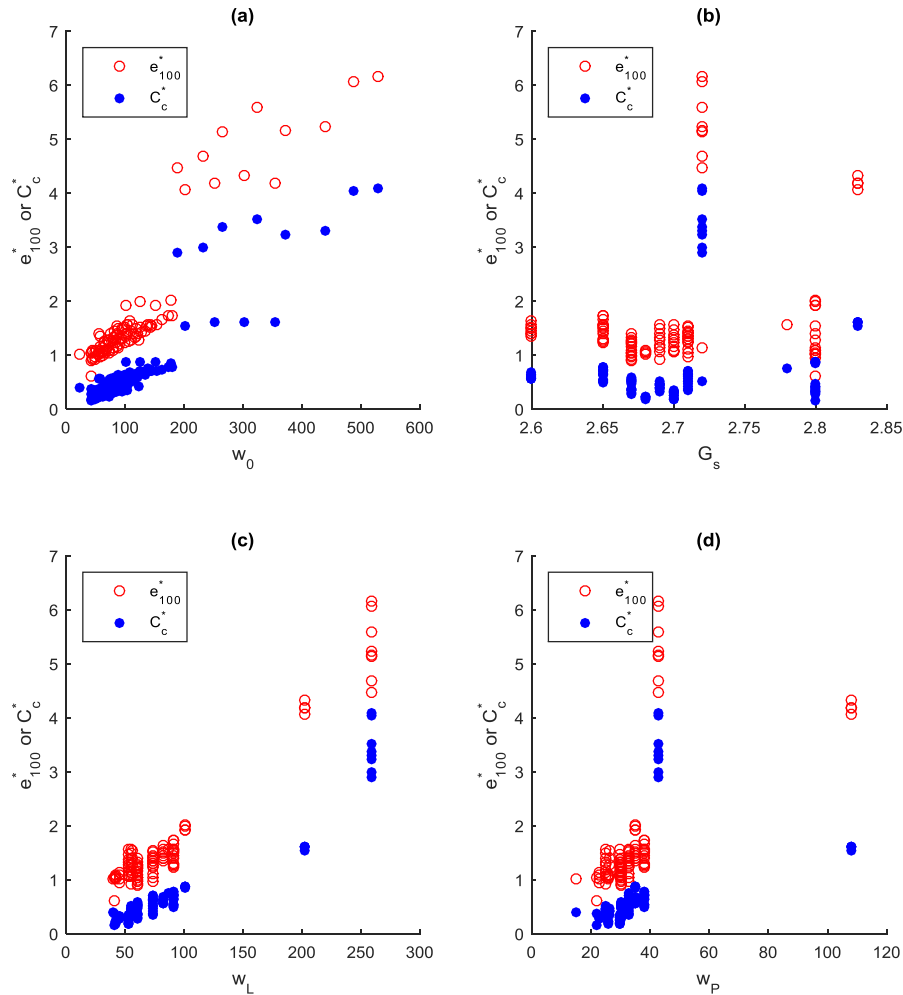


Figure 12-1. The relationships between intrinsic parameters and input parameters; a) initial water content b) specific gravity c) liquid limit and d) plastic limit (data extracted from (Al Haj & Standing, 2015; Burland, 1990; Cerato & Lutenegeger, 2004; Habibbeygi & Nikraz, 2018b; Habibbeygi, Nikraz, & Chegenizadeh, 2017; Hong et al., 2013; Hong et al., 2012; Hong et al., 2010; Lei et al., 2015; Liu et al., 2013; Polidori, 2014; Shi & Herle, 2015; Sridharan & Nagaraj, 2000; Sun et al., 2016; Xu & Yin, 2015))

Table 12-1. Summary statistics of the data used as input parameters

	w_0	G_s	w_L	w_P	e_{100}^*	C_c^*
Minimum	22	2.60	40	15	0.502	0.741
Maximum	529	2.83	259	108	1.130	1.568
Mean	118	2.70	88	35	0.816	1.154
Median	91	2.70	74	33	0.816	1.154
Mode	101	2.80	61	30	0.502	0.741
Standard deviation	92	0.06	59	16	0.444	0.585

To investigate the effect of each input parameter on the intrinsic constants, rank regression can be used, especially when there is a non-linear relationship between input data and outputs (Park & Lee, 2011). In this study, the Spearman rank correlation coefficient (Spearman's rho), which is based on a ranking method, was used to compare the effectiveness of each input parameter on the intrinsic constants. The Spearman rank coefficient r_s can be calculated for distinct parameters from Equation (12-1):

$$r_s = 1 - \frac{6 \sum d^2}{n(n^2 - 1)} \quad (12-1)$$

where d is the difference between the ranks of each observation, and n is the number of observation.

An r_s value of +1 means there is a perfect positive correlation, while $r_s = -1$ means a perfect negative correlation and $r_s = 0$ means that there is no correlation.

Figure 12-2 presents the r_s values for all five input parameters (i.e. w_0 , G_s , w_L , w_P and CLM) for both outputs (i.e. e_{100}^* and C_c^*). As can be seen, w_0 and G_s have the maximum and minimum values of the Spearman rank correlation coefficient for the output of e_{100}^* . The r_s value of w_0 is 0.90, which indicates that there is a very strong, positive, linear correlation. On the other hand, the r_s value of G_s is 0.10, which implies that there is a very weak linear correlation. Briefly, w_0 and w_L are the most linearly-correlated parameters, and are followed in order by w_P , CLM and G_s .

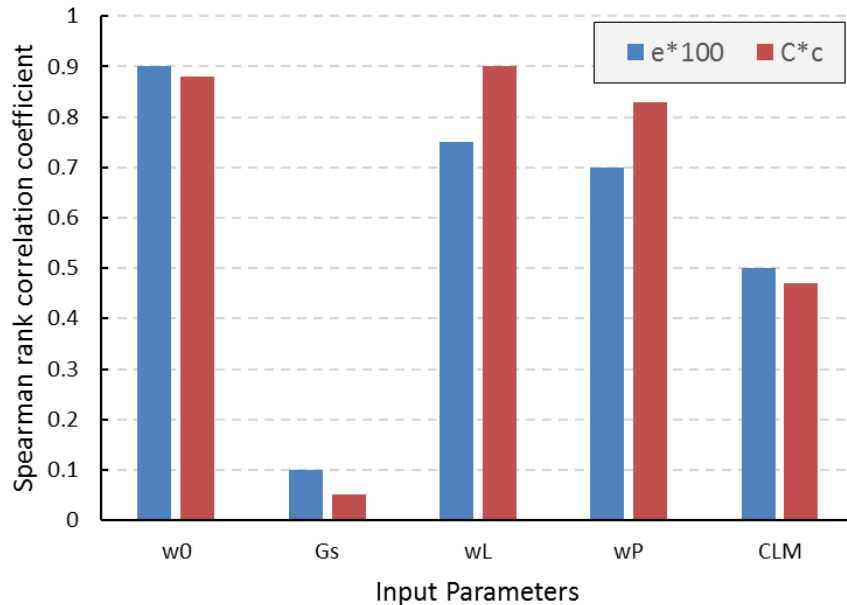


Figure 12-2. Spearman rank correlation coefficients of input parameters

Similarly, the r_s values of w_L , w_0 and w_P are 0.90, 0.88 and 0.83, respectively, for the intrinsic parameters of C_c^* , which indicates that there are very strong, positive, linear correlations for all these three variables. However, the r_s value of G_s is still low, in the order of 0.05 for this parameter, which indicates that there is a very weak linear correlation. Briefly, w_L , w_0 and w_P are the most linearly-correlated parameters for both outputs, while G_s is the least linearly-correlated variable.

12.2.4 Artificial Neural Networks

An artificial neural network (ANN) is a type of data processing system that has been developed in the past few decades and was inspired by the structure of biological nervous systems. They are much simpler than biological neural networks but can be taught to serve particular functions, such as running simulations and recognising compound patterns.

ANNs use a large number of parallel processing elements to process data and simulate responses. These simple but fully interconnected elements, or nodes, are named *neurons* due to their similarity to the nerve cells of the human nervous system. Generally, there are almost 100 billion nerve cells in the brain of a human, which are interconnected with thousands of other nerve cells (Hagan et al., 1996).

Some parts of a neural network can be structured through training, such as developing new connections and strengthening or weakening synaptic connections. Similar to a nervous system, the simple nodes of a mathematical neural network are highly

Chapter 12 - Prediction of intrinsic compressibility parameters of reconstituted clays using artificial neural network

connected to each other and can be used in an ANN to learn from predefined information to solve complex equations. Moreover, similar to a nervous system, the nerve cells are simple, tiny, elements and the function of the neural network depends on the connections between these simple elements. In fact, this connectivity is the common part of human nervous systems and ANNs that is used to solve complex problems.

Hundreds of ANNs have been developed using various nerve cells and neuron connections to run simulations more accurately and efficiently. Likewise, a biological neural system typically needs more than one neuron to handle complex problems. These multiple neurons which work in parallel are called a *layer*.

The feed-forward neural network is the simplest class of ANN, wherein the information transfers only in a forward direction from the input layer to the output layer of a multi-layer system. Therefore, in this method, each neuron only receives information from the previous layer (Demuth & Beale, 2001). In this type of ANN, the network has a layered structure comprising at least three distinct layers. The first layer receives the input information as given input data. The last layer is referred to as the *output layer* and presents the actual response of the ANN. Moreover, the layers between the input and output layers, which are responsible for learning from and processing the data, are referred to as *hidden layers* (Demuth & Beale, 2001). The hidden layers are the layers where the received information (i.e. input data) is processed and transferred to the output layer. Typically, the complexity and processing time increase with increases in the number of neurons in the hidden layers. In a multi-layer ANN, each layer may have its own characteristics, including a weight matrix, bias and transfer function. Multiple-layer networks have great ability to simulate almost all functions well (Demuth & Beale, 2001). Another class of neural network structures is the *recurrent neural network*, where a directed graph is developed by the connections between neurons. This network is able to use its memory to process dynamic behaviour and tasks such as speech and handwriting recognition (Demuth & Beale, 2001).

A single layer of neurons is presented in Figure 12-3. As shown in this figure, the layer contains S neurons. All neurons are fully connected to each other with a particular weight factor (w_{ij}); i represents the number of neurons and j represents the number of the neuron in the row. Each neuron has its own bias (b), summer and transfer function considering the number of neurons. Here in this structure, there are R input data and S

output elements. The input of a multiple-input neuron is a $R \times 1$ vector, the bias is a $S \times 1$ vector, the weight matrix is a $S \times R$ matrix and the output is also a $S \times 1$ vector.

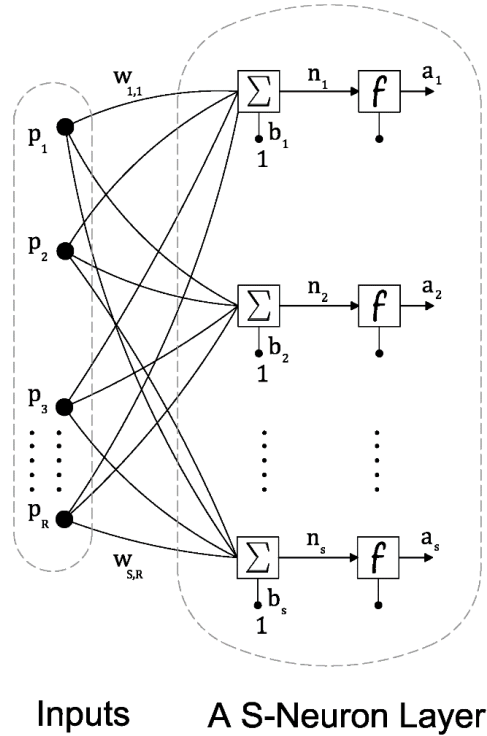


Figure 12-3. A single layer of neurons (redrawn from (Demuth & Beale, 2001))

In this model, the input parameter p of each neuron is multiplied by the weight parameter (w) and added to the offset or bias (b) to form a net input of (n), which is named the summer *output*. The summer then goes into a transfer function/activation function as an input and produces the output of the neuron (a).

A schematic of the architecture of a three-layer feed-forward ANN using abbreviated notation is presented in Figure 12-4. In this figure, there are input, hidden and output layers. To identify the layers, a superscript has been used along each invariant to make it clear which layer is being referred to. This network, like a single-layer network, has p inputs, and the numbers of neurons in layers one to three are S^1 , S^2 and S^3 , respectively. As can be seen in this figure, the output of each layer is the input for the next layer. The weight matrices of the three layers are named W^1 , W^2 and W^3 correspondingly. The last layer, whose output is the output of the entire network, is called *output layer*.

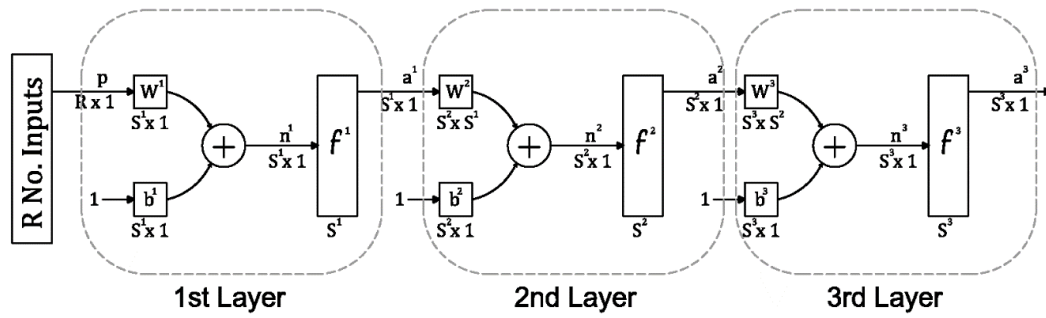


Figure 12-4. Schematic of the architecture of a three-layer ANN using abbreviated notation (redrawn from (Demuth & Beale, 2001))

Consistently, the other layers which connect the inputs to the output layer are named *hidden layers*. In this figure, layers 1 and 2 are hidden layers and layer 3 is the output layer of the network. The output vector can be calculated from Equation (12-2) below:

$$a^3 = f^3(W^3 f^2(W^2 f^1(W^1 p + b^1) + b^2) + b^3) \quad (12-2)$$

Similar to a biological neuron, the summation function and active function represent the cell body of a neuron called a *general neuron* and the weight relates to the synaptic strength. The output of the neuron depends on the adjustable parameters of the weight and the bias as well as the transfer function. The transfer function is chosen in the architectural design of a neural of network but w_{ij} and b , which are initially selected, will be modified to achieve the predefined goal, which may be to minimise the error between output and target values. The error is calculated at each iteration, which is called the *epoch*. The output of each layer passes through the next layer as an input to the neurons in the subsequent layer.

12.2.5 ANN structure used in this study

Three-layered ANNs comprising input, output and hidden layers were used in this study. In these ANN models, four index parameters—the liquid limit (w_L), plastic limit (w_P), specific gravity (G_s) and initial water content (w_0), as well as clay mineralogy (*CLM*)—are included as the input parameters and two intrinsic parameters (i.e. e_{100}^* and C_c^*) are used as the outputs. The structure of the three-layered ANN used in this study is presented in Figure 12-5.

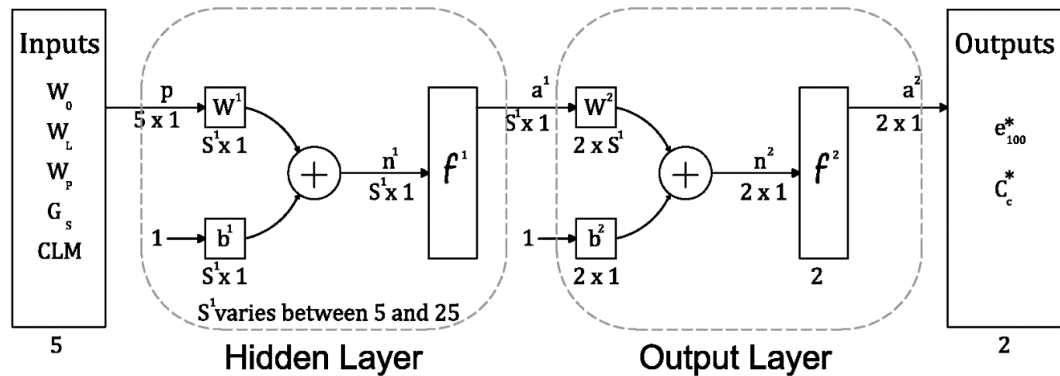


Figure 12-5. The ANN structure used in this study

In the studied ANN models, single hidden layers comprising between 5 and 25 neurons were used to investigate the optimal number of neurons in the hidden layer.

The training step is one of the most important steps in the use of ANN models. There are three different types of training procedures mentioned in the literature: *supervised learning*, *unsupervised learning* and *reinforcement learning* (Çelik & Tan, 2005). In supervised learning, the training is carried out using a series of training sets that include input and target values. The training procedure uses this set of data to minimise the error between the target and the ANN outputs by adjusting weight matrices and biases. On the other hand, in the unsupervised training procedure, there are no target values and the modification is only based on the network inputs. Furthermore, the reinforcement training procedure is similar to the supervised one, but instead of having the target values, there are some grades for adjusting the weights and biases (Çelik & Tan, 2005). There are a large number of training algorithms available in the literature to make ANN learn from a series of input and target (output) values. Some of the more common algorithms are *backpropagation with momentum*, *Levenberg-Marquardt*, *conjugate gradient descent*, *scaled conjugate gradient*, *quasi-Newton*, *backpropagation* and *quick propagation* (Demuth, Beale, & Hagan, 2008). Each algorithm has its own advantages and disadvantages, and its success is dependent on the learning rate and type of parameters used (Çelik & Tan, 2005). A trial-and-error method can be used to choose the most appropriate technique in the optimisation procedure.

One of the most popular algorithms in ANNs is the feed-forward with back propagation algorithm. The standard Levenberg-Marquardt learning algorithm was

used in this study as the training function. It is presented in Equation (12-3) (Demuth & Beale, 2001):

$$x_{k+1} = x_k - [J^T J + \mu I]^{-1} \cdot J^T e \quad (12-3)$$

where J is the Jacobian matrix that comprises the first error derivatives, e is the error vector, μ is the Marquardt parameter, I is a unit matrix and k is the iteration number. For a μ of zero, the Levenberg-Marquardt algorithm becomes a simple Newton's algorithm procedure.

In this study, the database was divided into three divisions for training of the ANNs. Seventy per cent of the available dataset was used for training (equivalent of 73 randomly-chosen data points), 15% was used for verification (equivalent of 15 randomly-chosen data points) and another 15% (equivalent to 15 randomly-chosen data points) was used for validation to verify the accuracy of the ANN in predicting the compression parameters.

The statistics of mean square error (MSE) and correlation coefficient (R) were used to assess the performance of the ANN structures and also to minimise the error function by adjusting the weight matrices and biases. Equations (12-4) and (12-5) present the equations for these parameters, which were used in the supervised training and performance analyses in this study:

$$MSE = \frac{\sum_{i=1}^n (x_i - y_i)^2}{n} \quad (12-4)$$

$$R = \frac{\sum_{i=1}^n (x_i - \bar{x}_i)(y_i - \bar{y}_i)}{\sqrt{\sum_{i=1}^n (x_i - \bar{x}_i)^2} \sqrt{\sum_{i=1}^n (y_i - \bar{y}_i)^2}} \quad (12-5)$$

where x_i and y_i are the measured (target) and predicted (output) values, \bar{x}_i and \bar{y}_i are the relative mean values, and n is the number of samples.

12.2.6 Results and Discussion

12.2.6.1 Comparison of ANNs with different structures

Many transfer functions are presented in the literature, such as linear (Lin.), hard limit, log-sigmoid (Logsig.), symmetric hard limit, positive linear, radial basis, saturating linear, hyperbolic tangent sigmoid (Tansig.) and softmax (Demuth et al., 2008). All of these transfer functions take the vector n and produce the argument a . In this study, some common transfer functions were used for developing the ANN structure to investigate their effect on the ANN's performance.

Chapter 12 - Prediction of intrinsic compressibility parameters of reconstituted clays using artificial neural network

In the ANN models, the number of neurons in the hidden layer was changed from 5 to 25 and the MSE was calculated for each model (189 ANN models in total). Afterwards, the optimal number of neurons in the hidden layer was chosen based on the best performance (i.e. the lowest MSE). MATLAB R2015a was used to develop ANN models. Artificial Neural Network Matlab Codes are presented in Appendix F.

Performance charts were drawn to determine the optimal number of neurons for minimising the MSE and, hence, optimising the ANN's performance. For instance, Figure 12-6 illustrates a performance graph for the three steps of training, validating and testing the ANN model comprised of a tangent sigmoid for both hidden and output layers. According to this figure, the best performance (i.e. a minimum $MSE = 0.0014$) for the validation step was achieved by a single-hidden layer ANN with 17 neurons in its hidden layer. Accordingly, the optimal iteration number (epoch) for achieving the best performance for this model was 44 (Figure 12-7).

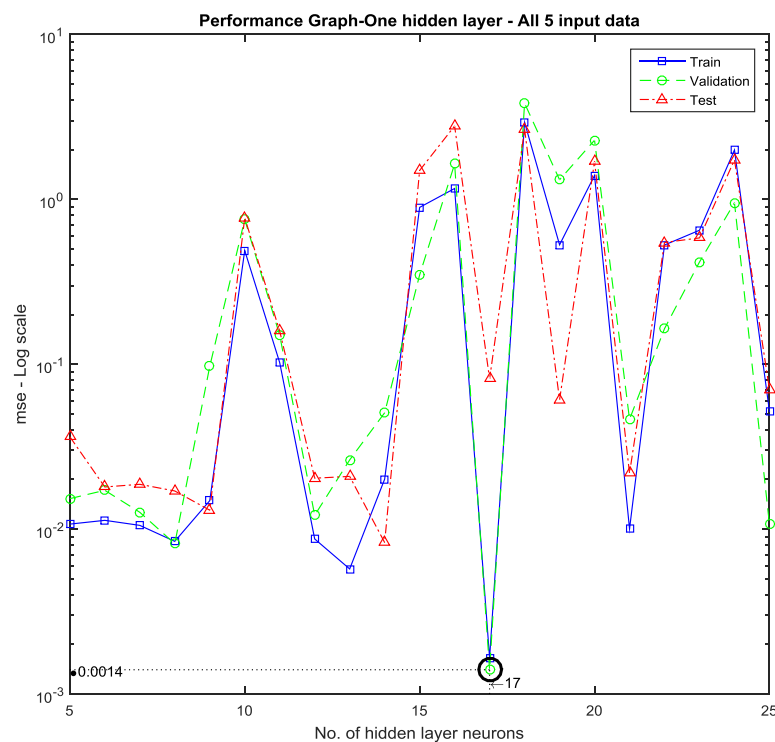


Figure 12-6. Performance graph of the number of neurons in the hidden layer

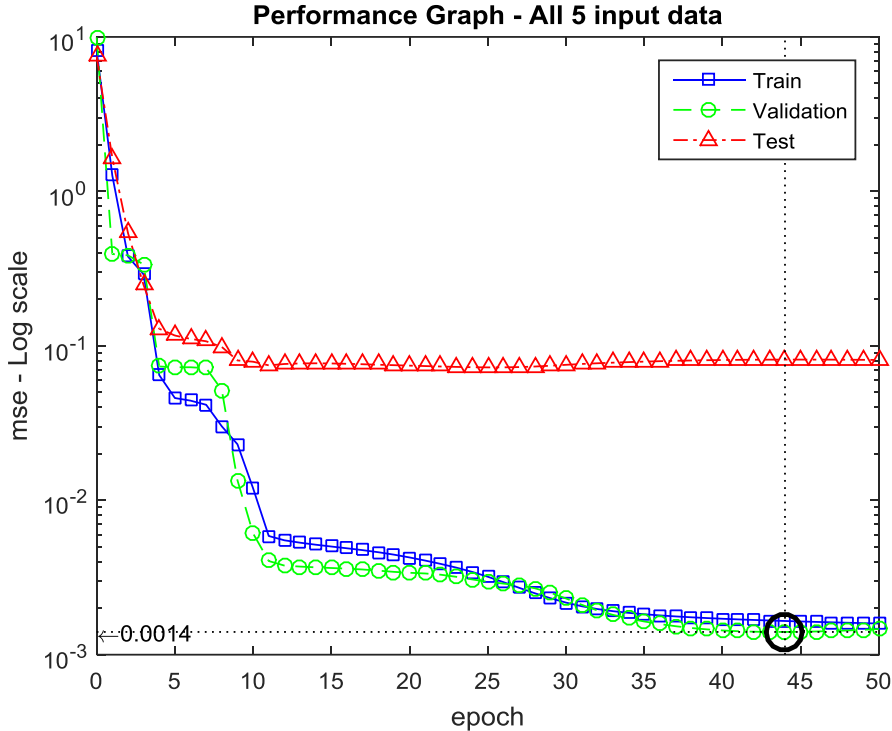


Figure 12-7. Performance graph of the number of iterations for 17 neurons

Table 12-2 summarises the results for various numbers of hidden cells and different transfer functions. Nine combinations of transfer functions with 21 different models comprising 5–25 neurons in the hidden layer, a total of 189 ANN models, were experimented with to optimise the ANN. However, for simplicity, only the results of the optimal structure for each transfer function are tabulated in Table 20. The results are also plotted in Figure 12-8. As shown in this figure, the ANN models using Sigmoid-Lin, Tansig.-Lin, Sigmoid.-Tan. and Tansig.-Tansig. transfer functions have the best performance. Among the above ANN models, however, Tansig.-Lin. has the least hidden neurons and was chosen as the optimal ANN model. The results of sensitivity analysis are presented for this optimal model in the following sections.

Chapter 12 - Prediction of intrinsic compressibility parameters of reconstituted clays using artificial neural network

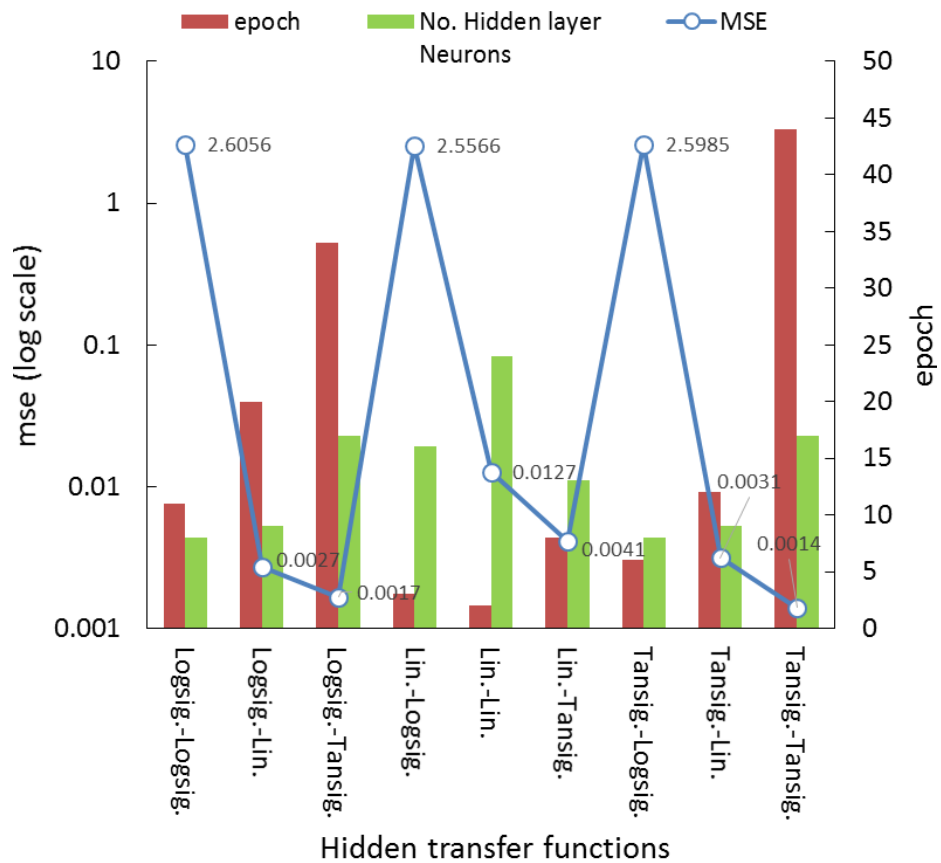


Figure 12-8. Performance charts for various ANN structures

Table 12-2. Summary of optimal ANN structures for various transfer functions and numbers of hidden neurons

ANN model	Hidden transfer function	Output transfer function	Epoch	No. of neurons	MSE
1	Logsig.	Logsig.	11	8	2.6056
2	Logsig.	Lin.	20	9	0.0027
3	Logsig.	Tansig.	34	17	0.0017
4	Lin.	Logsig.	3	16	2.5566
5	Lin.	Lin.	2	24	0.0127
6	Lin.	Tansig.	8	13	0.0041
7	Tansig.	Logsig.	6	8	2.5985
8	Tansig.	Lin.	12	9	0.0031
9	Tansig.	Tansig.	44	17	0.0014

12.2.6.2 Simulation Results

The relationship between target values and outputs obtained from the ANN are presented in Figure 12-9 and Figure 12-10 for compressibility parameters. The target values and outputs were compared for all data in the three data processing steps (i.e. training, validation and testing). The results confirm a good relationship between the target values and the ones predicted by the ANN models for both compression parameters.

Figure 12-11 and Figure 12-12 compare the target values (measured) and outputs (predicted) of both compression indices, (C_c^*) and (e_{100}^*), respectively. The graphs represent the differences in the training steps (Figure 12-11a and Figure 12-12a), validation step (Figure 12-11b and Figure 12-12b) and test step (Figure 12-11c and Figure 12-12c). Graphs are also plotted for all available data in Figure 12-11d and Figure 12-12d.

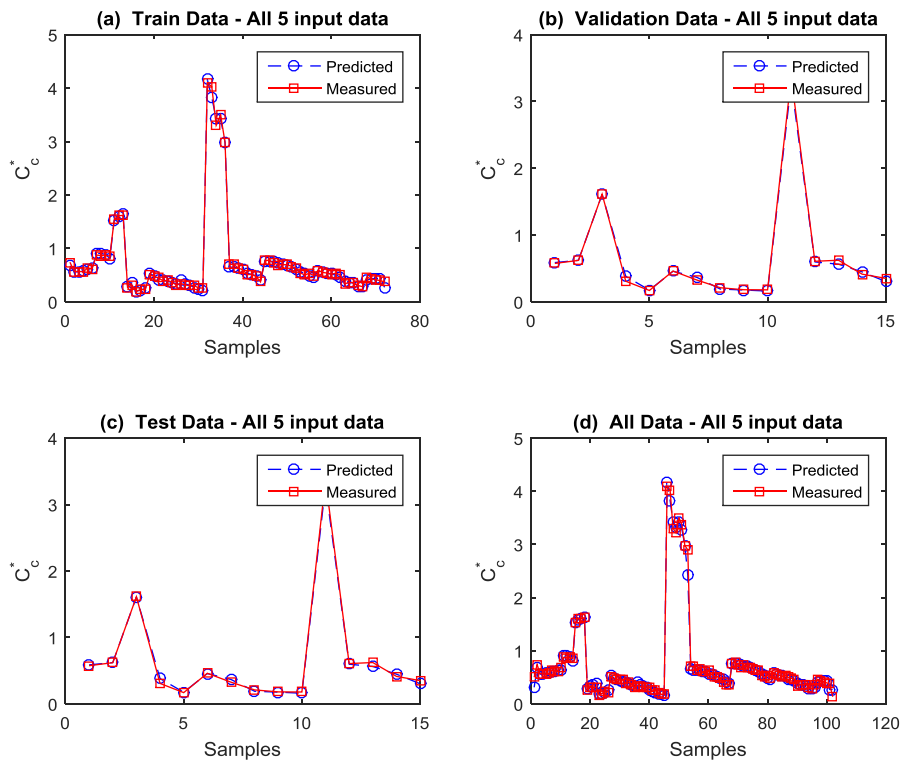


Figure 12-9. Simulation results for the three steps of data processing, and for all data (C_c^*).

The coefficients of correlation (R^2) were also calculated for all data. As shown, the calculated correlation coefficients are greater than 0.99 for both outputs, which

confirms that there are good agreements between the predicted and measured values for both compressibility parameters.

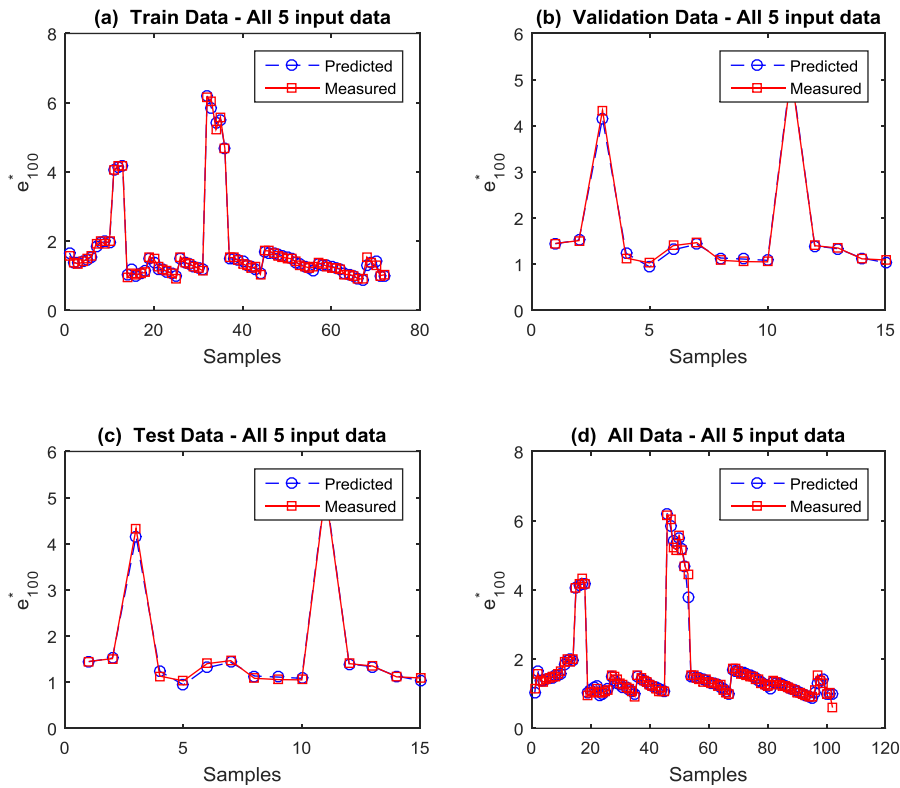


Figure 12-10. Simulation results for the three steps of data processing, and all data (e_{100}^*).

12.2.6.3 Sensitivity Analyses

To investigate the effect of input parameters on the accuracy of the ANN models, a series of sensitivity analyses were carried out by excluding each input parameter and developing a new ANN model. The results then were compared with the results of the main model (comprising all five input data).

A summary of the results is tabulated in Table 12-3. As shown, initial water content has a major effect on the performance of the ANN model. The *MSE* increases by three times for the validation and test steps by excluding w_0 . Liquid limit (w_L) has the second-highest effect on the performance of the ANN model. Excluding this parameter increases the *MSE* value from 0.0322 for all data to 0.0684 (i.e. approximately double for the main model). Then, w_p and *CLM* are ranked next in the order of influence on the results. As expected, the specific gravity of the samples has the least impact on the results, which is in agreement with the Spearman ranking values.

Chapter 12 - Prediction of intrinsic compressibility parameters of reconstituted clays using artificial neural network

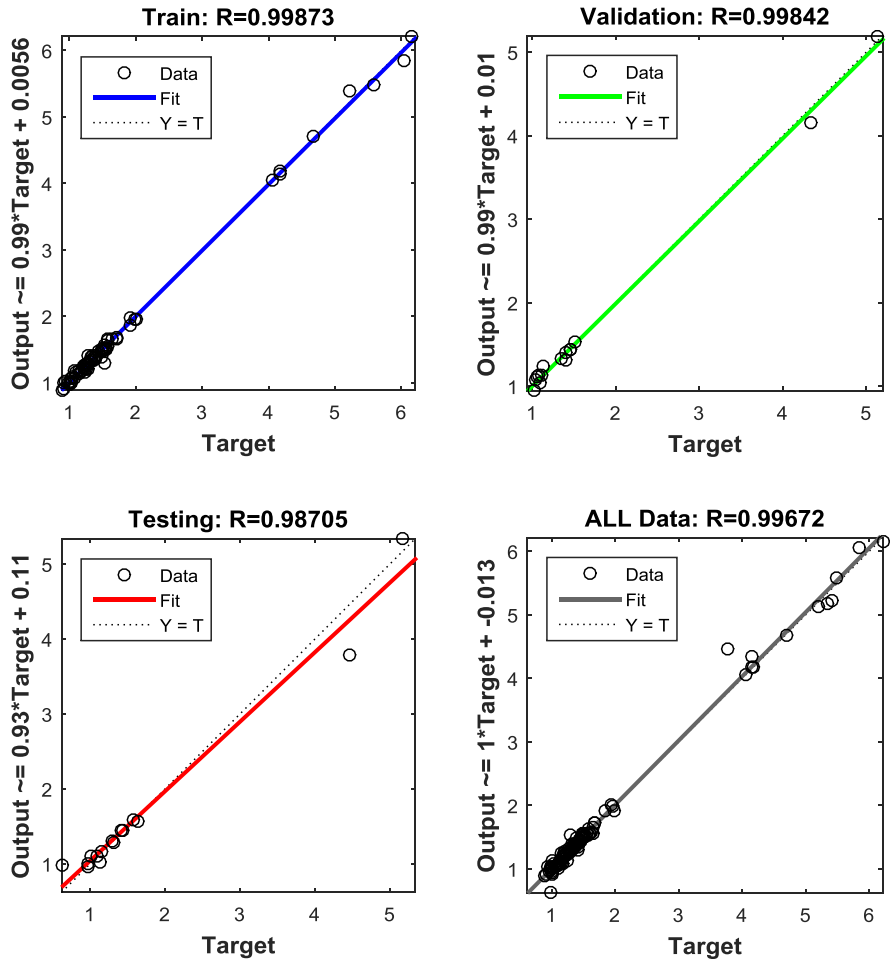


Figure 12-11. Comparison between the target values and outputs (C_c^*).

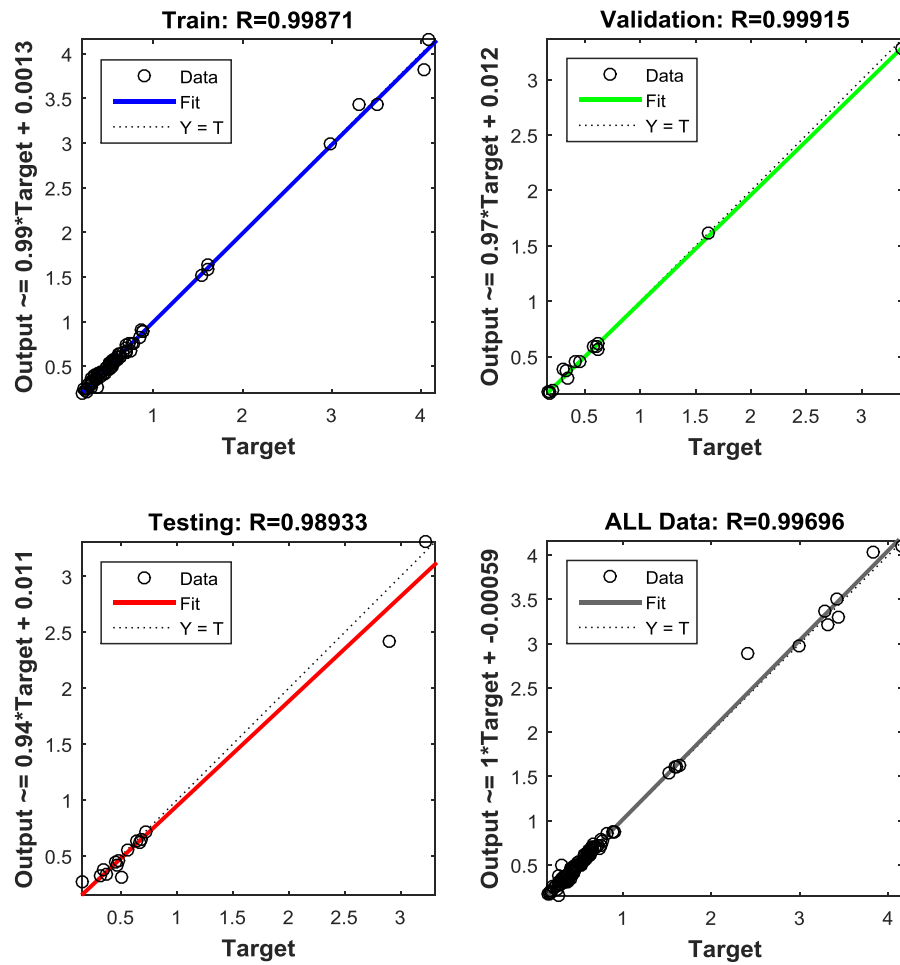


Figure 12-12. Comparison between target values and outputs (e_{100}^*).

Table 12-3. Mean square errors (MSE) for the optimal ANN structures excluding each input parameter

Data processing step	All data	Input parameters excluded from ANN model				
		w_0	G_s	w_L	w_P	CLM
Training	0.0028	0.0297	0.0018	0.0019	0.0019	0.0025
Validation	0.0031	0.0090	0.0016	0.0009	0.0014	0.0011
Testing	0.0322	0.0907	0.0127	0.0684	0.0384	0.0467

12.2.6.4 Proposed ANN Equation

The application of the ANN models makes it easy to predict the target values for any other series of input data. However, a relationship can be established to relate input parameters and output values by a mathematical equation. However, the difficulty of

Chapter 12 - Prediction of intrinsic compressibility parameters of reconstituted clays using artificial neural network

using a mathematical relationship increases with increases in the number of input parameters.

Table 12-4 presents the biases and weights of the inputs and outputs for the optimal ANN model. The relationship between the outputs and inputs can be written as follows:

$$y_j = f_{Lin} \left\{ b_o + \sum_{k=1}^9 \left[w_{kj} \times f_{Tansig} \left(b_{hk} + \sum_{i=1}^m w_{ik} \cdot x_i \right) \right] \right\} \quad (12-6)$$

where f_{Lin} is the pure-linear transfer function, b_o is the bias at the output layer, w_{kj} is the weight between the k^{th} neuron of the hidden layer and j^{th} output neuron ($j = 1$ and 2 for the ANN model with two output neurons), f_{Tansig} is the Tangent-sigmoid transfer function, b_{hk} is the bias at the k^{th} neuron of the hidden layer, w_{ik} is the weight between the i^{th} input variable ($i = 1$ to 5 for the ANN model with five input neurons) and the k^{th} neuron of the hidden layer, and x_i is the i^{th} input parameter.

Table 12-4. Biases and weights of the optimal ANN model

ANN model	Input weights					Output weights		Bias
	w_0	G_s	w_L	w_P	CLM	e_{100}^*	C_c^*	b_o
1	-0.7798	1.5022	2.5789	0.0396	1.1052	0.1691	0.1654	-1.6709
2	2.4442	-1.0211	1.2738	0.4260	-0.6232	0.8718	0.9966	-2.2466
3	-0.2616	1.7552	-0.4947	-0.6422	1.7632	0.5739	-0.1800	1.3397
4	1.7567	0.7710	-1.2375	0.2315	-1.2354	0.1232	0.0850	-0.7659
5	0.2743	0.5305	0.5914	-1.9327	0.3370	-0.5644	-0.3487	0.2177
6	-1.2005	0.7312	0.4353	-0.3655	-1.4575	-0.1026	-0.0266	-1.4556
7	-1.6905	-0.4215	1.2035	-1.2922	0.2499	1.1332	1.1717	-1.2797
8	0.0947	1.1459	1.1656	-2.2703	1.1640	-0.9400	0.6352	1.6908
9	2.1880	0.4428	-0.6114	0.4778	-0.2486	1.1830	1.0747	1.5984

12.2.7 Conclusions

In this chapter, neural network simulations were carried out to estimate intrinsic compression parameters based on the soil index of reconstituted clays and their clay mineralogy. Based on the results of the ANN models, the following conclusions can be made:

Chapter 12 - Prediction of intrinsic compressibility parameters of reconstituted clays using artificial neural network

- ANN models with two output neurons, which were developed based on five input parameters (comprising initial water content, liquid limit, plastic limit, specific gravity and clay mineralogy), can be used to reliably predict intrinsic compression parameters with considerable accuracy. The two output neuron ANN models can reduce the procedural time significantly without reducing the accuracy.
- The performance charts show that the Sigmoid-Lin, Tansig.-Lin, Sigmoid.-Tan. and Tansig.-Tansig. are the best-performing ANN transfer functions. In fact, Tansig.-Lin. also has the least hidden neurons and can be chosen as the optimal ANN model.
- The initial water content and liquid limit have major effects on the performance of the ANN model. Furthermore, the specific gravity of the samples has the least effect on the results. These results are also compatible with the Spearman ranking values calculated for the input parameters.
- The sensitivity analyses show that the intrinsic compression parameters are also influenced by the clay mineralogy, which cannot be ignored in the predictive models.
- The intrinsic compression parameters predicted using the ANN models are in good agreement with the measured values of these parameters.

13 CONCLUSIONS AND RECOMMENDATIONS

13.1 *Summary Discussion*

The mechanical and volumetric behaviour of expansive clays was investigated in this thesis by carrying out experimental tests, statistical and regression analyses, and constructing artificial neural networking models. A detailed discussion of the behaviour, alongside the results and methodology of each section, is presented in Chapters 4 to 12. In this section, the findings are summarised and some recommendations for future study are suggested.

13.1.1 *Inherent Compressibility and Remoulded Yield Stress*

The inherent compressibility of expansive clays are investigated in Chapter 4. Two methods of normalisation, comprising the normalised void ratio and void index, are investigated to assess their accuracy in predicting the behaviour of reconstituted clays. Moreover, a modified intrinsic compression line (ICL) is proposed to forecast the compression behaviour of such soils.

Experimental tests illustrate that the intrinsic baseline can be used to predict the volumetric behaviour of expansive clays at high initial water contents with considerable accuracy. According to one-dimensional consolidation testing, the intrinsic invariables of e_{100}^* and C_c^* are dependent on the initial status of the samples and increase progressively with increases in water content. The findings show that clay mineralogy has a great impact on these parameters.

The results of experimental tests illustrate that the compression curves of reconstituted clays (i.e. destructured clays) are inverse S-shaped, similar to those of natural clays. The normalised compression curves plotted on the void index – $\log \sigma'_v$ converge to a unique line; however, there is a disparity between the compression curves of samples prepared at various initial water contents at low stress levels. This shows that even for reconstituted clays, there is a definite structure that withstands external forces. However, this inherent structure will be destroyed with increases in the external force (i.e. consolidation stress). The clay particles are structured by both inter-particle locking and their particle arrangement (i.e. fabric).

The results of this research illustrate that there is a particular stress that differentiates between the pre-yield and post-yield behaviours of reconstituted clays. This particular

stress, which is referred to as the *remoulded yield stress* (σ'_{yr}), can be well defined by replotting the compression curves on a bi-logarithmic plane. The results of this research indicate that the remoulded yield stress is influenced by initial water content and clay mineralogy. Moreover, the remoulded yield stress plunges swiftly with increasing initial water content; however, it flattens out for normalised initial water contents greater than 1.2 times the liquid limit.

13.1.2 Compression, Recompression and Swell Indices

There are many empirical equations to predict the compression indices of clayey soils based on simple geotechnical parameters, thereby avoiding the need for consolidation tests. However, most of these equations are limited to certain types of clayey soils and are not suitable for expansive clays. In this research, an empirical equation was proposed by using the intrinsic baseline and the theoretical criterion for shear strength at the consistency limits. The equation of the normalisation line (i.e. void index vs consolidation stress) was employed to derive a general equation for the compression index that covers most clayey soils, including expansive clays (Chapter 6). The compression index predicted by this equation was compared with the measured one for a broad range of clays comprising low and high plasticities, low and high initial water contents and various clay mineralogies (kaolin, illite and montmorillonite). The findings show that the proposed equation can reasonably predict the compression index of clays which lie above the A-line of the plasticity chart with good accuracy. The effect of unloading/reloading cycles on the compression indices are investigated in Chapter 7. The experimental experiments indicate that the compression reloading index remains virtually constant after the first cycle of loading/reloading. This can be explained by the inherent structure of the studied clay at very low levels of stress. Afterwards, the clay structure starts to weaken with increases in consolidation stress and becomes completely destructured at higher deformations. The findings also indicate that the loading/reloading compression curves are hysteresis loops. Actually, the swell part is nearly linear, yet the reloading part is visibly nonlinear. It can be stated that irreversible deformation is governed by the alignment of clay particles.

The compression behaviour of clays is governed by physico-chemical forces when the clay particles are parallel. Conversely, compression behaviour is governed by mechanical forces when the contacts between clay particles are more skewed. The compression curves state that swelling due to unloading is typically affected by

physico-chemical forces. The parallel alignment of clay particles results in higher repulsion due to unloading, which leads to higher void ratios. On the other hand, with excessive repulsive forces, higher deformation and steeper slopes occur.

Finally, two equations for rebound compression indices based on the compression and swell indices were presented.

13.1.3 Consolidation Coefficient

The consolidation coefficient (C_v) is surely the most important parameter when the settlement rate of a clayey layer is being assessed. As part of this research, the effect of initial water content and sample disturbance on the consolidation coefficient is investigated in Chapter 8.

The results of this research show that the C_v values of expansive clays consisting mainly of montmorillonite (smectite) as their predominant clay mineral decrease with increases in consolidation pressure; while clays with a predominance of other minerals experience increases in their consolidation coefficients with increasing consolidation pressure. Likewise, an increase in consolidation pressure (for medium to high stress levels) results in a decrease in C_v . Conversely, at low stress levels, the trend is opposite for reconstituted samples prepared at higher initial water contents. Therefore, it was concluded that the value of C_v depends on both clay mineralogy and the stress level.

The mechanism governing the compression behaviour of expansive clays was used to explain this variation in the trend of C_v . As discussed in previous sections, mechanical and physicochemical forces are two major factors that control the behaviour of expansive clays. The results of this research illustrate that the deviation of C_v with consolidation pressure is affected by the type of clay mineral, initial water content and stress. The mechanical force controls the deviation of the consolidation coefficient when the initial water content is high. This shows that even for expansive clays with a predominance of montmorillonite, diffuse double-layer formation is suppressed by high amounts of water, such that the behaviour is solely governed by mechanical forces rather than physicochemical forces.

Nonetheless, C_v decreases with increasing consolidation pressure, such that the mechanism is governed by physicochemical forces for initial water contents less than the liquid limit. Likewise, the compression mechanism is controlled by the same force even at high initial water contents when the level of consolidation pressure is high.

The experimental tests on both remoulded and reconstituted samples indicate that the m_v values of reconstituted samples are typically greater than those of remoulded samples at the same consolidation pressure. Furthermore, m_v frequently decreases with increases in consolidation pressure. Based on the results of one-dimensional tests, C_v increases with decreases in initial water content, to the order of up to two times the relative value.

The effect of sample disturbance was also investigated in this research. The findings show that the C_v values of undisturbed samples are greater (up to four times) than those of remoulded ones. The results also suggest that the C_v of undisturbed samples decreases with increases in consolidation pressure. This can be explained by understanding that the factor governing compression behaviour is physicochemical forces, because the initial water contents of such samples are lower than their liquid limits.

13.1.4 Intrinsic Shear Strength

The intrinsic baseline is employed to forecast the undrained shear strength (S_u^*) of expansive clays in Chapter 9. Furthermore, an intrinsic strength line (IS_uL) is proposed to express the relationship between the void index and the undrained shear strength of expansive clays.

Based on the results of direct shear tests, S_u^* reduces with increases in the initial water content of samples at the same normal stress. This deviation increases even more for higher values of normal stress. This proves that S_u^* is significantly affected by initial water content, especially for high values of normal stress in expansive clays.

There is a linear relationship between the undrained shear strength of expansive clays and the applied normal stress for all studied initial water contents, as expected.

By using the intrinsic framework, the IS_uL was derived to predict the shear behaviour of expansive clays with reasonable accuracy. Additionally, a normalised undrained shear strength (R_{su}^*) was defined to investigate the effects of initial water content and normal stress. The findings show that R_{su}^* decreases with increases in normalised initial water content. The samples with higher initial water contents had higher void ratios, resulting in reduced shear strength of the samples. It has been shown by this research that R_{su}^* varies between 0.25 and 0.50 for the studied range of normal stresses and reduces with increasing normal stress.

13.1.5 Residual Shear Strength

An experimental study on the shear behaviour of a pre-sheared clayey soil and the shear rate affecting the residual shear strength was presented in Chapter 10. Based on ring shear test results, it is apparent that the fast residual strength is greater than the residual strength at slow rates for approximately 5 to 10 per cent.

The growth in residual strength at a slow rate reduces as the shear rate decreases from 50 to 1 mm/min. The residual strength increases as the applied normal stress increases by 1–3 times its value under low normal stress (i.e. 50 kPa).

The findings show that the fast residual strength grows almost instantly to a value higher than the slow residual strength as soon as the shear rate rises, then continues to reach the peak fast residual strength. This phenomenon, which is a positive impact of shear rate on residual stress, can be explained by the isotach behaviour of clays. Afterwards, it is usually followed by a negative impact (i.e. a decrease of up to 6%) with increasing shear displacement. This phenomenon was observed for all rates of shear displacement and normal stresses.

The intrusion of water along the shear surface may be the cause of this mechanism. The void ratio and water content increase due to the fast shearing, and the freed water penetrates the shear surface and reduces the shear strength. In contrast, structural change may be the cause of increases in shear strength at small displacements, as fast shearing results in structural disorder.

13.1.6 Swell Potential

To evaluate the swell potential of the studied expansive clay, zero-swell and free-swell tests were carried out to measure swell pressure and heave values. The results for both untreated and treated clays are presented in Chapter 11.

The findings show that swell curves can be divided into three distinctive phases: *initial*, *primary* and *secondary swelling*. In the first phase of swelling, the swell pressure increases steadily, then escalates substantially in the second phase where it almost reaches the final pressure.

The effect of a green stabiliser, magnesium chloride hexahydrate (industrial name: Bischofite and formula: $MgCl_2 \cdot 6H_2O$) on reducing the swell potential of the studied expansive clay was investigated. Experimental laboratory tests illustrate that the swell pressure of the treated clay can be reduced to one-fifth that the untreated one. The

optimum percentage of magnesium chloride hexahydrate was measured to be 8%, with additional improvements almost negligible with more. It was also found that the consistency limits (i.e. liquid and plastic limits) of expansive clays can be reduced by stabilisation with magnesium chloride. The thickness of the diffuse double layer decreases due to cation exchange, which results in improvement of the index parameters of expansive clays.

There are three distinct phases in the free swell curves, which is similar to the zero-swell test results. Approximately 90% of the total free swell occurs in the primary swell stage (i.e. second stage of the test). Five to ten per cent of free swell occurs in the last stage and the swell curves flatten-out four days afterwards. The results indicate that the secondary swell strain decreases when the samples are stabilised with magnesium chloride.

13.1.7 Regression models

Chapter 11 presents the results of regression analyses carried out to develop models for predicting the intrinsic invariables indirectly. Intrinsic invariables can be measured by undertaking one-dimensional consolidation tests. However, these tests are cumbersome and costly, especially for expansive clays with very low permeability. Existing empirical equations use one or a combination of geotechnical indices to predict intrinsic invariables. These predictors generally comprise initial water content, liquid and plastic limits, and the natural void ratio. In this research, clay mineralogy and initial water content were also included as input parameters in the models, and their impacts were assessed. Four models were developed based on the degree of available data, and the advantages and disadvantages of each model are discussed. All models were verified by large amounts of experimental data obtained from the literature.

The findings illustrate that the clay mineralogy of reconstituted clay has a significant effect on the intrinsic invariables. The results indicate that e_{100}^* increases with increases in the void ratio at the liquid limit for all types of clay mineralogy; however, the impact of mineralogy is crucial when the predominant mineral is smectite. Additionally, the models show that e_0 (void ratio at the initial state) has a lesser influence on the e_{100}^* of clay when the predominant mineral is smectite, in comparison to other clay minerals.

13.1.8 Artificial Neural Network Models

One common drawback of all regression models is the limited number of input parameters that can be used as predictors. The over-simplification of regression models leads to loss of accuracy in predicting compression invariables.

An artificial neural network (ANN) was employed to develop models for predicting compression invariants in Chapter 12. In these ANN models, a total of five input parameters comprising four numerical data (liquid and plastic limits, specific gravity, initial water content) and one categorical parameter (clay mineralogy) and two outputs (intrinsic invariants of e_{100}^* and C_c^*) are included. The two-output ANN structures were developed to considerably decrease the processing time while maintaining the predictive accuracy.

Various combination of transfer functions were employed in the ANN models. The results indicate that the combinations of the Sigmoid-Lin, Tansig.-Lin, Sigmoid.-Tan. and Tansig.-Tansig transfer functions for the hidden and output layers have the best performance. Amongst the above-mentioned transfer functions, Tansig.-Lin requires the least number of hidden neurons, which reduces the processing time as well.

The sensitivity analyses illustrate that the initial water content and liquid limit have significant impacts on the accuracy of ANN models, while specific gravity has the least impact. This finding is in agreement with the rank regression analyses (i.e. Spearman rank correlation coefficients). Moreover, the results illustrate that the compression parameters are influenced by clay mineralogy, and that this parameter cannot be ignored in the models. The simulation results are also plotted against the measured values (target values). The results indicate a good agreement between the simulated values (derived from ANN models) and those measured by oedometric tests. Finally, an equation for prediction of the compression parameters was developed using the biases and weighting factors of the ANN models.

13.2 Recommendations

Based on the findings of this research, the following recommendations are drawn:

- The intrinsic framework can be used to predict both the volumetric and mechanical behaviour of reconstituted clays with reasonable accuracy.
- Clay mineralogy has a significant impact on the compression behaviour of expansive clays. In fact, this parameter is recommended to be included in all

models comprising empirical equations and analytical models to estimate the compression parameters of expansive clays accurately.

- Magnesium chloride can be used as a green stabiliser for mitigating the swell potential of expansive clays. The geotechnical properties of clays treated with this agent showed considerable improvements compared with untreated samples.
- ANN models can be used to predict the compressibility of expansive clays with great accuracy, due to their ability to solve complex nonlinear problems containing multiple invariants.

13.3 Further Research

This research only scratches the surface of comprehending the behaviour of expansive clays, and more work needs to be carried out on this topic. Some recommendations for further research are presented as follows:

- Further research using unsaturated triaxial apparatus to investigate the effects of the degree of unsaturation.
- Further research on modifying ICLs based on various stress paths, and investigation of anisotropic effects on intrinsic parameters.
- Further research is required on undisturbed samples to provide more comprehensive information on the behaviour of black clay.
- Further research on the impact of wetting and drying cycles on the volumetric and mechanical behaviour of black clay.
- An investigation using triaxial apparatus that can measure and control suction is required to enhance our understanding of the compression behaviour of black clay.
- Development of a constitutive model based on the results of a suction-controlled triaxial apparatus is required.

14 REFERENCES

- Adams, A. L. (2011). *Laboratory evaluation of the constant rate of strain and constant head techniques for measurement of the hydraulic conductivity of fine grained soils*. Massachusetts Institute of Technology.
- Al-Mukhtar, M., Lasledj, A., & Alcover, J. F. (2014). Lime consumption of different clayey soils. *Applied Clay Science*, 95, 133-145. doi:10.1016/j.clay.2014.03.024
- Al Haj, K. M. A., & Standing, J. R. (2015). Mechanical properties of two expansive clay soils from Sudan. *Geotechnique*, 65(4), 258-273. doi:10.1680/geot.14.P.139
- Alonso, E. E., Gens, A., & Josa, A. (1990). A constitutive model for partially saturated soils. *Geotechnique*, 40(3), 405-430. doi:10.1680/geot.1990.40.3.405
- Alrubaye, A. J., Hasan, M., & Fattah, M. Y. (2016). Stabilization of soft kaolin clay with silica fume and lime. *International Journal of Geotechnical Engineering*, 1-7. doi:10.1080/19386362.2016.1187884
- American Society for Testing and Materials. (2011). Specifications: West Conshohocken, PA.
- American Society for Testing and Materials. (2015). Specifications. West Conshohocken, PA.
- Anon, O. (1979). Classification of rocks and soils for engineering geological mapping, Part 1—Rock and soil materials. *Report of the commission of engineering geological mapping, bulletin international association of engineering geology*, 19, 364-371.
- Arulrajah, A., Nikraz, H., & Bo, M. (2005). In-situ testing of Singapore marine clay at Changi. *Geotechnical & Geological Engineering*, 23(2), 111-130.
- Azzouz, A. S., KRIZEK, R. J., & Corotis, R. B. (1976). Regression analysis of soil compressibility. *Soils Foundations*, 16(2), 19-29.
- Barton, N., & Choubey, V. (1977). The shear strength of rock joints in theory and practice. *Rock mechanics*, 10(1-2), 1-54.
- Basma, A. A., Al-Homoud, A. S., & Husein, A. (1995). Laboratory assessment of swelling pressure of expansive soils. *Applied Clay Science*, 9(5), 355-368. doi:http://dx.doi.org/10.1016/0169-1317(94)00032-L
- Basma, A. A., Al-Homoud, A. S., Husein Malkawi, A. I., & Al-Bashabsheh, M. A. (1996). Swelling-shrinkage behavior of natural expansive clays. *Applied Clay Science*, 11(2-4), 211-227. doi:http://dx.doi.org/10.1016/S0169-1317(96)00009-9
- Biscontin, G., Cola, S., Pestana, J. M., & Simonini, P. (2007). Unified compression model for Venice lagoon natural silts. *Journal of Geotechnical and Geoenvironmental Engineering*, 133(8), 932-942.
- Bo, M. W., Choa, V., Wong, K. S., & Arulrajah, A. (2011). Laboratory validation of ultra-soft soil deformation model. *Geotechnical and Geological Engineering*, 29(1), 65-74.
- Bourokba Mrabent, S. A., Hachichi, A., Souli, H., Taibi, S., & Fleureau, J.-M. (2015). Effect of lime on some physical parameters of a natural expansive clay from Algeria. *European Journal of Environmental and Civil Engineering*, 1-18. doi:10.1080/19648189.2015.1093963
- Bowles, J. E. (1989). *Physical and geotechnical properties of soils*. New York: McGraw-Hill Book.

- Bucx, T. H. M., van Ruiten, C. J. M., Erkens, G., & de Lange, G. (2015). An integrated assessment framework for land subsidence in delta cities. *Proc. IAHS*, 372, 485-491. doi:10.5194/piahs-372-485-2015
- Burland, J. B. (1990). On the compressibility and shear strength of natural clays. *Geotechnique*, 40(3), 329-378. Retrieved from <http://www.scopus.com/inward/record.url?eid=2-s2.0-0025645141&partnerID=40&md5=a68763a789a6434fdd140d205588dbd4>
- Burland, J. B., Rampello, S., Georgiannou, V. N., & Calabresi, G. (1996). A laboratory study of the strength of four stiff clays. *Geotechnique*, 46(3), 491-514. Retrieved from <http://www.scopus.com/inward/record.url?eid=2-s2.0-0030238322&partnerID=40&md5=0b9fb6c863adcbe0e960eb534ffd7724>
- Butterfield, R. (1979). A natural compression law for soils (an advance on e-log p'). *Geotechnique*, 29(4).
- Butterfield, R. (2011). An improved model of soil response to load, unload and re-load cycles in an oedometer. *Soils and Foundations*, 51(2), 253-263.
- Casacrande, A., & Wilson, S. (1951). Effect of rate of loading on the strength of clays and shales at constant water content. *Geotechnique*, 2(3), 251-263.
- Casagrande, A. (1936). *The determination of the pre-consolidation load and its practical significance*. Paper presented at the Proceedings of the international conference on soil mechanics and foundation engineering.
- Casagrande, A., & Fadum, R. E. (1940). Notes on soil testing for engineering purposes. *Soil Mechanics Series No. 8*(Pub. No. 268), 37.
- Çelik, S., & Tan, Ö. (2005). Determination of preconsolidation pressure with artificial neural network. *Civil Engineering and Environmental Systems*, 22(4), 217-231. doi:10.1080/10286600500383923
- Cerato, A. B., & Lutenecker, A. J. (2004). Determining Intrinsic Compressibility of Fine-Grained Soils. *Journal of Geotechnical and Geoenvironmental Engineering*, 130(8), 872-877. doi:doi:10.1061/(ASCE)1090-0241(2004)130:8(872)
- Chandler, R. J. (2000). Clay Sediments in Depositional Basins: the Geotechnical Cycle. *Journal of Engineering Geology and Hydrogeology*, 33(1), 7-39.
- Chen, B., Sun, D. A., & Lü, H. B. (2013). Experimental study of compression behavior of marine soft clays. *Yantu Lixue/Rock and Soil Mechanics*, 34(2), 381-388. Retrieved from <http://www.scopus.com/inward/record.url?eid=2-s2.0-84875081525&partnerID=40&md5=58f6f7a3661dcf588c2afedff58e309f>
- Chen, F. H. (1988). *Foundations on expansive soils*. Developments in soils geotechnical engineering: Elsevier, New York.
- Coutinho, R., & Bello, M. (2011). Analysis and control of the stability of embankments on soft soils Juturnaiba and others experiences in Brazil. *Soils Rocks*, 34(4), 331-351.
- Coutinho, R., Oliveira, J., & Oliveira, A. (1998). Geotechnical site characterization of Recife soft clays (Vol. 2, pp. 1001-1006): Balkema.
- Cozzolino, V. (1961). *Statistical forecasting of compression index*. Paper presented at the Proceedings of the 5th international conference on soil mechanics and foundation engineering, Paris.
- Das, B. M. (2013). *Advanced soil mechanics*: CRC Press.
- Das, B. M., & Sobhan, K. (2013). *Principles of geotechnical engineering*: Cengage Learning.
- Demuth, H., & Beale, M. (2001). *Neural Network Toolbox For Use with Matlab-- User'S Guide Verion 4.0*.

- Demuth, H., Beale, M., & Hagan, M. (2008). Neural Network Tool Box™ 6 for Use with MATLAB R2008a. *The Math Works Inc., Natick, Massachusetts*, 5.2.
- Devin, S. C., & Sandford, T. C. (1990). *Stability of natural slopes in the Presumpscot Formation*: Maine Geological Survey, Department of Conservation.
- Fredlund, D. (1983). *Prediction of ground movements in swelling clays*. Paper presented at the Presentation of the 31st Annual Soil Mechanics and Foundation Engineering Conference, Minneapolis, Minn. American Society of Civil Engineers, New York.
- Fredlund, D. G., & Rahardjo, H. (1993). *Soil mechanics for unsaturated soils*: John Wiley & Sons.
- Garga, V. K., Khan, M. A., & Vanapalli, S. K. (2006). Stress-path dependent behavior of a weathered clay crust. *Geotechnical & Geological Engineering*, 24(6), 1481-1509.
- Geoscience Australia and Australian Stratigraphy Commission. (2017). Australian Stratigraphic Units Database. Retrieved from <http://www.ga.gov.au/products-services/data-applications/reference-databases/stratigraphic-units.html>
- Goodrich, B. A., Koski, R. D., & Jacobi, W. R. (2009). Condition of soils and vegetation along roads treated with magnesium chloride for dust suppression. *Water, air, and soil pollution*, 198(1-4), 165-188.
- Google Maps (Cartographer). [Baldvis] [Street map]. Retrieved from <https://www.google.com.au/maps/place/Perth+WA/@-32.1305172,115.8180173,11.25z/data=!4m2!3m1!1s0x2a32966cdb47733d0:x304f0b535df55d0> Accessed December 2017 [Street map]. Retrieved from <https://www.google.com.au/maps/place/Perth+WA/@-32.1305172,115.8180173,11.25z/data=!4m2!3m1!1s0x2a32966cdb47733d0:x304f0b535df55d0>
- Gratchev, I. B., & Sassa, K. (2015). Shear Strength of Clay at Different Shear Rates. *Journal of Geotechnical and Geoenvironmental Engineering*, 141(5), 06015002. doi:10.1061/(asce)gt.1943-5606.0001297
- Habibbeygi, F., & Nikraz, H. (2018a). Characterisation of the Undrained Shear Strength of Expansive Clays at High Initial Water Content Using Intrinsic Concept. *International Journal of GEOMATE*. doi:<https://doi.org/10.21660/2017.29.20455>
- Habibbeygi, F., & Nikraz, H. (2018b). Compression behaviour of highly expansive clays stabilised with a green stabiliser of magnesium chloride. *International Journal of GEOMATE*, 14(45), 144-150. doi:<https://doi.org/10.21660/2018.45.10697>
- Habibbeygi, F., & Nikraz, H. (2018c). The effect of unloading and reloading on the compression behaviour of reconstituted clays. *International Journal of GEOMATE*, 15(51), 53-59. doi:<https://doi.org/10.21660/2018.51.52643>
- Habibbeygi, F., & Nikraz, H. (2018d). Variation of Consolidation Coefficient of Expansive Clays at High Initial Water Content. *Journal of Engineering Science & Technology*, 13(9), 2644-2654.
- Habibbeygi, F., Nikraz, H., & Chegenizadeh, A. (2017). Intrinsic Compression Characteristics of an Expansive Clay from Western Australia. *International Journal of GEOMATE*, 12(29), 140-147. doi:<https://doi.org/10.21660/2017.29.20455>
- Habibbeygi, F., Nikraz, H., & Verheyde, F. (2017). Determination of the compression index of reconstituted clays using intrinsic concept and normalized void ratio.

- International Journal of GEOMATE*, 13(39), 54-60.
doi:<https://doi.org/10.21660/2017.39.98271>
- Hagan, M. T., Demuth, H. B., Beale, M. H., & De Jesús, O. (1996). *Neural network design* (Vol. 20): Pws Pub. Boston.
- Head, K. H. (1986). *Manual of soil laboratory testing* (Vol. 2): Pentech Press London.
- Herrero, O. (1983). Universal compression index equation; closure. *Journal of Geotechnical Engineering, ASCE*, 109(5), 755-761.
- Hong, Z., & Tsuchida, T. (1999). On compression characteristics of Ariake clays. *Canadian Geotechnical Journal*, 36(5), 807-814.
- Hong, Z. S. (2006). Void Ratio-Suction Behavior of Remolded Ariake Clays. *Geotechnical Testing Journal*, 30(3).
- Hong, Z. S., Gao, Y. F., Cui, Y. J., Bian, X., & Zeng, L. L. (2013). Effect of initial water content on undrained shear behaviour of reconstituted clays. *Geotechnique*, 63(6), 441-450. doi:10.1680/geot.11.P.114
- Hong, Z. S., Lin, C., Zeng, L. L., Cui, Y. J., & Cai, Y. Q. (2012). Compression behaviour of natural and reconstituted clays. *Geotechnique*, 62(4), 291-301. doi:10.1680/geot.10.P.046
- Hong, Z. S., Yin, J., & Cui, Y. J. (2010). Compression behaviour of reconstituted soils at high initial water contents. *Geotechnique*, 60(9), 691-700. doi:10.1680/geot.09.P.059
- Horpibulsuk, S., Liu, M., Zhuang, Z., & Hong, Z.-S. (2016). Complete Compression Curves of Reconstituted Clays. *International Journal of Geomechanics*, 06016005.
- Horpibulsuk, S., Yangsukkaseam, N., Chinkulkijniwat, A., & Du, Y. J. (2011). Compressibility and permeability of Bangkok clay compared with kaolinite and bentonite. *Applied Clay Science*, 52(1), 150-159.
- Hossanlourad, M., Rokni, M. N., Hassanlo, M., & Badrlou, A. (2017). DISPERSIVE CLAY STABILISED BY ALUM AND LIME. *International Journal of GEOMATE*.
- Hou, Y., Wang, J., & Jeng, D. (2011). Three-Dimensional Deformation Behavior of an Over-Sized Excavation in Shanghai Clay. *Geotechnical Engineering Journal of the SEAGS&AGSSEA*, 42(3), 22-29.
- Hough, B. K. (1957). *Basic soils engineering*. New York: Ronald Press.
- Hung, W.-C., Hwang, C., Liou, J.-C., Lin, Y.-S., & Yang, H.-L. (2012). Modeling aquifer-system compaction and predicting land subsidence in central Taiwan. *Engineering Geology*, 147-148, 78-90. doi:10.1016/j.enggeo.2012.07.018
- Hunt, C. E., Pestana, J. M., Bray, J. D., & Riemer, M. (2002). Effect of pile driving on static and dynamic properties of soft clay. *Journal of Geotechnical and Geoenvironmental Engineering*, 128(1), 13-24.
- Jha, A. K., & Sivapullaiah, P. V. (2015). Mechanism of improvement in the strength and volume change behavior of lime stabilized soil. *Engineering Geology*, 198, 53-64. doi:<http://dx.doi.org/10.1016/j.enggeo.2015.08.020>
- Jones, L. D., & Jefferson, I. (2012). *Expansive soils*: ICE Publishing.
- Jung, Y.-H., Choo, J., Cho, W., & Chung, C.-K. (2013). Patterns of Nonlinear Shear Stiffness Degradation of Reconstituted Clay with Different Stress Histories. *Marine Georesources & Geotechnology*, 31(4), 309-331. doi:10.1080/1064119x.2012.676158
- Kang, X., Ge, L., Kang, G.-C., & Mathews, C. (2015). Laboratory investigation of the strength, stiffness, and thermal conductivity of fly ash and lime kiln dust

- stabilised clay subgrade materials. *Road Materials and Pavement Design*, 16(4), 928-945. doi:10.1080/14680629.2015.1028970
- Khemissa, M., & Mahamedi, A. (2014). Cement and lime mixture stabilization of an expansive overconsolidated clay. *Applied Clay Science*, 95, 104-110. doi:http://dx.doi.org/10.1016/j.clay.2014.03.017
- Kootahi, K., & Moradi, G. (2016). Evaluation of Compression Index of Marine Fine-Grained Soils by Means of Index Tests. *Marine Georesources & Geotechnology*. doi:10.1080/1064119x.2016.1213775
- Latifi, N., Rashid, A. S. A., Siddiqua, S., & Horpibulsuk, S. (2015). Micro-structural analysis of strength development in low- and high swelling clays stabilized with magnesium chloride solution — A green soil stabilizer. *Applied Clay Science*, 118, 195-206. doi:10.1016/j.clay.2015.10.001
- Le, T. M., Fatahi, B., & Khabbaz, H. (2012). Viscous Behaviour of Soft Clay and Inducing Factors. *Geotechnical and Geological Engineering*, 30(5), 1069-1083. doi:10.1007/s10706-012-9535-0
- Le, T. M., Fatahi, B., & Khabbaz, H. (2015). Numerical optimisation to obtain elastic viscoplastic model parameters for soft clay. *International Journal of Plasticity*, 65, 1-21.
- Lee, C., Hong, S.-J., Kim, D., & Lee, W. (2015). Assessment of Compression Index of Busan and Incheon Clays with Sedimentation State. *Marine Georesources & Geotechnology*, 33(1), 23-32. doi:10.1080/1064119x.2013.764947
- Lee, H. J., Kayen, R. E., & McArthur, W. G. (1990). Consolidation, triaxial shear-strength, and index-property characteristics of organic-rich sediments from the Peru margin.
- Lei, H., Wang, X., Chen, L., Huang, M., & Han, J. (2015). Compression characteristics of ultra-soft clays subjected to simulated staged preloading. *KSCE Journal of Civil Engineering*. doi:10.1007/s12205-015-0343-y
- Li, J., Zhang, D.-M., Hicher, P.-Y., & Wei, C.-F. (2016). Three-dimensional modelling of stress relaxation of soft clay under complex loading conditions. *European Journal of Environmental and Civil Engineering*, 1-13.
- Li, Y. R., Wen, B. P., Aydin, A., & Ju, N. P. (2013). Ring shear tests on slip zone soils of three giant landslides in the Three Gorges Project area. *Engineering Geology*, 154, 106-115. doi:10.1016/j.enggeo.2012.12.015
- Liu, M. D., Zhuang, Z., & Horpibulsuk, S. (2013). Estimation of the compression behaviour of reconstituted clays. *Engineering Geology*, 167, 84-94. doi:10.1016/j.enggeo.2013.10.015
- Mesri, G., & Olson, R. (1970). Shear strength of montmorillonite. *Geotechnique*, 20(3), 261-270.
- Mesri, G., & Olson, R. E. (1971). Consolidation characteristics of montmorillonite. *Geotechnique*, 21(4), 341-352.
- Mitchell, J. K., & Soga, K. (1976). *Fundamentals of soil behavior* (Vol. 422): Wiley New York.
- Mohd Amin, J., Taha, M. R., Ahmed, J., Abu Kassim, A., Jamaludin, A., & Jaadil, J. (1997). Prediction and determination of undrained shear strength of soft clay at Bukit Raja. *Pertanika Journal of Science & Technology*, 5(1), 111-126.
- Nacci, V. A., Wang, M. C., & Demars, K. R. (1975). *Engineering behavior of calcareous soils*. Paper presented at the Proceedings of Civil Engineering in the Oceans III, ASCE Specialty Conference, Newark, Del.
- Nagaraj, T., & Miura, N. (2001). *Soft clay behaviour analysis and assessment*. Rotterdam, Netherlands: A. A. Balkema.

- Nagaraj, T., & Murthy, S. (1983). Rationalization of Skempton's compressibility equation. *Geotechnique*, 33(4), 433-443.
- Nagaraj, T., & Murthy, S. (1986). A critical reappraisal of compression index equations. *Geotechnique*, 36(1), 27-32.
- Nagaraj, T., Pandian, N., Narasimha Raju, P., & Vishnu Bhushan, T. (1995). *Stress-state-time-permeability relationships for saturated soils*. Paper presented at the Proceedings of the International Symposium on Compression and Consolidation of Clayey Soils.
- Nagaraj, T. S., Basavapatna, R., & Murthy, S. (1985). Prediction of the preconsolidation pressure and recompression index of soils.
- Nath, A., & DeDalal, S. (2004). The role of plasticity index in predicting compression behaviour of clays. *Electronic Journal of Geotechnical Engineering*, 9.
- Nelson, J. D., & Chao, K. C. (2014). *Relationship between swelling pressures determined by constant volume and consolidation-swell oedometer tests*. Paper presented at the Unsaturated Soils: Research and Applications - Proceedings of the 6th International Conference on Unsaturated Soils, UNSAT 2014.
- Nelson, J. D., & Miller, D. J. (1992). *Expansive soils: Problems and Practice in Foundation and Pavement Engineering*. the United States of America: John Wiley & Sons.
- Nelson, J. D., Reichler, D. K., & Cumbers, J. M. (2006). *Parameters for heave prediction by oedometer tests*. Paper presented at the Geotechnical special publication.
- Newland, P., & Allely, B. (1955). Results of some investigations on two sensitive clays. *New Zealand Engineering*, 10(11), 403.
- Ni, J., Indraratna, B., Geng, X.-Y., Carter, J. P., & Chen, Y.-L. (2014). Model of soft soils under cyclic loading. *International Journal of Geomechanics*, 15(4), 04014067.
- Ogawa, F. (1978). Correlation of the mechanical and index properties of soils in Harbor districts. *Report of the Port and Harbor Research Institute*, 17(3), 4-89 (in Japanese).
- Ouhadi, V. R., Yong, R. N., Amiri, M., & Ouhadi, M. H. (2014). Pozzolanic consolidation of stabilized soft clays. *Applied Clay Science*, 95, 111-118. doi:<http://dx.doi.org/10.1016/j.clay.2014.03.020>
- Park, H. I., & Lee, S. R. (2011). Evaluation of the compression index of soils using an artificial neural network. *Computers and Geotechnics*, 38(4), 472-481. doi:10.1016/j.compgeo.2011.02.011
- Park, J., & Koumoto, T. (2004). New compression index equation. *Journal of Geotechnical and Geoenvironmental Engineering*, 130(2), 223-226.
- Peduto, D., Huber, M., Speranza, G., van Ruijven, J., & Cascini, L. (2016). DInSAR data assimilation for settlement prediction: case study of a railway embankment in The Netherlands. *Canadian Geotechnical Journal*, 54(4), 502-517.
- Phanikumar, B. R., Sreedharan, R., & Aniruddh, C. (2014). Swell-compressibility characteristics of lime-blended and cement-blended expansive clays – A comparative study. *Geomechanics and Geoengineering*, 10(2), 153-162. doi:10.1080/17486025.2014.902120
- PLAXIS2D. (2011). *Reference Manual*.
- Polidori, E. (2014). On the intrinsic compressibility of common clayey soils. *European Journal of Environmental and Civil Engineering*, 19(1), 27-47. doi:10.1080/19648189.2014.926295

- Powell, J. S., Siemens, G. A., Take, W. A., & Remenda, V. H. (2013). Characterizing the swelling potential of Bearpaw clayshale. *Engineering Geology*, 158, 89-97. doi:10.1016/j.enggeo.2013.03.006
- Puppala, A. J., Manosuthikij, T., & Chittoori, B. C. S. (2014). Swell and shrinkage strain prediction models for expansive clays. *Engineering Geology*, 168, 1-8. doi:10.1016/j.enggeo.2013.10.017
- Puppala, A. J., Punthutaecha, K., & Vanapalli, S. K. (2006). Soil-water characteristic curves of stabilized expansive soils. *Journal of Geotechnical and Geoenvironmental Engineering*, 132(6), 736-751. doi:10.1061/(ASCE)1090-0241(2006)132:6(736)
- Ranganatham, B., & Satyanarayana, B. (1965). *A rational method of predicting swelling potential for compacted expansive clays*. Paper presented at the Proceedings of the 6th International Conference on Soils Mechanics and Foundation Engineering, Montreal.
- Rashwan, M., & Koumoto, T. (2007). UNDRAINED SHEAR STRENGTH OF ARIAKE CLAY BY ELECTRONIC CONE PENETRATION TESTING. *Lowland technology international: the official journal of the International Association of Lowland Technology (IALT)/Institute of Lowland Technology, Saga University*, 9(1), 28-40.
- Retnamony, G., Robinson, R., & Allam, M. (1998). Effect of clay mineralogy on coefficient of consolidation. *Clays and Clay Minerals*, 46(5), 596-600.
- Richardson, A. M., & Whitman, R. V. (1963). Effect of strain-rate upon undrained shear resistance of a saturated remoulded fat clay. *Geotechnique*, 13(4), 310-324.
- Samang, L., Miura, N., & Sakai, A. (2005). Geotechnical Properties of Soft Cohesive Lowland Soils Deposited in Saga Airport Highway, Japan. *MEDIA KOMUNIKASI TEKNIK SIPIL*, 13(3), 19-35.
- Saride, S., Puppala, A. J., & Chikyala, S. R. (2013). Swell-shrink and strength behaviors of lime and cement stabilized expansive organic clays. *Applied Clay Science*, 85, 39-45. doi:10.1016/j.clay.2013.09.008
- Scaringi, G., & Di Maio, C. (2016). Influence of Displacement Rate on Residual Shear Strength of Clays. *Procedia Earth and Planetary Science*, 16, 137-145. doi:10.1016/j.proeps.2016.10.015
- Seed, H. B., Woodward, R. J., Jr, & Lundgren, R. (1962). Prediction of swelling potential for compacted clays. *Journal of the Soil Mechanics and Foundations Division*, 88(3), 53-88.
- Sharma, B., & Bora, P. (2004). Determination of plastic limit of soils by cone penetration method. *Indian Geotech J*, 34(4), 297-312.
- Sharma, B., & Bora, P. K. (2003). Plastic limit, liquid limit and undrained shear strength of soil-reappraisal. *Journal of Geotechnical and Geoenvironmental Engineering*, 129(8), 774-777.
- Sharma, B., & Bora, P. K. (2015). A Study on Correlation Between Liquid Limit, Plastic Limit and Consolidation Properties of Soils. *Indian Geotechnical Journal*, 45(2), 225-230.
- Shi, B., Jiang, H., Liu, Z., & Fang, H. (2002). Engineering geological characteristics of expansive soils in China. *Engineering Geology*, 67(1), 63-71.
- Shi, J., Qian, S., Zeng, L. L., & Bian, X. (2015). Influence of anisotropic consolidation stress paths on compression behaviour of reconstituted Wenzhou clay. *Geotechnique Letters*, 5(4), 275-280. doi:doi:10.1680/jgele.15.00113

- Shi, X. S., & Herle, I. (2015). Compression and undrained shear strength of remoulded clay mixtures. *Geotechnique Letters*, 5(2), 62-67. doi:doi:10.1680/geolett.14.00089
- Simons, N. E., Menzies, B. K., & Matthews, M. C. (2002). *A short course in geotechnical site investigation* (Vol. 5). London: Thomas Telford Ltd.
- Skempton, A., & Bishop, A. (1954). *Soils, Chapter 10 of Building Materials- their Elasticity and Inelasticity*. Amsterdam: North-Holland Publ. Co.
- Skempton, A. W. (1985). Residual strength of clays in landslides, folded strata and the laboratory. *Geotechnique*, 35(1), 3-18.
- Skempton, A. W., & Jones, O. (1944). Notes on the compressibility of clays. *Quarterly Journal of the Geological Society*, 100(1-4), 119-135.
- Sridharan, A., & Gurtug, Y. (2004). Swelling behaviour of compacted fine-grained soils. *Engineering Geology*, 72(1), 9-18.
- Sridharan, A., & Gurtug, Y. (2005). Compressibility characteristics of soils. *Geotechnical & Geological Engineering*, 23(5), 615-634.
- Sridharan, A., & Nagaraj, H. (2000). Compressibility behaviour of remoulded, fine-grained soils and correlation with index properties. *Canadian Geotechnical Journal*, 37(3), 712-722.
- Standards Australia (2003). Soil reactivity tests-Determination of the shrinkage index of a soil-Shrink-swell index (AS 1289.7.1.1-2003).
- Sun, L., Lu, J., Guo, W., Yan, S., & Jia, T. (2016). Models to Predict Compressibility and Permeability of Reconstituted Clays. *Geotechnical Testing Journal*, 39(2), 20150145. doi:10.1520/gtj20150145
- Takashi, T. (2015). e-log σ_v' Relationship for Marine Clays Considering Initial Water Content to Evaluate Soil Structure. *Marine Georesources & Geotechnology*. doi:10.1080/1064119x.2015.1113577
- Tan, B. B. (2004). *Geotechnical characterization of sediments from Hydrate Ridge, Cascadia continental margin*. Massachusetts Institute of Technology.
- Tatsuoka, F., Di Benedetto, H., Enomoto, T., Kawabe, S., & Kongkitkul, W. (2008). Various viscosity types of geomaterials in shear and their mathematical expression. *Soils and Foundations*, 48(1), 41-60.
- Taylor, D. (1948). *Fundamentals of Soil Mechanics*. New York: John Wiley and Sons.
- Terzaghi, K., & Peck, R. B. (1967). *Soil mechanics in engineering practice* (2nd ed.). New York: John Wiley & Sons.
- Thenoux, G., & Vera, S. (2002). Evaluation of hexahydrated magnesium chloride (Bischofite) performance as a chemical stabilizer of granular road surfaces. *Materiales de Construcción*, 52(265), 5-22.
- Tika, T. E., & Hutchinson, J. (1999). Ring shear tests on soil from the Vaiont landslide slip surface. *Geotechnique*, 49(1), 59-74.
- Tika, T. E., Vaughan, P., & Lemos, L. (1996). Fast shearing of pre-existing shear zones in soil. *Geotechnique*, 46(2), 197-233.
- Turkoz, M., Savas, H., Acaz, A., & Tosun, H. (2014). The effect of magnesium chloride solution on the engineering properties of clay soil with expansive and dispersive characteristics. *Applied Clay Science*, 101, 1-9. doi:10.1016/j.clay.2014.08.007
- Van der Merwe, D. (1956). The prediction of heave from the plasticity index and percentage clay fraction of soils. *Civil Engineering= Siviele Ingenieurswese*, 6(6), 103-107.

- Vanapalli, S. K., & Lu, L. (2012). A state-of-the art review of 1-D heave prediction methods for expansive soils. *International Journal of Geotechnical Engineering*, 6(1), 15-41. doi:10.3328/ijge.2012.06.01.15-41
- Vulliet, L., & Hutter, K. (1988). Viscous-type sliding laws for landslides. *Canadian Geotechnical Journal*, 25(3), 467-477.
- Walton, W., Sangrey, D., & Miller, S. (1983). Geotechnical engineering characterization of hydraulically piston-cored deep ocean sediments. *INITIAL REPORTS OF THE DEEP SEA DRILLING PROJECT*, 72(DEC), 537-549.
- Wang, D., & Abriak, N. E. (2014). Compressibility Behavior of Dunkirk Structured and Reconstituted Marine Soils. *Marine Georesources & Geotechnology*, 33(5), 419-428. doi:10.1080/1064119x.2014.950798
- Wang, D., Abriak, N. E., & Zentar, R. (2014). One-dimensional consolidation of lime-treated dredged harbour sediments. *European Journal of Environmental and Civil Engineering*, 19(2), 199-218. doi:10.1080/19648189.2014.939309
- Wang, D., Zentar, R., & Abriak, N. E. (2016). Interpretation of Compression Behavior of Structured and Remolded Marine Soils. *Journal of Materials in Civil Engineering*, 0(0), 04016005. doi:doi:10.1061/(ASCE)MT.1943-5533.0001503
- Whittle, J. F. (1974). *Consolidation behavior of an embankment on Boston blue clay*. Massachusetts Institute of Technology.
- Wilkinson, G., & Rogers, C. (1973). Symbolic description of factorial models for analysis of variance. *Applied Statistics*, 22(3), 392-399.
- Wood, D., & Wroth, C. (1976). *The Correlation of Some Basic Engineering Properties of Soils*. Paper presented at the Proc. Conf. On Behaviour of Offshore Structures.
- Wroth, C., & Wood, D. (1978). The correlation of index properties with some basic engineering properties of soils. *Canadian Geotechnical Journal*, 15(2), 137-145.
- Xu, G.-Z., Gao, Y.-F., & Xu, C. (2015). Permeability Behavior of High-Moisture Content Dredged Slurries. *Marine Georesources & Geotechnology*, 33(4), 348-355. doi:10.1080/1064119x.2014.890258
- Xu, G.-Z., & Yin, J. (2015). Compression Behavior of Secondary Clay Minerals at High Initial Water Contents. *Marine Georesources & Geotechnology*, 34(8), 721-728. doi:10.1080/1064119x.2015.1080333
- Xu, G., Gao, Y., Yin, J., Yang, R., & Ni, J. (2014). Compression Behavior of Dredged Slurries at High Water Contents. *Marine Georesources & Geotechnology*, 33(2), 99-108. doi:10.1080/1064119x.2013.805287
- Yan, W., & Ma, Y. (2010). Geotechnical characterization of Macau marine deposits. *Engineering Geology*, 113(1), 62-69.
- Yanase, Y., Tsuboi, H., Hamamoto, S., Kawamoto, K., Takemura, T., Kurukulasuriya, L. C., & Oda, M. (2010). *Consolidation characteristics for Sri lankan and Japanese clays: void index in relation to stress states and sedimentation environment*. Paper presented at the International Conference on Sustainable Built Environment (ICSBE-2010), Kandy.
- Yin, J., & Miao, Y. (2013). Intrinsic Compression Behavior of Remolded and Reconstituted Clays-Reappraisal. *Open Journal of Civil Engineering*, 03(03), 8-12. doi:10.4236/ojce.2013.33B002
- Yunus, N. M., Wanatowski, D., & Stace, L. (2013). The influence of chloride salts on compressibility behaviour of lime-treated organic clay. *International journal*

- of GEOMATE: geotechnique, construction materials and environment*, 5(1), 640-646.
- Zeng, L.-L., Hong, Z.-S., Cai, Y.-Q., & Han, J. (2011). Change of hydraulic conductivity during compression of undisturbed and remolded clays. *Applied Clay Science*, 51(1–2), 86-93. doi:<http://dx.doi.org/10.1016/j.clay.2010.11.005>
- Zeng, L.-L., Hong, Z.-S., & Cui, Y.-J. (2015). Determining the virgin compression lines of reconstituted clays at different initial water contents. *Canadian Geotechnical Journal*, 52(9), 1408-1415. doi:10.1139/cgj-2014-0172

Chapter 14 - REFERENCES

Every reasonable effort has been made to acknowledge the owners of copyright material. I would be pleased to hear from any copyright owner who has been omitted or incorrectly acknowledged.

Appendix A - Test Pitting Photos

Appendix A Test Pitting Photos

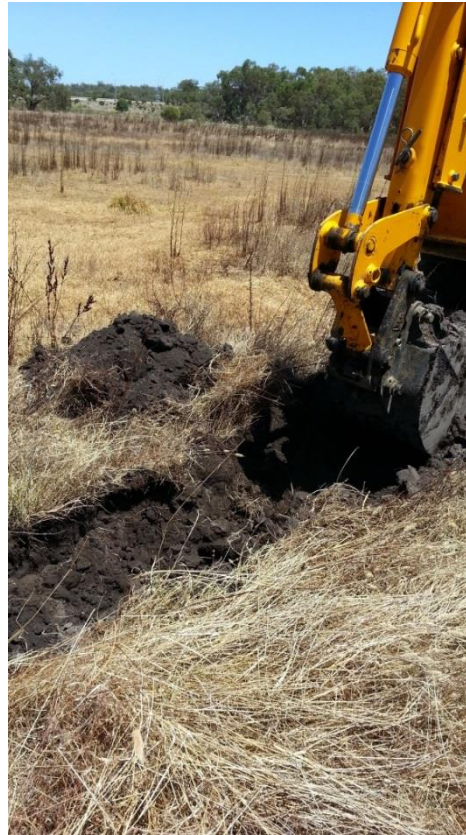


Figure A.1 . Test pitting procedure (cont.)

Appendix A - Test Pitting Photos



Figure A.1 . Test pitting procedure

Appendix B One-dimensional Consolidation Results

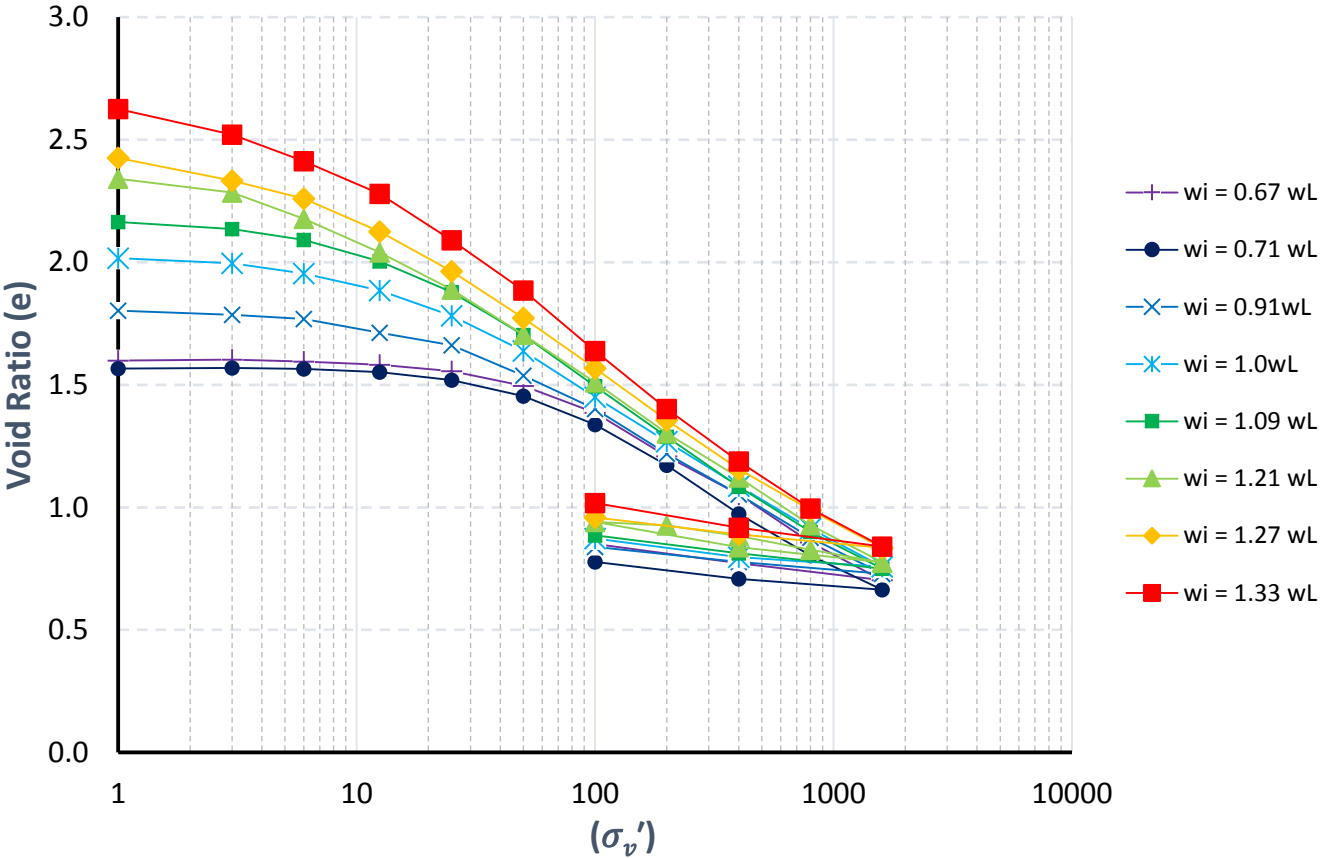


Figure B. 1. Compression Curves

Appendix B - One-dimensional Consolidation Results

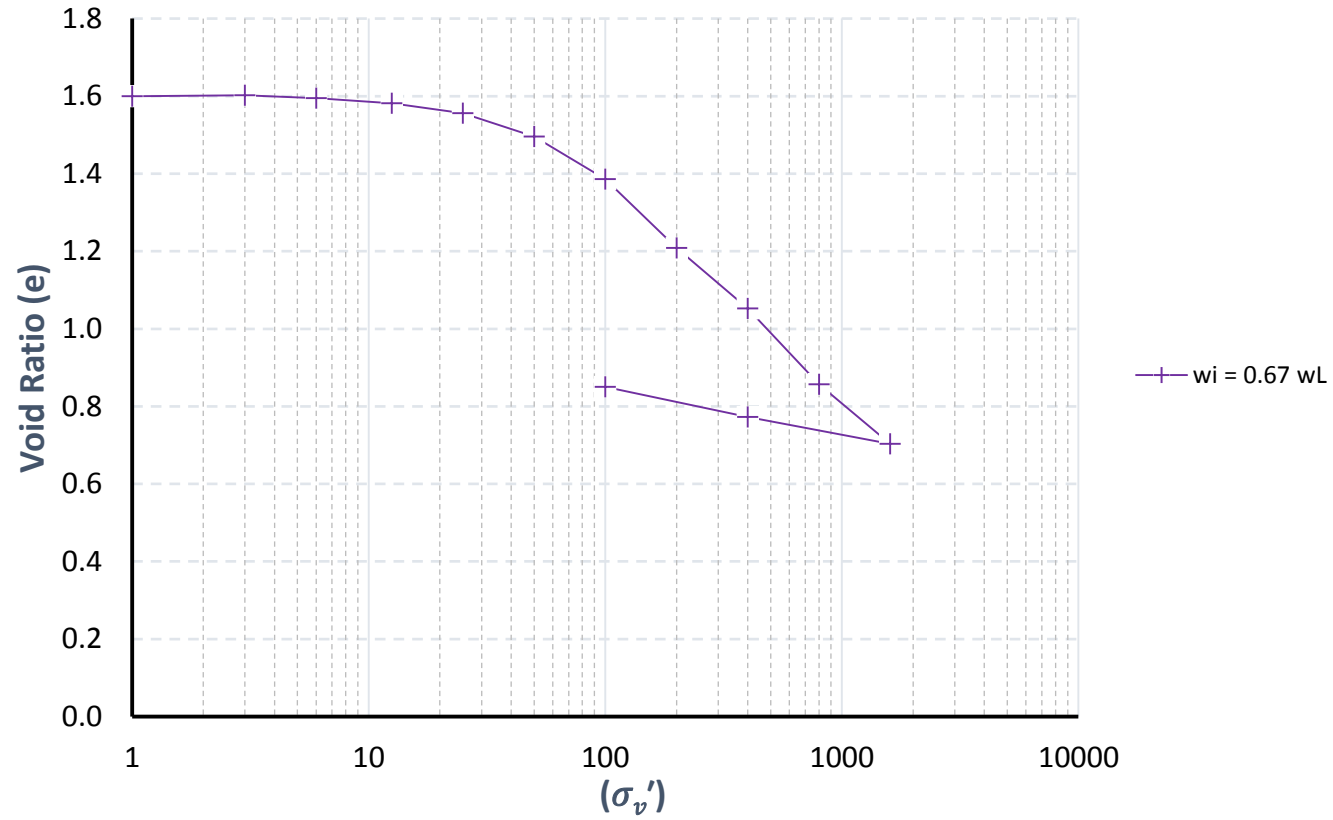


Figure B.2 . Compression Curves ($w_0 = 0.67 w_L$)

Appendix B - One-dimensional Consolidation Results

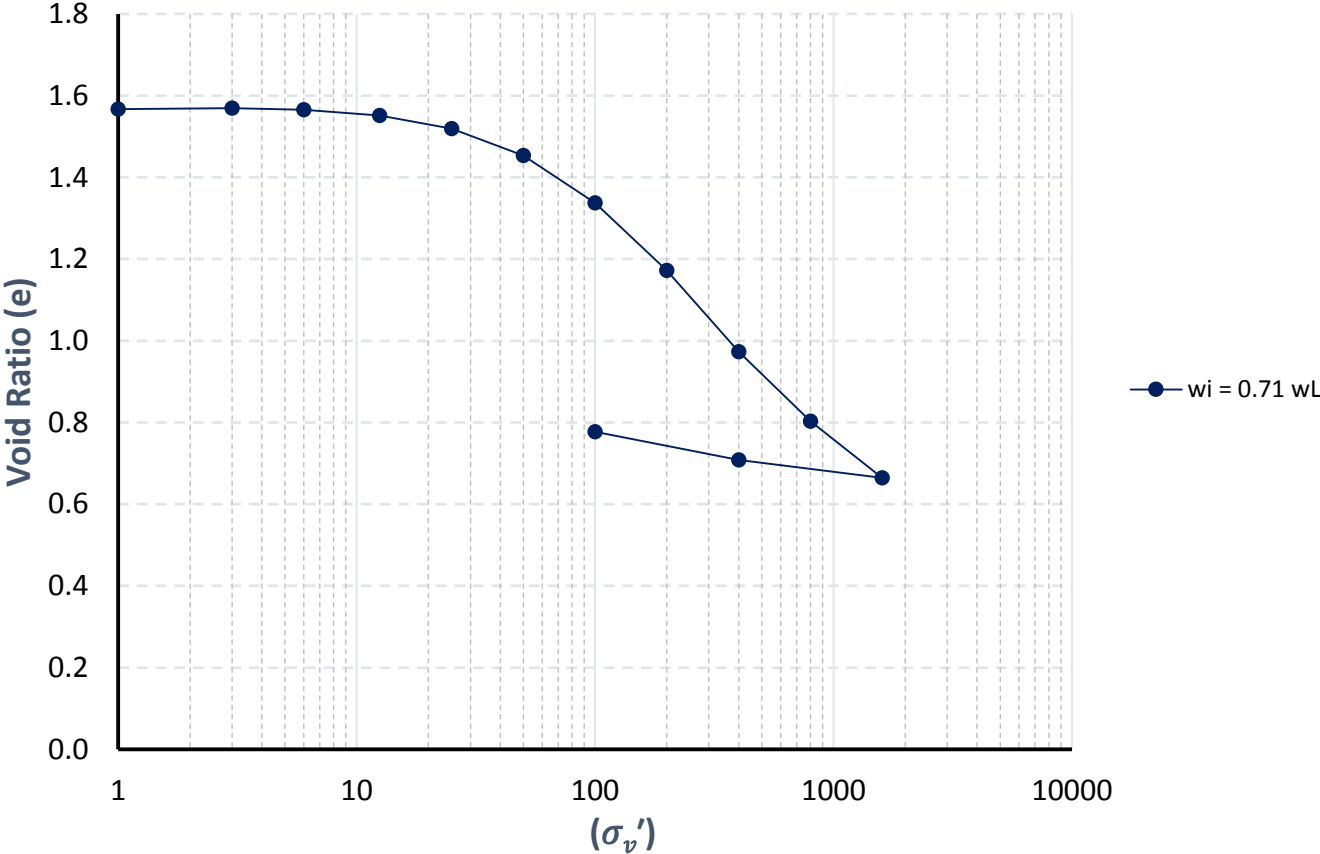


Figure B.3 . Compression Curves ($w_0 = 0.71 w_L$)

Appendix B - One-dimensional Consolidation Results

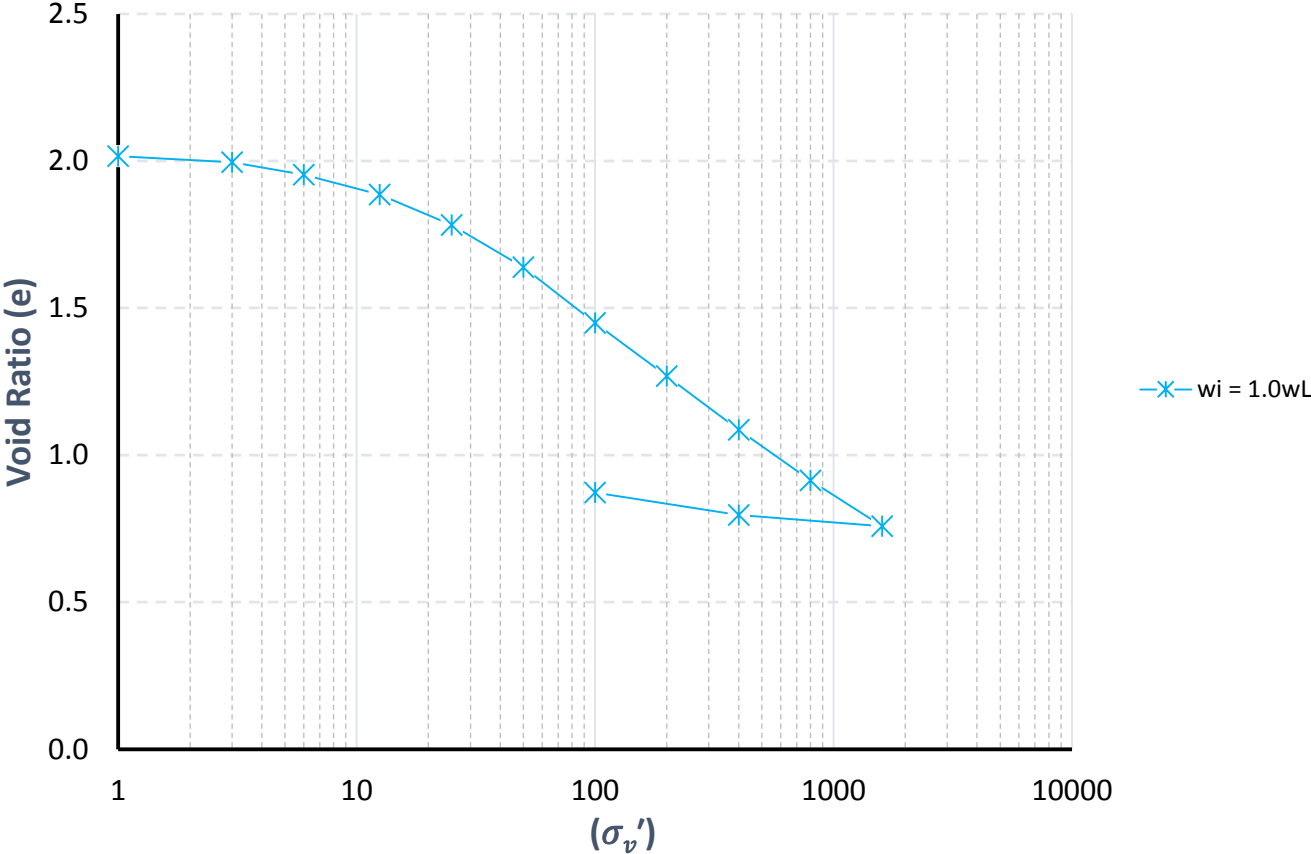


Figure B.4 . Compression Curves ($w_0 = 0.91 w_L$)

Appendix B - One-dimensional Consolidation Results

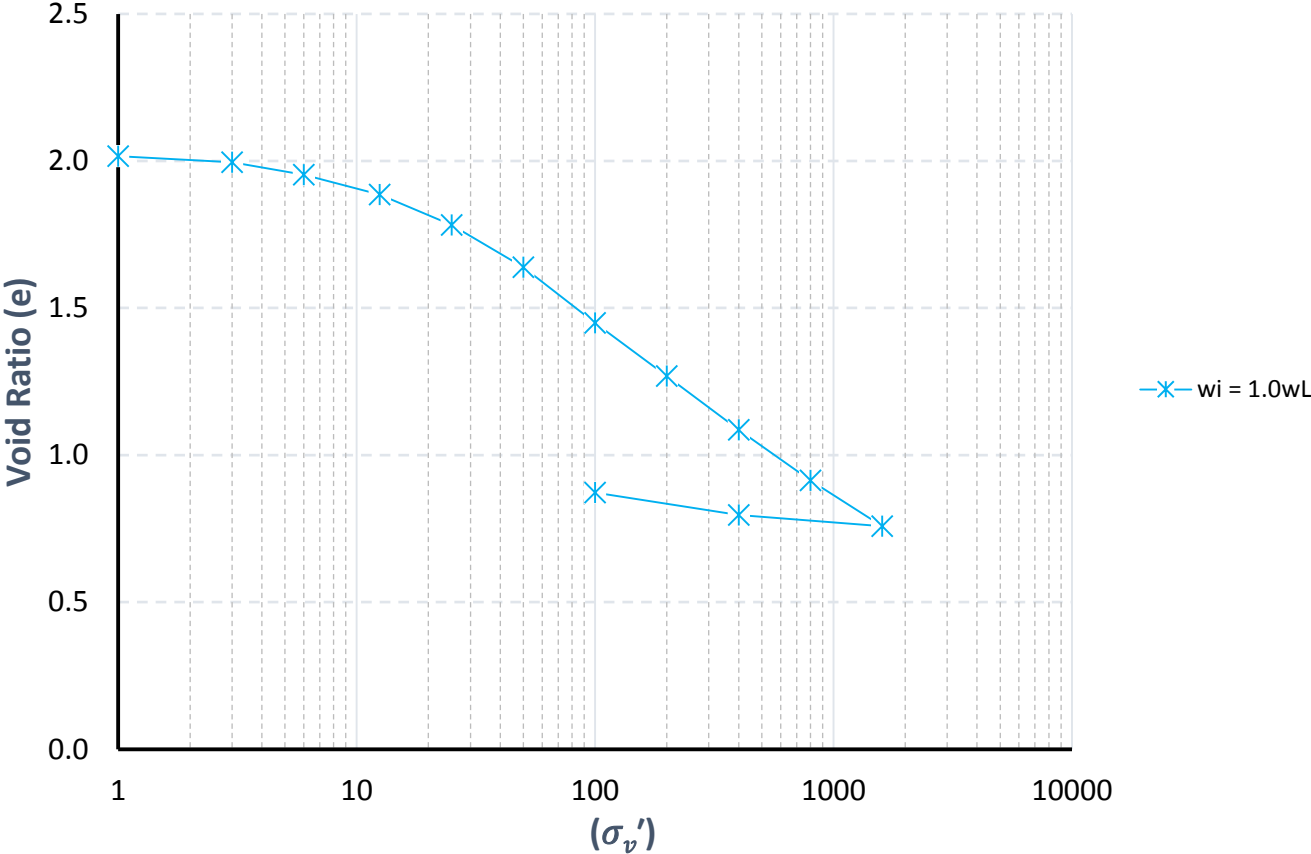


Figure B.5 . Compression Curves ($w_0 = 1.0 w_L$)

Appendix B - One-dimensional Consolidation Results

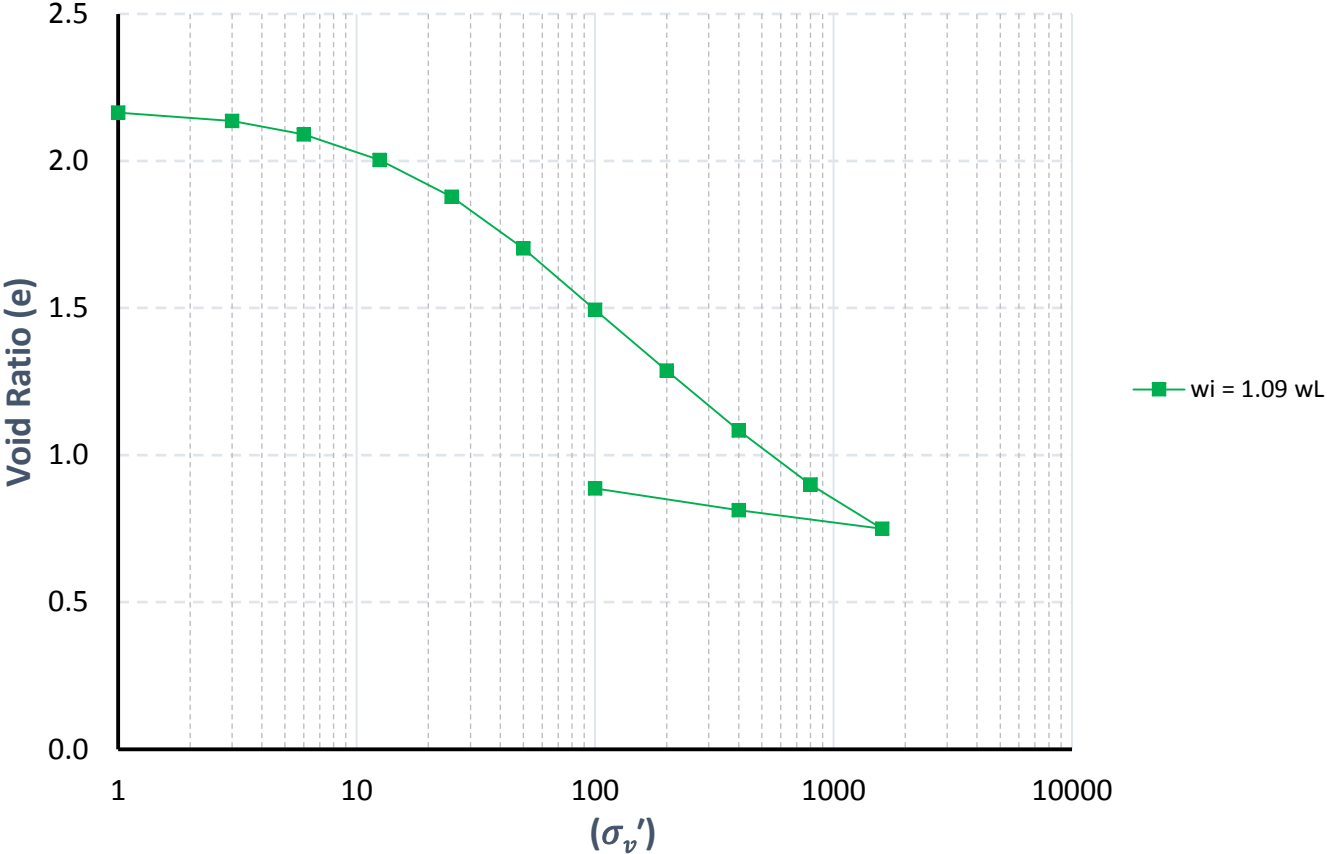


Figure B.6 . Compression Curves ($w_0 = 1.09 w_L$)

Appendix B - One-dimensional Consolidation Results

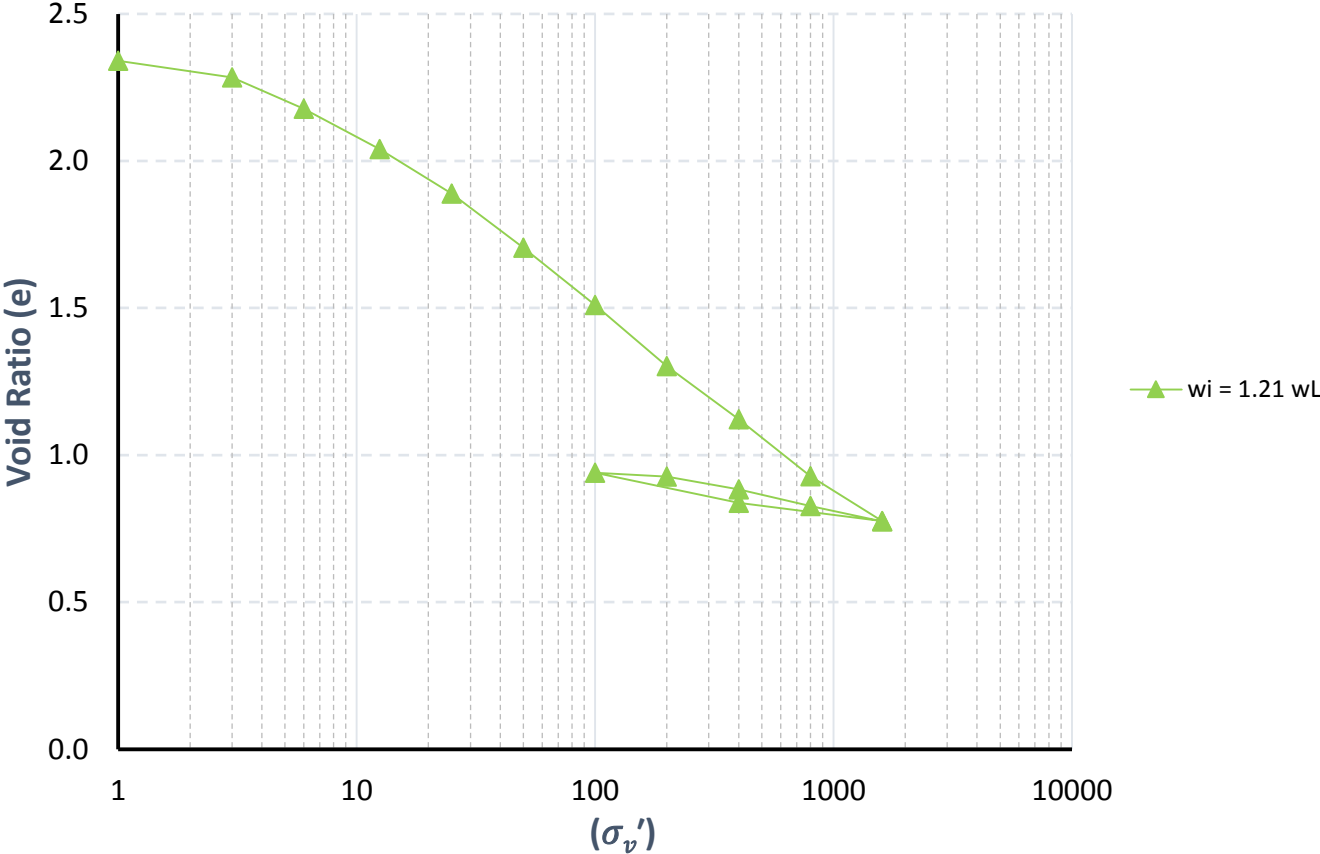


Figure B.7 . Compression Curves ($w_0 = 1.21 w_L$)

Appendix B - One-dimensional Consolidation Results

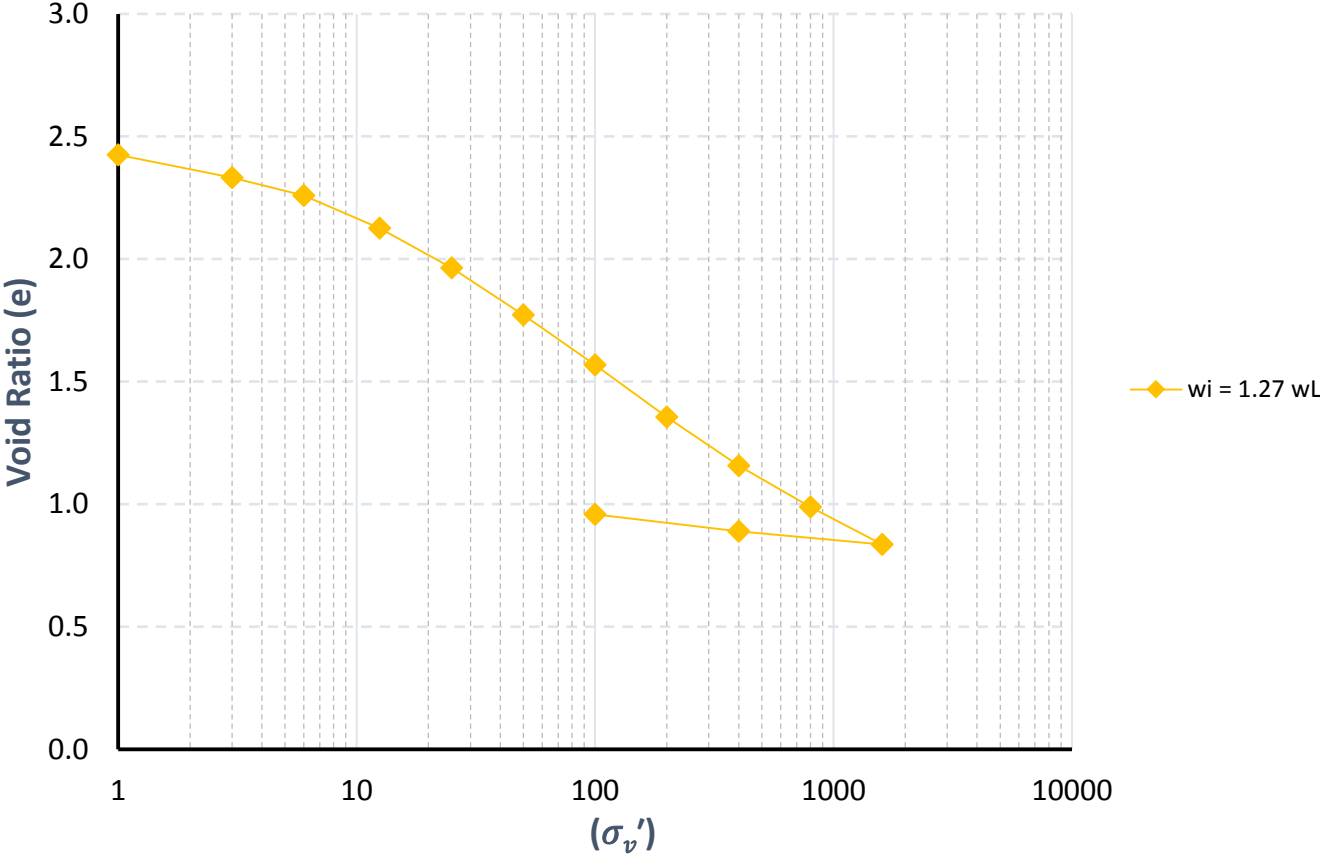


Figure B.8 . Compression Curves ($w_0 = 1.27 w_L$)

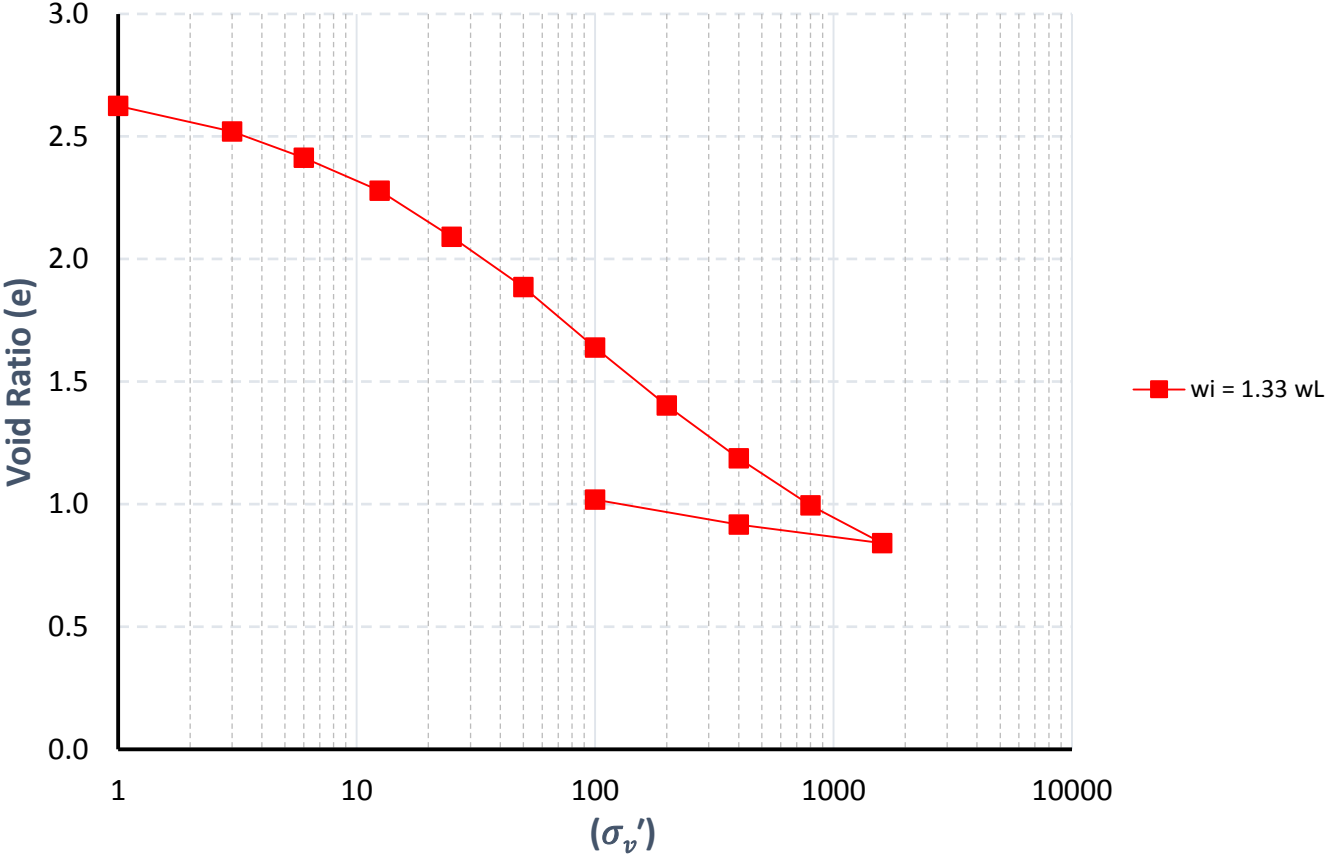


Figure B.9 . Compression Curves ($w_0 = 1.33 w_L$)

Appendix C Direct Shear Test Results

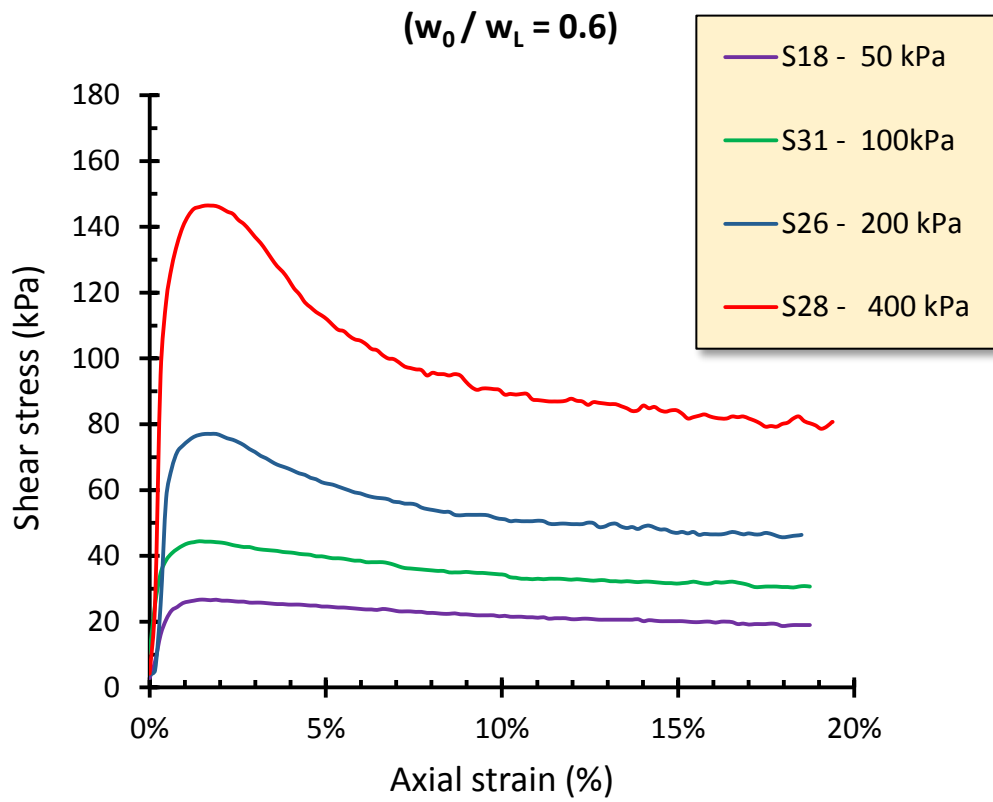


Figure C.1 . Shear strength vs horizontal strain ($w_0 = 0.6 w_L$)

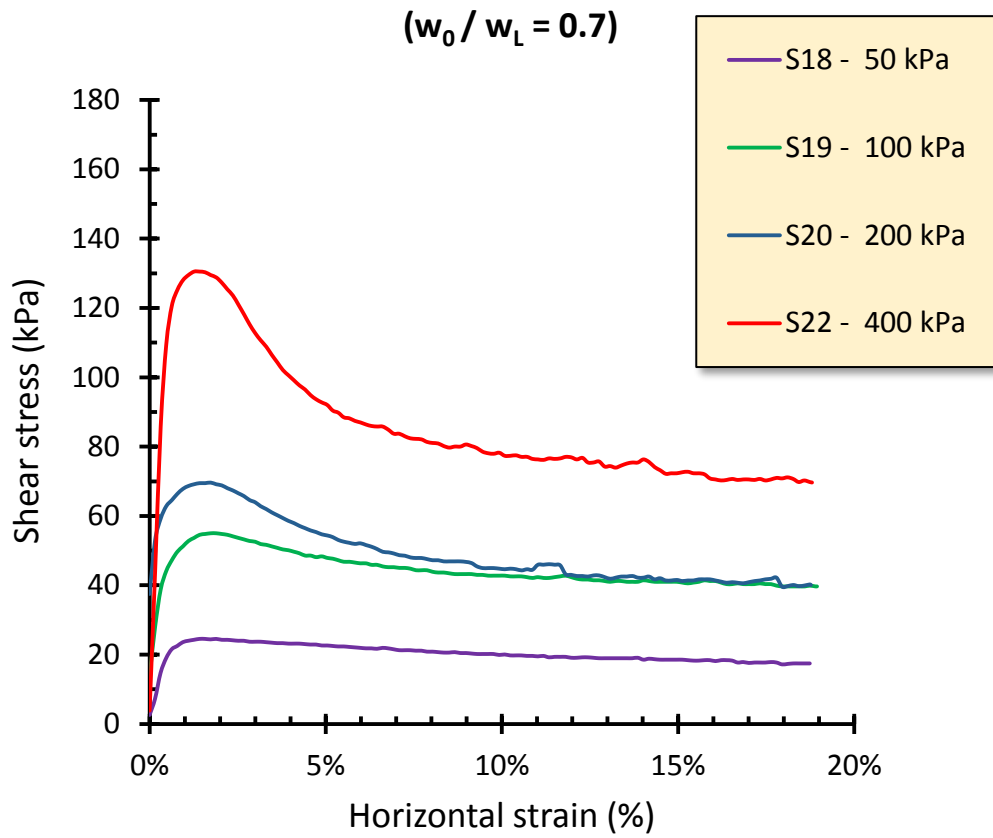


Figure C. 2 . Shear strength vs horizontal strain ($w_0 = 0.7 w_L$)

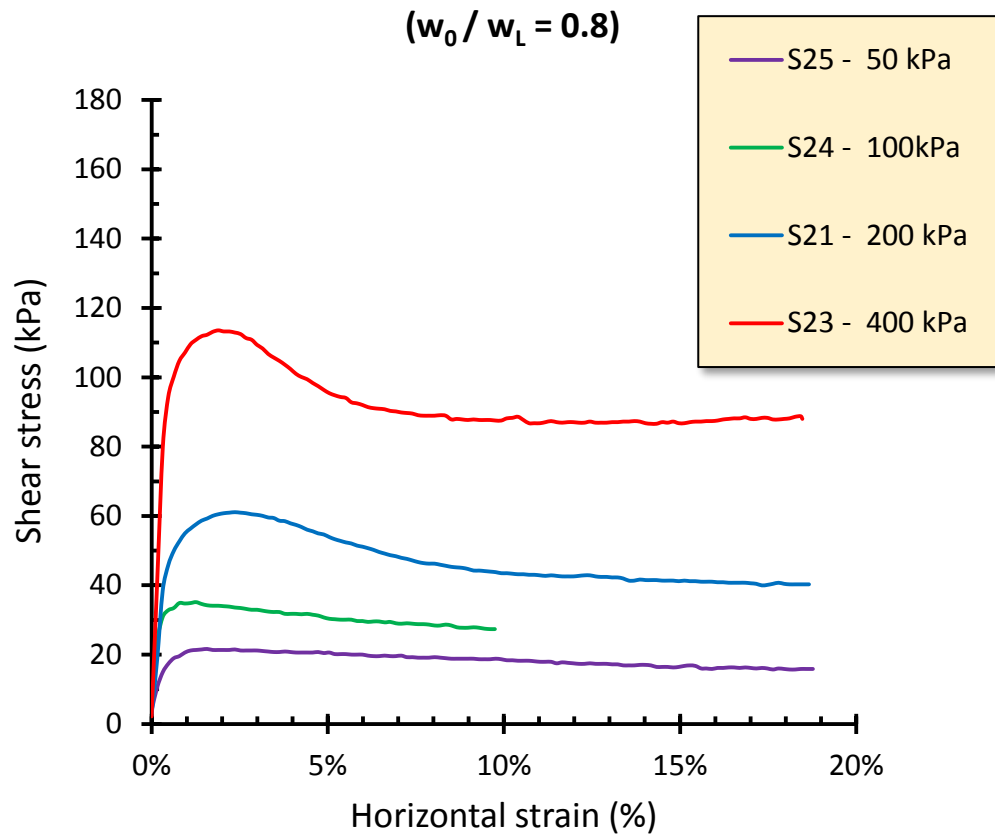


Figure C. 3 . Shear strength vs horizontal strain ($w_0 = 0.8 w_L$)

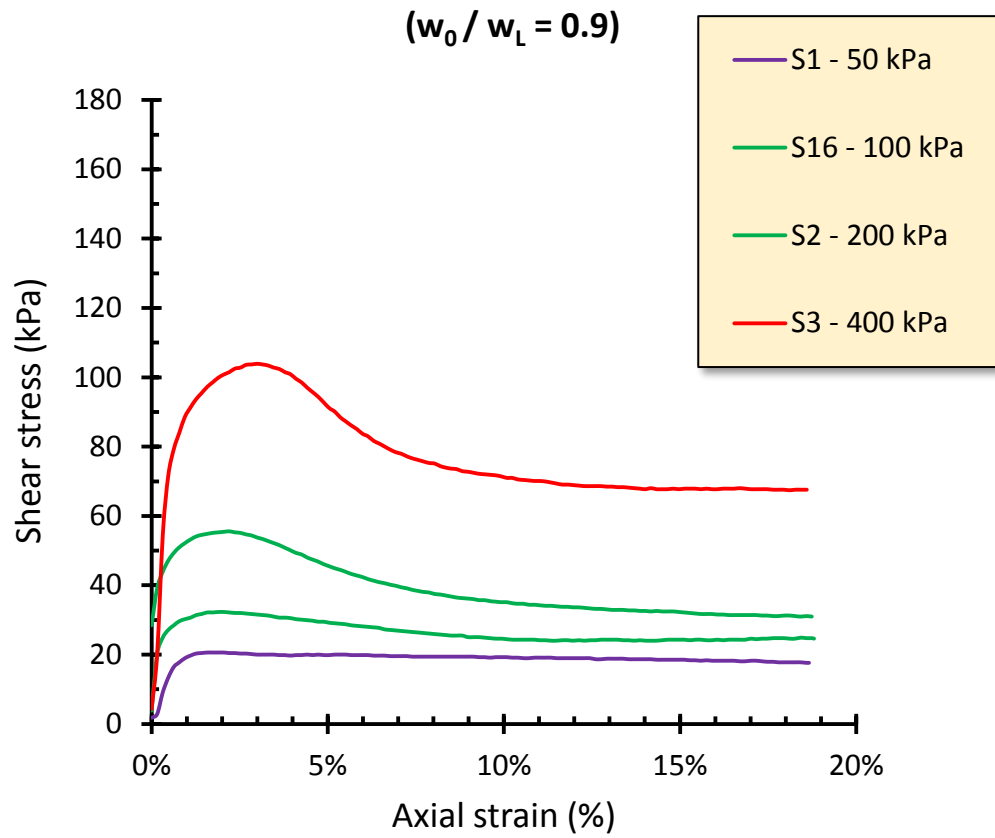


Figure C. 4 . Shear strength vs horizontal strain ($w_0 = 0.9 w_L$)

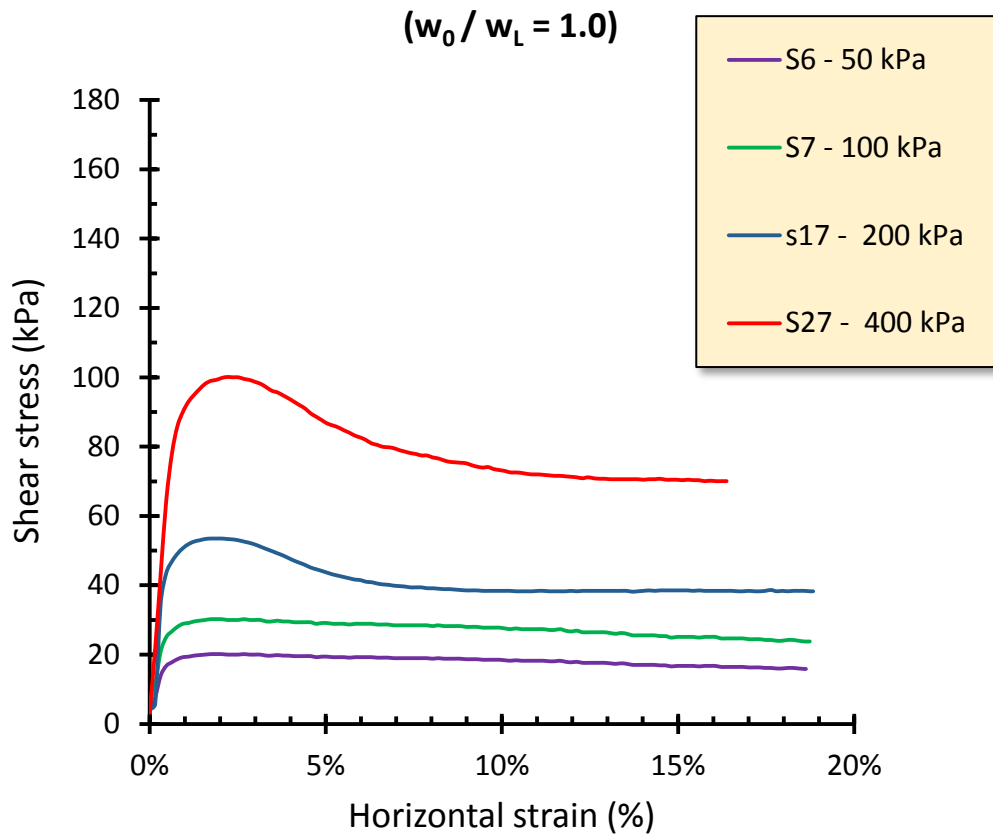


Figure C. 5 . Shear strength vs horizontal strain ($w_0 = 1.0 w_L$)

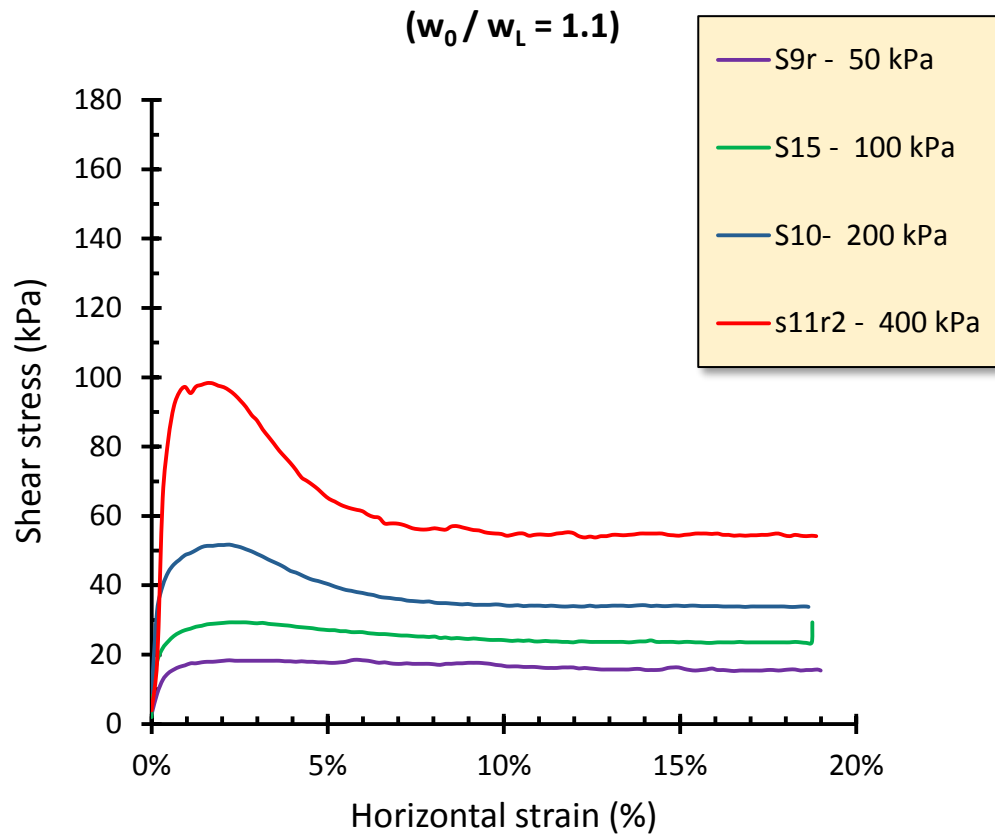


Figure C. 6 . Shear strength vs horizontal strain ($w_0 = 1.1 w_L$)

Appendix C - Direct Shear Test Results

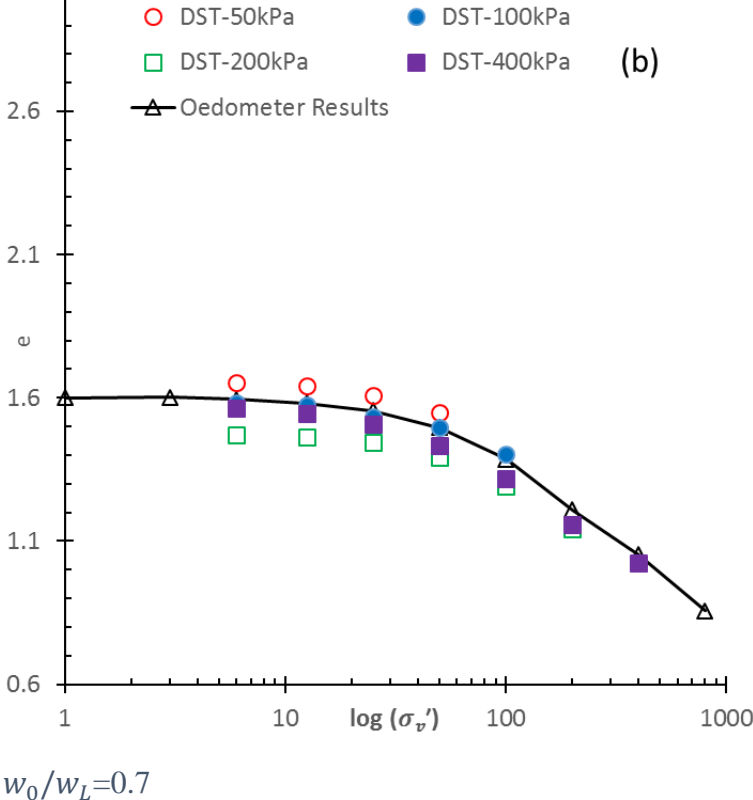
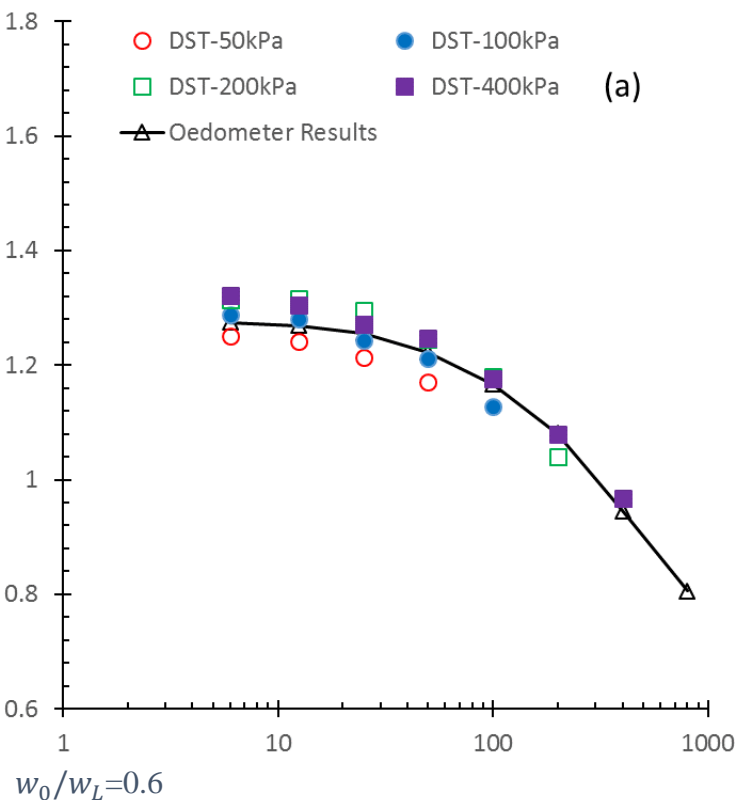
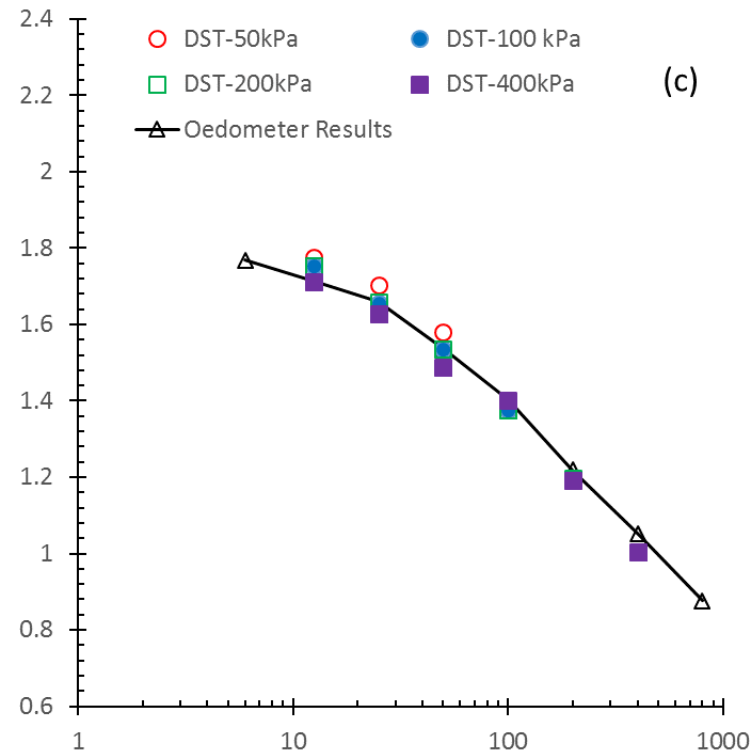
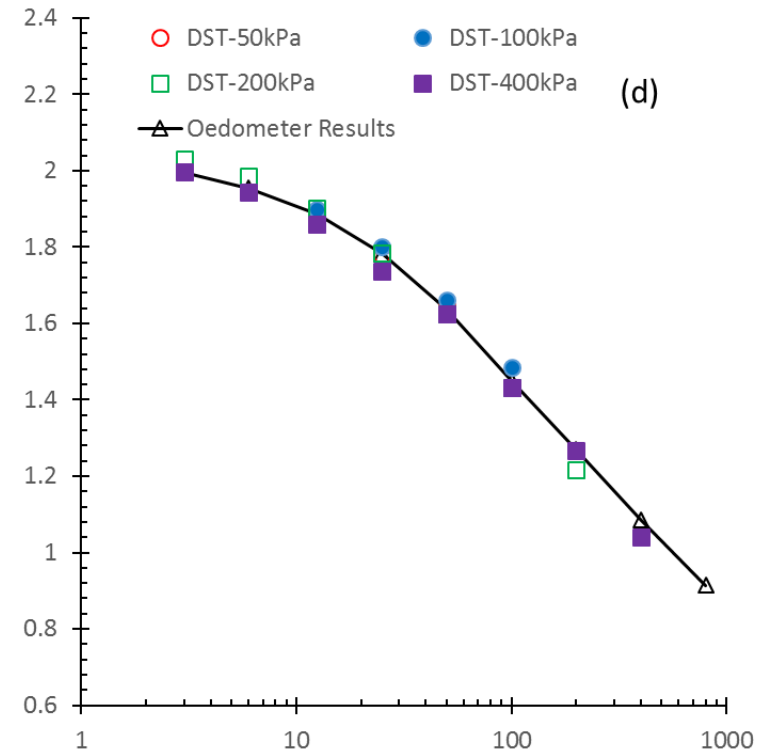


Figure C. 7 . Compression curves for the pre-consolidation stage and the one-dimensional consolidometer test

Appendix C - Direct Shear Test Results



$$w_0/w_L=0.8$$



$$w_0/w_L=0.9$$

Figure C. 8 . Compression curves for the pre-consolidation stage and the one-dimensional consolidometer test

Appendix C - Direct Shear Test Results

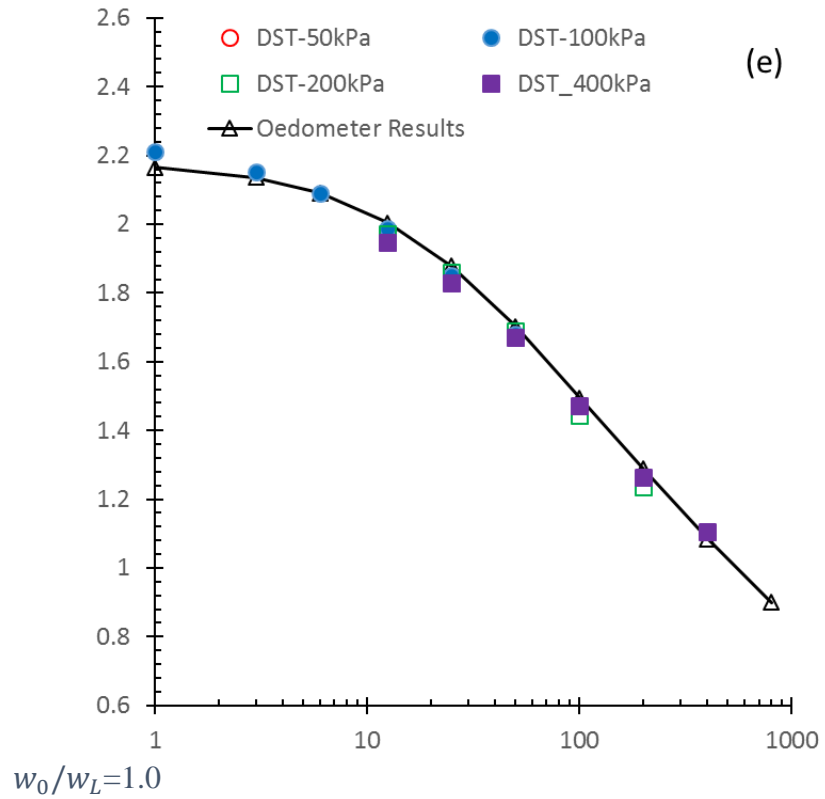


Figure C. 9 . Compression curves for the pre-consolidation stage and the one-dimensional consolidometer test

Appendix D Torsional Shear Test Results

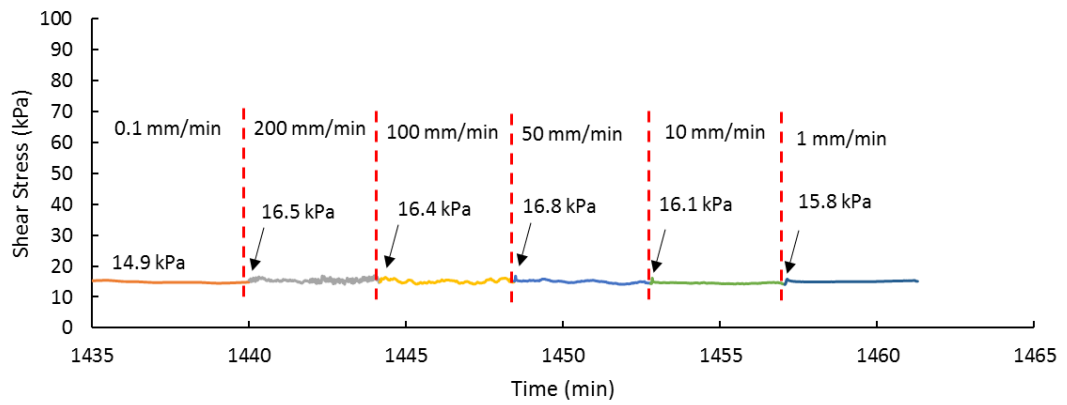


Figure D. 1 . Residual shear strength against elapsed. Time ($\sigma'_v = 50$ kPa).

Appendix D - Torsional Shear Test Results

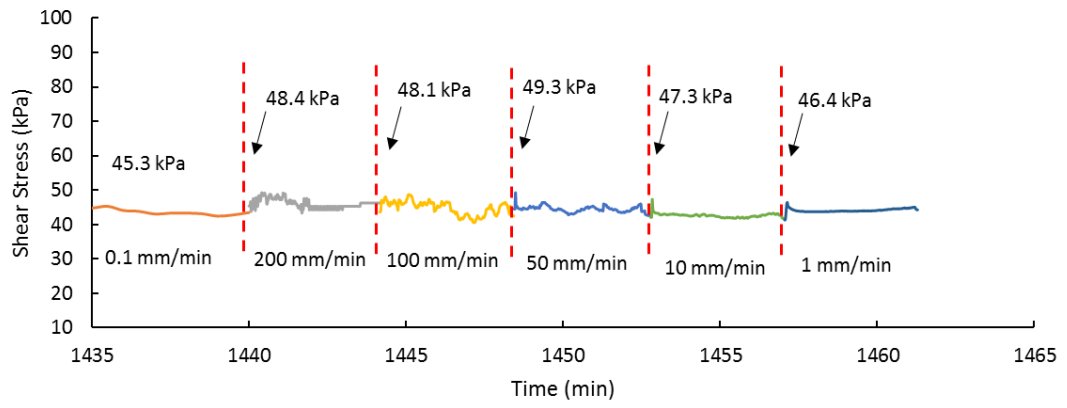


Figure D. 2. Residual shear strength against elapsed. Time ($\sigma'_v = 100$ kPa).

Appendix D - Torsional Shear Test Results

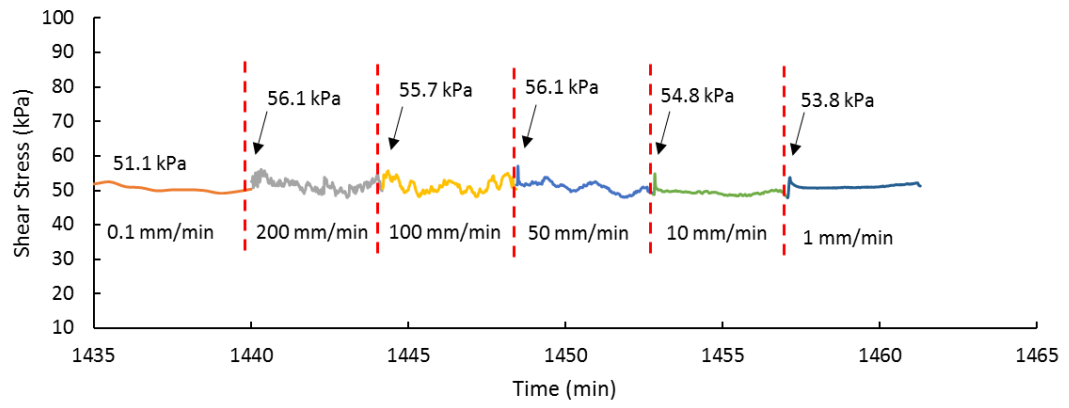


Figure D. 3. Residual shear strength against elapsed. Time ($\sigma'_v = 200$ kPa).

Appendix E Artificial Neural Network Results

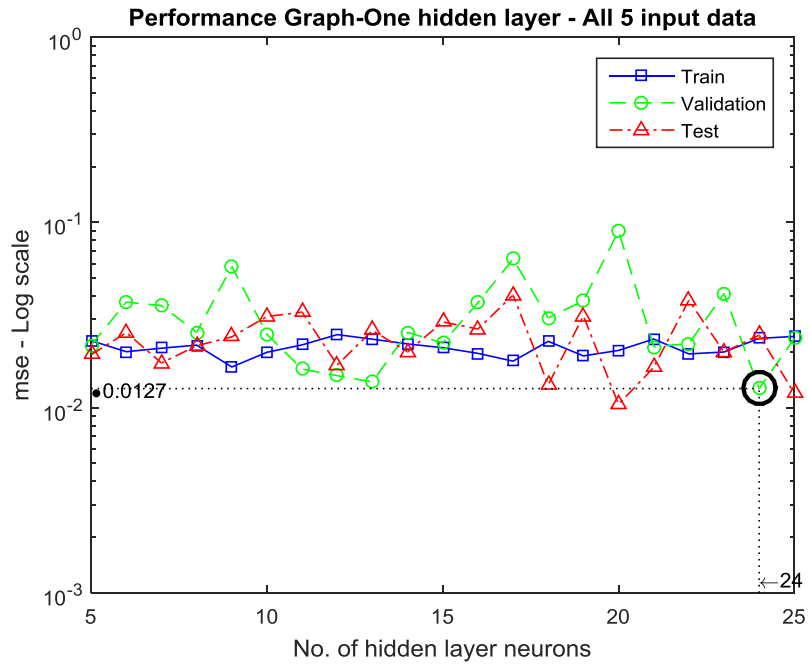


Figure E. 1 . The performance graphs of the number of neurons in the hidden layer (Linear –Linear Transfer functions).

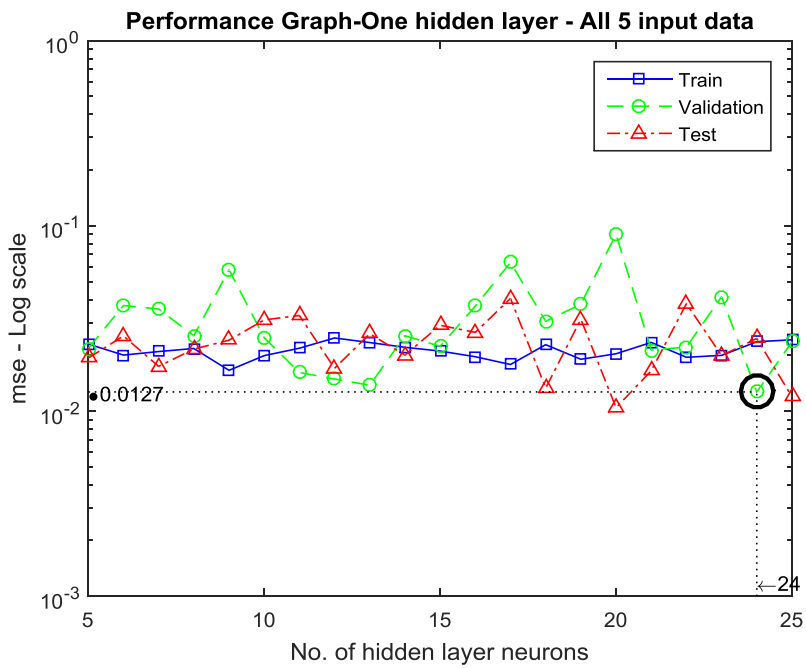


Figure E. 2. The performance graphs of the number of iterations

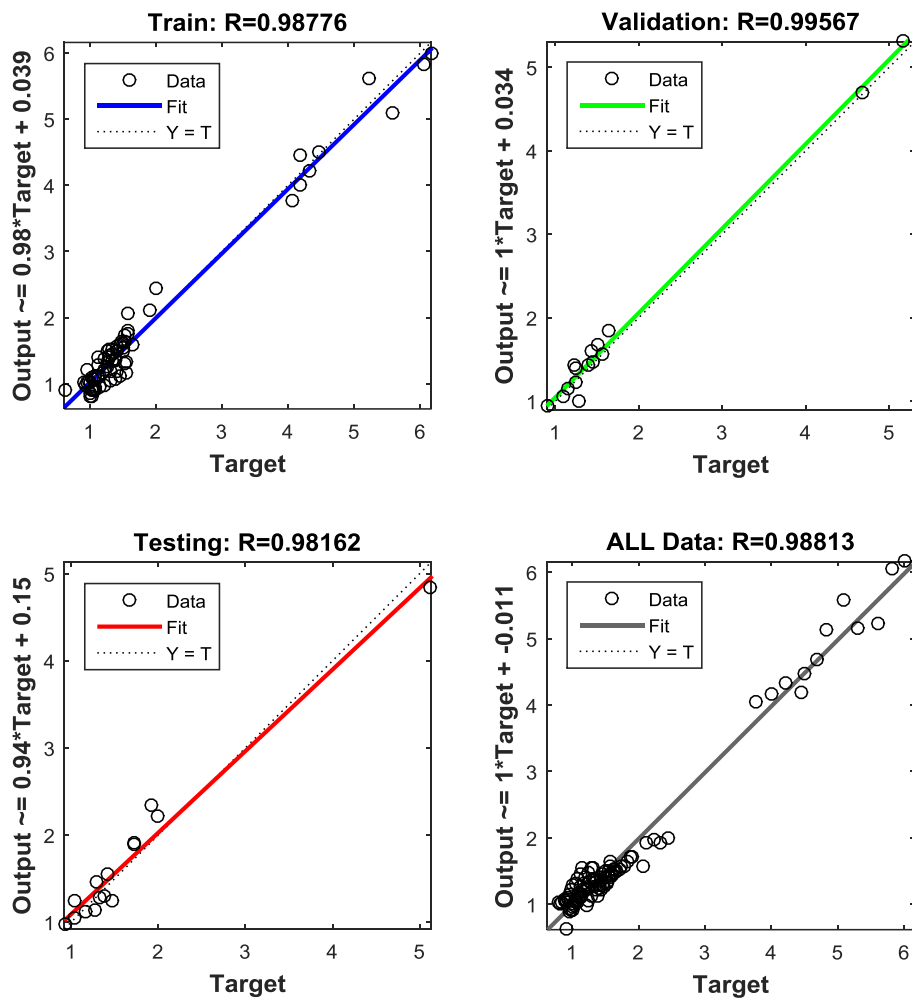


Figure E. 3 . A comparison between target values and outputs (e_{100}^*) - (Linear – Linear Transfer functions).

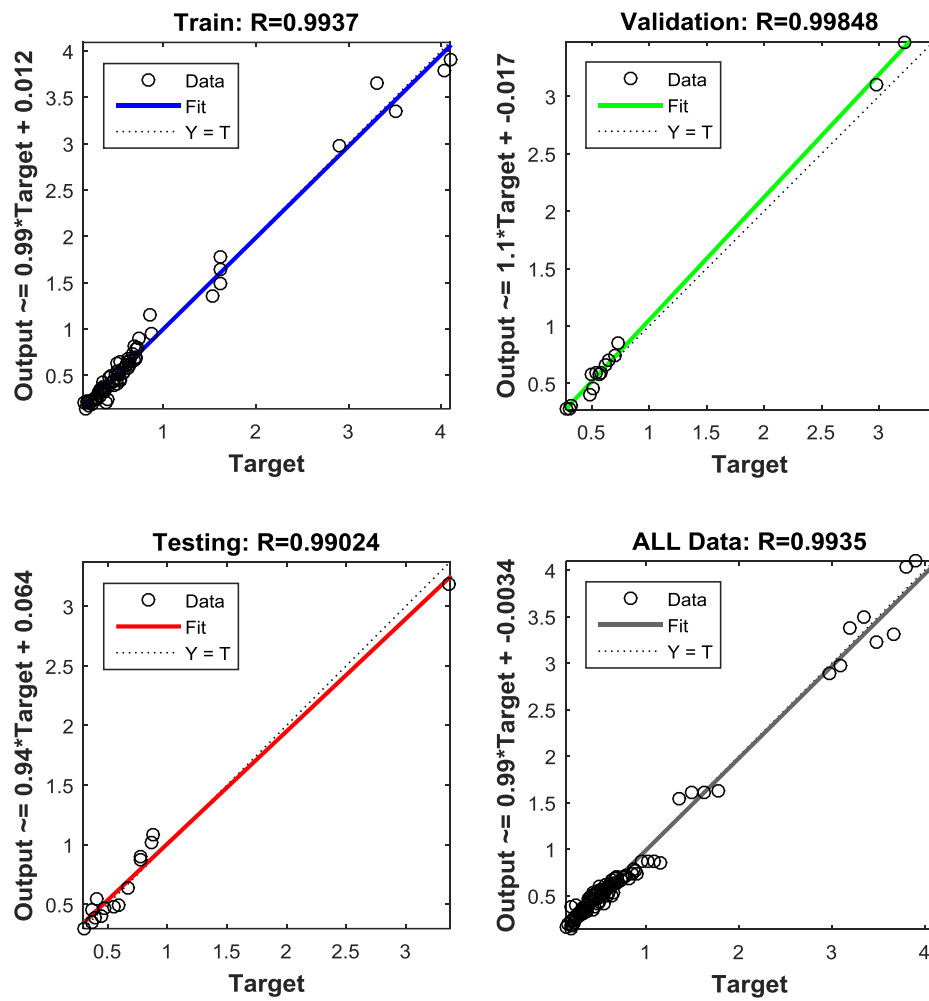


Figure E. 4 . A comparison between target values and outputs (C_c^*)- (Linear –Linear Transfer functions).

Appendix E - Artificial Neural Network Results

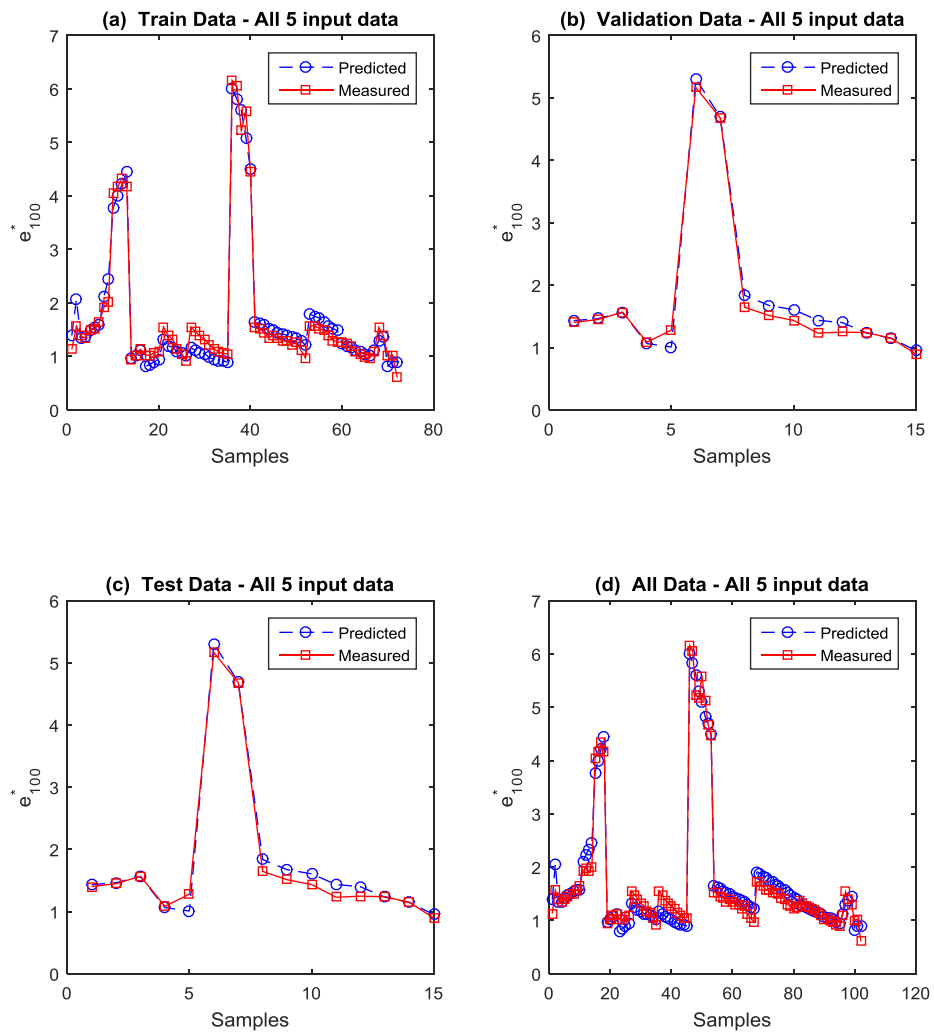


Figure E. 5 The simulation results for three steps of data processing and all data (e_{100}^*) - (Linear –Linear Transfer functions)..

Appendix E - Artificial Neural Network Results

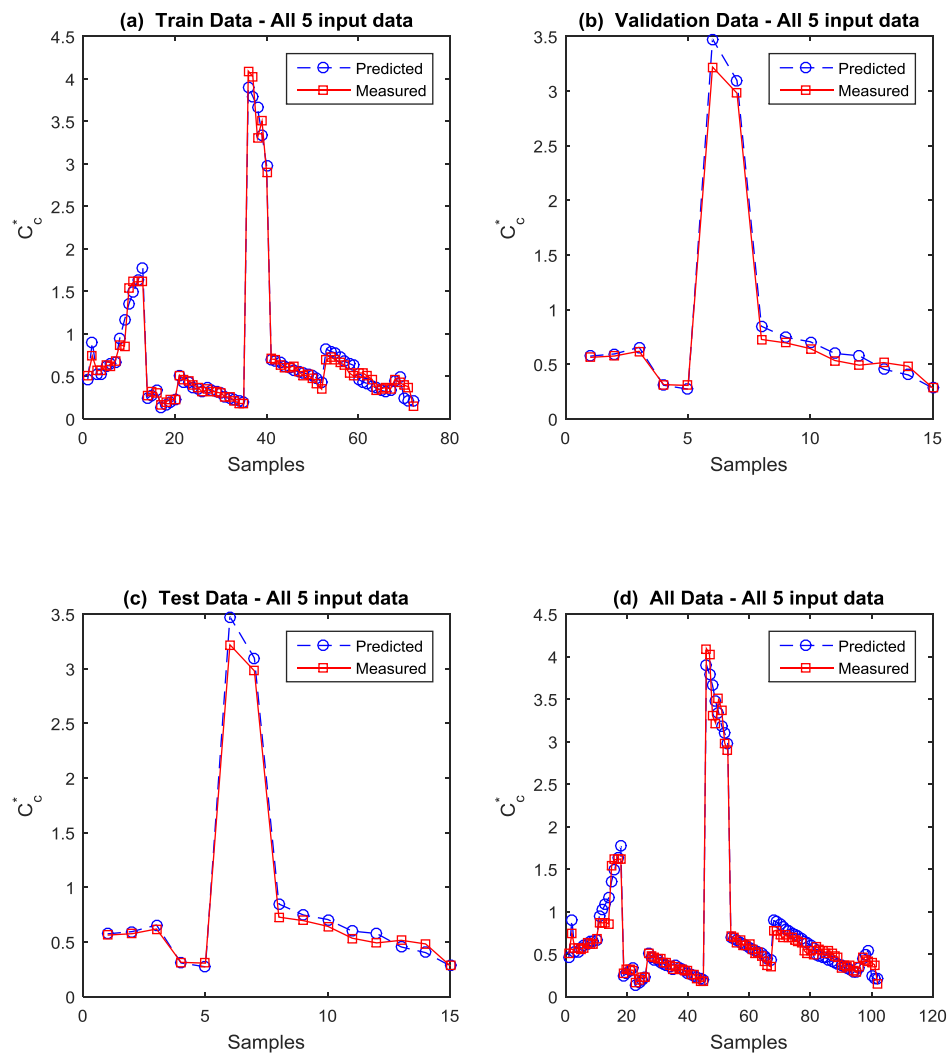


Figure E. 6 . The simulation results for three steps of data processing and all data (C_c^*) - (Linear –Linear Transfer functions).

Appendix E - Artificial Neural Network Results

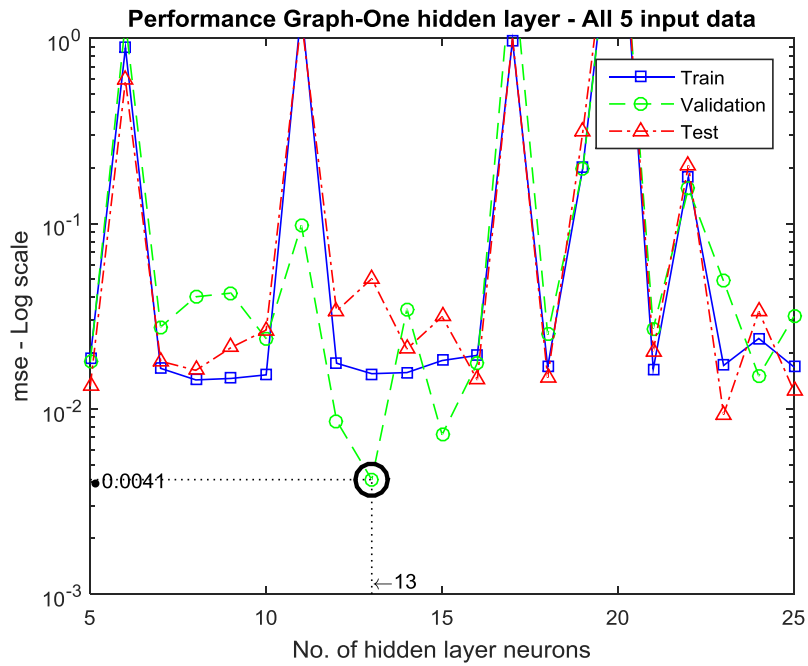


Figure E. 7 . The performance graphs of the number of neurons in the hidden layer (Linear –Tangent sigmoid Transfer functions).

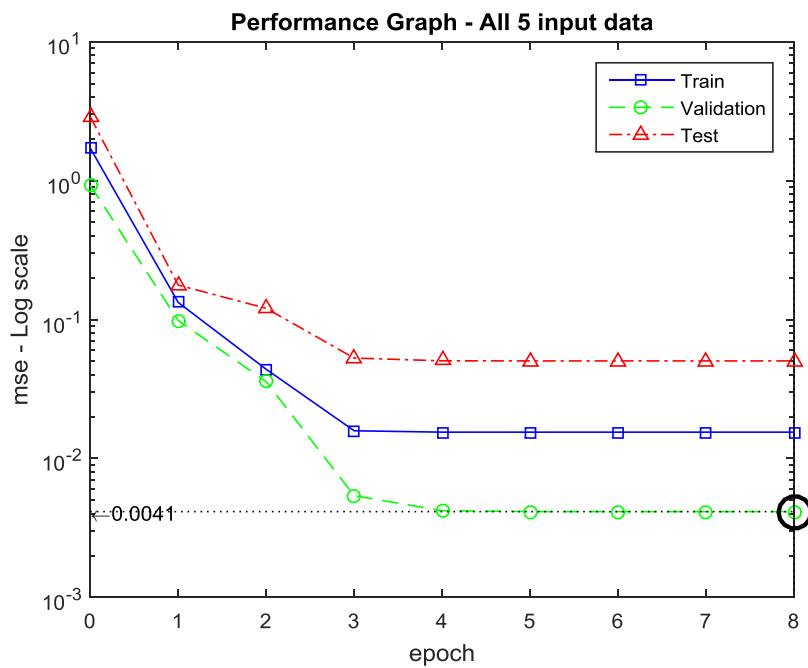


Figure E. 8. The performance graphs of the number of iterations

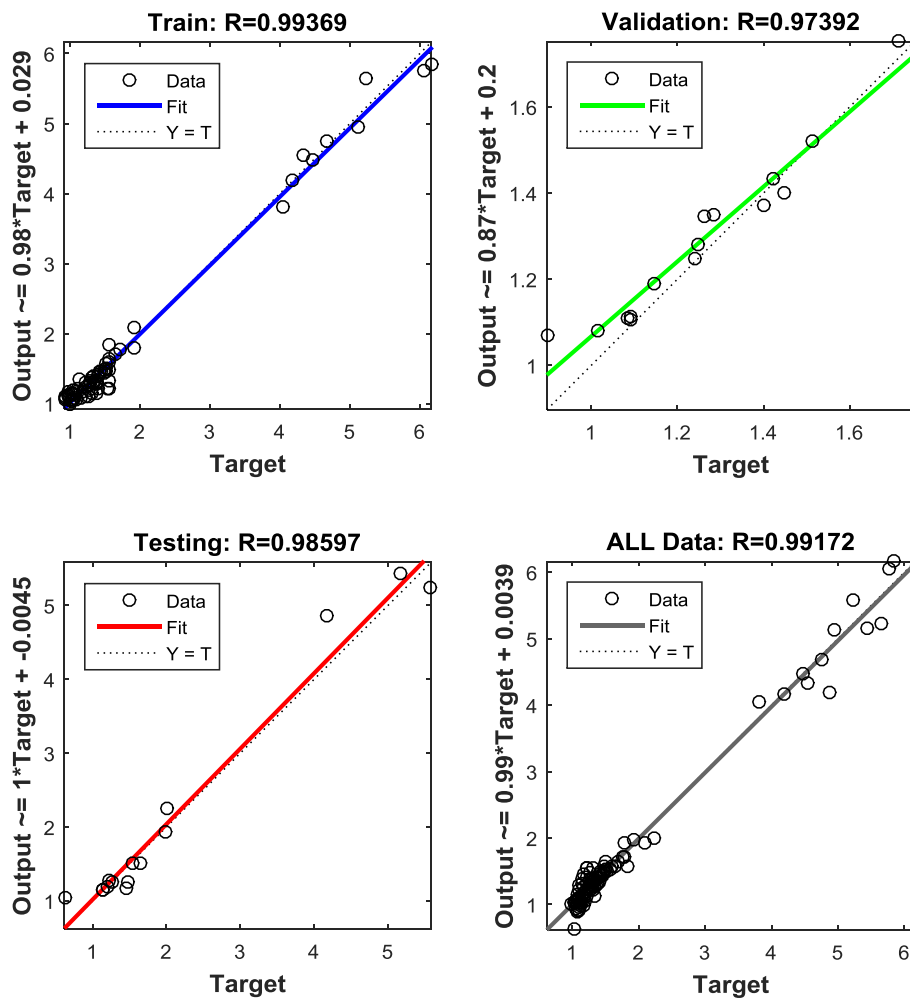


Figure E. 9 . A comparison between target values and outputs (e_{100}^*) - (Linear - Tangent sigmoid Transfer functions).

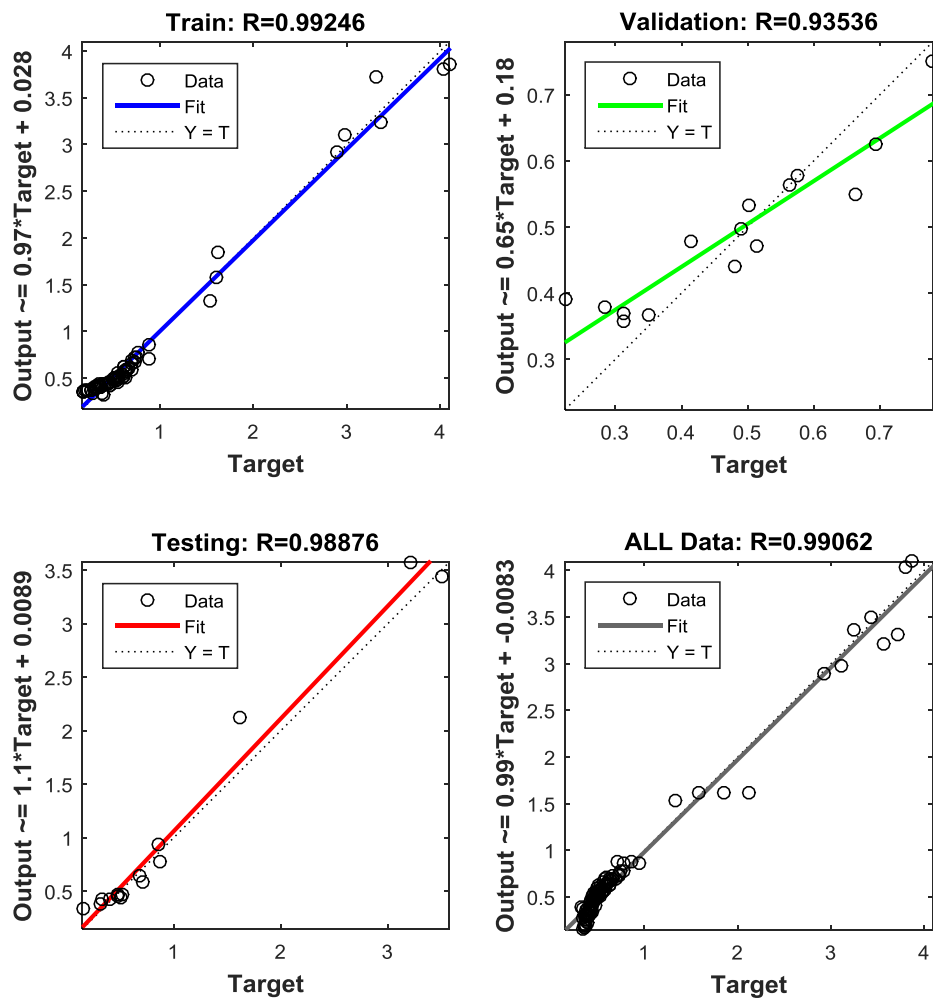


Figure E. 10 . A comparison between target values and outputs (C_c^*)- (Linear - Tangent sigmoid Transfer functions).

Appendix E - Artificial Neural Network Results

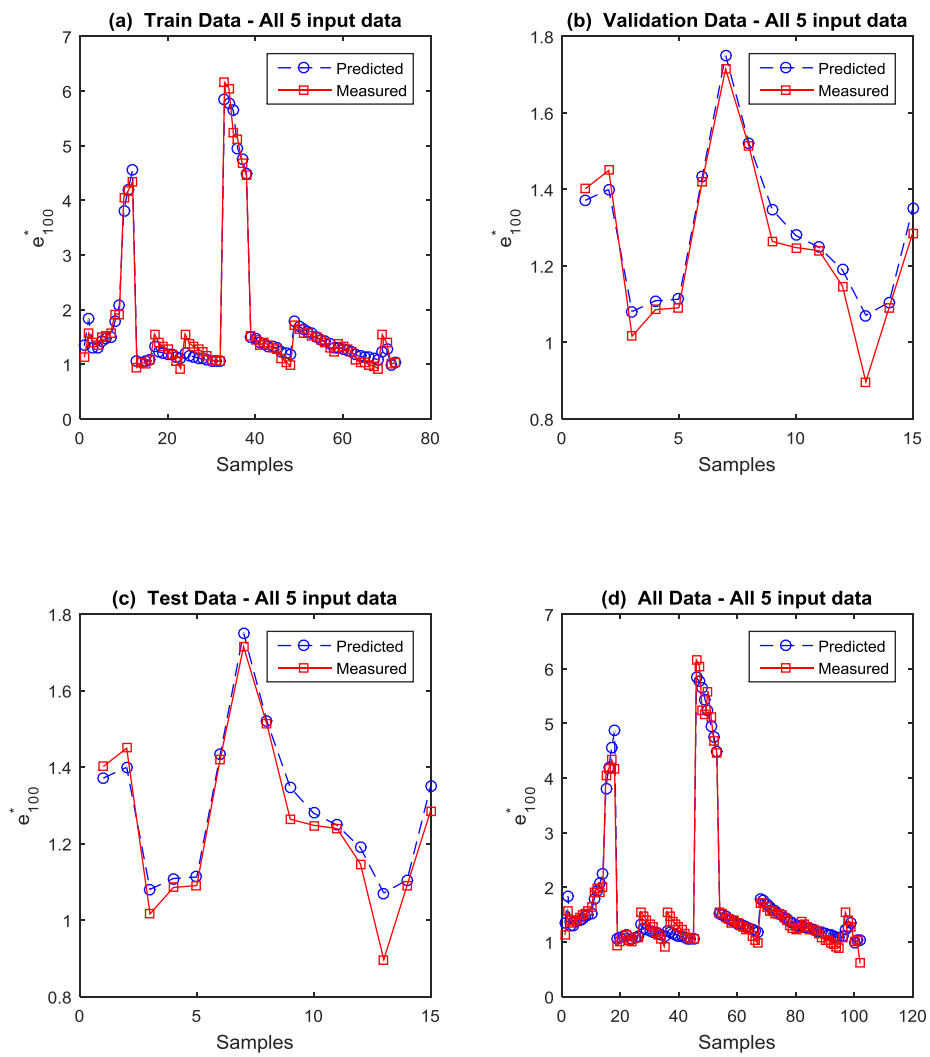


Figure E. 11 The simulation results for three steps of data processing and all data (e_{100}^*) - (Linear -Tangent sigmoid Transfer functions)..

Appendix E - Artificial Neural Network Results

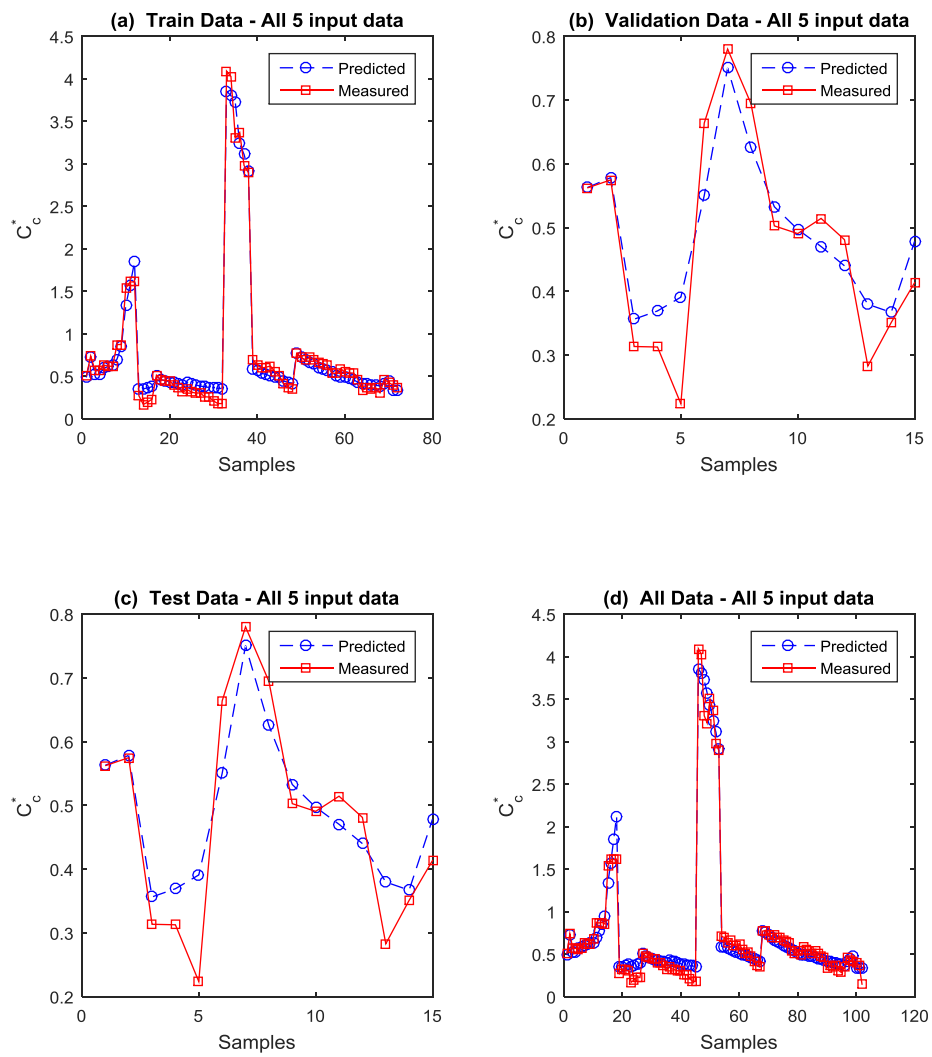


Figure E. 12 . The simulation results for three steps of data processing and all data (C_c^*) - (Linear -Tangent sigmoid Transfer functions).

Appendix E - Artificial Neural Network Results

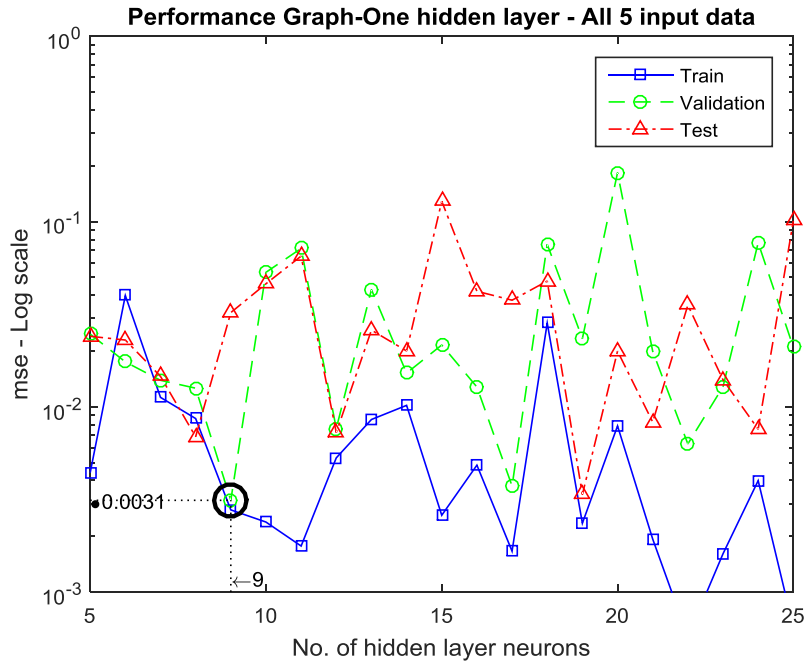


Figure E. 13 . The performance graphs of the number of neurons in the hidden layer (Tangent sigmoid - linear Transfer functions).

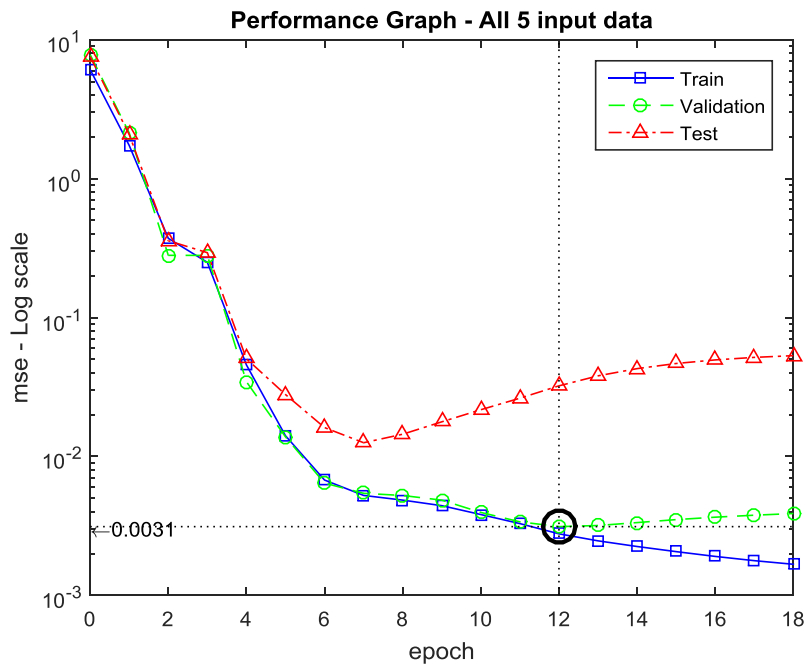


Figure E. 14. The performance graphs of the number of iterations

Appendix E - Artificial Neural Network Results

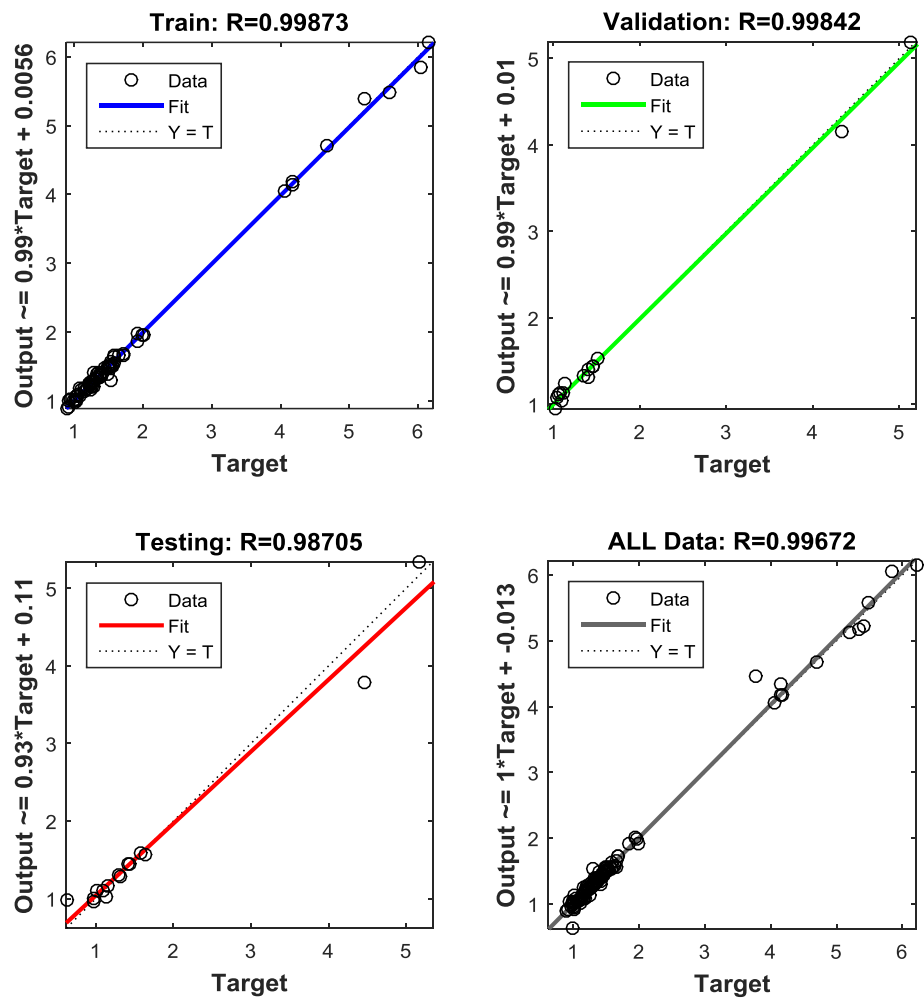


Figure E. 15 . A comparison between target values and outputs (e_{100}^*) - (Tangent sigmoid - linear Transfer functions).

Appendix E - Artificial Neural Network Results

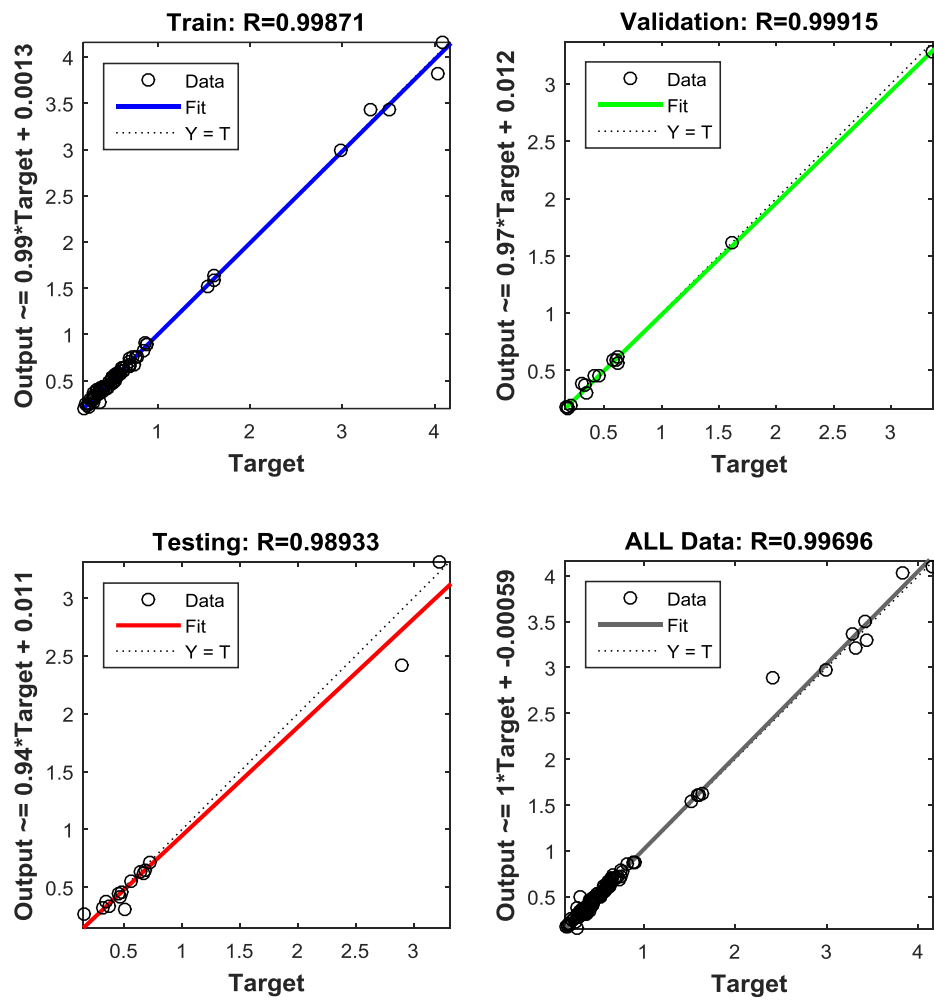


Figure E. 16 . A comparison between target values and outputs (C_c^*)- (Tangent sigmoid - linear Transfer functions).

Appendix E - Artificial Neural Network Results

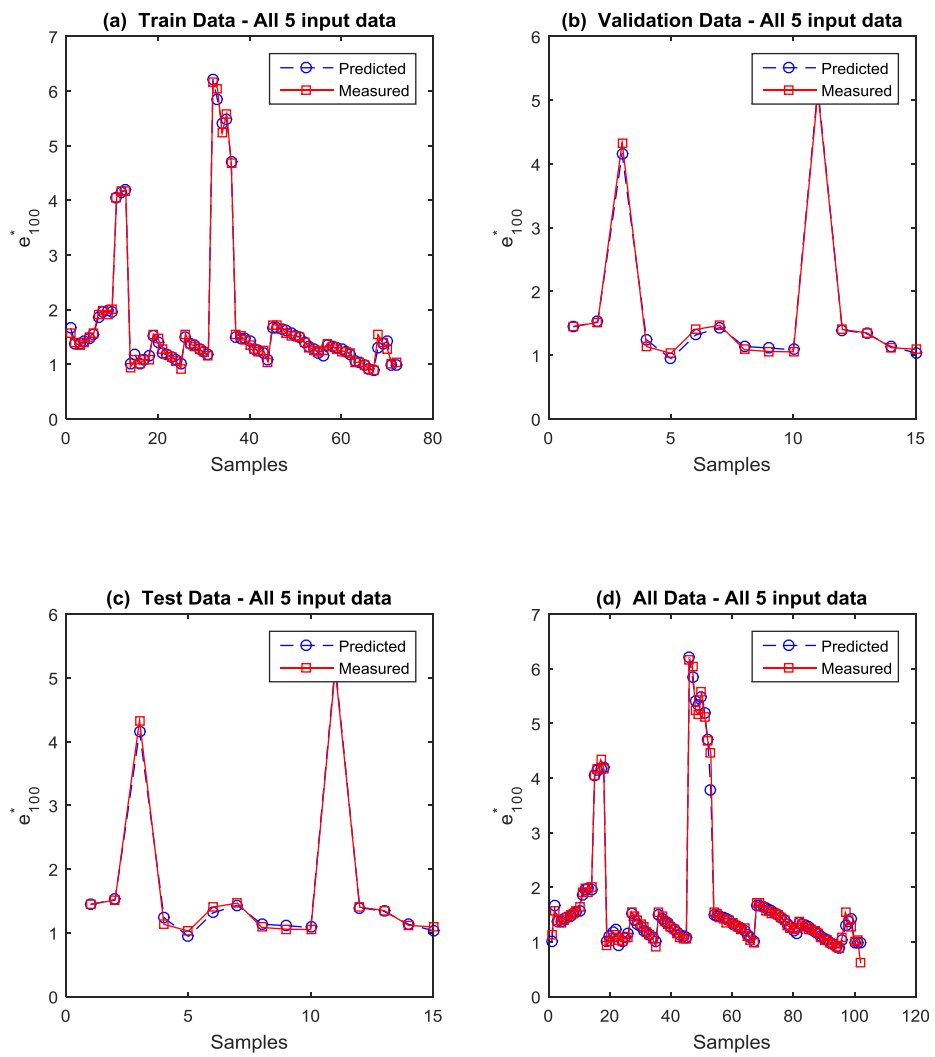


Figure E. 17 The simulation results for three steps of data processing and all data (e_{100}^*) - (Tangent sigmoid - linear Transfer functions)..

Appendix E - Artificial Neural Network Results

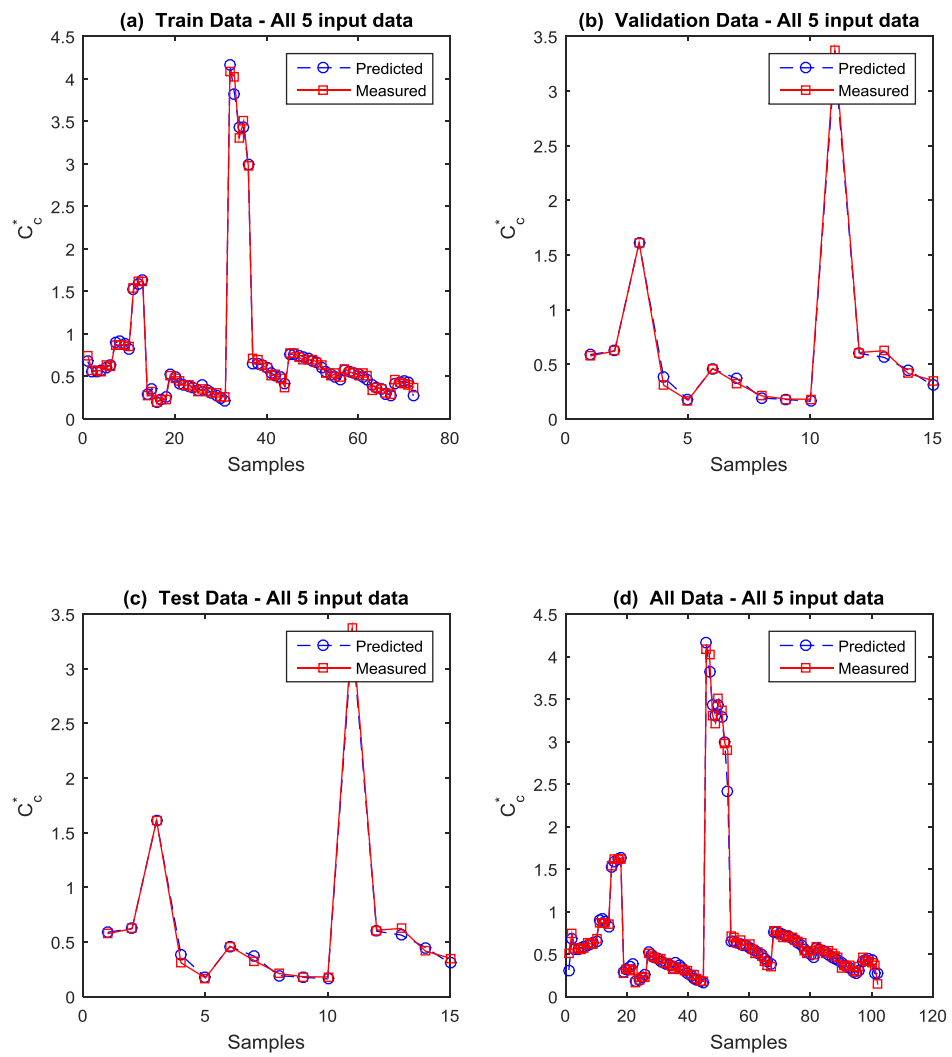


Figure E. 18 . The simulation results for three steps of data processing and all data (C_c^*) - (Tangent sigmoid - linear Transfer functions).

Appendix E - Artificial Neural Network Results

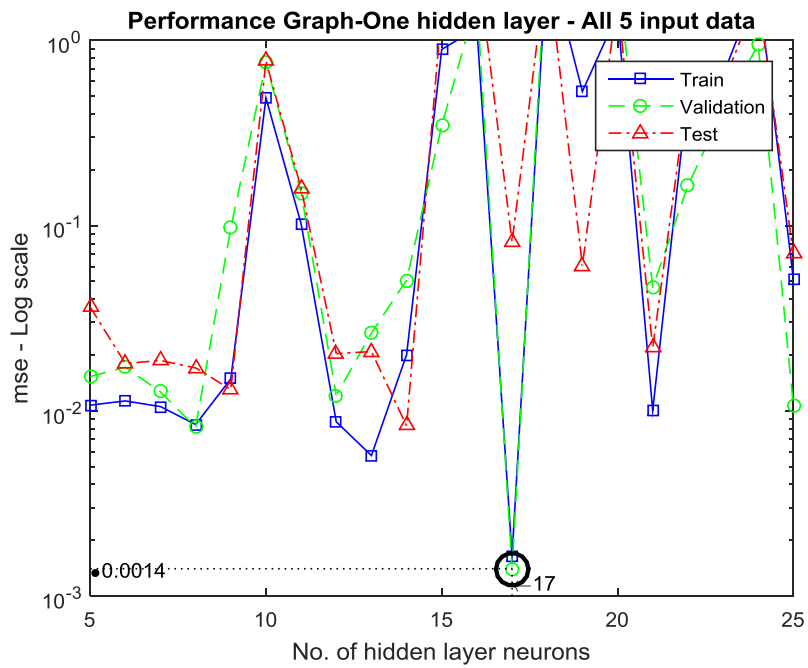


Figure E. 19 . The performance graphs of the number of neurons in the hidden layer (Tangent sigmoid - Tangent sigmoid Transfer functions).

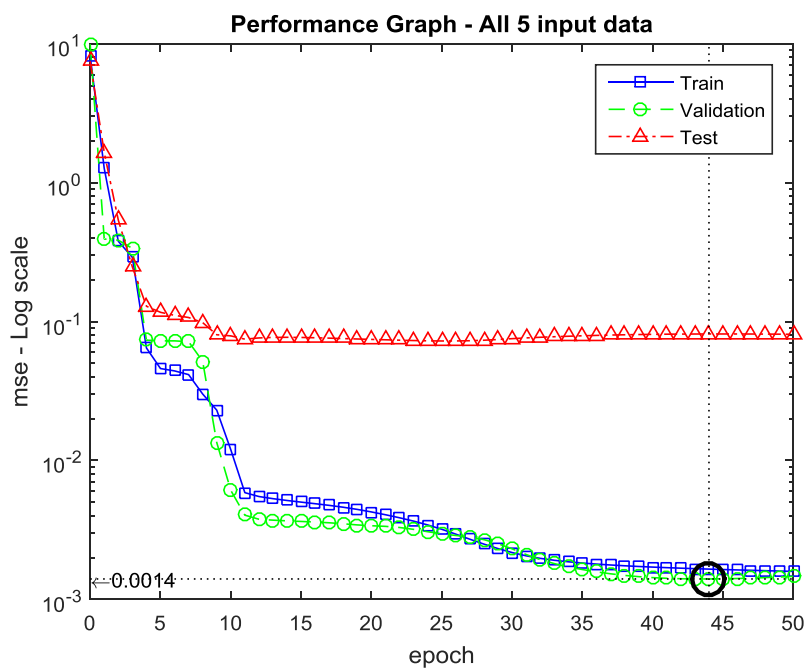


Figure E. 20. The performance graphs of the number of iterations

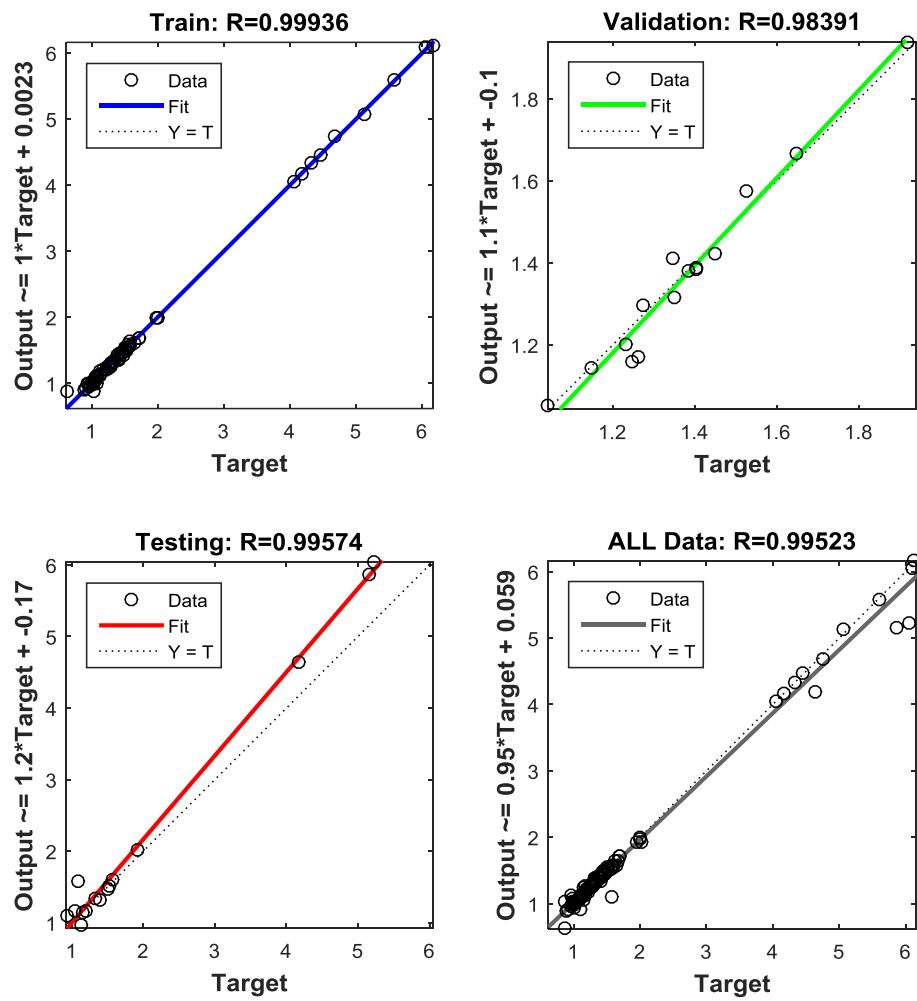


Figure E. 21 . A comparison between target values and outputs (e_{100}^*) - (Tangent sigmoid -Tangent sigmoid Transfer functions).

Appendix E - Artificial Neural Network Results

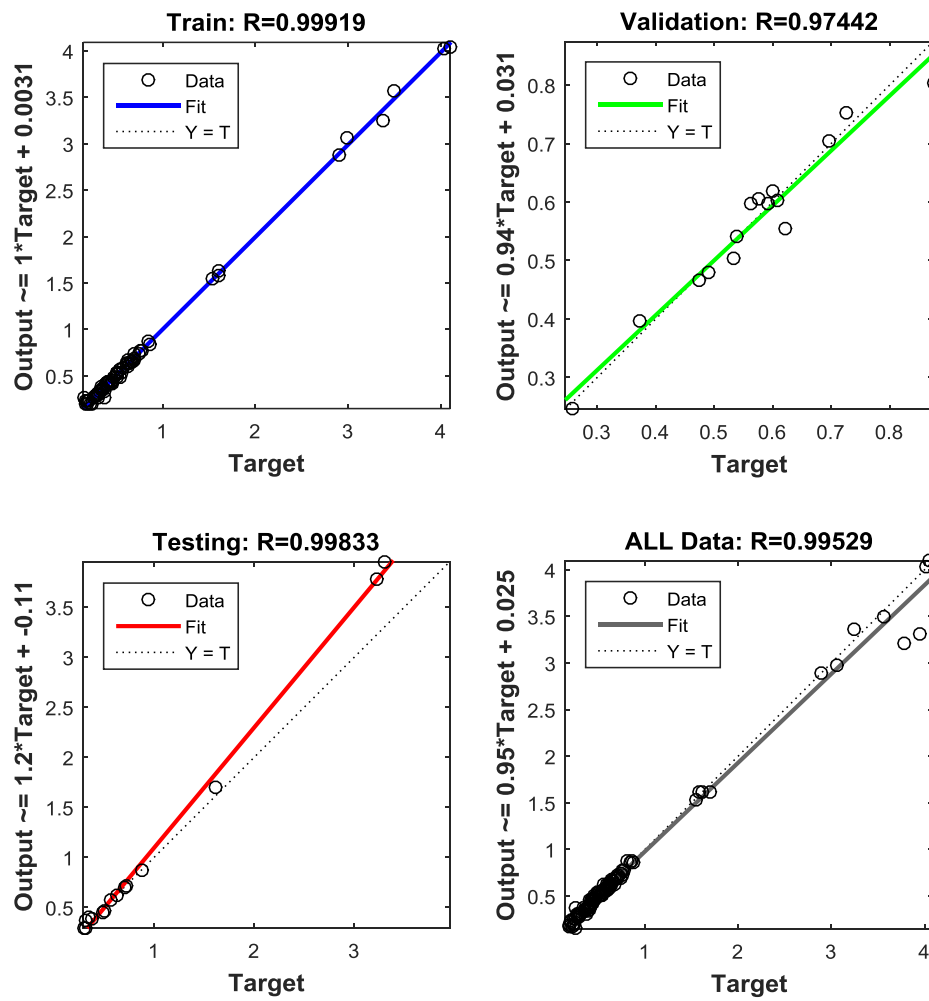


Figure E. 22 . A comparison between target values and outputs (C_c^*)- (Tangent sigmoid -Tangent sigmoid Transfer functions).

Appendix E - Artificial Neural Network Results

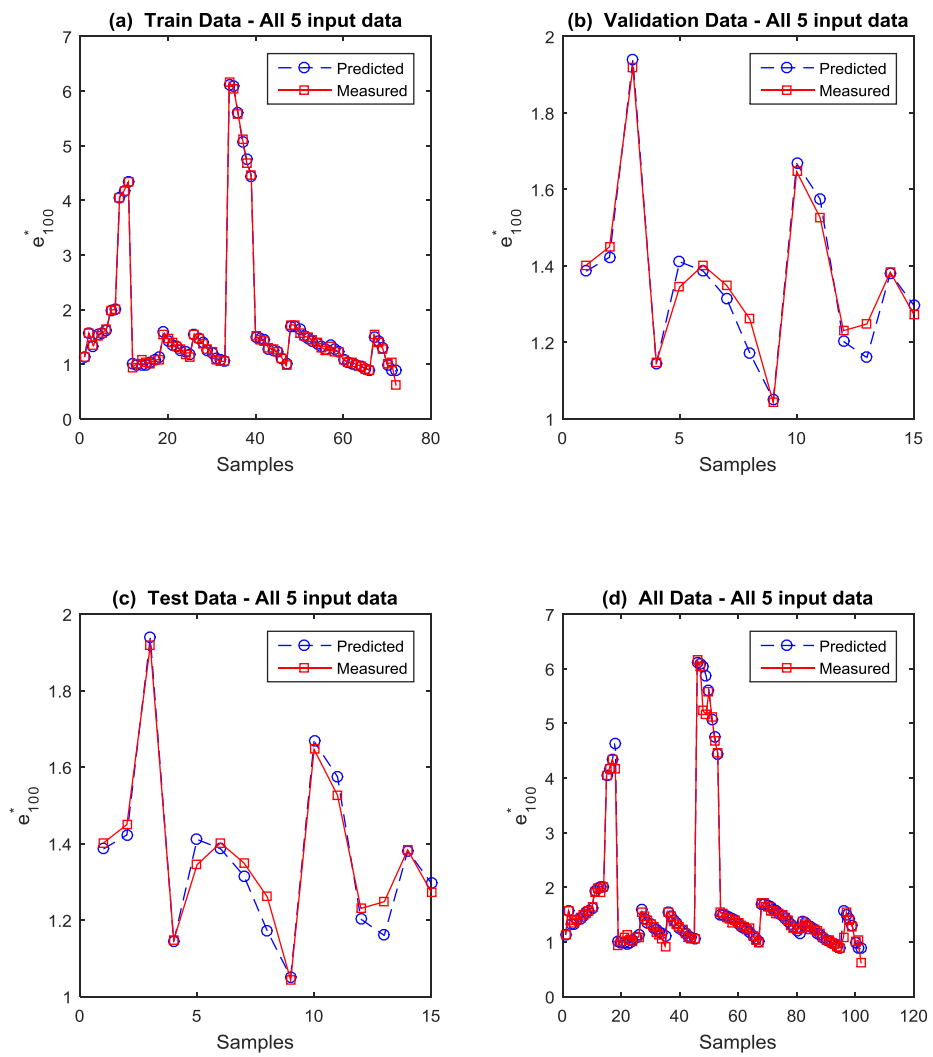


Figure E. 23 The simulation results for three steps of data processing and all data (e_{100}^*) - (Tangent sigmoid -Tangent sigmoid Transfer functions)..

Appendix E - Artificial Neural Network Results

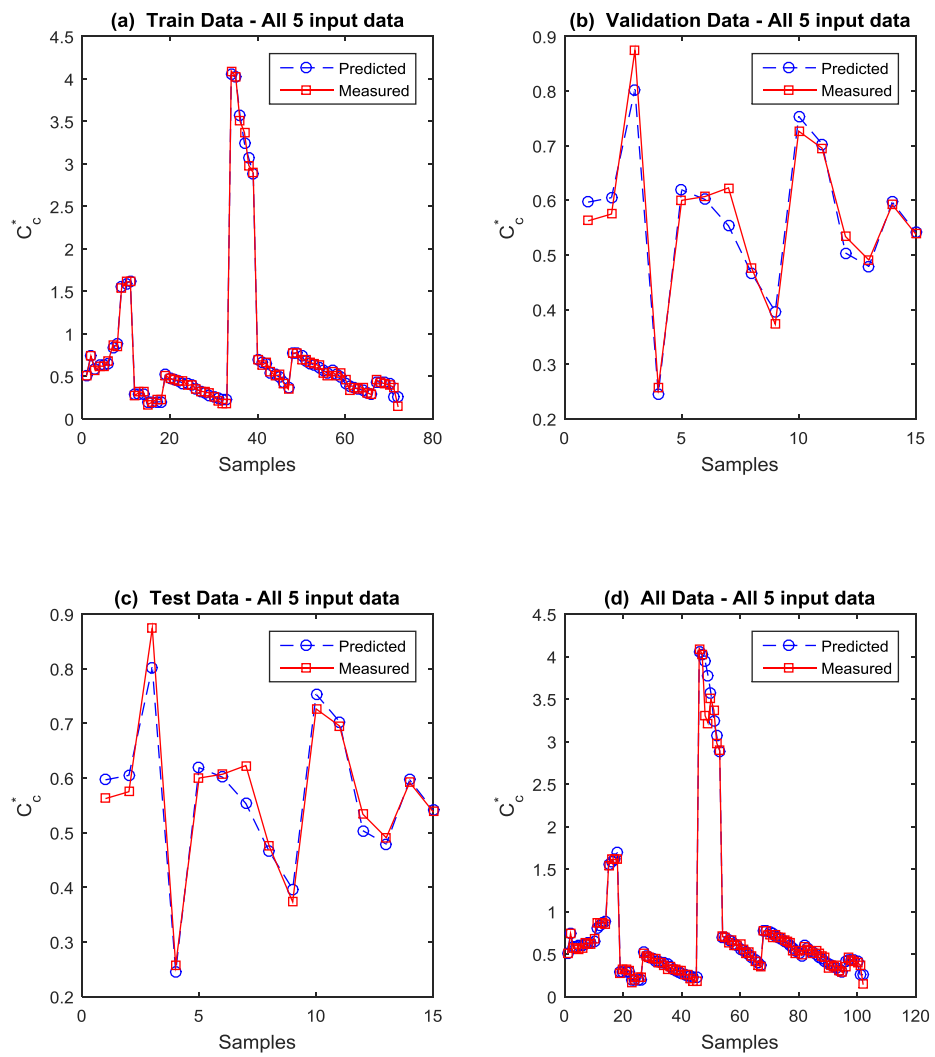


Figure E. 24 . The simulation results for three steps of data processing and all data (C_c^*) - (Tangent sigmoid -Tangent sigmoid Transfer functions).

Appendix E - Artificial Neural Network Results

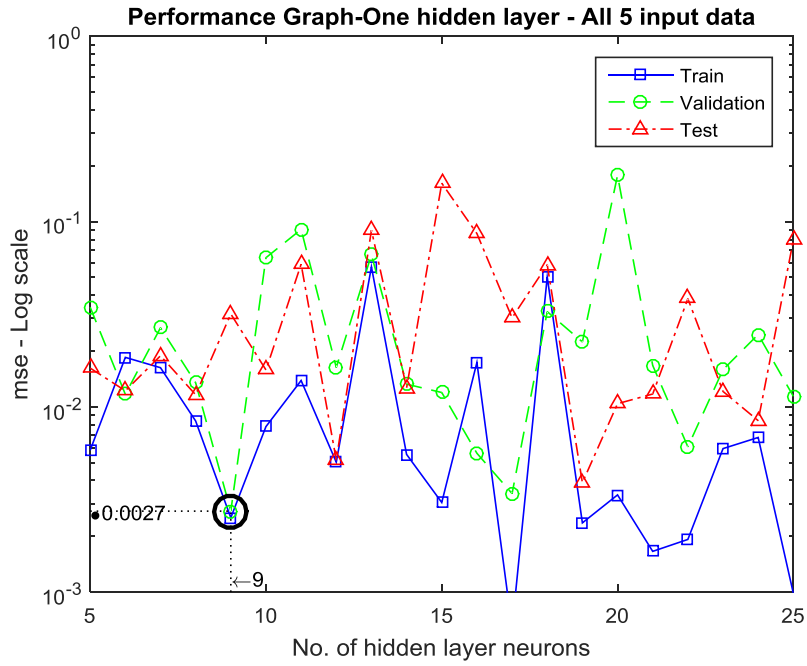


Figure E. 25 . The performance graphs of the number of neurons in the hidden layer (log-sigmoid-linear Transfer functions).

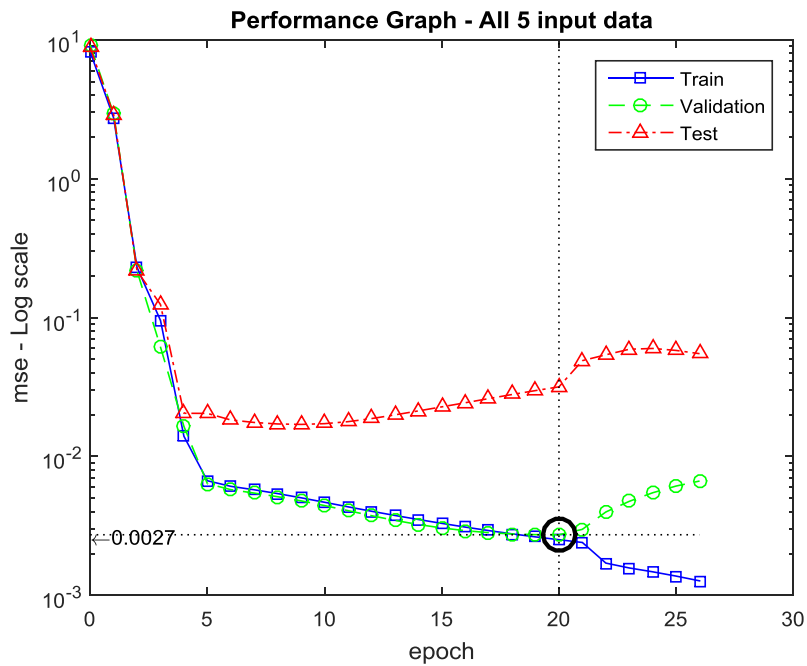


Figure E. 26. The performance graphs of the number of iterations

Appendix E - Artificial Neural Network Results

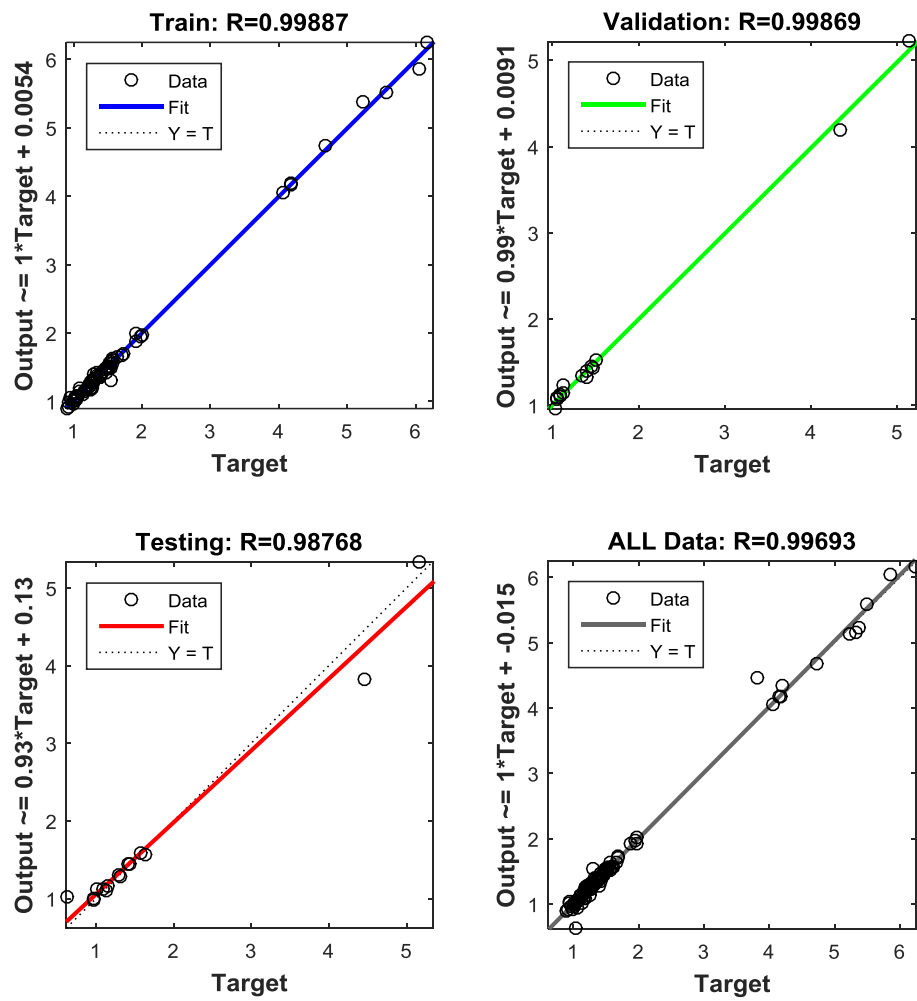


Figure E. 27 . A comparison between target values and outputs (e_{100}^*) - (log-sigmoid-linear Transfer functions).

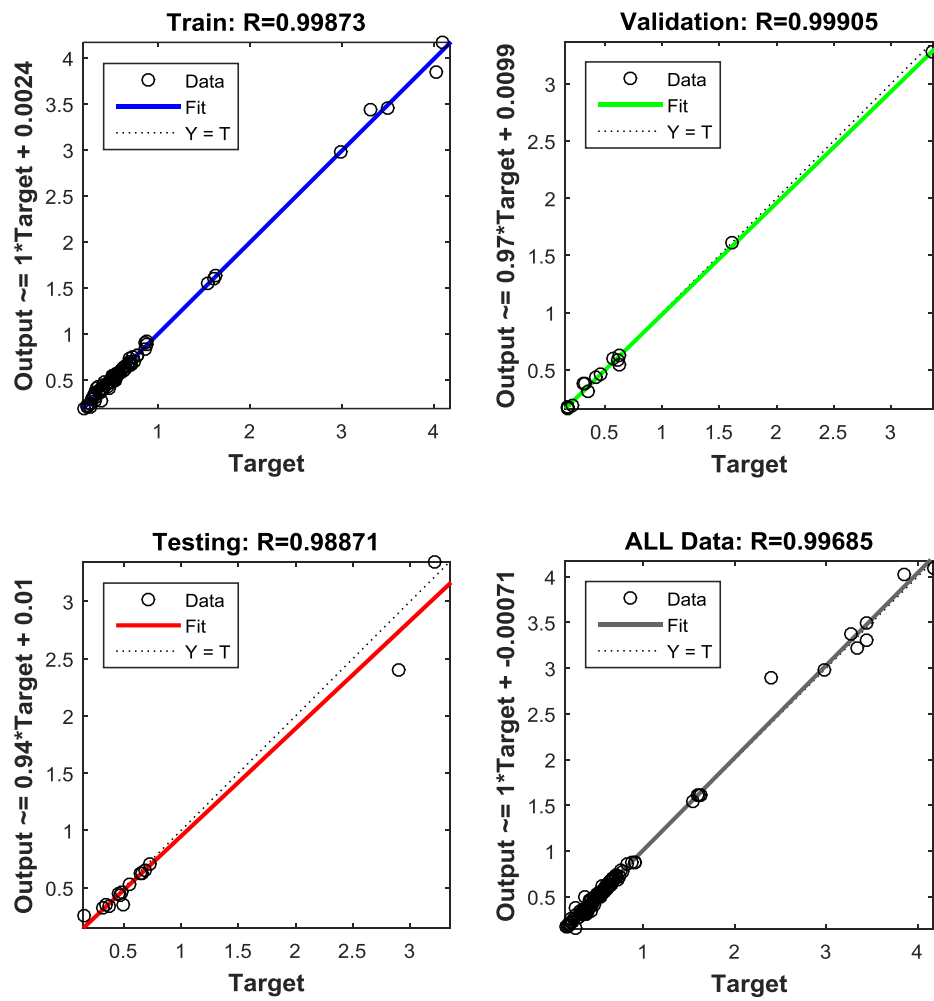


Figure E. 28 . A comparison between target values and outputs (C_c^*)- (log-sigmoid-linear Transfer functions).

Appendix E - Artificial Neural Network Results

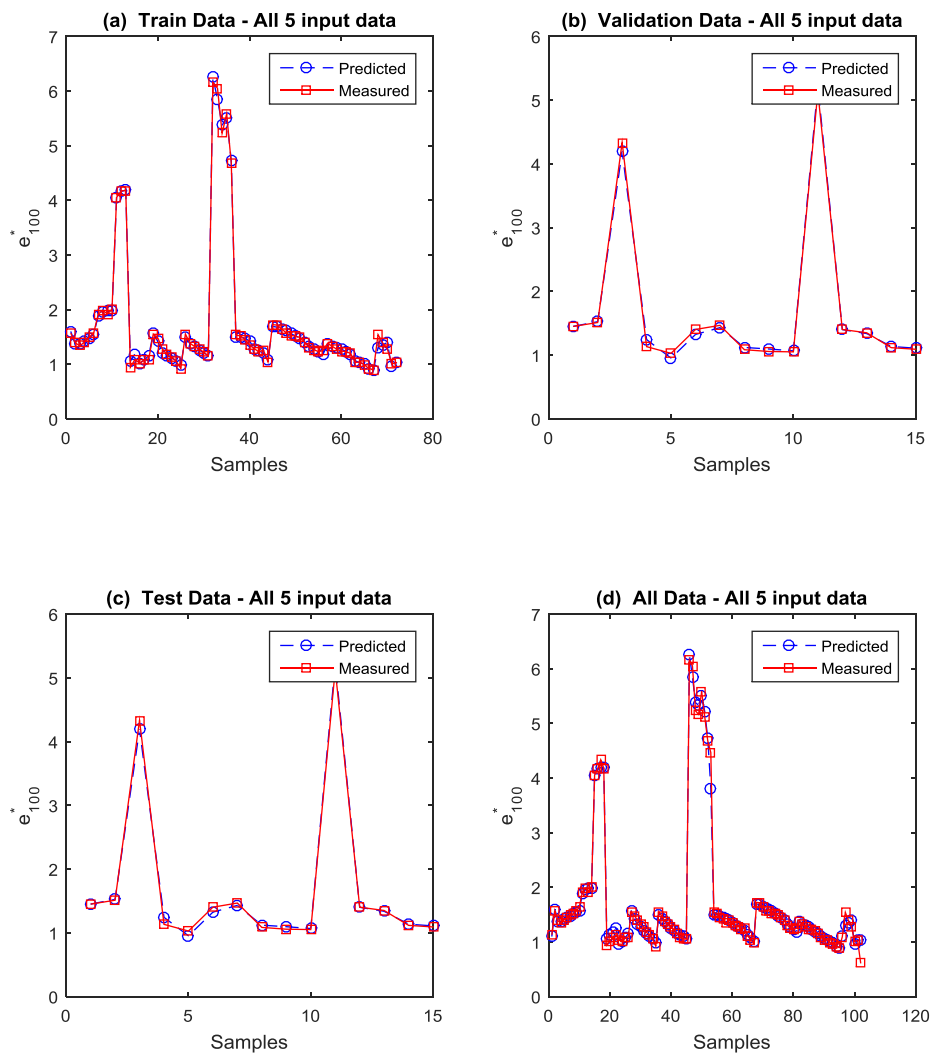


Figure E. 29 The simulation results for three steps of data processing and all data (e_{100}^*) - (log-sigmoid-linear Transfer functions)..

Appendix E - Artificial Neural Network Results

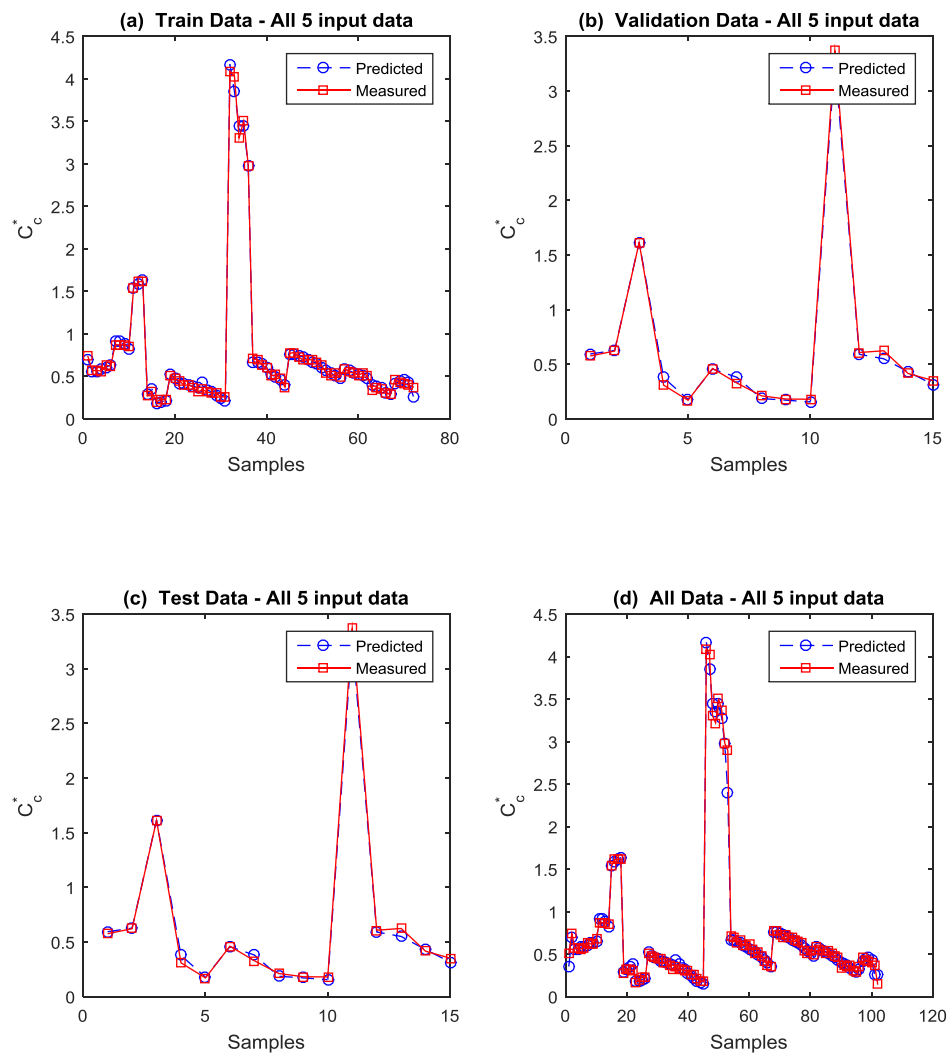


Figure E. 30 . The simulation results for three steps of data processing and all data (C_c^*) - (log-sigmoid-linear Transfer functions).

Appendix E - Artificial Neural Network Results

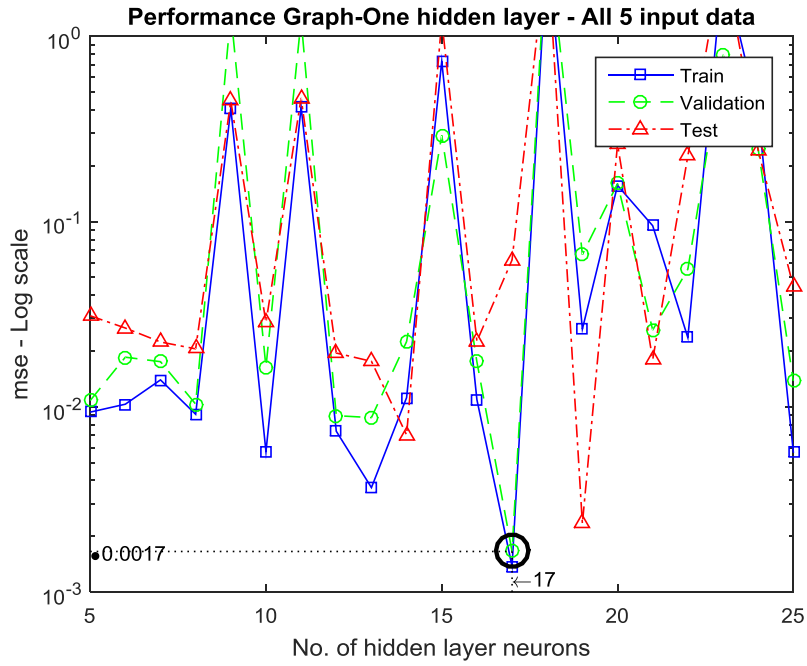


Figure E. 31 . The performance graphs of the number of neurons in the hidden layer (log-sigmoid-Tangent sigmoid Transfer functions).

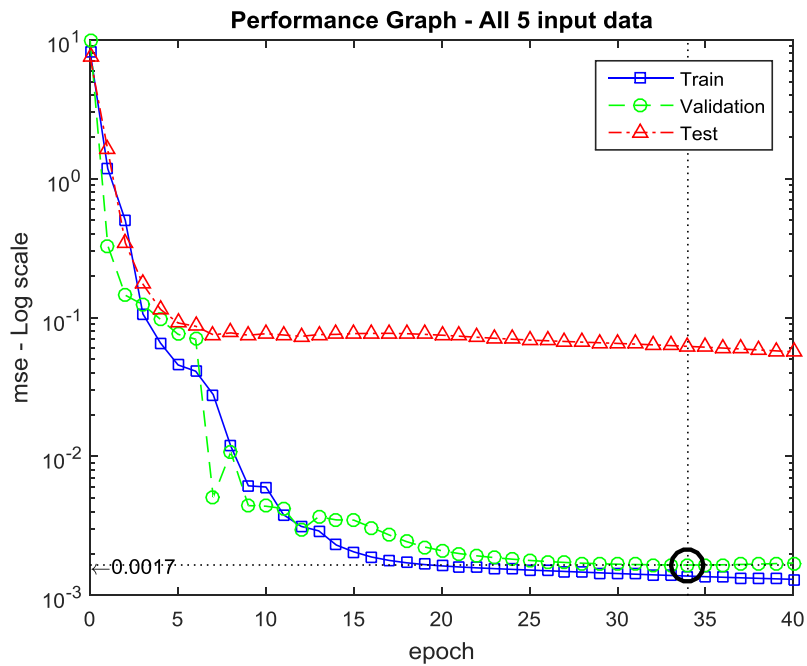


Figure E. 32. The performance graphs of the number of iterations

Appendix E - Artificial Neural Network Results

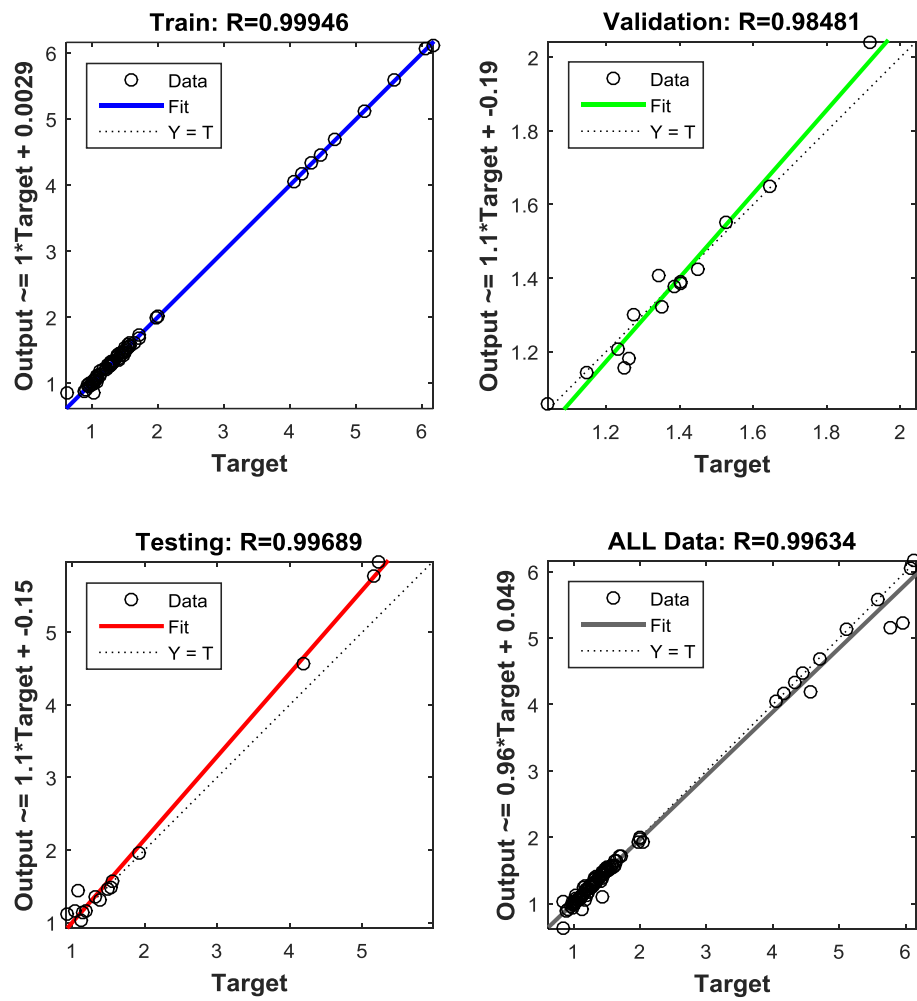


Figure E. 33 . A comparison between target values and outputs (e_{100}^*) - (log-sigmoid-Tangent sigmoid Transfer functions).

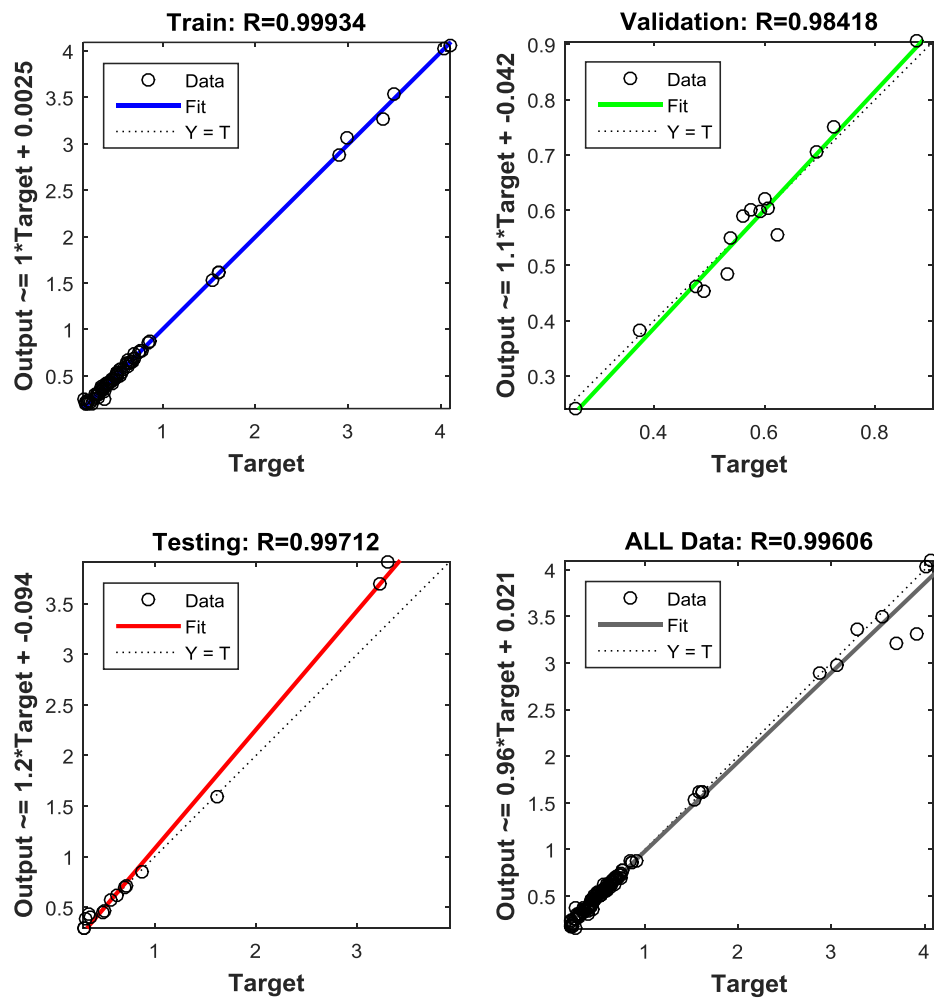


Figure E. 34 . A comparison between target values and outputs (C_c^*)- (log-sigmoid-Tangent sigmoid Transfer functions).

Appendix E - Artificial Neural Network Results

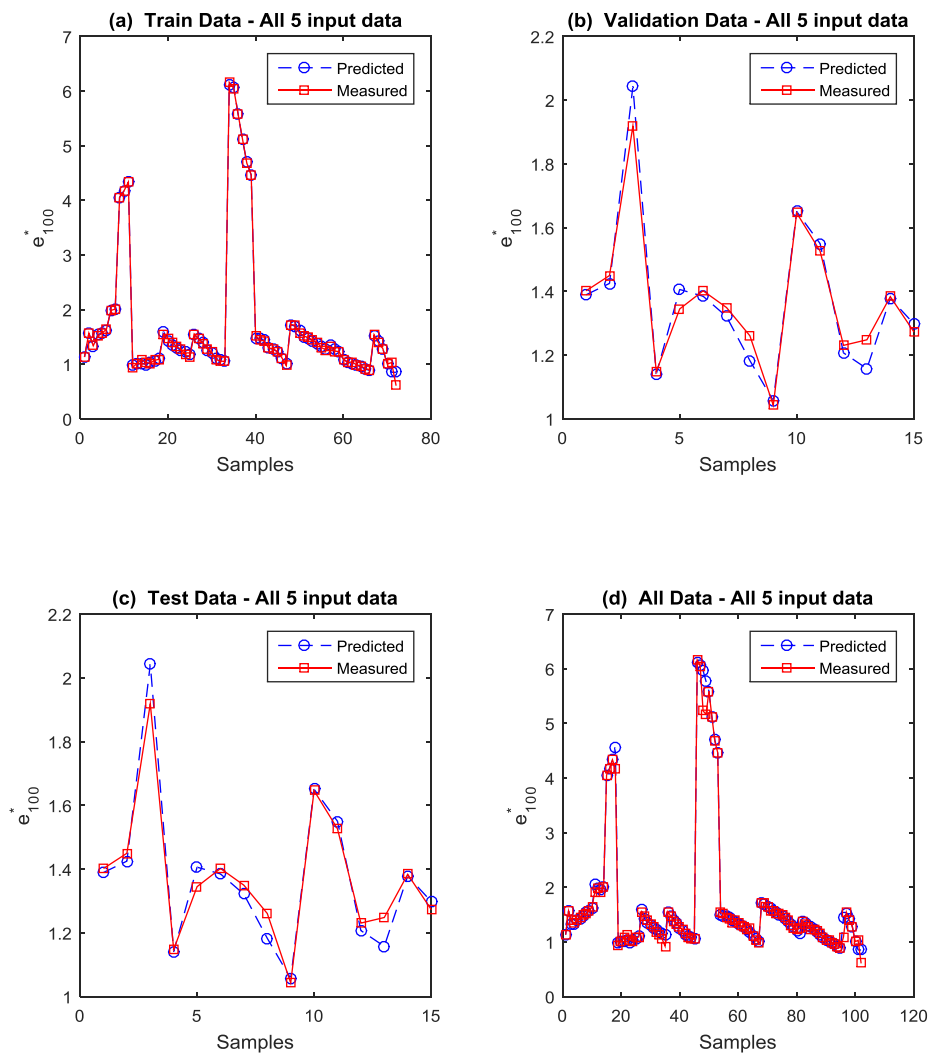


Figure E. 35 The simulation results for three steps of data processing and all data (e_{100}^*) - (log-sigmoid- Tangent sigmoid Transfer functions)..

Appendix E - Artificial Neural Network Results

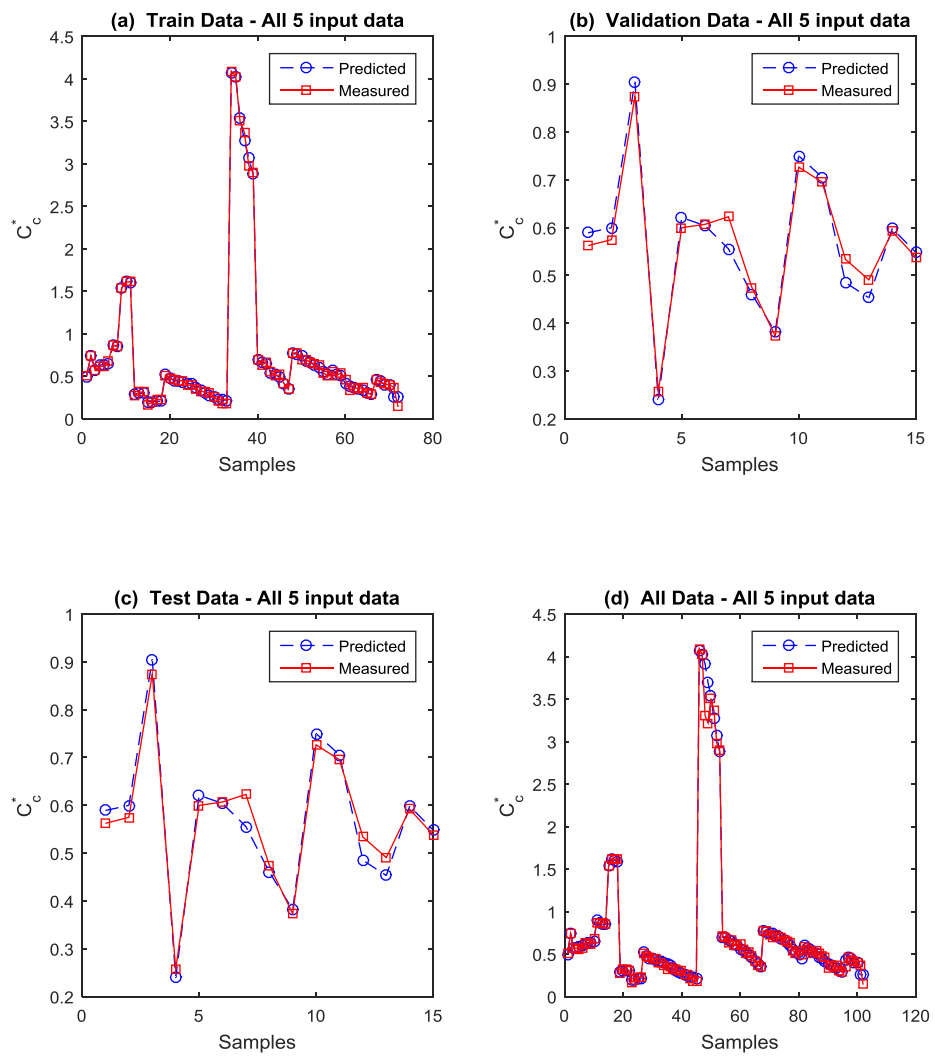


Figure E. 36 . The simulation results for three steps of data processing and all data (C_c^*) - (log-sigmoid -Tangent sigmoid Transfer functions).

Appendix F Artificial Neural Network Matlab Codes

```

%%
=====
% Determination of intrinsic parameters e*100 and C*c: ANN approach
% Artificial Neural Network (ANN)
% last version 6: Updated Date 19/12/2016
%
% v.7: set rng to default if a new net is developing
% v.67: Different TFN1, TFN2 & write fig in a DATE folder
% v.52: Summerize the perf. in one sheet & the possibility of TFN
change
% v.5: Statistics of studied data
% v.4: Excl. each input to see the sensitivity of the nwk to them
% v.3: Add do-loop to find the optimum no. of hidden layer neurons
% v.2: Two-output nwk (e100,Cc)
% v.1: One-output nwk (e100)
% Excluding one parameter (i.e. 4 input parameters)
%
=====
% 102 samples from literature used in this study
%
% Two-output network
% 1st target : simulation of e*100
% 2nd target : simulation of C*c
%
%
% Read data from xls file in the path using function of ANN_inp
% Path: C:\Users\17441722\Documents\My PhD\My papers\ANN\xls'
% filename: ANN-01.xlsx
%
% input to this file:
% i - input data.
% t_e100 - target data of 1st ANN.
% t_Cc - target data of 2nd ANN.

% General Definition:
% Target = Measured = Observed
% Output = simulated = predicted

% variables definition:
%
% t:      targets (1*102)
% e:      error (t-y1)
% x:      input all data (5*102)
% y:      Output all data (1*102)
% trOut:  output trained data
% vOut:   output validation
% tsOut:  Output test data
% trTarg: Target trained data
% vTarg:  Target Validation data
% tsTarg: Target test data
% n_all:  vector to the size of No. of all data
% n_tr:   vector to the size of No. of trained data
% n_ts:   vector to the size of No. of test data
% n_v:    vector to the size of No. of validation data

% trainFcn: training function
% hiddenLayerSize: Hidden layer neruon size
close ALL;clear; clc;
PLOT=true; %change to true if plot req'd
path_out='C:\Users\17441722\Documents\My PhD\My papers\ANN';

```

Appendix F - Artificial Neural Network Matlab Codes

```
cd(path_out);
stat_out='stat_out.xlsx'; %output for table of statistics

Result_folder=date;
mkdir(Result_folder)
path_out=fullfile(path_out,Result_folder);

cd(path_out);

% c2_n=0; % no. of input data put it 0 if Excl is not neccessary
% str_exc='N'; % Do you want to run Excl. procedure?

prompt = 'Exclude data? [N]: ';
str_exc = input(prompt,'s');
if isempty(str_exc)
    c2_n=0;
    str_exc='N';
else
    c2_n=5;
    str_exc='Y';
end

%% Solve an Input-Output Fitting problem with a Neural Network

for c5=1:3 %TFN1

    switch c5
        case 1
            TFN1='purelin';
        case 2
            TFN1='tansig';
        case 3
            TFN1='logsig'
    end

    for c6=1:3 %TFN2

        switch c6
            case 1
                TFN2='purelin';
            case 2
                TFN2='tansig';
            case 3
                TFN2='logsig'
        end

        filename=strcat('wb_',TFN1,'_',TFN2,'.xlsx'); %output file name which
        is stored in xls folder
        filename_out=fullfile(path_out,filename);

        for c2=0:c2_n % Excluding one input in each iteration

            % 1: Excl. w0
            % 2: Excl. Gs
            % 3: Excl. wL
            % 4: Excl. wP
            % 5: Excl. CLM
            % 0: For all 5 data
```


Appendix F - Artificial Neural Network Matlab Codes

```

switch c2
    case 0
        x_bar={'w_0';'G_s';'w_L';'w_P';'CLM'};
        str_title=' - All 5 input data';
    case 1
        x_bar={'G_s';'w_L';'w_P';'CLM'};
        str_title=' - Excluding w_0';
    case 2
        x_bar={'w_0';'w_L';'w_P';'CLM'};
        str_title=' - Excluding G_s';
    case 3
        x_bar={'w_0';'G_s';'w_P';'CLM'};
        str_title=' - Excluding w_L';
    case 4
        x_bar={'w_0';'G_s';'w_L';'CLM'};
        str_title=' - Excluding w_P';
    case 5
        x_bar={'w_0';'G_s';'w_L';'w_P'};
        str_title=' - Excluding CLM';
end

% This script assumes these variables are defined by input func.:
%

[i, t_e100, t_Cc] = ANN_inp03(c2);

x = i'; % order of input data: Matrix rows
t = [t_e100,t_Cc]' ; % 2 targets

if and(and(c2==0,c5==1),c6==1) % Data statistics calculation!!!

    stat_out=fullfile(path_out,stat_out);
    sheet = 1;
    l_s={'w_0','G_s','w_L','w_P','e*100','C*c'};

    xlRange = 'B1';
    xlswrite(stat_out,l_s,sheet,xlRange); %input titles

    xlRange = 'A2';
    l_s={'Min. ','Max. ','Mean','Median','Mode','Stand. Dev.'};
    xlswrite(stat_out,l_s,sheet,xlRange); %input titles

    % Ordinal input parameters
    for c3=1:4
        switch c3
            case 1
                xlRange = 'B2';
            case 2
                xlRange = 'C2';
            case 3
                xlRange = 'D2';
            case 4
                xlRange = 'E2';
        end

        PPP=ANN_stat(i(:,c3));
        xlswrite(stat_out,PPP,sheet,xlRange); %input titles

```

Appendix F - Artificial Neural Network Matlab Codes

```

end
% Output variables
for c3=1:2
    switch c3
        case 1
            xlRange = 'F2';
        case 2
            xlRange = 'G2';
        end
        PPP=ANN_stat(t(:,c3)');
    xlswrite(stat_out,PPP,sheet,xlRange); %input titles
end

end

% Create a Fitting Network with different neuron size of hidden layer
c1=1;
for hiddenLayerSize=5:25

rng default;

% Choose a Training Function
% For a list of all training functions type: help nntrain
% 'trainlm' is usually fastest.
% 'trainbr' takes longer but may be better for challenging problems.
% 'trainscg' uses less memory. Suitable in low memory situations.
trainFcn = 'trainlm'; % Levenberg-Marquardt backpropagation.

net = fitnet(hiddenLayerSize,trainFcn);

% Choose Input and Output Pre/Post-Processing Functions
% For a list of all processing functions type: help nnprocess
net.input.processFcns = {'removeconstantrows','mapminmax'};
net.output.processFcns = {'removeconstantrows','mapminmax'};

% Setup Division of Data for Training, Validation, Testing
% For a list of all data division functions type: help nndivide
net.divideFcn = 'dividerand'; % Divide data randomly
net.divideMode = 'sample'; % Divide up every sample
net.divideParam.trainRatio = 70/100;
net.divideParam.valRatio = 15/100;
net.divideParam.testRatio = 15/100;

%Choose Transfer functions from : tansig/logsig/purelin
% Before train command & after fitnet command
net.layers{1}.transferFcn = TFN1; % hidden layer TFN
net.layers{2}.transferFcn = TFN2; % output TFN

% Choose a Performance Function
% For a list of all performance functions type: help nnperformance
net.performFcn = 'mse'; % Mean Squared Error

% Choose Plot Functions
% For a list of all plot functions type: help nnplot
net.plotFcns = {'plotperform','plottrainstate','ploterrhist', ...
    'plotregression','plotfit'};

```

Appendix F - Artificial Neural Network Matlab Codes

```

% Train the Network
[net,tr] = train(net,x,t); % tr is training record epoch and perf

% Test the Network
y = net(x);
e_xls = gsubtract(t,y);
performance = perform(net,t,y)

%% Performance array of net
perf_array(c1,1)=hiddenLayerSize;
perf_array(c1,2)=tr.best_perf %train data min performance
perf_array(c1,3)=tr.best_vperf; %Validation data min performance
perf_array(c1,4)=tr.best_tperf %test data min performance
c1=c1+1

end
[max_perf,I_perf]= min(perf_array);

% plot graph for best performance for No of hidden layer and
% only for "ALL DATA" condition (5 inputs)c2==0
if and(c2==0,PLOT) % plot of mse vs no. of neurons of Hidden layer

figure

semilogy(perf_array(:,1),perf_array(:,2),'b-s',...
         perf_array(:,1),perf_array(:,3),'g--o',...
         perf_array(:,1),perf_array(:,4),'r-.^')

title(strcat('Performance Graph-One hidden layer',str_title))
xlabel('No. of hidden layer neurons')
ylabel('mse - Log scale')
legend('Train','Validation','Test','Location','northeast')
% Add a circle at best performance of validation to graph:
hold on;

min_x=perf_array(1,1);
max_x=perf_array(end,1);
axis([min_x max_x .001 1]);
plot(perf_array(I_perf(3)),max_perf(3),'ko',...
      'LineWidth',2,...
      'MarkerSize',15)
% Add refrence line
line([perf_array(I_perf(3))
perf_array(I_perf(3))],[.001,max_perf(3)],...
      'Color','black','LineStyle',':');
line([perf_array(1,1)
perf_array(I_perf(3))],[max_perf(3),max_perf(3)],...
      'Color','black','LineStyle',':');
% Add texts
str=strcat('\leftarrow',num2str(perf_array(I_perf(3))));
text(perf_array(I_perf(3)),0.0012,str,'HorizontalAlignment','left');
str=strcat('\bullet',num2str(round(max_perf(3),4)));
text(min_x,max_perf(3),str,'HorizontalAlignment','left');
saveas(gcf,strcat(int2str(get(gcf,'Number')),'_',TFN1,'_',TFN2,'HLNo
',int2str(perf_array(I_perf(3))),str_title,'.fig'));
end

%% Final network:

```

Appendix F - Artificial Neural Network Matlab Codes

```
% no. of hidden layer-neurons for best performance of validation data
rng default;
hiddenLayerSize=perf_array(I_perf(3));

net = fitnet(hiddenLayerSize,trainFcn);

% Choose Input and Output Pre/Post-Processing Functions
% For a list of all processing functions type: help nprocess
net.input.processFcns = {'removeconstantrows','mapminmax'};
net.output.processFcns = {'removeconstantrows','mapminmax'};

% Setup Division of Data for Training, Validation, Testing
% For a list of all data division functions type: help nndivide
net.divideFcn = 'dividerand'; % Divide data randomly
net.divideMode = 'sample'; % Divide up every sample
net.divideParam.trainRatio = 70/100;
net.divideParam.valRatio = 15/100;
net.divideParam.testRatio = 15/100;

%Choose Transfer functions from : tansig/logsig/purelin
% Before train & after fitnet
net.layers{1}.transferFcn = TFN1; % hidden layer TFN
net.layers{2}.transferFcn = TFN2; % output TFN

% Choose a Performance Function
% For a list of all performance functions type: help nnperformance
net.performFcn = 'mse'; % Mean Squared Error

% Choose Plot Functions
% For a list of all plot functions type: help nnplot
net.plotFcns = {'plotperform','plottrainstate','ploterrhist', ...
    'plotregression','plotfit'};

% Train the Network
[net,tr] = train(net,x,t); % tr is training record epoch and perf

% Test the Network
y = net(x);
e_xls = gsubtract(t,y);
performance = perform(net,t,y)

% Extract train, validation and test data
trOut = y(:,tr.trainInd);
vOut = y(:,tr.valInd);
tsOut = y(:,tr.testInd);
trTarg = t(:,tr.trainInd);
vTarg = t(:,tr.valInd);
tsTarg = t(:,tr.testInd);

%% Weights and biases
wb = getwb(net);
[b,IW,LW] = separatewb(net,wb); %Separate biases and weight values
from weight/bias vector

%Input
sheet = c2+1;
```

Appendix F - Artificial Neural Network Matlab Codes

```

xlRange = 'A1';
xlswrite(filename_out,x_bar',sheet,xlRange); %input titles

xlRange = 'F1';
A={'Bias'};
xlswrite(filename_out,A,sheet,xlRange); %Biases title

xlRange = 'A2';
xlswrite(filename_out,IW{1,1},sheet,xlRange); %input weights

xlRange = 'F2';
xlswrite(filename_out,b{1,1},sheet,xlRange); %Biases values

%Output weights
A = {'e^*_100','C*_c'};
xlRange = 'H1';
xlswrite(filename_out,A,sheet,xlRange);

xlRange = 'H2';
xlswrite(filename_out,LW{2,1}',sheet,xlRange); %weights

%% Spearman's rank correlation coefficient
rho=corr(i, t', 'type', 'Spearman');

xlRange = 'K2';
xlswrite(filename_out,x_bar,sheet,xlRange);

xlRange = 'K1';
A = {'rho','e^*_100','C*_c'};
xlswrite(filename_out,A,sheet,xlRange);

xlRange = 'L2';
xlswrite(filename_out,rho,sheet,xlRange);
%% performance
xlRange = 'O1';
A = {'Data type';'Train';'Validation';'Test';'epoch';'No. Hidden
Layer neurons';'mse_Val_Optimized nwk';'TFN1';'TFN2'};
xlswrite(filename_out,A,sheet,xlRange);

xlRange = 'P1';
A = {'mse'};
xlswrite(filename_out,A,sheet,xlRange);

xlRange = 'P2';
A
[tr.best_perf;tr.best_vperf;tr.best_tperf;tr.best_epoch;perf_array(I
_perf(3));max_perf(3)];
xlswrite(filename_out,A,sheet,xlRange);

% xlswrite(filename_out,{TFN1},sheet,'P8');
% xlswrite(filename_out,{TFN2},sheet,'P9');

xlswrite(filename_out,{net.layers{1}.transferFcn},sheet,'P8');
xlswrite(filename_out,{net.layers{2}.transferFcn},sheet,'P9');

% Gather all performances of diff Excl. input in the last sheet(c2_n+2)
if str_exc=='Y'

```

Appendix F - Artificial Neural Network Matlab Codes

```

A = {'Data type';'Train';'Validation';'Test';'epoch'};
xlswrite(filename_out,A,c2_n+2,'A1');

switch c2
    case 0
        xrange_t1='B1';xrange_t2='B2';AT={'All data'};
    case 1
        xrange_t1='C1';xrange_t2='C2';AT={'Excl. w0'};
    case 2
        xrange_t1='D1';xrange_t2='D2';AT={'Excl. Gs'};
    case 3
        xrange_t1='E1';xrange_t2='E2';AT={'Excl. wL'};
    case 4
        xrange_t1='F1';xrange_t2='F2';AT={'Excl. wP'};
    case 5
        xrange_t1='G1';xrange_t2='G2';AT={'Excl. CLM'};
end

xlswrite(filename_out,AT,c2_n+2,xrange_t1);

A = [tr.best_perf;tr.best_vperf;tr.best_tperf;tr.best_epoch];
xlswrite(filename_out,A,c2_n+2,xrange_t2);
end

%% PLOT SECTION

if c2==0

% Relationship graphs between outputs against inputs
% e*100 and C*c vs w0,Gs,wL,wP
% CLM (5th input parameter has not been plotted)
    if PLOT % Draw relation graphs just for 5 inp data
        figure
        % w0
        subplot(2,2,1);

        scatter(i(:,1),t_e100,'ro')
        title(' (a) ')
        xlabel('w_0')
        ylabel('e^*_1_0_0 or C^*_c')
        hold on

        scatter(i(:,1),t_Cc,'filled','bo')
        legend('e^*_1_0_0','C^*_c','Location','northwest')

        % Gs
        subplot(2,2,2);

        scatter(i(:,2),t_e100,'ro')
        title(' (b) ')
        xlabel('G_s')
        ylabel('e^*_1_0_0 or C^*_c')
        hold on

        scatter(i(:,2),t_Cc,'filled','bo')
        legend('e^*_1_0_0','C^*_c','Location','northwest')

        % wL
        subplot(2,2,3);
    end
end

```

Appendix F - Artificial Neural Network Matlab Codes

```

scatter(i(:,3),t_e100,'ro')
title(' (c) ')
xlabel('w_L')
ylabel('e^*_1_0_0 or C^*_c')
hold on

scatter(i(:,3),t_Cc,'filled','bo')
legend('e^*_1_0_0','C^*_c','Location','northwest')

% wP
subplot(2,2,4);

scatter(i(:,4),t_e100,'ro')
title(' (d) ')
xlabel('w_P')
ylabel('e^*_1_0_0 or C^*_c')
hold on

scatter(i(:,4),t_Cc,'filled','bo')
legend('e^*_1_0_0','C^*_c','Location','northwest')

saveas(gcf, strcat(int2str(get(gcf,'Number')), '_ ',TFN1, '_ ',TFN2, 'HLNo
',int2str(hiddenLayerSize),str_title, '.fig'));
end

if PLOT
%Plot regression
for c1=1:2
figure
plotregression(trTarg(c1,:),trOut(c1:,:), 'Train',...
vTarg(c1,:),vOut(c1:,:), 'Validation',...
tsTarg(c1,:),tsOut(c1:,:), 'Testing',...
y(c1,:),t(c1:,:), 'ALL Data')
legend

saveas(gcf, strcat(int2str(get(gcf,'Number')), '_ ',TFN1, '_ ',TFN2, 'HLNo
',int2str(hiddenLayerSize),str_title, '.fig'));
end
end

if PLOT
% Simulation results:
% plot target and output data vs sample no for comparison.
% c1 indicates that which target is plotting
% c1=1 :e1*100 c1=2: C*c
for c1=1:2
figure
if c1==1
ylabel_char='e^*_1_0_0';
else
ylabel_char='C^*_c';
end
subplot(2,2,1);
n_tr=1:length(trOut);
plot(n_tr,trOut(c1,:), 'b--o',n_tr,trTarg(c1:,:), 'Rs-')
title(strcat(' (a) Train Data',str_title))
xlabel('Samples')
ylabel(ylabel_char)
legend('Predicted','Measured','Location','northeast')

```

```

subplot(2,2,2);
n_v=1:length(vOut);
plot(n_v,vOut(c1,:), 'b--o', n_v,vTarg(c1,:), 'Rs-')
title(strcat('(b) Validation Data', str_title))
xlabel('Samples')
ylabel(ylable_char)
legend('Predicted', 'Measured', 'Location', 'northeast')

subplot(2,2,3);
n_ts=1:length(tsOut);
plot(n_ts,vOut(c1,:), 'b--o', n_ts,vTarg(c1,:), 'Rs-')
title(strcat('(c) Test Data', str_title))
xlabel('Samples')
ylabel(ylable_char)
legend('Predicted', 'Measured', 'Location', 'northeast')

subplot(2,2,4);
n_all=1:length(y);
plot(n_all,y(c1,:), 'b--o', n_all,t(c1,:), 'Rs-')
title(strcat('(d) All Data', str_title))
xlabel('Samples')
ylabel(ylable_char)
legend('Predicted', 'Measured', 'Location', 'northeast')
saveas(gcf, strcat(int2str(get(gcf, 'Number')), '_', TFN1, '_', TFN2, 'HLNo',
int2str(hiddenLayerSize), str_title, '.fig'));
end
end

% plot of performance vs epoch
if PLOT
figure

semilogy(tr.epoch, tr.perf, 'b-s', ...
tr.epoch, tr.vperf, 'g--o', ...
tr.epoch, tr.tperf, 'r-.^')

% Add reference lines to graph at minimum mse of validation data
% (i.e.best epoch)
line([tr.best_epoch tr.best_epoch], [.001,10], ...
'Color', 'black', 'LineStyle', ':');
line([0 tr.num_epochs], [tr.best_vperf, tr.best_vperf], ...
'Color', 'black', 'LineStyle', ':');

title(strcat('Performance Graph', str_title))
xlabel('epoch')
ylabel('mse - Log scale')
legend('Train', 'Validation', 'Test', 'Location', 'northeast')
% Add a circle at best performance to graph:
hold on;
plot(tr.best_epoch, tr.best_vperf, 'ko', ...
'LineWidth', 2, ...
'MarkerSize', 15)

% Add texts _____
str=strcat('\leftarrow', num2str(round(tr.best_vperf, 4)));
text(0, tr.best_vperf, str, 'HorizontalAlignment', 'left');

```


Appendix F - Artificial Neural Network Matlab Codes

```

saveas(gcf, strcat(int2str(get(gcf, 'Number')), '_ ', TFN1, '_ ', TFN2, 'HLNo
', int2str(hiddenLayerSize), str_title, '.fig'));
end

if PLOT %Spearman Coeff
    figure
    y_bar=rho;
    b=bar(y_bar)
    set(gca, 'XTick', 1:5, 'XTickLabel', x_bar);
    legend('e^*_1_0_0', 'C^*_c');
    ylabel('e^*_1_0_0 or C^*_c');
    b(2).LineWidth = 2;
    b(2).EdgeColor = 'black';
    b(2).FaceColor = 'white';
    b(2).LineWidth = 1.0;
    b(2).LineStyle='-';
    b(1).EdgeColor = 'black';
    b(1).FaceColor = 'black';
    title(strcat('Spearman Correlation Coeff.', str_title))

saveas(gcf, strcat(int2str(get(gcf, 'Number')), '_ ', TFN1, '_ ', TFN2, 'HLNo
', int2str(hiddenLayerSize), str_title, '.fig'));
end
end
end
%% Rename excel sheet name of output file
e_xls = actxserver('Excel.Application'); % # open Activex server

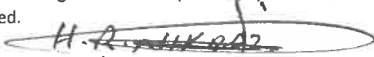
ewb = e_xls.Workbooks.Open(filename_out); % # open file (enter full
path!)
ewb.Worksheets.Item(1).Name = 'All data'; % # rename 1st sheet
if str_exc=='Y'
ewb.Worksheets.Item(2).Name = 'Excl w0';
ewb.Worksheets.Item(3).Name = 'Excl Gs';
ewb.Worksheets.Item(4).Name = 'Excl wL';
ewb.Worksheets.Item(5).Name = 'Excl wP';
ewb.Worksheets.Item(6).Name = 'Excl CLM';
ewb.Worksheets.Item(7).Name = 'Comparison';
end
ewb.Save % # save to the same file
ewb.Close(true)
e_xls.Quit
end
end

```

Appendix G - Co-author Attribution Tables



Appendix G Co-author Attribution Tables

Co-author Attribution Prof Hamid Nikraz



Paper No.	No. 1	No. 2	No. 3	No. 4	No. 5	No. 6	No. 7	No. 8	No. 9
Conception	X	X	X	X	X	X	X	X	X
Method guidance	X				X	X			
Introduction/ Conclusion	X								
Technical Advice							X		
Data acquisition & Analysis									
Approval	X	X	X	X	X	X	X	X	X
Paper No.	Paper Title								
1	Intrinsic Compression Characteristics of an Expansive Clay from Western Australia								
2	Determination of the compression index of reconstituted clays using intrinsic concept and normalized void ratio								
3	The effect of unloading and reloading on the compression behaviour of reconstituted clays								
4	Variation of Consolidation Coefficient of Expansive Clays at High Initial Water Content								
5	Characterisation of the Undrained Shear Strength of Expansive Clays at High Initial Water Content Using Intrinsic Concept								
6	Effect of shear rate on the residual shear strength of pre-sheared clays								
7	Compression behaviour of highly expansive clays stabilised with a green stabiliser of magnesium chloride								
8	Regression Models for Intrinsic Constants of Reconstituted Clays								
9	Prediction of intrinsic compressibility parameters of reconstituted clays using artificial neural network								
I acknowledge that these represent my contribution to the above research output.									
Signed. 									

Paper No. 1



Habibbeygi, F., Nikraz, H., & Chegenizadeh, A. (2017). Intrinsic Compression Characteristics of an Expansive Clay from Western Australia. International Journal of GEOMATE, 12(29), 140-147.
 doi:https://doi.org/10.21660/2017.29.20455

	Conception	Method guidance	Introduction/Conclusion	Technical Advice	Data acquisition & Analysis	Approval
Prof Hamid Nikraz	X	X	X			X
I acknowledge that these represent my contribution to the above research output. Signed. 						
Dr Amin Chegenizadeh	X	X	X			X
I acknowledge that these represent my contribution to the above research output. Signed. 						

Habibbeygi, F., Nikraz, H., & Verheyde, F. (2017). Determination of the compression index of reconstituted clays using intrinsic concept and normalized void ratio. International Journal of GEOMATE, 13(39), 54-60. doi:<https://doi.org/10.21660/2017.39.98271>

	Conception	Method guidance	Introduction/Conclusion	Technical Advice	Data acquisition & Analysis	Approval
Prof Hamid Nikraz	X					X
I acknowledge that these represent my contribution to the above research output. Signed. 						
Fred Verheyde		X		X		X
I acknowledge that these represent my contribution to the above research output. Signed. 						

Habibbeygi, F., Nikraz, H & Koul B. (2018). Prediction of intrinsic compressibility parameters of reconstituted clays using artificial neural network. Unpublished

	Conception	Method guidance	Introduction/Conclusion	Technical Advice	Data acquisition & Analysis	Approval
Prof Hamid Nikraz	X					X
I acknowledge that these represent my contribution to the above research output. Signed: 						
Bill Koul		X		X		X
I acknowledge that these represent my contribution to the above research output. Signed: 						

Appendix H - Copyright Permissions

Appendix H Copyright Permissions

23 Sep. 2018

International Journal of GEOMATE ISSN:2186-2982 (Print) 2186-2990 (Online)
Geotechnique, Construction Materials and Environment, Tsu, Mie, Japan

Dear International Journal of GEOMATE

It is my understanding that you are the copyright holder for the following papers which I have published with your journal during my research study:

- Habibbeygi, F., & Nikraz, H. (2018). Characterisation of the Undrained Shear Strength of Expansive Clays at High Initial Water Content Using Intrinsic Concept. *International Journal of GEOMATE*. doi:<https://doi.org/10.21660/2017.29.20455>
- Habibbeygi, F., & Nikraz, H. (2018). Compression behaviour of highly expansive clays stabilised with a green stabiliser of magnesium chloride. *International Journal of GEOMATE*, 14(45), 144-150. doi:<https://doi.org/10.21660/2018.45.10697>
- Habibbeygi, F., & Nikraz, H. (2018). The effect of unloading and reloading on the compression behaviour of reconstituted clays. *International Journal of GEOMATE*, 15(51), 53-59. doi:<https://doi.org/10.21660/2018.51.52643>
- Habibbeygi, F., Nikraz, H., & Chegenizadeh, A. (2017). Intrinsic Compression Characteristics of an Expansive Clay from Western Australia. *International Journal of GEOMATE*, 12(29), 140-147. doi:<https://doi.org/10.21660/2017.29.20455>
- Habibbeygi, F., Nikraz, H., & Verheyde, F. (2017). Determination of the compression index of reconstituted clays using intrinsic concept and normalized void ratio. *International Journal of GEOMATE*, 13(39), 54-60. doi:<https://doi.org/10.21660/2017.39.98271>

I would like to reproduce an extract of this work in a doctoral thesis which I am currently undertaking at Curtin University in Perth, Western Australia. The subject of my research is 'Experimental study on the behaviour of expansive soils'. I am carrying out this research in my own right and have no association with any commercial organisation or sponsor.

The specific material / extract that I would like to use for the purposes of the thesis is '**whole of the papers mentioned above as the chapters of my thesis**'.

Once completed, the thesis will be made available in online form via Curtin University's Institutional Repository espace (<http://espace.curtin.edu.au>). The material will be provided strictly for educational purposes and on a non-commercial basis.

I would be most grateful for your consent to the copying and communication of the work as proposed. If you are willing to grant this consent, please complete and sign the attached approval slip and return it to me at the address shown. Full acknowledgement of the ownership of the copyright and the source of the material will be provided with the material.

If you are not the copyright owner of the material in question, I would be grateful for any information you can provide as to who is likely to hold the copyright.

I look forward to hearing from you and thank you in advance for your consideration of my request.

Yours sincerely

Farzad Habibbeygi

PERMISSION TO USE COPYRIGHT MATERIAL AS SPECIFIED BELOW:

- Habibbeygi, F., & Nikraz, H. (2018). Characterisation of the Undrained Shear Strength of Expansive Clays at High Initial Water Content Using Intrinsic Concept. *International Journal of GEOMATE*. doi:<https://doi.org/10.21660/2017.29.20455>
- Habibbeygi, F., & Nikraz, H. (2018). Compression behaviour of highly expansive clays stabilised with a green stabiliser of magnesium chloride. *International Journal of GEOMATE*, 14(45), 144-150. doi:<https://doi.org/10.21660/2018.45.10697>
- Habibbeygi, F., & Nikraz, H. (2018). The effect of unloading and reloading on the compression behaviour of reconstituted clays. *International Journal of GEOMATE*, 15(51), 53-59. doi:<https://doi.org/10.21660/2018.51.52643>
- Habibbeygi, F., Nikraz, H., & Chegenizadeh, A. (2017). Intrinsic Compression Characteristics of an Expansive Clay from Western Australia. *International Journal of GEOMATE*, 12(29), 140-147. doi:<https://doi.org/10.21660/2017.29.20455>
- Habibbeygi, F., Nikraz, H., & Verheyde, F. (2017). Determination of the compression index of reconstituted clays using intrinsic concept and normalized void ratio. *International Journal of GEOMATE*, 13(39), 54-60. doi:<https://doi.org/10.21660/2017.39.98271>

I hereby give permission for **Farzad Habibbeygi** to include the abovementioned material(s) in his/her higher degree thesis for Curtin University, and to communicate this material via the space institutional repository. This permission is granted on a non-exclusive basis and for an indefinite period.

I confirm that I am the copyright owner of the specified material.

Signed: 

Name: Professor Dr. Zakaria Hossain

Position: Editor-in-Chief, International Journal of GEOMATE

Date: 25 September 2018

Please return signed form to Farzad Habibbeygi farzad.habibbeygi@postgrad.curtin.edu.au

23 Sep. 2018

Journal of Engineering Science and Technology (JESTEC)

Taylor's University, Malaysia

ISSN: 1823-4690

Dear Journal of Engineering Science and Technology

It is my understanding that you are the copyright holder for the following paper, which I have published, with your journal during my research study:

Habibbeygi, F., & Nikraz, H. (2018). Variation of Consolidation Coefficient of Expansive Clays at High Initial Water Content. *Journal of Engineering Science & Technology*, 13(9), 2644-2654.

I would like to reproduce an extract of this work in a doctoral thesis, which I am currently undertaking at Curtin University in Perth, Western Australia. The subject of my research is '**Experimental study on the behaviour of expansive soils**'. I am carrying out this research in my own right and have no association with any commercial organisation or sponsor.

The specific material / extract that I would like to use for the purposes of the thesis is '**whole of the paper mentioned above as one chapter of my thesis**'.

The paper will be cited in the thesis appropriately.

Once completed, the thesis will be made available in online form via Curtin University's Institutional Repository espace (<http://espace.curtin.edu.au>). The material will be provided strictly for educational purposes and on a non-commercial basis.

I would be most grateful for your consent to the copying and communication of the work as proposed. If you are willing to grant this consent, please complete and sign the attached approval slip and return it to me at the address shown. Full acknowledgement of the ownership of the copyright and the source of the material will be provided with the material.

If you are not the copyright owner of the material in question, I would be grateful for any information you can provide as to who is likely to hold the copyright.

I look forward to hearing from you and thank you in advance for your consideration of my request.

Yours sincerely

Farzad Habibbeygi

PERMISSION TO USE COPYRIGHT MATERIAL AS SPECIFIED BELOW:

Habibbeygi, F., & Nikraz, H. (2018). Variation of Consolidation Coefficient of Expansive Clays at High Initial Water Content. *Journal of Engineering Science & Technology*, 13(9), 2644-2654.

I hereby give permission for **Farzad Habibbeygi** to include the abovementioned material in his higher degree thesis for Curtin University, and to communicate this material via the espace institutional repository. This permission is granted on a non-exclusive basis and for an indefinite period.

I confirm that I am the copyright owner of the specified material.

Signed:



Name: Abdulkareem Sh. Mahdi Al-Obaidi

Position: Associate Professor, Executive Editor / Journal of Engineering Science and Technology

Date: Wednesday, 26 September 2018

Please return signed form to Farzad Habibbeygi farzad.habibbeygi@postgrad.curtin.edu.au

Re: Copyright permission request #TrackingId:1967385

Farzad Habibbeygi

Thu 10/11/2018 8:30 PM

Sent Items

To: geoscience@cogentoa.com <geoscience@cogentoa.com>;

Dear Melissa

Thank you for your email.

Best regards,
Farzad Habibbeygi

From: geoscience@cogentoa.com <geoscience@cogentoa.com>

Sent: Thursday, October 11, 2018 8:18:19 PM

To: Farzad Habibbeygi

Subject: Copyright permission request #TrackingId:1967385

Dear Farzad,

Thank you for your patience while I looked into this further for you. Since your article is published under a CC-BY license, you, as the author, retain copyright and you can reproduce it as long as you attribute the original source in the new piece of work.

I hope this proves helpful to you, and, again, thank you for your patience in awaiting my reply.

Best,
Melissa

Cogent Geoscience

From: farzad.habibbeygi@postgrad.curtin.edu.au

Sent: 23-09-2018 01:23

To: farzad.habibbeygi@postgrad.curtin.edu.au

Cc:

Subject: Copyright permission request

Dear Journal of Cogent Geoscience

It is my understanding that you are the copyright holder for the following paper which I have published with your journal during my research study:

Habibbeygi, F., & Nikraz, H. (2018). Effect of shear rate on the residual shear strength of pre-sheared clays. *Cogent Geoscience*, 4(1), 1453989. doi:<https://doi.org/10.21660/2017.29.20455>

I would like to reproduce an extract of this work in a doctoral thesis which I am currently undertaking at Curtin University in Perth, Western Australia. The subject of my research is '**Experimental study on the behaviour of expansive soils**'. I am carrying out this research in my own right and have no association with any commercial organisation or sponsor.

The specific material / extract that I would like to use for the purposes of the thesis is '**whole of the paper mentioned above as one chapter of my thesis**'.

Once completed, the thesis will be made available in online form via Curtin University's Institutional Repository espace (<http://espace.curtin.edu.au>). The material will be provided strictly for educational purposes and on a non-commercial basis.

I would be most grateful for your consent to the copying and communication of the work as proposed. If you are willing to grant this consent, please complete and sign the attached approval slip and return it to me at the address shown. Full acknowledgement of the ownership of the copyright and the source of the material will be provided with the material.

If you are not the copyright owner of the material in question, I would be grateful for any information you can provide as to who is likely to hold the copyright.

I look forward to hearing from you and thank you in advance for your consideration of my request.

Best regards,
Farzad Habibbeygi



Open Access License to Publish (CC-BY)

<http://creativecommons.org/licenses/by/4.0/>

ARTICLE TITLE:	Effect of Shear Rate on the Residual Shear Strength of Pre-Sheared Clays
ARTICLE DOI:	10.1080/23312041.2018.1453989
AUTHOR(S):	Farzad Habibbeygi, Hamid Nikraz
JOURNAL TITLE:	Cogent Geoscience
JOURNAL ISSN:	2331-2041

You retain copyright in your Article

You grant **Cogent OA** a non-exclusive license to publish the Version of Record of your article named above, including any abstract, visual abstract, tables, figures, data, and supplemental material (together, the "Article"), in the Journal, subject to the Terms and Conditions set out below.

If the Article is accepted for publication by the Editors of the Journal, Cogent OA will publish the Article under the terms of a Creative Commons Attribution 4.0 (CC BY 4.0) License (<http://creativecommons.org/licenses/by/4.0/>).

You grant **Anyone** (and retain for yourself) the right to share (copy and redistribute the material in any medium or format) or adapt (remix, transform, and build upon the material) the Article as published in the Journal for any purpose, even commercially provided appropriate credit is given, a link to the license is provided and details of changes made are indicated.

I own copyright, and I am granting Cogent OA the non-exclusive license to publish the Version of Record of my Article on an Open Access basis, with the copyright statement '© <YEAR> The Author(s). Published by Cogent OA'.

I confirm that I have read and accept the full terms of the Open Access License to Publish including the **Terms & Conditions** and author warranties below.

I confirm that I agree to assume responsibility for payment of any applicable Open Access Article Publishing Charges.

Signed and dated: Farzad Habibbeygi, 17 March 2018

Taylor and Francis, 17 March 2018



Open Access License to Publish (CC-BY)

<http://creativecommons.org/licenses/by/4.0/>

ARTICLE TITLE:	Regression models for intrinsic constants of reconstituted clays
ARTICLE DOI:	10.1080/23312041.2018.1546978
AUTHOR(S):	Farzad Habibbeygi, Hamid Nikraz, Bill Koul
JOURNAL TITLE:	Cogent Geoscience
JOURNAL ISSN:	2331-2041

You retain copyright in your Article

You grant Cogent OA a non-exclusive license to publish the Version of Record of your article named above, including any abstract, visual abstract, tables, figures, data, and supplemental material (together, the "Article"), in the Journal, subject to the Terms and Conditions set out below.

If the Article is accepted for publication by the Editors of the Journal, Cogent OA will publish the Article under the terms of a Creative Commons Attribution 4.0 (CC BY 4.0) License (<http://creativecommons.org/licenses/by/4.0/>).

You grant Anyone (and retain for yourself) the right to share (copy and redistribute the material in any medium or format) or adapt (remix, transform, and build upon the material) the Article as published in the Journal for any purpose, even commercially provided appropriate credit is given, a link to the license is provided and details of changes made are indicated.

I own copyright, and I am granting Cogent OA the non-exclusive license to publish the Version of Record of my Article on an Open Access basis, with the copyright statement '© <YEAR> The Author(s). Published by Cogent OA'.

I confirm that I have read and accept the full terms of the Open Access License to Publish including the Terms & Conditions and author warranties below.

I confirm that I agree to assume responsibility for payment of any applicable Open Access Article Publishing Charges.

Signed and dated: Farzad Habibbeygi, 09 November 2018

Taylor and Francis, 09 November 2018